



## **DISCLAIMER**

This report was prepared as an account of work sponsored by an agency of the United States Government. Neither the United States Government nor any agency thereof, nor any of their employees, makes any warranty, express or implied, or assumes any legal liability or responsibility for the accuracy, completeness, or usefulness of any information, apparatus, product, or process disclosed, or represents that its use would not infringe privately owned rights. Reference herein to any specific commercial product, process, or service by trade name, trademark, manufacturer, or otherwise does not necessarily constitute or imply its endorsement, recommendation, or favoring by the United States Government or any agency thereof. The views and opinions of authors expressed herein do not necessarily state or reflect those of the United States Government or any agency thereof.

This report has been reproduced directly from the best available copy.

Available to DOE and DOE contractors from the Office of Scientific and Technical Information, P.O. Box 62, Oak Ridge, TN 37831; prices available from (615)576-8401, FTS 626-8401.

Available to the public from the National Technical Information Service, U.S. Department of Commerce, 5285 Port Royal Rd., Springfield, VA 22161.

*U.S. Govt. - Strategic*

SELECTION AND INITIAL CHARACTERIZATION OF A SECOND BARRIER  
ISLAND RESERVOIR SYSTEM AND REFINING OF METHODOLOGY FOR  
CHARACTERIZATION OF SHORELINE BARRIER RESERVOIRS

Topical Report

By  
M. Szpakiewicz  
R. Schatzinger  
S. Jackson  
B. Sharma  
A. Cheng  
M. Honarpour

January 1991

Work Performed Under Cooperative Agreement No. DE-FC22-83FE60149

Prepared for  
U.S. Department of Energy  
Assistant Secretary for Fossil Energy

Edith Allison, Project Manager  
Bartlesville Project Office  
P.O. Box 1398  
Bartlesville, OK 74005

Prepared by  
IIT Research Institute  
National Institute for Petroleum and Energy Research  
P.O. Box 2128  
Bartlesville, OK 74005

## TABLE OF CONTENTS

	<u>Page</u>
Abstract .....	1
Executive summary.....	2
Chapter I - Introduction.....	5
Objectives of the project.....	5
General characteristics of tidal sedimentation in shoreline barrier system .....	6
Chapter II - Process for selecting a second shoreline barrier reservoir system (Milestone 1).....	9
Initial candidates.....	9
Ranking of top five candidate reservoirs.....	10
Selection of Almond formation, Patrick Draw field.....	11
Advantages/disadvantages of Almond formation/Patrick Draw field.....	12
Other activities related to final selection and evaluation of Almond formation/ Patrick Draw field .....	13
Chapter III - Patrick Draw field; preliminary geological and engineering analyses (Milestone 2)	
Paleogeographic setting of the Almond formation .....	14
Depositional environments .....	15
Geology of Patrick Draw field .....	16
Tectonics of Patrick Draw field and adjacent area.....	17
Geochemistry of fluids in Patrick Draw field.....	18
Mineralogical composition of the Almond formation, Patrick Draw field .....	20
Texture of Almond reservoir sandstones.....	22
Rock Structure and anisotropy.....	23
Diagenesis of Almond reservoir rocks.....	24
Porosity .....	25
Permeability and pore throat sizes .....	26
Stratigraphic and petrophysical properties of reservoir sandstones of Upper Almond formation - Patrick Draw field, WY .....	27
Stratigraphic units .....	27
Petrophysical and reservoir properties of UA-5 sandstone.....	28
Analysis of outcrop core and log data to determine characteristics of sandstones deposited under different environmental condition in Patrick Draw (WY) field.....	30
Characteristics of sandbodies.....	30
Comparison of grain size distribution of Barrier Island sandstones in Bell Creek and Patrick Draw fields.....	31
Comparison of facies distribution and petrophysical properties of sandstones at Patrick Draw and Bell Creek fields.....	31
Preliminary engineering data analysis of Patrick Draw field .....	32
Reservoir history.....	32
Oil-in-Place.....	32
Core analyses.....	32
Chapter IV - Generic engineering methodology for reservoir characterization (Milestones 3 & 4)...	33
Introduction.....	33
Injection/production monitoring: an effective method for reservoir characterization.....	34
Analyses of waterflood data during linedrive water injection .....	36
Analyses of water and chemical injection wells during EOR process .....	37
Analysis of chemical injection wells using Hall method .....	38
Integration of production, injection and pressure data for dynamic characterization of TIP area, Bell Creek field.....	39
Results and conclusions .....	40

TABLE OF CONTENTS (continued)

	<u>Page</u>
Effect of geological heterogeneities on distribution of initial and post waterflood oil saturations .....	41
Integration of data from various sources for oil saturation studies .....	41
Results of correlations studies .....	42
Application of differential oil-in-place to quantify the effect of geological heterogeneities in oil production .....	43
Determination of oil-in-place distribution by material balance equation .....	43
Determination of oil-in-place distribution by volumetric equation .....	44
Differential oil-in-place method .....	45
Testing of differential oil-in-place method .....	45
Analysis of differential oil-in-place (DOIP) index in Bell Creek field, Unit 'A' .....	46
Conclusions .....	47
Application of fractals for quantitative reservoir characterization .....	48
The Method .....	48
Results and discussion .....	49
 Chapter 5 - Summary .....	 50
 References .....	 52
Acknowledgments .....	51
Appendix A .....	57
Appendix B .....	90

TABLES

1. Oil fields producing from shoreline barrier deposit. Initial candidates for comparative study and generalization of geological-engineering models .....	99
2. Top five shoreline barrier reservoir candidates for comparison with Bell Creek field .....	100
3. Comparison of depositional setting, some rock, and some fluid properties for Bell Creek field Unit 'A', and the top five candidates for a comparative study .....	101
4. Shoreline barrier outcrops considered for generalization of reservoir models .....	102
5. Modern shoreline barriers considered for generalization of reservoir models .....	103
6. Reservoir data and history for Patrick Draw field .....	104
7. Chemical composition of a Patrick Draw oil sample .....	105
8. Range and mean of whole-rock X-ray diffraction analyses of 46 sandstone and 30 shale samples from the upper Almond formation. From Keighin, Law, and Pollastro, 1989 .....	106
9. Mean clay-mineral compositions of sandstone and shale from the upper Almond formation as determined by X-ray diffraction .....	107
10. Whole rock X-ray diffraction analysis, in weight percent, for samples from Patrick Draw upper Almond formation core samples .....	108
11. Characteristics of sands encountered in corehole #2 deposited under different environmental conditions .....	109

TABLES (continued)

Page

12. Characteristics of sand in corehole #1.....	110
13. Permeability reduction of core samples from Patrick Draw field as a result of fresh water injection.....	111
14. Injectivity reduction as a result of chemical injection, TIP, Unit A, Bell creek field.....	112
15. Comparison of water relative permeabilities from well test analysts with those from core analysis .....	112
16. Analysis of petrophysical data in Bell Creek field, Unit A .....	113
17. Analysis of differential oil-in-place in Bell Creek field, Unit A.....	115
18. Analysis of overlay results of differential oil-in-place on various geological and engineering variables, Bell Creek field, Unit A.....	117

ILLUSTRATIONS

1. Three "end-member" facies models of barrier island stratigraphic sequences.....	118
2. Worldwide distribution of microtidal (<2m), mesotidal (2-4m), and macrotidal (>4m) ranges.....	119
3. The influence of inlet spacing on the interconnectedness ratio of tidal delta deposits.....	120
4. Reconstruction of a landward expanding flood-tidal delta.....	121
5. Three-dimensional reconstruction of the wedge-shaped geometry of flood tidal delta sandstone.....	122
6. Models for the vertical stacking of flood tidal deltas in an environment of relative rise of sea level.....	123
7. Diagrammatic map showing relative locations of ancient oil productive shoreline barrier sandstones in Wyoming and Montana.....	124
8. Vertical sequence of facies from outcrop core hole #1, Almond formation.....	125
9. Vertical sequence of facies in cored interval from well Arch 78-14-6, Patrick Draw field, WY.....	126
10. Typical regressive sequence of the shoreline barrier sediments in Southeastern Colorado; the lower and upper Cretaceous Dakota Sandstone with an average thickness of 80 feet.....	127
11. Paleogeographic setting of the Almond formation shoreline/barrier island system on the western shoreline of the Late Cretaceous epeiric sea.....	128

## ILLUSTRATIONS (Continued)

12. Nomenclature and anatomy of facies deposited in a mesotidal barrier island system.....	129
13. Map showing location of wells within Arch and Monell units of Patrick Draw field and location of log-based dip-oriented stratigraphic section illustrated in fig. 33. ....	130
14. Isopach map of interval from the "A" marker bentonite to the top of the lower Almond (same as interval 2 of Weimer, 1966) approximately equivalent to the upper Almond sequence in the outcrop.....	131
15. Combined geochemical anomalies and faults at Patrick Draw oil field from the 1980 Geosat study.....	132
16. Hydrochemical cross-section east of the Rock Springs Uplift, Greater Green River Basin. ....	133
17. Quartz-feldspar-rock fragment composition and rock type classification (after Folk, 1968) <sup>42</sup> for thin section samples from the upper Almond formation at Patrick Draw field.....	134
18. CT scan and density profile for porous, cross bedded sandstone from Patrick Draw field well 49-1 3 at 4,552 ft. ....	135
19. CT scan and density profile for thinly laminated sandstone from Patrick Draw field well 49-1 3 at 4,531 ft.....	135
20. CT scan and density profile for interlaminated silty, very fine sandstone and silty shale from Patrick Draw field well 7-18-1 at 4,957 ft.....	136
21. CT scan and density profile for black, coaly siltstone and shale from Patrick Draw field well 78-14-6 at 4,344 ft.....	136
22. Diagenetic sequence for upper Almond Formation, typical of Patrick Draw field.....	137
23. Dolomite is dominantly cement, however, it locally replaces framework grains.....	138
24. Feldspar (right of center) has been severely leached leaving kaolinized remnants and secondary intercrystalline microporosity.....	138
25. Microcline with characteristic crossed spindle twinning (left) is not corroded while another grain of feldspar immediately adjacent (right) has had its center leached and kaolinized resulting in a significant increase of secondary intercrystalline microporosity. Well 7-18-1, 4,955 ft. ....	139
26. Strongly leached feldspar with abundant secondary intraparticle porosity (center) could not have been transported to the site of deposition in its current state of preservation. ....	139
27. Scanning electron image shows well-developed books and scattered flakes of kaolinite cement within interparticle porosity. ....	140
28. The relationship between natural log (Ln) of permeability and porosity for core analysis from the upper Almond formation at Patrick Draw field. ....	141

ILLUSTRATIONS (Continued)

	<u>Page</u>
29. The relationship between natural log (Ln) of permeability and amount of dolomite cement in reservoir sandstones from the upper Almond formation at Patrick Draw field. ....	142
30. Porosity and permeability plotted for samples from various depositional facies recognized in the upper Almond formation at Patrick Draw field. ....	143
31. Stratigraphic cross section of upper Almond formation, showing major stratigraphic units. ....	144
32. Log responses and petrophysical properties of producing UA-5 sandstone and other geological features of the Upper Almond formation, Patrick Draw field, well no. 10-A. ....	145
33. Log responses and petrophysical properties of producing UA-5 sandstone and other geological features in upper Almond formation, Patrick Draw field, well no. 102. ....	146
34. Depth sequential crossplot of resistivity and porosity to distinguish various facies in the 140 ft sand in corehole No. 1 in the Almond formation. ....	147
35. Depth sequential crossplot of gamma ray and porosity to distinguish various facies in the 140 ft sand in corehole No. 1 in the Almond formation. ....	147
36. Depth sequential crossplot of resistivity and porosity to distinguish various sandstone facies in well W-4 from Bell Creek (MT) field. ....	148
37. Imbibition and drainage oil-water relative permeability analysis conducted on a core sample from the Almond formation at Patrick Draw field. ....	149
38. Mercury capillary pressure test results on five core samples from well no. 15, Arch unit, Patrick Draw field. ....	150
39. Location map of Bell Creek (MT) field, Unit 'A', tertiary incentive project (TIP) area. ....	151
40. Structural cross-sections across TIP area parallel to the dip (X - X') and strike (Y - Y') of Muddy formation. ....	152
41. Comparison of the location of 70% water-cut advancement superimposed on fault map (a) and that from the full-scale areal simulation (b) of TIP area. ....	153
42. Comparison of residual oil saturation distribution after 10 years of linedrive waterflooding, obtained by full-scale simulation without the inclusion of a major fault, in % (a) and with the inclusion of a major fault (b). ....	154
43. Pressure-pulse and falloff test results prior to initiation of chemical flooding. ....	155
44. Hall plot of injection performance of all pattern water injection wells in TIP area. ....	156
45. Hall plot of injection performance of all chemical injection wells in TIP area. ....	157
46. Hall plot of early performance of all chemical injection wells in TIP area. ....	158

ILLUSTRATIONS (Continued)

Page

47.	Distribution of Hall plot slopes based on performance of water injection and early performance of chemical injection wells, TIP area.....	159
48.	Average transmissivity map.....	160
49.	Superposition of projected Hall plot chemical injection wells (Region 1) based on their early performance and their actual performance (Region II) of Hall plot of water injection wells. ....	161
50.	Distribution of initial oil saturation and other reservoir properties in well 26-4.....	162
51.	Distribution of water saturation and other reservoir properties in well P-2 drilled after 13 years of combined primary and waterflood production. ....	163
52.	Oil-in-place distribution in TIP area of Bell Creek (MT) field using material balance equation.....	164
53.	Differential oil-in-place for the four sections surrounding the Tertiary Incentive Project area.....	165
54.	Log derived heterogeneity index (LHI) vs. differential oil-in-place (DOIP), Bell Creek field, Unit 'A'.....	166
55.	R/S analysis regression curve of bulk density log as measured in well P2 of Bell Creek field. ....	167
56.	Bulk density log for well P2, Bell Creek field.....	168
57.	R/S analysis regression curve of bulk density log as measured in well W7 of Bell Creek field. ....	169
58.	Bulk density log for well W7, Bell Creek field. ....	170

# SELECTION AND INITIAL CHARACTERIZATION OF A SECOND BARRIER ISLAND RESERVOIR SYSTEM AND REFINING OF METHODOLOGY FOR CHARACTERIZATION OF SHORELINE BARRIER RESERVOIRS

By

M. Szpakiewicz, R. Schatzinger, S. Jackson, B. Sharma, A. Cheng, and M. Honarpour

---

## ABSTRACT

Generalization of shoreline barrier reservoir characteristics is a primary objective of the BE1 project, "Reservoir Assessment and Characterization." The Upper Cretaceous Almond formation in Patrick Draw oil field, southwestern Wyoming, has been selected from 18 primary candidates for comparison with the Lower Cretaceous Muddy formation in Bell Creek field, southeastern Montana (Milestone 1). Both oil productive reservoirs selected for broadening geological and engineering understanding of the system represent a combination of "end-member" models of shoreline barriers developed under different hydrodynamic conditions. The hydrodynamic conditions primarily involve changes in sea level and the dominant tide and wave regime of a coastline.

The productive Muddy formation in Bell Creek field predominantly consists of fine-grained littoral (intertidal) and neritic (shallow marine) sandstones deposited as shoreface and foreshore facies in a shoreline barrier system, whereas the Almond formation in Patrick Draw field contains two distinct units consisting of fine- to medium-grained estuarine sandstones deposited in a tidal channel/tidal delta environment associated with migrating tidal inlets within a barrier-island coastline and some fine to very fine-grained littoral and shallow neritic sandstones. For broadening comparative aspects of these oil-productive shoreline barrier systems, geologic information on a number of well documented outcrops and several representatives of the Holocene barriers have also been collected.

The study of similarities and contrasts of the microtidal (Bell Creek) and mesotidal (Patrick Draw) types of ancient oil-producing shoreline barrier deposits provides an improvement in quantification of a generalized shoreline barrier model (Milestone 2). By incorporating the Patrick Draw field model into the generalized barrier island model, the product will become more broadly applicable. A spectrum of geologic and engineering data is being collected from Patrick Draw field and analyzed to reach that goal.

An integrated study was conducted to correlate geological heterogeneities with log signatures, pressure, injection, and production characteristics (Milestone 3); and fractal distribution (Milestone 4). This work provides an effective, efficient, and economical methodology for characterization of shoreline barrier reservoirs.

## EXECUTIVE SUMMARY

The broad objectives of the Department of Energy program for geoscience research are to develop methods for determining mobile and immobile oil saturation distribution in reservoirs and evaluating suitable methods for recovering oil. The specific objective is to develop a better understanding of heterogeneity factors that influence the movement and trapping of fluids in reservoirs. Accurate descriptions of the spatial distribution of critical reservoir parameters (e.g., permeability, porosity, pore geometry, mineralogy, and oil saturation) were considered essential for improving sweep efficiency by implementation of fluid diversion techniques and for reliable predictions of oil recovery. This information, in the near- to mid-term, will assist producers to implement better reservoir management strategies such as placing infill wells or planning fluid displacement methods. The methodology developed based on this information will help operators determine which reservoir parameters are critical for reliable performance prediction through mathematical simulation.

So far as we know, this project is the only one which systematically addresses the integration of geological and engineering parameters for all genetic varieties of a depositional system.

Shoreline barrier depositional systems contain a substantial amount of petroleum resource in the United States that can be the target of infill drilling and/or enhanced oil recovery.

Shoreline barrier depositional settings encompass a variety of sandbody types. Shoals, spits, barrier peninsulas, barrier islands, and sandy barrier bars attached to the mainland are subtypes of shoreline barriers formed by long-shore currents and modified by movements of relative sea level, direction of sandbody buildup, wave and/or tide action, local tectonics, and diagenetic processes.

In previous years, NIPER selected an example of a microtidal, wave-dominated, progradational barrier island reservoir that was a prolific producer: Bell Creek (MT), field. An interdisciplinary team approach was applied to characterize this field.

The scope of the work for FY90 consisted of three main areas. First, a mesotidal, tide-dominated shoreline barrier/barrier island reservoir, Patrick Draw (WY) field was selected for expanding the methodology for effective shoreline barrier characterization. Advantages and disadvantages of numerous candidate reservoirs were used to rank them. A group of five fields with the greatest potential for comparative study were selected as final candidates prior to selection of Patrick Draw field as the field which best fulfills the criteria established to meet the objectives of the project.

The second area of FY90 work included the fundamental relationships between geological, petrophysical, and reservoir production/injection characteristics. Much of the work in this area was conducted using previously available data from Bell Creek field.

The third area of FY90 work included investigation of more efficient and economical methods for shoreline barrier/barrier island reservoir description and simulation (methodology). Bell Creek data and data from related outcrops were also used in this area of work.

FY90 Task 1 was the selection of a second shoreline barrier/barrier island reservoir for testing and generalizing the NIPER characterization methodology and collection of data. Preliminary geological investigation of Patrick Draw field indicates that mesotidal processes (1 to 3.5 m range) dominated the depositional setting and that tidal inlet, tidal delta, and tidal channel facies are much more dominant than in a microtidal system such as the Muddy formation at Bell Creek field. Geometry of the various depositional facies reflects the different depositional processes.

FY90 Task 2 was analysis of fundamental relationships between geological, petrophysical, and reservoir production characteristics to improve quantification of the barrier island model. Petrographic analysis of rock samples indicates that feldspar content of the Almond formation at Patrick Draw field averages 8.5%, which is about 4 times the amount of feldspar present in the Muddy formation at Bell Creek field. The abundance of detrital feldspar at Patrick Draw field is probably the source of much of the diagenetic kaolinite and is related to the origin of common secondary porosity within the producing Almond formation sandstones. Little interlayered illite/smectite is present in the upper Almond sandstones and formation damage due to swelling clays is negligible; however, the small pore throat size associated with diagenetic kaolinite indicates that the formation is susceptible to mobile fines damage.

Improvement in methodology for reservoir characterization was made by identifying heterogeneities through engineering analysis and evaluating the influence of these heterogeneities on production, injection performance, and residual oil saturation. Once integrated with other sources of information, the Hall plot method and water advancement monitoring provide dynamic, quantitative characterization of geological heterogeneities. The Hall plot can be used as a diagnostic method for performance evaluation of waterflood and EOR processes.

Comparisons of calculated oil-in-place values from material balance equations (MBE) with those from volumetric calculations on a well-by-well basis can provide information about geological heterogeneities early in the life of a field.

FY90 Task 3 was to improve the quantitative barrier island model from detailed correlation of log signatures with geological heterogeneities. The log study found that among shoreline-barrier facies, barrier beach has the highest average porosity and tidal channel, the lowest porosity. Because grain size is similar for these two facies, the higher average porosity in the beach facies is attributed to better sorting.

FY90 Task 4 was to investigate the use of fractal distributions for improvement of the shoreline barrier/barrier island model. NIPER developed and applied an algorithm and a program for processing many types of data using the fractal method to the recognition, quantification, and characterization of log signatures.

Based on FY90 work, future directions for this project should include: detailed investigation of external and internal geometry and spatial variation of reservoir rock properties in a mesotidal shoreline barrier system (Patrick Draw field) and comparison with the same characteristics of microtidal shoreline barrier systems (Bell Creek field).

## CHAPTER I. - INTRODUCTION

### Objectives of the Project

The overall objective of NIPER's Reservoir Characterization Program is to identify critical reservoir heterogeneities and to develop a better understanding of the influence of reservoir heterogeneities on the movement and trapping of fluids and develop a methodology for characterization of shoreline barrier reservoirs. This deposystem-specific methodology should outline methods for prediction of the residual oil saturation at interwell scales and the flow patterns of injected and produced fluids.

A quantitative geological/engineering model has been constructed and used to evaluate the influence of heterogeneities found in microtidal shoreline barriers on primary, secondary, and tertiary production; patterns of injected and produced fluids; and residual oil saturation distribution and magnitude. An integrated methodology for constructing a quantified hydrodynamic model for application to shoreline barrier reservoirs was developed based on Bell creek (MT) field, nearby analogous outcrops, and the literature. Selection of a second shoreline barrier/barrier island reservoir for characterization was an integral part of this project in FY90.

In order to expand the developed methodology, a mesotidal shoreline barrier reservoir was selected (a) to test the earlier methodology, (b) to generalize the geological/engineering model of shoreline barrier reservoirs, and (c) to improve the predictability of shoreline barrier production performance based on the geological/engineering model. Patrick Draw (WY) field, a mesotidal reservoir, was chosen as a second reservoir for generalization of the methodology (Task 1).

Preliminary engineering and geological studies were conducted to investigate and identify fundamental relationships between heterogeneities in shoreline barrier reservoirs and production, injection, and pressure performance (Task 2).

Depositional facies were identified through crossplotting log signatures. Production, injection, and pressure histories were integrated for identification of geological heterogeneities and their influence on reservoir performance (Task 3).

The application of fractal geostatistics for improvement of a quantitative shoreline barrier model was investigated by developing an algorithm and a program for processing many types of data such as log signature, core, and production data (Task 4).

### General Characteristics of Tidal Sedimentation In Shoreline Barrier System

Prior to the 1970s, the prograding Galveston Island depositional model was considered by many geologists as the "one and only" facies model for interpreting ancient barrier-island sequences. Studies conducted within the past 20 years indicate that the use of one normative model is unrealistic.<sup>1</sup> Three generalized facies models to barrier island sequences can be recognized: (1) regressive barrier, (2) transgressive barrier, and (3) barrier-inlet<sup>1</sup> (see fig. 1). Most ancient shoreline barrier sequences can be classified through comparative analyses with individual "end-member" models or a combination of them.

The shoreline barrier depositional system consists of (1) supratidal sediments such as aeolian and backshore (backbeach) facies, (2) intertidal sediments such as foreshore, tidal flat, and upper tidal delta facies, and (3) subtidal sediments such as shoreface, shoal, tidal inlet, tidal channel, lower tidal delta, and lagoonal/estuarine facies.

Hydrodynamic conditions such as wave and tidal action lead to reworking original barrier island sediments in a transgressive setting. Redeposition of sands brought about by migration and infilling of tidal channels may become the single most important depositional process restructuring facies arrangement in a barrier island system.<sup>2</sup>

Facies architecture depends much on the magnitude of tide action. Mesotidal conditions predominate on contemporary shorelines except in polar regions (fig. 2). Tidal delta deposits attached to frequent inlets, which are characteristic for mesotidal coasts, may create extensive and almost interconnected lobate sand bodies on the backbarrier side (fig.3). Isolated flood tidal delta bodies form on coasts with long barrier islands and few, wide-space tidal inlets. Long barrier islands typically form on coasts with a micro-tidal regime. (fig. 3A). Coasts with short barrier islands and abundant, close-spaced tidal inlets are normal on mesotidal coasts.<sup>3</sup> In this setting, flood tidal deltas can connect to form a continuous sheet (fig. 3B).<sup>4</sup>

The anatomy of flood tidal delta is shown in figure 4. Geometry of the wedge-shaped flood tidal delta is exemplified by a 3-D reconstruction of sandstone exposures investigated in northern Spain by Cuevas et al.,<sup>5</sup> (fig. 5). Donselaar<sup>4</sup> provided synthetic models for vertical stacking of flood tidal deltas attached to inlets of different spacing and dynamism (fig. 6). The delta deposits are schematically represented by plano-convex lenses. The use of the plano-convex shape is justified by the preserved geometries of the flood tidal delta deposits in the Menefee formation, San Juan Basin, northwest New Mexico. Formation of flood tidal delta deposits connected to ephemeral inlets (fig. 6A) takes place only when the inlets are open. When the inlets are closed, the flood tidal delta deposits are covered with lagoonal fines. In time, this results in the formation of isolated sandstone lenses. Permanent tidal inlets

(fig. 6B) either are fixed, or migrate lateral. A fixed position of tidal inlets is generally related to preexisting depressions in the substrate, such as flooded river valleys. Accumulation of flood tidal delta deposits connected to fixed inlets, or to inlets that migrate within a limited zone only (fig. 6B.1), results in the formation of pillar-like sedimentary bodies. Close spacing of tidal inlets leads to the interconnection of the sedimentary bodies. Accumulation of flood tidal delta deposits adjacent to freely migrating permanent inlets (fig. 6B.2) results in the formation of extensive tidal delta belts.

The preservation potential of the barrier island depositional system in a transgressive setting is higher on the barrier-sheltered lagoonal side. The best preservation potential represents facies deposited in erosional depressions such as tidal inlet channel fills and tidal deltas including the distributary channel fills of tidal deltas. This may lead to a hypothesis that in mesotidal transgressive settings the barrier-sheltered and barrier-associated sandstones may predominate over the barrier island facies (in the strict sense) such as those described in case of the Bell Creek field on a microtidal coast.<sup>6</sup>

The variety of ancient oil producing sandstones and morphologies that can be encountered in a barrier island depositional system is illustrated by a diagrammatic map (fig. 7) showing the position of four major Rocky Mountain oil reservoirs within a paleosystem.

The barrier island associated reservoir sandstones are from the Lower and Upper Cretaceous formations in Powder River Basin and Green River Basin in Wyoming and Montana. The Muddy consists of interbedded nonmarine to marine sandstone and shales in an overall transgressive sequence. Recluse field has an estuarine sequence from a basal fluvial-channel fill to overlying transgressive marine sandstones. Bell Creek field displays a wave-dominated barrier-island sandstone and adjacent lagoonal deposits on the microtidal coast. Hilight field has a coastal-marsh section succeeded by shoreline sandstones that were partly eroded or reworked during transgressions. The Almond formation in Patrick Draw field consists of estuarine sandstones deposited in a tidal channel/tidal delta environment associated with migrating tidal inlets within a barrier island coastline. Some shallow neritic shoreface sandstones are also represented.

According to Donselaar,<sup>4,7</sup> Cuevas et al.,<sup>5</sup> and Tillman<sup>8</sup> the dominant features of the flood tidal deltas, which develop at the distal part of tidal inlets in response to flow expansion of the tidal current that passed through the inlet, are as follows:

- Simple or multiple plano-convex, lobate or wedge-shaped geometry of sandstone bodies
- Bipolar transport direction resulting in the bimodal distribution of foreset dips with a dominant landward component
- Arrangements of the internal structures such as:

- coarsening upward units; occasionally no vertical or lateral grain size variation within the sandstone body
- the flat lower surface is only slightly erosive
- occurrence of bundle sequences
- the uniform landward inclination of set boundaries and reactivation surfaces
- the mud drapes on foresets and bottomsets
- the dominance of smaller, trough-shaped sets in the upper part of the bodies, as opposed to higher, tabular to wedge-shaped sets and inclined laminane in the lower part
- upper surfaces convex to undulating, often wave rippled
- often deep erosive scours in the upper part of sandstone body filled with cross-bedded sandstones (flood tidal delta feeder channels).

Dominant features of the tidal inlet channel deposits (fills) are as follows according to the same sources as above:

- erosive (scoured) base
- fining upward sequence
- shell lag layers common at base
- bi-directional flow structures (couplets present)
- poor sorting
- commonly consists of high and low angle large scale tabular crossbeds
- drapes in low flow velocity (silt dominated clayey mud)
- contrasting lithologies and sedimentary structures in tide-and wave dominated deposits due to variations in modes of migration and channel abandonment.

Tidal deposits such as tidal deltas (flood and ebb), tidal inlet channels, and flood tidal delta distributary channels may possess excellent reservoir properties within a barrier island system if preserved in a transgressive setting and if not extensively cemented by postdepositional diagenetic processes. Their geometry and internal architecture, however, significantly differ from a typical open marine shoreface and foreshore facies; therefore, their performance as hydrocarbon reservoirs should also differ.

High confidence identification of certain facies in the shoreline barrier system such as, for example, shoreface and tidal delta and their lateral correlation may be difficult in reservoir cores. Studying outcrops, where directional features can be identified, should significantly increase the level of confidence. Figures 8 and 9 (Almond formation at Patrick Draw field) and figure 10 (Dakota Sandstone) illustrate characteristic

sequences of facies in shoreline barrier systems which differ considerably from those earlier described in the Bell Creek reservoir.

The previously studied Muddy formation in Bell Creek (MT) field and analogous Muddy formation outcrops in NE Wyoming (New Haven area) consist of a dominantly regressive (prograding) sequence of facies with minor elements from a transgressive event at the base of the sequence.<sup>9-10</sup> Thus to broaden the range of studied end-members for barrier island reservoir characterization (Task 1 of Project BE1, FY90) and to make the geological/engineering model more broadly applicable to a wider range of reservoirs, our attention was drawn to the selection of reservoirs where barrier island and associated tidal inlet sequences of facies dominate in productive intervals.

## **CHAPTER II. - PROCESS FOR SELECTING A SECOND SHORELINE BARRIER RESERVOIR SYSTEM (MILESTONE 1)**

### **Initial Candidates**

Eighteen candidates were chosen (table 1) among numerous shoreline barrier reservoirs based on NIPER established criteria. A shoreline barrier literature data base has been continually updated and now contains the collected references about the Almond formation, Patrick Draw field, stratigraphy, sedimentology and petrography of barrier sediments, and references about the formations and specific fields considered in our selection process (See appendix A.) A review of these cases indicated that a similar spectrum of facies occurs in most barrier systems. The variations of processes, however, control the predominance of the various facies. For example, in mesotidal deposition, tidal processes dominate, and tidal inlet, tidal channel, and tidal delta facies are predominant; whereas, in a microtidal system, marine processes dominate, and foreshore, shoreface, and washover facies are predominant. The data base was supplemented by discussions with consultants and specialists in industry, visits to core repositories, and examinations of cores from various sources.

The following criteria were established for selection of a second reservoir:

1. The reservoir must comprise a shoreline barrier that will expand the model developed based on Bell Creek field.
2. It should be a prolific oil producer (OOIP>100 MM STB).
3. A complete suite of geological and engineering data from the reservoir should be available to NIPER.
4. Nearby analogous outcrops should be available.
5. The reservoir should have a history of some primary and secondary production and should be a potential EOR candidate.

6. The reservoir should be in the continental U.S. , preferably within the Rocky Mountain Region.

Based upon the above criteria, the number of candidate reservoirs was reduced. A list of the top five candidate reservoirs and a comparative summary of their reservoir properties with Bell Creek field are shown in tables 2 and 3. Because shoreline barriers comprise a variety of genetic types,<sup>11</sup> it was necessary to know which type of barrier the candidates represented. It was also important to select a reservoir which is at a stage of oil recovery comparable with that of Bell Creek. The reported environments of deposition are, therefore, summarized along with some other important parameters for each of the top five candidate reservoirs (tables 2 and 3).

Sandbodies that are originally detached from the strandplain may through time become connected to the mainland by vertical accretion on the lee side of the barrier, or by bay-head delta progradation. An example is provided by the Upper Cretaceous Gallup Sandstone within the San Juan Basin where a lagoon became a coal swamp and the associated barrier island in the strict sense became attached to the mainland as the swamp replaced the lagoon.<sup>12</sup> Such sequences that record the vertical (and therefore temporal) shift from detached shorelines to attached shoreline sands actually may be very common and play an important role in development and growth of strandplains and chenier plains such as seen on the Gulf Coast. Knowledge of this natural complexity in the relationship between attached and detached, submerged and emergent shoreline barriers meant that the search for barrier island reservoir settings in the strict sense must be de-emphasized. Instead, more emphasis was placed on determining the type of shoreline barrier candidates represented and whether they would be the best reservoir for comparing and contrasting the setting of Unit 'A' at Bell Creek and for testing the reservoir characterization methodology.

Outcrop exposures and modern environments provide extremely useful information about geometry and lateral extent of facies for developing shoreline barrier models. Information on a number of well documented outcrops (table 4) and several representative modern shoreline barriers (table 5) were collected and may be considered for future use in shoreline barrier model developments.

#### **Ranking of Top Five Candidate Reservoirs**

The top five candidate reservoirs of 18 which were considered are summarized in tables 2 and 3. The first candidate reservoir is Patrick Draw field, located on the east side of the Rock Springs Uplift, Greater Green River Basin, Wyoming. Barrier-related production is from the Upper Almond formation, between 4,000 and 5,000 ft below surface. The reported depositional environment is barrier island (probably prograding) and associated inlet fill.<sup>13</sup> Patrick Draw field was selected as first choice because it fulfills the criteria established to meet the objectives of the project (listed above) more than any of the other reservoirs.

The second candidate was Hilight field producing from the Muddy formation in Powder River Basin, south of Bell Creek field. The barrier island sandstones are the most prolific producers there, followed by the underlying fluvial and delta front sandstones.<sup>14</sup> Analyses of facies and facies sequences in cores from Hilight field provide direct lithologic evidence of depositional paleoenvironments, but cannot reliably distinguish between some paleoenvironments with similar deposits; e.g. wave-dominated delta front vs. shoreface, or lagoon vs. bay.<sup>14</sup> The top-most sandstone interval--Springer Ranch Member--is interpreted as progradational barrier island/spit and tidal inlet deposits.

The third rated choice was West Ranch field, which produces from the Oligocene Frio formation between 5,100 and 5,700 ft in the Texas Gulf Coast. This large field contains three barrier intervals developed under microtidal regime and classified as aggrading, transgressive, and progradational barrier islands.<sup>15</sup> The three producing intervals are responsible for an estimated 499 million barrels OOIP. Unfortunately the amount of core available from these intervals is questionable. Much of the known core was unconsolidated and has become disaggregated.<sup>16</sup> Ranking of this reservoir was also somewhat lowered because it is not located within the same general geological province (Rocky Mountain region) as was the first study at Bell Creek.

The fourth candidate was Elk City field, which produces from relatively deep (9,400 ft) Pennsylvanian sandstones in the Anadarko Basin of southwestern Oklahoma. This field is reported to produce from deltaic and associated barrier bar deposits. The type of bar remains unclear at this time, and it is uncertain whether the barrier portion accounts for more than 10% of the reservoir.

The fifth candidate reservoir was Bisti field which produces from the Gallup sandstone in the San Juan Basin of northwestern New Mexico. Based on the recent literature,<sup>17</sup> the depositional environment for Bisti field does not appear to meet the requirements for a shoreline barrier.

In addition to the five reservoirs listed in tables 2 and 3, two cores from the Almond formation at Sun Ranch (TX) field, operated by Oryx Oil Co., were studied. One of the cores was too tight for consideration, and barrier facies could not be identified in the other core. A third Oryx core was sent to NIPER for analysis.

#### **Selection of Almond Formation, Patrick Draw Field**

Of the five reservoirs that showed the greatest potential for a comparative study and test of the developed reservoir characterization methodology, Patrick Draw field is the highest rated candidate and has been selected. Therefore, somewhat more detailed descriptions of the advantages/disadvantages of the reservoir and geological characteristics are presented.

### Advantages/Disadvantages of Almond Formation/Patrick Draw Field

The advantages include the following:

1. Reservoir location. This field is located within a similar geographic area (Rocky Mountain region) as was the reservoir in the previous work. Similarities between the reservoirs include geological province, age of the formation, and tectonic regime although Patrick Draw is located in a different basin (Powder River vs. Green River). These similarities would allow meaningful comparisons of the two sandbodies. In addition, our expertise in the Rocky Mountain region will facilitate the collection and interpretation of data and the determination of similarities and differences between the two reservoirs.
2. Extensive outcrop exposure. Outcrops of the upper Almond formation exist within 10 miles of the subsurface production in Patrick Draw field (fig. 11). More than 100 miles of outcrop are available along the Rock Springs Uplift which exposes a barrier island 60 miles long and 4 miles wide.<sup>18</sup> Two core holes were drilled behind the outcrop providing close to 200 ft of cores that are available to NIPER for examination and normalization of shoreline barrier characteristics.
3. Available cores and logs. More than 80 cores from the Arch Unit of Patrick Draw field are available from the USGS core repository for analysis, many electric and nuclear logs are available from Union Pacific Resources Co.
4. Variation of shoreline barrier type. The Almond formation represents a different "end-member" of barrier/island deposition (fig. 1) compared to the Muddy formation in Bell Creek field. Although both formations were deposited in a shoreline barrier setting, the low tidal range during Muddy deposition (microtidal) resulted in long, laterally uninterrupted barrier core sand bodies. In contrast, the higher tidal range during Almond deposition (mesotidal) produced short, drumstick-shaped barriers.<sup>13</sup> The Almond deposits are complicated with a mosaic of associated barrier system facies such as tidal deltas and tidal creek channels.

The similarities and contrasts of these two types of barrier shoreline deposits will indicate the extent to which coastal barriers can be generalized in a meaningful manner. By adding models of Patrick Draw field to that developed for Bell Creek field, the model will become more broadly applicable to other barrier fields.

The disadvantages include the following:

1. The reservoir thickness within Patrick Draw is rather thin (20 ft); however, this is a common thickness for one-cycle shoreline barrier reservoirs and is nearly the same as that at Bell Creek.
2. No EOR processes have been implemented in the field although EOR is believed to be under consideration.
3. Few foreshore and shoreface intervals have been identified in examined reservoir cores.

#### **Other Activities Related to Final Selection and Evaluation of Almond Formation/Patrick Draw Field**

The process used to select the second reservoir for testing NIPER reservoir characterization methodology was presented to the BPO Project Manager in January 1990, and tentative approval for studying the Almond formation at Patrick Draw (WY) field was obtained. A trip was made to the USGS core-storage facility in Denver, and Upper Cretaceous Almond formation cores from Patrick Draw field were examined. The objective of this examination was to evaluate the quality of 34 slabbed cores from wells primarily in the Arch Unit of Patrick Draw field for the development of a generalized shoreline barrier model and comparison with the Muddy formation at Bell Creek (MT) field. It was concluded that the Arch Unit of Patrick Draw field was deposited in a mesotidal setting, whereas Bell Creek field is a microtidal shoreline barrier.

Union Pacific Resources Co., the operator of Patrick Draw field, was visited to examine the quality of geological and engineering data for the development of a generalized shoreline barrier model. It was learned that adequate core analyses and production-injection data are available from both the Arch and Monell Units. However, few well test data were collected in this field. A second meeting with the BPO Project Manager was arranged in March 1990, for the purpose of sharing information about similarities and differences between Patrick Draw and Bell Creek fields based on initial findings.

An agreement for releasing reservoir data from Patrick Draw field was reached with Union Pacific Resources Co. Log and completion information about Patrick Draw field was received representing virtually all the data that were available from the USGS. Compilation into a computer data file of all the collected data was continued in this fiscal year.

Data from Patrick Draw field were entered into a spreadsheet data file (appendix B). This organized, digitized form allows easy access to digitized data for any purpose including direct input of various parameters into computer mapping, log analysis, statistical analysis, graphics, and simulation programs. Direct transfer into a multi-use geological data base will be possible when the data base

becomes available. Additional well, engineering, and production data will be added as they become available.

Currently the following parameters for 200 wells have been input into the spreadsheet data file:

- (1) Location (section, township, range, footage from section lines);
- (2) Elevation (ground level and Kelly bushing);
- (3) Core information (slabbed or full, interval cored, photographs available/on hand, percent core recovered, quality of core);
- (4) Total depth and tops of formations;
- (5) Logs run;
- (6) Well status (gas/oil producer, gas/water injector, shutin, plugged and abandoned, temporarily abandoned, dry and abandoned, never drilled);
- (7) Initial production (rate, perforated zones, perforation density); and
- (8) Oil gravity

Lithostratigraphic profiles and facies interpretation of two Almond formation cores from core holes drilled behind outcrops on the eastern slope of the Rock Springs Uplift, about 40 miles apart,<sup>19</sup> have been reexamined by NIPER geologists at the Occidental Petroleum Co. research facility in Tulsa, OK. The primary objective of the reexamination was to identify the sedimentologic criteria used by Meyers<sup>19</sup> in the late 1970s for identification of facies in the Patrick Draw area and to compare the criteria used by NIPER geologists in the late 1980s in the Bell Creek area. Such "calibration" is necessary in comparative studies based on facies interpretations by geologists representing different schools of thought but who must deal with assemblages of facies representing the same general environment of deposition that is formed under different dynamic conditions. Average grain size was measured on a foot-by-foot basis in a 300-ft interval of barrier/shoreline in Almond core hole No. 2. Descriptions of sedimentary/biogenic structures were also recorded. Alternative interpretations were suggested from those concluded by Meyers for some intervals and additional work is being conducted to resolve these differences.

### **CHAPTER III. - PATRICK DRAW FIELD; PRELIMINARY GEOLOGICAL AND ENGINEERING ANALYSES (MILESTONE 2)**

#### **Paleogeographic Setting of the Almond Formation**

The Almond formation, the upper interval within the Mesaverde formation, was deposited during a local regression in the overall transgression of the marine Lewis formation over the Mesaverde formation.<sup>20</sup> It ranges in thickness from 250 to 750 ft and can be divided into lower and upper members. The lower Almond (100 to 600 ft thick) contains a fresh water fauna including dinosaur, crocodile, turtle, and fish and consists of small, lenticular channel sandstones; thin, finer-grained levee; overbank and

floodplain sandstones, siltstones and mudstones; and carbonaceous shales and coal beds deposited in a fresh water, coastal swamp environment.<sup>21</sup> The upper part of the lower Almond (125 to 250 ft thick) consists of a cyclic sequence of coals deposited in a fresh-water coastal-marsh environment and fossiliferous, slightly carbonaceous shales, mudstones, siltstones and thin sandstones deposited in a brackish-water, salt-marsh tidal flat, estuarine setting.

The upper Almond (100 to 400 ft thick) produces prolific amounts of oil and gas in the Greater Green River Basin and has been interpreted as a shoreline/barrier deposit.<sup>13,18,21-24</sup> It contains two distinct units consisting of fine-to medium-grained tidal channel/inlet deposits, and fine- to very fine-grained shallow marine deposits. In the Rock Springs/Patrick Draw area, barrier islands were deposited at the head of an embayment (Rock Springs Embayment) in an inter-deltaic area between the Red Desert delta<sup>21, 24-26</sup> to the north and an unnamed delta west of Craig in northwestern Colorado (fig. 11). Moderately high tides (greater than 3 ft) affected the development of the barrier islands and probably resulted from a focusing of tidal currents as they flowed westward and became constricted toward the head of the Rock Springs embayment.<sup>18</sup>

### Depositional Environments

Tidal channel/inlet deposits are common in mesotidal barriers (tidal range 3 to 12 ft)<sup>27</sup> and are also present in the upper Almond formation in the Rock Springs area. Mesotidal channel/inlet sand bodies are associated with laterally migrating barrier-island tidal inlets (fig. 12). Inlet migration is the result of longshore drift which transports sediment in one dominant direction (shoreline parallel) resulting in deposition on the updrift side and erosion on the downdrift side of each inlet. In the upper Almond, three sand bodies can be identified as components of the tidal inlet setting: (a) flood tidal delta, which forms on the landward (lagoonal) side of the inlet, interfingers with tidal flat and salt marsh deposits, and commonly contains oysters (*Crassostrea* sp.) at the base of the deposit; (b) tidal channel, characterized by scoured erosional bases, shell lags of abraded oyster valves and bimodal ebb and flood oriented cross-stratification; and (c) ebb tidal delta, which formed on the seaward side of tidal inlets, and exhibit ebb oriented cross-strata where associated with tidal channel sandstones, and in a seaward direction, become massive and grade into marine sandstones.

The shallow marine sandstones were deposited on the seaward side of the barrier islands and represent outer shelf, subshoreface, shoreface and foreshore (beach) deposits.<sup>21</sup> Outer shelf deposits consist of commonly bioturbated shale and siltstones which grade upward into the subshoreface environments of interbedded sandstone, siltstone and shale deposited below daily wave base and commonly contain the trace fossils *Thalassinoides* and a miniature form of *Ophiomorpha*.<sup>21</sup> The shoreface sandstones were deposited below low tide and above effective wave base and commonly contain burrows of deposit feeders in the lower part and low-angle cross-stratification and abundant

*Ophiomorpha* burrows in the upper part. In the Rock Springs/Patrick Draw area, the laterally extensive shallow marine sands are truncated by tidal inlet/channel deposits resulting in rapid lateral facies changes and complex reservoir unit geometries.

### Geology of Patrick Draw Field

The Almond formation is one of the most important hydrocarbon units in the Rocky Mountain region. This Upper Cretaceous (Maestrician) shallow marine and coastal, coal-bearing sandstone has produced 100 million bbl of oil and 0.7 trillion cu ft of gas through 1986.<sup>23</sup>

Hydrocarbon production from the Almond formation is located in the Greater Green River Basin, Sweetwater County, Wyoming and occurs on the eastern flank of the Rock Springs Uplift, northeastern flank of the Washakie Basin, and Wamsutter arch. The major fields producing oil from the Almond formation are Patrick Draw, Table Rock, and West Desert Springs. Desert Springs field produces gas. All of the fields are stratigraphic traps except Table Rock, which is a structural trap. Two hundred feet of productive beach deposits have been reported at Table Rock.<sup>29</sup>

Patrick Draw field is divided into two units, the northern Arch Unit and the southern Monell<sup>1</sup> Unit (fig. 13). Table 6 presents reservoir properties and field data for Patrick Draw field. The Monell Unit, however, has been successfully waterflooded for 10 to 15 years, with current consideration of applying EOR methods to further enhance production. Attempts to waterflood the Arch Unit were not as successful.

Oil production in Patrick Draw field is from the upper 60 ft of the Almond formation which consists of two sands designated as the UA-6, the lower sand with an average thickness of 12 ft, and the UA-5.

The UA-6 is oil productive in West Desert Springs field (fig. 14) and in the northern part (Arch Unit) of Patrick Draw field.<sup>31</sup> The sandstone is gray, very fine- to fine-grained, calcareous and ranges from a wedge-edge to more than 25 ft thick. The UA-6 sandstone trends southwest to northeast and has been interpreted as tidal creek channels and tidal flat sands deposited landward (west) of a shoreline sand trend based on the erratic distribution of productive sandstone, the fine grain size, and the close association above and below with coal beds and lagoonal shale.<sup>31</sup> An alternative interpretation as a distributary channel has also been suggested.<sup>30</sup>

A second sandstone labeled UA-5 occurs near the top of the Almond formation and is the main oil productive sandstone at Patrick Draw. The UA-5 sandstone is interpreted as a prograding, shoreline sand that was deposited in a mesotidal regime (4 to 8 ft tidal range).<sup>24</sup> The UA-5 sandstone ranges in thickness from 0 to more than 30 ft within Patrick Draw. The porous and permeable UA-5 sandstone zone occurs over an area at least 20 miles long and 6 to 8 miles wide. The reservoir is sealed by the overlying marine

Lewis Shale, by oyster-bearing (*Ostrea glabra*) coquina layers in the central part of the field, or by 5 to 10 ft of carbonaceous shale and impermeable sandstone.

The UA-5 interval has at least two distinct bars and a resulting low-permeability zone which runs mainly north-south and splits the Arch unit into two parts. Although the two bars are similar in lithologic character,<sup>25</sup> they are nearly separate reservoirs with different oil-water contacts, one having a gas cap while the other does not. The permeability barrier represents a depositionally controlled heterogeneity consisting of oyster coquina layers, carbonaceous shale and impermeable sandstone which probably formed in a lagoonal setting.

The UA-5 also can be divided vertically into two main, mappable units in the Monell Unit (Champlin Interoffice correspondence). The upper part (A) is present over most of the west half of the Monell Unit, while the lower part underlies a consistent shale interval, and sometimes a coquina marker below the shale, in both the Arch and Monell Units. The best part of both the Arch and Monell Units is the lower UA-5 (B) sand, which normally has three to ten times the permeability of the upper UA-5 (A) sand.

The UA-5 (A) sand is also present in the Arch Unit and is thought to be correlative with the sand in the Monell Unit, but not hydraulically connected.<sup>25</sup> This is supported by the fact that in the Arch Unit, the sand is wet and nonproductive.

A great portion of Patrick Draw field is unexplored beneath the UA-6 sandstone in both Arch and Monell units.<sup>29</sup> According to Union Pacific Resources Co. data<sup>32</sup> UA-8 sandstone production has been proven in limited areas.

### **Tectonics of Patrick Draw Field and Adjacent Area**

Patrick Draw oil field is located in the Greater Green River Basin, east of the Laramide-Aged Rock Springs Uplift, which divides the Green River sub-basin on the west from the Washakie sub-basin on the east. The Wamsutter Arch, which is an east-west structural nose on the east flank of the Rock Springs Uplift, separates the Great Divide sub-basin on the north from the Washakie sub-basin on the south. Thus, Patrick Draw field is structurally located on the eastern flank of the Rock Springs Uplift and on the southern limb of the east-west trending Wamsutter Arch dipping into the Washakie Basin.<sup>24</sup>

Post-Laramide tectonism affected the present position of the Wamsutter arch and subsequently affected the position of oil and gas reservoirs exploited in the Patrick Draw area.<sup>18</sup> Vitrinite reflectance data,<sup>25</sup> recent thermal modeling, and general reconstruction of structural developments clearly indicate that the tectonic history in the Patrick Draw area played a decisive role in generation, original entrapment, and relocation of oil to the present position after the axis of the Wamsutter Arch migrated in the mid-

Tertiary to the north and the Almond formation developed a dip of about 4 degrees in the Patrick Draw field area.

Post lower-Almond to early-upper Almond Uplift was an early positive expression of the present Rock Springs Uplift-Wamsutter arch that caused truncation and westward thinning of lower Almond strata.<sup>14</sup> Structural downwarping west of Patrick Draw combined with the incipient Wamsutter Arch placed the Patrick Draw sandstone in a structurally high position with closure to the west, south, and north by the time the upper Almond strata were deposited.<sup>21</sup> The structurally high position promoted early hydrocarbon accumulation.<sup>33</sup> Much of the present-day Cretaceous section near Patrick Draw is currently in the oil window zone, actively generating hydrocarbons from the marine, organic-rich Lewis Shales.<sup>34</sup>

A number of east to northeast trending normal faults have been documented in the outcrop belt of Almond on the Rock Spring Uplift. Few of these faults, however, cut through Patrick Draw field (fig. 14). The movements on these faults is thought to be dominantly vertical. Several faults have fault dips that approach 45 degrees.<sup>21</sup> Richers et al.<sup>34-35</sup> studied a relationship between geochemical anomalies observed in the Patrick Draw area and the distribution of faults and linaments (fig. 15). They concluded that fractures and faults are the preferred migration pathways of hydrocarbons leaking from the subsurface source beds and reservoirs to the surface.

Law et al. (1986)<sup>36</sup> pointed out that vitrinite reflectance "anomalies" in the region of northeast trending faults cutting across Patrick Draw field indicate the possibility that hydrocarbons have migrated vertically along these faults from deeper basin pre-Almond source beds.

Weimer (pers. comm. in Van Horn, 1979)<sup>21</sup> indicated that the oil produced from the overlying Fox Hills formation as well as oil produced west of Patrick Draw migrated vertically from the Almond along east-west trending faults. The strong indications of lateral and vertical cross-formational flow through faults in the Patrick Draw area should be confirmed by independent geochemical tools such as isotopy.

### **Geochemistry of Fluids in Patrick Draw Field**

Patrick Draw oil is moderately mature and paraffin with 44.4° API gravity and density of 0.7977 g/cm<sup>3</sup> at 25° C.<sup>34</sup> The chemical composition of a Patrick Draw oil sample is shown in table 7. Whole oil chromatogram analysis indicates a preponderance of lighter n-paraffin components, a large amount of the isoprenoid pristane, and a composition supporting the premise that the oil is derived from terrigenous rather than marine organic matter.<sup>34</sup> Most geochemists believe that pristane to phytane ratios greater than 3.0 characterize input from terrigenous material common to lacustrine, fluvial, and deltaic environments, which fits the local geology of Patrick Draw. Vitrinite reflectance anomalies in the region<sup>36</sup> indicate the possibility of the hydrocarbons migrating vertically along northeast-trending faults from

deeper terrigenous facies. This finding may imply geochemical heterogeneity of oils in different sections of Patrick Draw reservoir. Few data are available in the literature on lateral and vertical distribution of chemical, physical, and isotopic properties of oil from the Patrick Draw field area.

Salinity and chemical composition of formation water in the Almond formation east of the Rock Springs Uplift vary significantly.<sup>37</sup> In Patrick Draw field, the downdip oil productive section of the Almond formation contains brackish waters with total dissolved solids (TDS) of 4 g/L and brines with a TDS of 70 g/L occur in the updip section (fig. 16). Chemical composition of the waters is highly variable. Chlorides, sulfates, or bicarbonates may predominate locally as the major anions in wells located about 1 mile apart.<sup>37</sup>

Geochemical inversion can be readily seen on a hydrochemical cross section (fig. 16). At depths of 3,000 to 4,000 ft in the updip mostly non-hydrocarbon-productive portion of Almond, highly saline waters (TDS = 50 to 70 g/L) overlay downdip formation waters associated with oil and gas accumulation having a salinity as low as 2 to 20 g/L. Mechanisms for forming these anomalies and heterogeneities can only be speculated at this time. Analyses of the stable isotope content of fluids could provide more definite answers. The problem is of more than academic nature because an anomalous inversion like that in Patrick Draw field seems to be a rule rather than exception in major petroliferous intermontane basins of the U.S. Rocky Mountains.<sup>37</sup> Little attention has been reported in the petroleum literature about the geochemical inversions in petroliferous basins which seem to be widespread in geologically young basins.

A definite reverse gradient in water salinity existing in both the Arch and Monell Units of Patrick Draw field has been noticed by operators. Analyses of produced water also differ significantly in Monell and Arch Units. All Arch Unit wellhead samples contain large quantities of sulfate ion (above 1 g/L), and bicarbonates predominate over chloride, whereas in Monell Unit water samples, sulfates are virtually absent, and chloride is a dominant anion. These facts strongly indicate that Almond waters in both units are not in hydraulic contact and belong to two different genetic systems.

A systematic study of chemical and isotopic characteristics of oils, waters, and gases in the geochemically heterogeneous Patrick Draw system could provide vital information for improvement of further development of the field and proper selection of EOR strategy.

### Mineralogical Composition of the Almond Formation, Patrick Draw field

Bulk mineral composition based on X-ray diffraction (XRD) of sandstones and shales of the upper portion of the Almond formation was presented by Keighin, Law, and Pollastro (1989).<sup>28</sup> Their results, reproduced here in table 8, indicate that sandstones in Patrick Draw reservoir tend to contain more carbonate minerals and less quartz than do upper Almond sandstones which are buried to greater depths east of Patrick Draw. Carbonates include calcite, dolomite, ankerite, and siderite. Keighin and others<sup>28</sup> noted that the amount of carbonate in the sandstone varies greatly on the scale of a few inches. In addition, ankerite is the most common carbonate cement in tightly cemented sandstones.

In a study of porosity occlusion in Upper Cretaceous sandstones from the Rocky Mountain Region (including the Almond formation), Jacka<sup>38</sup> noted that tops and bottoms of progradational barrier island sandstone bodies commonly exhibit greater concentrations of calcite cement than middle (foreshore beach and surfzone) intervals. It was noted that locally common concentrations of oyster shells in backshore beach or lagoonal sediments of Upper Cretaceous Rocky Mountain barriers may be so tightly calcite cemented that they could locally form seals to trap hydrocarbons. Where oyster shells are not concentrated in lagoonal backshore (backbarrier) portions of barrier island sandbodies, porosity-occluding calcite cement is lacking.<sup>38</sup> It was concluded that calcite cement in the Upper Cretaceous barrier island sandstones of the Rocky Mountains is a function of the abundance of calcite nuclei upon which the calcite crystals can grow. Calcite nuclei may be provided by oyster fragments, disaggregated *Inoceramus* prisms, and planktonic and benthic foraminifera.

Table 8 indicates that total feldspar content of the Almond sandstones averages 5%. The average feldspar content of 10 thin sections analyzed for this project is 8.5%, with minimum and maximum values of 2.0 and 17.7% respectively. However, as much as 30 to 40% feldspar has been reported.<sup>32</sup> Much detrital feldspar has been removed by dissolution, and some has been replaced by carbonate minerals. Potassium feldspar (dominantly orthoclase) is more common in upper Almond sandstones at depths of less than 6,000 ft in contrast to plagioclase feldspar which is more common in the more deeply buried upper Almond sandstones.

Upper Almond sandstones contain between about 15 and 25 wt % clay minerals (table 8). Mean clay-mineral compositions in the less than 2 $\mu$  (clay size) fraction show that kaolinite is the most abundant clay within the shallower reservoir sandstones. Kaolinite abundance decreases with increasing depth (table 9) and is rare to absent in reservoir sandstones below 9,000 ft.<sup>28</sup> Small amounts of chlorite were detected in Almond shales, but none was detected in any sandstone samples.<sup>28</sup> Illite dominates the clay size fraction below 9,000 ft and includes discrete illite and interstratified illite/smectite. Illite/smectite is of the ordered variety and contains less than 25% expanded layers.<sup>28</sup> Little smectite is found in either the

upper Almond formation sandstones or in the shales. These characteristics of the clay composition indicated that even the shallowest upper Almond formation reservoir rocks, now at depths of approximately 4,500 ft, may have been buried to depths where the temperature exceeded 212° F, or may have experienced a heating event.<sup>28</sup>

Four additional samples from Patrick Draw field have been analyzed by X-ray diffraction in this work. The results (table 10) tend to support the results of Keighin et al.<sup>28</sup> in that quartz is the dominant mineral except in sample 45-14-3 (50 ft), which was from an oyster rubble bed. K-feldspar is dominant over plagioclase, kaolinite is the dominant clay mineral, and illite and mixed-layer illite/smectite are present.

Excluding the sample from an oyster bed, calcite comprises less than 5 wt % of the samples; however, combined dolomite and ferroan dolomite comprise up to 25% in one sample. Total carbonate content ranges from 12 to 93 wt % of the samples and is dominated by ferroan dolomite. The amount of dolomite from samples listed in table 10 is much greater than that indicated by Keighin et al.<sup>28</sup> (table 9). The greatest amount of dolomite plus ankerite (ferroan dolomite) reported by Keighin et al. was only 12%, although the greatest amount of total carbonate was 20 wt %, which is in line with most of the values in the Patrick Draw samples (table 10).

Interparticle cement crusts of high magnesium calcite up to 30 mm thick are presently forming in coastal marsh and barrier island complexes of the Gulf Coast of Louisiana.<sup>39</sup> If preserved, such crusts could be responsible for laterally extensive calcite-cemented horizons in ancient barrier islands.

Petrographic analyses of Almond formation outcrop thin sections<sup>40</sup> indicate a very similar mineralogical composition as compared to analyses by Keighin et al.<sup>28</sup> Point count analysis by Pryor<sup>30</sup> indicates an immature chert arenite composition. Twenty-nine Almond reservoir samples examined<sup>41</sup> were classified as quartz arenite; however, chert and other quartzose rock fragments were plotted on the same pole of a sandstone composition classification diagram. If corrections for rock fragments were taken into account, the samples<sup>41</sup> would plot in the sublitharenite to chert arenite range.<sup>42</sup> Detrital matrix contributed 16.5% of the rock volume while rock fragments contributed 25% of the total rock composition in the samples.<sup>40</sup> A generic classification of the rock fragments include the following: shale, 0.5%; siltstone, 1.5%, chert, 19.5%; and polycrystalline quartz, 3.5%. Van Horn<sup>21</sup> noted that chert decreases volumetrically with respect to feldspar in an up-section direction within the upper Almond formation. He also concluded that the abundance of pelitic rock fragments in upper Almond sandstones places the feldspar and lithic (rock fragment) content nearly equal. The finer grained sandstones (with an abundance of pelitic rock fragments) fall into the litharenite to sublitharenite category, while the coarser sandstones (which are relatively deficient in the pelitic rock fragments) fall into the arkosic to subarkosic category. If, however, the pelitic rock fragments are fecal pellets (which is not unlikely), then the coarser upper Almond

sandstones could all be classified as arkoses.<sup>42</sup> Heavy mineral content was less than 0.8% for all Mesaverde Group sandstones analyzed. Garnet and zircon comprised 94% of the heavy mineral abundance in an Almond sample,<sup>40</sup> indicating crystalline schists, gneiss, and acid igneous source rocks.

Petrographic analyses of Almond formation sandstone thin sections from cores from Patrick Draw field indicate dominantly feldspathic litharenite, chert arenite, and sublitharenite compositions (fig. 17). In only one case was feldspar more abundant than rock fragments, resulting in a lithic arkose composition. Mineralogically the sandstones are quite immature as is reflected by the abundance and variety of rock types and feldspars, including plagioclase. The dominant lithic fragments include chert and other sedimentary rock fragments, although metamorphic and even sparse volcanic rock fragments were identified. During these analyses the original (unaltered) grain types were interpreted to ensure that original (syndepositional) rock composition was recorded.

The Almond formation sandstones examined from Patrick Draw field are generally texturally submature because they contain less than 5% detrital clay, but sand grains are only moderately to well sorted and not well rounded.

#### **Texture of Almond Reservoir Sandstones**

Lower Almond formation (fluvial and freshwater coastal marsh<sup>21</sup>) reservoir rocks consist of pods of poorly sorted, very fine-grained, silty, argillaceous (illitic) sandstone. Lower Almond sandstones would be moderately-well to well-sorted if it were not for the abundance of silt and clay matrix.<sup>21</sup> In contrast, upper Almond reservoirs consist predominantly of medium-grained sandstones.<sup>21</sup> Visual scans of sandstone thin sections from Patrick Draw field, however, indicate an average grain size of 188  $\mu\text{m}$  (fine-grained sand) with a distinct difference between samples from facies tentatively identified as tidal delta (average 210 microns, N=6) and abandoned inlet (average 145  $\mu\text{m}$ , N=3). These coastal and barrier sandbodies<sup>13,25,43</sup> consist of well sorted, linear belts containing much smaller percentages of authigenic clay, which is dominantly kaolinite.<sup>41</sup> The major carbonate mineral in upper Almond reservoirs is calcite or dolomite, whereas it is frequently siderite in the lower Almond. Carbonate cement and compacted clay-rich rock fragments significantly reduce porosity in most upper Almond sandstones,<sup>21</sup> and thinner, finer-grained units are more tightly cemented by authigenic carbonate than are thicker upper Almond sandstone units.

Fine-grained and medium-grained upper Almond sandstones have similar fabrics dominated by point contacts and include many floating grains, suggesting that early cementation prevented later compaction.<sup>21</sup> In thin sections where dolomite cement comprises greater than about 25% of bulk volume, permeability is less than 1 md and the resulting texture is undercompacted. Undercompacted textures are not necessarily the product of early cementation alone, as is evidenced by dolomite-replaced margins of

quartz framework grains, dolomite-filled re-entrants in otherwise normal grains, grains with highly irregular shape, "ghosts" of replaced grains within dolomite crystals, and "floating" silt to very fine sand grains encased in dolomite cement.

Lower permeability zones (< 30 md) in otherwise good reservoir quality sandstones are often created by processes other than dolomite cementation. Four major causes for such low-permeability zones have been recognized in samples from Patrick Draw field:

1. Preserved clay matrix seams.
2. Clay-cemented zones, particularly by kaolinite.
3. Altered and selectively leached zones where the collapsed remnants tend to block pore throats. Processes involved include replacement by kaolinite, corrosion and leaching, vacuolization, and sericitization.
4. Compaction, particularly after weakening of grains by alteration and leaching. Compaction creates low permeability zones by rotating, bending, breaking, and shattering grains; creating long contacts, sutured contacts, interpenetrating grains, and stylolitic contacts between grains; compression of softer grains and creating pseudomatrix.

### **Rock Structure and Anisotropy**

Three slabbed rock samples from Patrick Draw cores well 49-1-3, 4,522 ft (fig. 18), 4,531 ft (fig. 19), and well 7-18-1, 4,957 ft (fig. 20) were CT-scanned perpendicular to bedding to evaluate the extent of CT density variation within facies having different reservoir quality. Sample 7-18-1, 4,957 ft, has the best reservoir quality (greatest apparent porosity based on visual scan) and has a CT density that varies from 600 to 700 HU (Hounsfield Unit, a measure of X-ray attenuation where -1,000 HU = air, 0 HU = water, and <1,000 HU = rock). This sample is a porous, cross-laminated fine-grained sandstone with a few partly cemented thin laminae. The intermediate reservoir quality sample (49-1-3, 4,522 ft), which is a thinly laminated silty sandstone with more visible lamination, has CT density variation from 650 to 750 HU. The sample with the poorest reservoir quality (49-1-3, 4,531 ft) comprises interlaminated silty very fine sandstone and silty shale. It has a CT density variation of 750 to 850 HU. Note that CT density increases with generally decreasing reservoir quality and that even the "better" layers (lower CT values) in successively poorer reservoir quality rock do not seem to overlap.

This type of CT density variation reflects a high degree of vertical anisotropy related to interlayering of lithologies within the core samples. The CT density variation in the best reservoir quality sample is determined by relatively small amounts of clay cementation based on thin section analysis.

A sample of black, coaly siltstone and shale (well 78-14-6, 4,344 ft) was also scanned (fig. 9) and shows CT density increasing from 0 to about 450 HU as one proceeds away from the thin pure coal layers into dark-colored siltstone and shale. This transitional behavior, shown on the scan profile in figure 21, reflects several coal-rich laminae that can be distinguished from the surrounding silty shale and indicates a transitional or alternating environment.

### **Diagenesis of Almond Reservoir Rocks**

The diagenetic history of the Almond marine reservoirs is complex. Nine stages have been evaluated (fig. 22).<sup>28</sup> Quartz overgrowths on detrital quartz grains were found in all samples examined. Most quartz overgrowths precipitated early in the paragenetic sequence; however, some were found to reduce porosity within secondary pores. Five to 15% of the primary porosity in upper Almond formation sandstones has been filled by silica cement. The diagenetic sequence for upper Almond sandstones proposed by Thomas<sup>41</sup> is somewhat more simplified; however, it is in very close agreement with the scheme presented by Keighin et al.<sup>28</sup>

Much of the porosity in the Almond sandstones at Patrick Draw field has been created by the dissolution of mineral grains and cement. Most intragranular and moldic porosity was formed by dissolution of feldspars, chert, and shale rock fragments. Because the reservoir sandstones generally contain a significant amount of leached feldspar and easily decomposed rock fragments (such as chert and shale), these components also make the reservoir rock sensitive to compaction and subsequent decrease in porosity and permeability.

In addition, 13 to 81% (average 58%) of all feldspar in examined Almond formation sandstone from Patrick Draw field is altered or completely replaced (fig. 23), mostly by kaolinite. Commonly, altered margins or entire feldspar grains are partly leached resulting in a complex maze of secondary microporosity, which contribute to high initial water saturation but little to permeability (fig. 24). In most of the thin sections examined, both perfectly fresh feldspars and all intermediate stages of leached feldspars are present in the same sample, often immediately adjacent to one another (fig. 25). The complex porous remnants of feldspar remaining after more than 90% of the grain has been leached surely could not have been transported to the site of deposition in that condition (fig. 26). The presence of fresh and leached plagioclase and potassium feldspars, mainly orthoclase and microcline, in the same sample implies, however, that some of the partially leached grains must have been incorporated into the sediments in the altered state. Neither selective leaching of one type of feldspar nor a general leaching of all feldspars can explain the preserved textures or the types of feldspars preserved in the upper Almond sandstones at Patrick Draw field. The diagenetic history of the upper Almond formation feldspars is significant because

more than one-third of the total porosity in many examined thin sections was created by corrosion or leaching of part to all of the feldspar assemblage.

Ferroan dolomite is the most common cement in the more permeable upper Almond formation sandstones examined. Dolomite locally replaces calcite and quartz and has also been identified as syntaxial overgrowths on prior dolomite and calcite. Thin section analysis of Patrick Draw samples indicates that dolomite can locally contribute up to 35% rock volume, thereby reducing permeability to less than 1 md.

Clay minerals play an important role in the development of reservoir quality (fig. 27). Partial dissolution and replacement of feldspar and rock fragments by clays is very common in Patrick Draw sandstones where this process created abundant microporosity. The difference between laboratory-derived porosity and thin section point count derived porosity (always the smaller of the two) should give an index of the amount of microporosity within a sample. The distribution of clays within the pore system indicates that the reservoir should be sensitive to migration of fines.<sup>44</sup> Cementation and replacement of detrital chert, quartz grains, shale rock fragments, and clay matrix by kaolinite is extensive in examined sandstones from the upper Almond formation at Patrick Draw field.

Illite cementation is a major mid- to late-stage event in the Almond, particularly in the deeper (>8,000 ft) reservoir sandstones. Illite replacement of rock fragments was reported in Almond sandstones from 4,500 to 12,000 ft.<sup>28</sup> Illite with "flame-like" and acicular habits is also present within secondary pores. The development of authigenic illite in Almond reservoir rocks is thought to be partly due to the conversion of smectite to illite<sup>45</sup> and partly to earlier leaching of K-feldspars.

It may be expected that outcrop samples from analogous sandstones may have a somewhat different diagenetic sequence which may, at least in part, be controlled by their more complicated tectonic history. It has been suggested that as a result of uplift into the vadose zone, iron hydroxide may be deposited as coatings or as "ironstone" concretions.<sup>38</sup> Also, calichefication of calcite-cemented horizons may occur upon uplift and exposure to vadose conditions. Distinguishing caliche created by outcrop weathering from that produced by early re-emergence of calcite-cemented reservoir barrier sandstones will require careful stratigraphic and petrographic studies.

### **Porosity**

A plot of porosity versus depth for sandstone core samples from the Almond formation<sup>28</sup> indicates the expected relationship of decreasing porosity with increasing depth. There is, however, a much greater scatter for data in the lower porosity rocks (<8%) that generally occur below about 9,000 ft. The shallower sandstones are conventional reservoirs with porosities as great as 22% (Patrick Draw field), while

the deeper sandstones have porosities that range from 3.5 to 8% and are generally unconventional (tight) reservoirs.

A plot of natural log of permeability versus porosity (fig. 28) for samples from the upper Almond formation at Patrick Draw field displays a positive correlation with a relatively high correlation coefficient of  $R = 0.83$ .

Based on vitrinite reflectance, there is also a generic relationship between decreasing porosity with increasing thermal maturity.<sup>28</sup> Another conclusion about the development of porosity in the Almond formation is that Patrick Draw area fields had experienced a heating event. Law et al. (1986)<sup>36</sup> concluded that the unusually high levels of thermal maturity in the field and the area around Patrick Draw were due to upward migration of hot fluids along faults and fractures. Such conditions may enhance or decrease porosity depending on the composition of the fluids and the nature of their interaction with the reservoir rocks.

### **Permeability and Pore Throat Sizes**

Based on petrographic examination, permeability of upper Almond reservoir sandstone at Patrick Draw field is an inverse function of dolomite content (fig. 29). Interestingly, there is no statistical relationship and only a weak visual trend for the relationship between permeability and clay cement plus dolomite cement, the two dominant authigenic minerals in the better reservoir quality sandstones.

Porosity-permeability-depositional facies relationships are portrayed for a number of Patrick Draw samples in fig. 30. Observations based on this figure include:

1. Two straight-line relationships become evident when the data for permeability are plotted using an arithmetic scale as in fig. 30.
2. Permeability values greater than 1 or 2 md are present in those samples with more than 21% porosity.
3. The two linear relationships are generally facies controlled: the more permeable samples tend to be from facies tentatively identified as tidal delta and abandoned inlet, whereas the low-permeability facies include tidal creek and tidal flat facies. Thus distinction of facies groups based on porosity-permeability makes us optimistic that with additional work major facies or facies groups may be clearly distinguished using core-calibrated wireline logs.

Thin section analysis of the two low-permeability tidal delta samples in fig. 30 indicates that permeability has decreased in these samples because of diagenetic processes (cementation). Such variations from the otherwise well delineated porosity-permeability-facies relationship illustrated in fig. 30 indicate that diagenetic heterogeneity may completely scramble well established permeability-porosity

trends based on depositional facies; therefore, log-derived facies designations must be verified with core whenever possible.

Porosity versus permeability for Almond formation sandstones show two distinct permeability regions. The more porous sandstones (>10%  $\phi$ , >1 md) show a well-defined trend of increasing permeability with increasing porosity.<sup>28</sup> The data from lower porosity/lower permeability (generally less than 1 md) rocks display greater scatter and a much more poorly defined trend. Based on mercury injection-capillary pressure data<sup>28</sup> and thin section examinations, the pore throats in Almond formation sandstones are frequently smaller than 1 micron in diameter. Effective pore throat size (where mercury begins to enter the pore throats) for samples from Patrick Draw field is generally between 10 and 15  $\mu\text{m}$ , whereas effective pore throat size for deeper Almond sandstones is much more variable and generally smaller. The variations in pore throat size for deeper samples is controlled by grain size, amount of carbonate cement and presence or absence of microfractures.

#### **Stratigraphic and Petrophysical Properties of Reservoir Sandstones of Upper Almond Formation -- Patrick Draw (WY) Field**

The distribution pattern and continuity of sandstones and other stratigraphic units of the upper Almond formation in Patrick Draw field were investigated from a dip-oriented stratigraphic section in the north central part of the field (see fig. 13 for location). The stratigraphic section (fig. 31) was constructed from available induction and spontaneous potential logs (SP), but other logs, such as sonic and density, were also studied when available. Preliminary lithological description of cores performed by NIPER geologists and earlier workers were available from a few wells along this section for calibration of log signatures with the dominant geological features.

#### **Stratigraphic Units**

The following stratigraphic units are important to the oil and gas accumulations and could be differentiated on the stratigraphic section (fig. 31).

1. The lowermost unit of upper Almond formation consists of a cyclic sequence of shales, sandstones, and coals each of which has a typical log signature. Particularly, the numerous coal beds are distinguishable by their sharp resistivity 'kicks' on induction log and very high transit time 'kicks' on the sonic logs. Three distinct cycles in this sequence were previously distinguished,<sup>43</sup> out of which cycle II is important because it contains the oil producing UA-6 sandstone. The UA-6 sandstone is either absent or is very thin (4 ft or less as shown in fig. 31) and is not always easily distinguishable on logs from the few other thin sandstone beds in this area. The UA-6 sand has good development slightly north of the section such as at well 64, section 11.

2. The lowermost of the shale units in this sequence can be easily distinguished and correlated on electric logs across the entire stratigraphic section. This unit has been called the 'marker shale' <sup>43</sup> and is indicated in figure 31.

3. Above the 'marker shale' and separated from it by another cycle of sandstones, shales and coals in most parts of the stratigraphic section is the producing UA-5 sandstone, which has been interpreted to be a shoreline/barrier deposit. The UA-5 sandstone is the principal reservoir in Patrick Draw field and is easily distinguishable on electric logs. It may be seen in fig. 31 that the UA-5 sandstone deposit is composed of two distinct 'bars', (the so-called 'western' and the 'eastern' bar) separated from each other by a zone where the sandstone is absent.

4. All along the western bar and partly along the eastern bar, an oyster-bearing layer of shales and sandstones overlie the UA-5 sandstone. This oyster-bearing layer is thickest where it fills the low between the two bars (about 30 ft) and is easily distinguishable on electric logs by its characteristic sharp response.

5. Directly overlying the Almond formation are the marine 'Lewis' shales. The contact between the Lewis and the oyster layer is easily distinguishable and correlatable on all the logs in the study area.

### **Petrophysical and Reservoir Properties of UA-5 Sandstone**

The oil and gas accumulation in UA-5 sandstone at Patrick Draw is the result of a stratigraphic trap formed by updip pinchout of the bar westward into impermeable lithologies. Generally the UA-5 sandstone is well sorted, fine-grained, and has uniform texture and composition with a minor degree of stratification. X-ray diffraction and clay/mineral analyses (tables 8-10) show that the UA-5 sandstone consists of (in decreasing order) quartz, carbonate minerals, clay minerals, and feldspar. Substantial amounts of authigenic clays are also present as pore-lining and pore-filling material.

The distribution of porosity and permeability along the entire thickness of the UA-5 sandstone can be studied from the type of logs such as the ones from wells 10-A and 102 (figs. 32 and 33) located close to the stratigraphic section (see fig. 13 for location). Typically the average porosity is around 20% which is sometimes drastically reduced at the top of the sand due to dolomite cementation (well 102, fig. 33). If the upper cemented zone is excluded, the amount of cement in the remaining sandbody is small. The uniform distribution in porosity is sometimes also disturbed by the presence of bioturbated zones and 'shell beds' which drastically reduce porosity and permeability (fig. 32). The vertical distribution of permeability follows the same trend as the porosity but its variation is more drastic, and in the two wells (figs. 32 and 33) permeability values range between 0 and 150 md.

The distribution of grain sizes in the UA-5 sandstone, on which the petrophysical properties depend to a large extent, is usually fairly uniform in the vertical direction, except that in many of the wells the sand is coarsest at or very near the base of the sandstone.<sup>43</sup> This increase in the grain sizes at the base of the sandstone is reflected by high permeability values in well 102 (fig. 33) at a depth of around 4,895 to 4,898 ft. From a few feet above the base, where the sandstone is finest, the grain size generally increases upward, suggesting deposition in progressively shoaling water. Laterally, the UA-5 sandstone becomes finer and less well sorted<sup>43</sup> to the east of the eastern bar where the sandstone grades laterally into marine shales in that direction. Presumably the petrophysical property will also continue to deteriorate in that direction.

### Analysis of Outcrop Core and Log Data to Determine Characteristics of Sandstones Deposited Under Different Environmental Conditions In Patrick Draw (WY) field

The core and log data available from two wells drilled through outcrops in the Rock Springs (WY) area located about 14 miles west of the producing Patrick Draw field were analyzed to determine the characteristics of sandstones deposited in the area under a variety of depositional environments. A few of the sandstones in the outcrop wells were from barrier island system of depositional environments; therefore, the characteristics of these sandstones could also be compared with the barrier island sandstone deposit in Bell Creek (MT) field.

#### **Characteristics of Sandbodies**

The induction, spontaneous potential, gamma ray, and density logs available from the two wells drilled through outcrops were interpreted to determine the characteristics of sandstones deposited under different environmental conditions in the area. A geological interpretation of depositional environment of the different sandstones in the two cored wells was already available<sup>19</sup> from core data interpretations of trace fossils, sedimentary structures, sand size distribution, and polymorphs in the core samples. Information from wireline log responses was intergrated with the geological information to determine the fluid flow characteristics and the geological heterogeneities of the different types of sandstones.

The sandstones encountered in the two outcrop wells were deposited under a wide variety of depositional environments,<sup>19</sup> such as, fluvial, distributary channel, tidal flat and tidal channel, shallow marine barrier island, and beach. Sandstones from each environment were analyzed using gamma ray, density, and induction log data. Because of fresh water penetration, the SP logs were featureless for the most part in the two wells. The results of analyses of seven sandstones from core hole 1 (fig. 8) and three sandstones encountered in core hole 2 are shown in figure 8 and tables 11 and 12. The depositional environments of these sandstones are known from geological studies.<sup>19</sup> The mean and standard deviations of vertical distribution of clay content and porosity of the different sandstones calculated from gamma ray and density logs are given in (tables 11 and 12). Because gamma ray logs do not respond sufficiently to potassium-deficient kaolinite clay, the clay figures will not effectively reflect the presence of kaolinite. The vertical distribution of grain sizes from which the mean and the range were calculated were obtained from visual examination of cores.

From tables 11 and 12, the barrier beach and/or distributary channel seem to have the highest average porosity and the tidal channel the lowest. The grain sizes and clay content in these two sandstones are quite similar; therefore, the significantly higher average porosity in the beach/distributary channel sandstone must be attributed to better sorting of grain sizes in this sandstone. All the marine sandstones in this area show high clay content compared to that of other current dominated sandstones, and since these sandstones also have appreciable porosities it must be concluded that the grain size

sorting in these sandstones usually is also fairly good. The significantly larger spread (high standard deviation) in clay content and porosity in the barrier beach/distributary channel sandstone in core hole No. 2 is due to the large range in particle size distribution (125 to 350  $\mu$ ) of this sandstone. The smallest average particle size was encountered in the marine sandstones and the largest in the current dominated channel sandstones and the beach deposit. The large grain sizes of the channel sands in this area should make these sandstones more permeable compared to the marine sandstones which have a much larger amount of clays.

#### **Comparison of Grain Size Distribution of Barrier Island Sandstones In Bell Creek and Patrick Draw Fields**

From this limited study, the grain sizes in the barrier island sandstone in the studied core holes was found to vary from 115 to 250 microns; the lower value was observed in a particularly clayey sandstone and the higher value in sandstones which had a particularly clean barrier beach component. The dominant grain size in the barrier island facies appeared to be around 170 microns at Patrick Draw field. At Bell Creek field also, the mean grain size in the main barrier island facies (foreshore, middle and upper shoreface), varied between 144 to 181<sup>46</sup> microns which is quite comparable to the size distribution observed in Patrick Draw field.

#### **Comparison of Facies Distribution and Petrophysical Properties of Sandstones at Patrick Draw and Bell Creek Fields**

The producing Muddy sandstones in Bell Creek field were primarily shallow marine barrier island and non-barrier valley fill deposits. A method to distinguish the dominant facies of the Muddy sandstones using a crossplot technique was previously discussed.<sup>46,47</sup> To determine if the shallow marine sandstones from the two outcrop wells also have similar facies distribution in the two crossplots (porosity vs. resistivity and porosity vs gamma ray), porosities were calculated from density logs and plots for porosity against deep resistivity (from induction log), and porosity against gamma rays were constructed for a number sandstones whose depositional environments were determined from previous geological studies.<sup>19</sup> Figs. 34 and 35 show the two crossplots for the shallow marine sandstone at a depth of 140 ft from outcrop corehole #1. Clear separation of the upper and lower shoreface facies is indicated in the two crossplots just as in the case of Bell Creek field. The porosity, resistivity plot for well no. W-4 from Bell Creek field is shown in figure 36 for comparison.

Crossplots for sandstones from other environments were also constructed but the porosity, resistivity and gamma ray values for these sandstones were observed to have a larger spread (large standard deviations) compared to those from the shallow marine environments, which is a consequence of the processes involved in the deposition of these sandbodies.

## Preliminary Engineering Data Analysis of Patrick Draw field

### **Reservoir History**

Patrick Draw field is located in townships 18 and 19 north, ranges 98 and 99 west, Sweetwater County, in southwestern Wyoming. The field was discovered on April 11, 1959, with the completion of the discovery well, El Paso Natural Gas Co., Patrick Draw Unit 1. Initial production rate for this well was 638 BOPD. Average well diameter is 8 inches. Most wells were completed with 5 1/2-inch casing and 2-inch tubing and were perforated at four (most frequently used) or two shots per foot. All wells were stimulated by using acidization and hydraulic fracturing. The reservoir drive mechanism for primary production was mainly solution-gas, and no active water encroachment was reported. Gas was generally not produced but reinjected through five injection wells for reservoir pressure maintenance. Waterflooding was initiated in 1963 and 1966 for the Monell and Arch Units, respectively. A full-scale waterflood was implemented on 80 acres with a 5-spot pattern along with water injection at the gas-oil contact for improving injectivities. About 239 wells have been drilled, and about 128 of these have been water injection wells. Both initial reservoir and saturation pressures were 1,790 psig. A comparison of reservoir properties of Patrick Draw and Unit 'A' Bell Creek field is shown in table 6. Lower waterflood recovery from Patrick Draw field indicates a higher degree of reservoir heterogeneities as compared to that of Bell Creek field.

### **Oil-in-Place**

The total original oil-in-place (OOIP) for both the Arch and Monell units was estimated to be between 200 and 250 MMSTB<sup>31</sup> from volumetrics, and between 140 and 150 MMSTB from material balance calculations. A total of approximately 78.5 MMSTBO has been produced through primary and secondary operations. Table 6 also shows the primary and secondary reserves for Arch and Monell Units. These data indicate that the Monell Unit has a higher recovery efficiency than the Arch Unit. As of July 1983, the daily oil production for the Arch and Monell Units was 180 and 1,300 BOPD, respectively.

### **Core Analyses**

From reported studies,<sup>43</sup> the average permeability of the UA-5 sandstone ranges between 10.4 and 54.4 md. Routine core analyses conducted at NIPER on core samples from well 120 in the, Arch Unit show that the average vertical permeability measured on full-diameter core (10 md) is about half as much as the horizontal permeability (18.6 md) of plugs samples using air. Similar conclusions were reached when a 6-inch-long core from higher energy facies of well 7-18-1, Arch Unit was CT scanned (fig. 20). The density profile along the long axis of the core indicates that CT density fluctuation due to lamination in the core is not very significant. The average grain density of core plugs from this well is 2.65 g/cm<sup>3</sup>.

Table 13 shows results of permeability tests conducted on 154 samples from 26 wells in Patrick Draw field.<sup>48</sup> Results indicate moderate formation sensitivity to fresh water flow. The reduction of

permeability to fresh water is attributed to fines migration resulting from illite and kaolinite presence in Patrick Draw field.

An imbibition and drainage oil-water relative permeability analysis conducted on a core sample from well 1 (Core Laboratories Scale 309-81274) is shown in figure 37. The residual water and oil saturations are between 51 and 58% and 18 and 20%, respectively. The water relative permeability at residual oil saturation is 3.5%. The preservation and core preparation is not known at this time; however, the fluid flow performance of the core indicates that the wetting preference is strongly water-wet.

Typical mercury injection measurements performed on five core samples from Arch Unit of Patrick Draw field are shown in figure 38. More than half of the pore throat diameters of productive sandstone cores from that study are between 2 and 20 microns, which is in agreement with previously published results.<sup>28</sup>

A correlation between porosity and depth of burial showing decreasing porosity with increasing depth, has been reported.<sup>28</sup> Porosity reduction of as much as 20% with increase in the net confining pressure up to 2,750 psi has also been reported. Pore volume compressibility associated with the porosity reduction is between  $4 \times 10^{-6}$  and psi.

#### **CHAPTER IV. - GENERIC ENGINEERING METHODOLOGY FOR RESERVOIR CHARACTERIZATION (MILESTONES 3 AND 4)**

Improvement in methodology for reservoir characterization was made by identifying heterogeneities through engineering analysis and evaluating the influence of these heterogeneities on production/injection performance and residual oil saturation. Readily available data from Bell Creek field were analyzed using conventional methods such as Hall Plot analysis, comparison of material balance and volumetric methods of oil-in-place calculation, and core-log correlation. These methods of analysis provided insight into the nature of heterogeneities and their influence on fluid flow and trapping.

A new approach to reservoir characterization was initiated. This method, fractal analysis, was applied to log signatures in an effort to quantify distribution of heterogeneities within the reservoir.

##### **Introduction**

A comprehensive reservoir description has been recognized in recent years as an important prerequisite for successful design and operation of both secondary and EOR projects. However, a comprehensive reservoir description, usually a multidisciplinary team or synergistic approach, can be very expensive and time consuming. Thus, it is very desirable to develop a reservoir description technique that is effective, efficient, and economical.

The primary objective of this engineering study was to show that through integrated analysis of well testing and production/injection/pressure monitoring methods an improved reservoir evaluation is obtainable. Thus, the influence of various geological heterogeneities on fluid flow during primary, waterflooding and the implementation of chemical flooding can be identified.

Front advancement monitoring and Hall plot analysis were effective and useful tools for evaluating performances of injection wells and identifying interwell geological heterogeneities.<sup>49-50</sup> In conjunction with production/injection data, periodic pressure falloff tests and pulse tests provided adequate information for refined analysis of in situ reservoir properties.

A new method was developed to quantify the effect of reservoir heterogeneities on oil production by examining the differential oil-in-place (OIP) of each well in a given reservoir. A well differential oil-in-place, DOIP is defined by the equation:  $DOIP = \text{volumetric OIP at a given spacing} - \text{material balance equation OIP}$ . This method only requires readily available production and basic petrophysical data and can be applied at or before the end of primary reservoir production. Main applications of this method (DOIP) are to determine: (1) remaining oil reserves, (2) geological heterogeneities, (3) well drainage area and efficiency, (4) optimal well spacing, and (5) best injection and production well sites for waterflood, infill, and EOR programs. Results of the method can be used independently or integrated with other information for optimal reservoir production planning. These methods were tested using the fairly complete geological and engineering data of Bell Creek field (MT), Unit 'A'.

#### **Injection/Production Monitoring: An Effective Method for Reservoir Characterization**

Many infill drilling, completion, stimulation, and enhanced oil recovery operations are inefficient because of insufficient reservoir characterization. Refined knowledge of the distribution of reservoir properties, critical heterogeneities, and potential formation damage is needed to reduce risk and improve productivity.<sup>49</sup> The main challenge of reservoir characterization is to obtain information about reservoir architecture, continuity, and interwell fluid flow patterns within a reservoir through integrated geological/engineering analysis of reservoir data, so that a plan can be developed for selecting the most favorable location and optimum completion and injection methods for maximum resource utilization.

The development of reliable geological and engineering models requires data collection, organization, evaluation, reconciliation, and integration of geological, petrophysical, diagenetic, rock-fluid, production, injection, and pressure data.<sup>49</sup>

Volumes, rates, pressures, cuts, fluid samples, fluid level monitoring, pressure transient testing, tracer testing, and production logging have been used for determination of productivity/injectivity indices, location of fronts, transmissivities, reservoir discontinuities, distance to fronts, and interwell pressure

communication.<sup>51</sup> Regular systematic and consistent production/injection monitoring and testing have provided a basis for decisions involving field development, more effective reservoir management, and improved recovery efficiency.<sup>52-54</sup> Because each of these techniques provides an average property around a well, in the drainage area of a well, or between wells, the data represent the combined effect of several reservoir parameters in a heterogeneous reservoir.<sup>55-56</sup> Complementary techniques must be utilized and integrated to identify the influence of various heterogeneities on fluid flow.

Integrative analysis of well tests has not received adequate attention<sup>50</sup> even though this type of approach is needed for improved characterization of a reservoir. Integrative analysis of well tests is necessary to identify and evaluate the effects of various heterogeneities on fluid flow in a reservoir at various stages of production. The integrative approach is most effective when it is based on a detailed geological model of a reservoir.

Bell Creek (MT) field was selected for characterization using production/injection monitoring and pressure transient testing (see fig. 39). Fairly complete production/injection and wellhead pressure data were recorded while the field was under primary and secondary recovery and chemical flooding. Good geological data of the central part of Unit 'A' were already available based on detailed core descriptions and analyses.<sup>10</sup> Several falloff and pulse tests for evaluation of reservoir anisotropy were conducted in the (TIP) area prior to the initiation of a chemical flood project. However, no integrative analysis was available in the literature to evaluate in situ flow behavior and identify the role of various heterogeneities on waterflood and enhanced oil recovery (EOR) performance.

Injection and production data over 10 years of linedrive waterflooding and 6 years of micellar-polymer injection for Unit 'A' of Bell Creek (MT) field were analyzed using front advancement monitoring and Hall plot analysis. The results were integrated with geological information to characterize a project area for geological heterogeneities and to determine their influence on waterflood and chemical EOR performance.

Preflush waterflood performance and late waterflood performance of chemical injection wells were compared with the performance of surrounding water injection wells to evaluate the overall performance of these wells as compared to that of similar injection wells in the TIP area. Component parts of this study include analysis of front advancements at low and high water cuts (20 to 70%), production, injection, wellhead pressure information, pressure transient data, and mathematical simulation. The production and injection data are analyzed in light of a thorough geological model of the reservoir which was developed<sup>10,55,57-58</sup> through a detailed analysis of cores and wireline logs. The geological and engineering information about Bell Creek field is discussed in references 10, 46, 52, 54, and 55 and provide a basis for analysis of production, injection, and pressure data.

The Muddy formation in Unit 'A' of Bell Creek field generally strikes in a NE-SW direction and dips northwest on an average of 100 ft/mile. Detailed structural analyses has revealed, several faults in the TIP and adjacent are (fig. 40). The faults are discontinuous and are generally parallel to the NW and NE trending lineaments recognized throughout Powder River Basin. Fig. 40 shows two cross sections of the Muddy sandstone along the dip (X - X') and the strike (Y - Y') in the TIP area (see fig. 39). The most common vertical displacements of these postdepositional faults are from 10 to 20 ft although displacements greater than 40 ft were also identified in section 27. Separation of the barrier island reservoir into small tectonic blocks has influenced the continuity of flow paths. Natural fractures have not been reported from core examination, but their presence has been inferred from exceptionally high productivity and injectivity of some wells, as well as pressure analyses of well test data. For these wells, the measured permeabilities on core samples do not in themselves justify such behavior.<sup>10</sup>

#### **Analyses of Waterflood Data During Linedrive Water Injection**

An attempt was made to relate water advancement information to geological heterogeneities in the TIP area. A water advancement map was constructed on the basis of the monthly production data from the whole Unit 'A'. Construction of a fault map was based on more detailed core data and wireline log data and regional geology data that were available after infill drilling in the TIP area.<sup>55</sup>

Advancement of the 20 and 70% water-cut production in Unit 'A' of Bell Creek field from the initiation of linedrive injection in the western part of the field through January 1981 was examined. The water movement in the 4-section area which contains the TIP area ranged from 0 to 14 ft/d. The fault map was superimposed with the 70% waterfront advancement information (fig. 41). This map clearly demonstrates that southwestern-northeastern faults have locally acted as sealing/semisealing discontinuities and have impeded fluid communications toward the southeast, whereas northwesterly oriented faults have enhanced the advancement of the water front. Fig. 41A also indicates that faults and associated flow conduits extend laterally beyond the faults as they appear in the background fault map. This may be taken as evidence for faults and flow conduits which extend beyond the zones of formation offset that cannot be demonstrated by log correlations.

Mathematical simulation of linedrive waterflooding in this region confirmed the presence of flow barrier and associated flow conduits.<sup>58</sup> The simulated waterflood advancement based on matrix permeability alone proved to be faster than the actual water advancement in the TIP area. This means that flow barriers associated with faults played an important role in impeding waterfront advancement in the TIP area. Fig. 41B shows results of mathematical simulation of the linedrive waterflood based on 10 years of history matching with the inclusion of one sealing fault in the northwest corner of the TIP area in the model. A closer correspondence between simulated and actual front advancement was observed in the

western part of the TIP. Moreover, the eastern part of the TIP shows faster simulated front advancement than the actual one (fig. 41B), meaning that semi-sealing faults have definitely slowed the waterfront movement.

The 1980 residual oil saturation for the TIP area was obtained from areal field simulation without (fig. 42A) and with (fig. 42B) the inclusion of one sealing fault in the northwest corner of the TIP area in the model. Comparison of the spatial distribution of the residual oil saturation for the two cases indicates that the presence of faults has influenced the residual oil saturation distribution in the TIP area. Accurate distribution of residual oil saturation requires the inclusion of all faults and high-permeability conduits in the simulation model.

Several pressure-pulse and falloff tests were conducted in the TIP area prior to the initiation of micellar-polymer flooding. The pulse tests provided information that indicated the degree of sealing across some of the faults where measurements were conducted<sup>55</sup> (fig. 42). The variation of water transmissivities in the TIP area is just under 700%. A large part of this variation is due to the presence of a diagenetically affected area. When areas with similar "matrix" permeabilities are compared, flow barriers seem to decrease the permeability to water only a few hundred percent.

#### **Analyses of Water and Chemical Injection Wells During EOR Process**

Injection, production, pressure, and fluid samples during the chemical injection process from all injection and production wells in the TIP area were examined. Performances of chemical injection wells as well as surrounding water injection wells in the TIP area were analyzed by the Hall plot method.<sup>50</sup> The objectives of this analyses were to identify the influence of any geological heterogeneities on fluid flow path and to compare the early performance of chemical injection wells with their later performance and to compare the performance of chemical injection wells with that of surrounding water injection wells.

Hall plots of water injection wells based on calculated bottomhole pressure from wellhead pressure data with the inclusion of friction and cumulative water injection were prepared (fig. 44) for the entire 6-year (1981-1987) project history. Linear trends, as noticed in all the wells, indicate no permeability reduction as a result of long-term water injection. However, diagenetic and structural heterogeneities in the drainage area of some wells caused sudden changes in the slope of some wells. Northwestern and southwestern wells showed greater magnitudes of slopes, and, therefore, lower permeabilities as compared to that of northeastern and southeastern wells. Wells W-1, W-3, and W-8 exhibited extremely low slopes indicating the presence of high-permeability conduits. Similar behavior was identified by monitoring the waterfront advancement during linedrive secondary recovery in this area. Wells W-1, W-5, W-6, W-8, W-11, W-13, W-14, W-18, and C-11 show change of slope due to changes in transmissivity in their drainage area resulting from the presence of semisealing faults. The estimated transmissivity across these semisealing faults is

close to one-half of the formation transmissivity. This value is obtained based on Buell's quantitative analysis of the Hall plot method, and it is in agreement with the rate of front advancement in fig. 41A and common vertical displacements of faults in the TIP area. Wells C-10, W-6, W-19, W-13, W-14, W-15 and W-16 showed extremely high slopes throughout their water injection histories. All of these wells are in a highly diagenetically affected area of the TIP having comparatively lower permeability.

### **Analysis of Chemical Injection Wells Using Hall Method**

All chemical injection wells underwent 4 months of preflush, 4 months of soluble-oil micellar injection, and 40 months of viscosity-graded, emulsion-type polyacrylamide polymer injection. Polymer solution was used as a mobility buffer behind a micellar slug and finally was followed by water injection for nearly 2 years.

Hall plots of chemical injection wells based on calculated bottomhole pressure and cumulative water, micellar, and polymer injection were prepared for the entire 6-year (1981-1987) project history of the TIP area (fig. 45). The early part of the plot (about 20 months) is expanded in fig. 46. An increase in slope of 300 to 400% at an average of 350% was noticed in all the wells when a micellar slug (45 cP wellhead viscosity) was injected. The estimated in situ viscosity of the micellar slug calculated based on Hall plot slopes is in the range of 55-75 cp. This value is close to the measured wellhead value of 45 cP. The calculated value takes into account a decrease in oil saturation and corresponding increase in water relative permeability resulting from miscible displacement of oil around the wellbores.

The slopes of the Hall plots decrease to values closer to those of original preflush slopes when polymer injection is initiated. Polymer injection started with 75-cP fluid at the wellhead condition and gradually reduced to a 3-cP level over a period of 4 years and was followed by injection of water (1 cP viscosity). Partial improvement in apparent permeability after the micellar injection is attributed to the lower in situ polymer viscosity as a result of temperature increase, salinity of formation water, and shear thinning and shear degradation. The estimated value for the in situ apparent viscosity of polymer solution based on Hall plot analysis is in the range of 12 to 25 cP; whereas, the calculated value based on the polymer and brine concentration in the Bell Creek field with the consideration of shear thinning is in the range of 3.3 to 21 cP. This behavior has been reported by Buell et al.<sup>59</sup> and Todd et al.<sup>60</sup> The final Hall plot slope (fig. 45) is an average of 316% greater than the original slope during the preflush period, indicating a gradual plugging effect of the formation by long-term, low-concentration polymer solution injection (table 14). Gradual reduction in apparent permeability of chemical injection wells during polymer flooding was unlike the linear behavior of any water injection wells in the TIP area (fig. 44).

Minor criss-crossing of performance lines occurred during the preflush, micellar, and early polymer injection, meaning that reservoir discontinuities around the chemical injection wells played minor roles

during their early chemical injection history. Reservoir permeability and clay content variation were also important in dictating the degree of permeability reduction during long-term injection.

### **Integration of Production, Injection and Pressure Data for Dynamic Characterization of TIP Area, Bell Creek Field**

Front advancement monitoring confirmed the presence of sealing/semisealing faults mapped by geological analysis. In addition, it showed the preferential flow direction and indicated the overall prominent role of sealing and semisealing faults in the TIP area.

Analyses of the performance of chemical injection wells by Hall's method show no other heterogeneities except the presence of clay and permeability variations around chemical injection wells. Applications of pattern flooding and micellar-polymer injection after the linedrive injection did not change the effective flow pattern appreciably, as evidenced in the plots of the chemical injection performance using Hall's method. Permeability variation as a result of barriers/semibarriers and flow conduits dictated the time of arrival of sulfonate in the producing wells from surrounding chemical injector wells. It seems that high-permeability conduits have influenced the Hall plot performance of some water injection wells (W-1, W-3, and W-8). Sudden increases in slopes of some water injection wells such as W-1, W-5, W-6, W-8, W-10, W-11, W-13, W-14, W-18, and C-11 are attributed to the surrounding semisealing faults. Interwell transmissivities have commonly dropped by half and agree with the vertical displacement equal to half of the formation thickness.

By combining the performance of water injection wells with the early performance of chemical injection wells, a map was prepared showing the distribution of Hall plot slopes in the TIP area (fig. 47). This map identifies the western corner of the TIP area as well as the regions around wells W-6 and W-7 that are diagenetically affected and have lower permeabilities and correspondingly higher slopes. The high-transmissivity region in the northeastern portion of the TIP area coincides with the low slope values of this map. An elongated portion in the central part of the TIP area around wells W-9, P-12, C-9, P-14, and C-11 exhibits low values of slopes in the region where transmissivities based on core measurements (fig. 48) do not support this behavior. Examination of total fluid production during the EOR operation shows correspondingly highest values of total fluid production in this area. This area has been characterized as a region that is strongly affected by high-permeability conduits orthogonal to the direction of sealing/semisealing faults (fig. 40A). Similar areas with low values of slopes appear in the southeastern edge of the TIP area. Again, this area is also associated with fault/high-permeability conduits and low values of Hall slopes. Water injection wells such as W-6, W-9, W-10, W-14, W-15, W-16, W-17, and W-18 had higher slopes in Hall's plot. All of these wells are located in highly diagenetic affected areas, as indicated by the low values in the transmissivity map (fig. 48). Variation in water transmissivity ( $k_{wh}$ ) calculated from the analysis of pressure pulse and falloff tests before the initiation of the TIP project (fig.

43) is due to the combined effects of structural discontinuity and variation of transmissivities in the area. The contribution of faults, however, hardly exceeded that of the role diagenesis has played in creating variation in permeabilities.

Water relative permeabilities based on transient well tests and Hall plot analyses were compared with those from laboratory-measured values on several W-5 core samples (table 15). Results of this comparison show that calculated water transmissivity values based on well test analyses are influenced by high-permeability conduits in the vicinity of some of the wells (C-4, C-6 and C-8). The presence of these high-permeability channels was described previously (fig. 41A).

Long-term, predicted performances of 'C' wells based on short-term preflush performances (Region I) and long-term actual performances of 'C' wells (Region II) when water injection was resumed after chemical injection were prepared. They were superimposed on long-term, water-injection performances of all water injection wells (fig. 49). The result showed that chemical injection wells were initially similar in performance to water injection (Region I) wells. In fact, they exhibited better performance than most of the water-injection wells. The late water injection performance of chemical injection wells (Region II) was similar to the performance of lower quality, diagenetically affected wells in TIP area. The application of the micellar-polymer process reduced permeability contrast and magnitude of permeability by factors of 3 to 5. These performances resulted from filtering/adsorption/retention of the injected polymer and permeability modification as a result of chemical injection.

### **Results and Conclusions**

1. Water front advancement monitoring at Bell Creek when integrated with fault maps based on geological analyses provides useful information about flow characteristics associated with faults. It was concluded from this work that sealing or partially sealing faults in a southwest-northeast direction and highly conductive channels perpendicular to this direction have influenced flow paths appreciably. Sealing/semisealing faults slowed waterfront advancement all through the TIP area during linedrive waterflooding.

2. The Hall plot is a good diagnostic method for performance evaluation of waterfloods and micellar-polymer floods. It gives strong indication of permeability and its variation, skin effects, and variation in drainage area for improved reservoir characterization.

3. Application of the Hall plot method showed that micellar-polymer injection drastically reduced both the magnitude of the permeability and the permeability contrast. The in situ apparent residual resistance factor for polymer injection could be calculated.

4. The presence of high-permeability conduits and sealing/semi-sealing faults in drainage areas of some wells in the TIP area has influenced their pressure transient behavior. The presence of tectonic discontinuities in the vicinities of some chemical injection wells has only a moderate effect. Whereas, in the vicinity of some water injection wells, a pronounced effect on Hall plot slopes was identified and attributed to the local variation in tectonic intensity.

5. In the TIP area of Bell Creek field, faults behaved as sealing or semisealing in the SW-NE direction and as a permeability conduit in the NW-SE direction.

6. The presence of faults contributed to variations in residual oil saturation distribution during 40-acre-spacing, linedrive waterflooding.

7. Improved reservoir evaluation for designing successful recovery projects is obtainable through systematic collection and integration of inexpensive conventional reservoir data if knowledge of geological heterogeneities is provided.

#### **Effect of Geological Heterogeneities on Distribution of Initial and Post Waterflood Oil Saturations**

Relationships between geological and reservoir parameters controlling the nonuniform distribution of oil saturations in clastic reservoirs were investigated from abundant log, core, and geological information available from Bell Creek field. Information on a number of rock and fluid properties obtained from interpretation of log and core data were integrated with petrographic and production data to study the nature of the distribution of oil saturation during primary and secondary recovery operations at Bell Creek.

#### **Integration of Data From Various Sources for Oil Saturation Studies**

Correlations of facies, sedimentary structure, lithology, and fluid properties with water saturations were initiated in wells 26-4 and P-2 located 660 ft apart in one of the most productive parts of Bell Creek field. Well 26-4 was drilled during the discovery phase of the field and provided information on distribution of initial oil saturation in the area. Although cores were not available from this well, information on facies boundaries and distribution of sedimentary structures in the different facies was available from applications of the cross-plot technique<sup>46,47</sup> and from correlations with neighboring wells P-1, P-2, and W-7 from which core data were available. In figure 50, the interpreted facies boundaries are shown along with log-derived total clay content and water saturation profiles and core-measured permeability and water saturation profiles. The high permeabilities of the main barrier sandstones (consisting of predominantly foreshore, upper, and middle shoreface facies) in this well with negligible clay content and very low water saturation (averaging 18%) explain the very high initial oil production (840 bbl/d) rates from the well. The log-derived water saturation profile obtained by application of Simandoux's method gives realistic values

compared to the core-measured values which seem to have been affected by dynamic mud filtrate invasion in cores and/or problems with core preservation. The pattern of distribution of water saturation derived from log analysis shows very little effect of the small amount of clays.

Figure 51 shows the oil saturation profiles in well P-2, (located 660 ft north of well 26-4) drilled after 13 years of primary and waterflood production. The permeability and total clay content profiles indicate that this well also has good reservoir properties, and productivity of this well should be only slightly inferior to that of well 26-4. Descriptions of facies, sedimentary structures, and lithology in this well are available from detailed examination of cores. The salient features of the core descriptions in this well are indicated in the left-hand margin in figure 51. Distribution of grain sizes in the sandstones obtained from thin section studies and core examination have also been plotted in figure 51 because grain size distribution and the distribution of the type and the amount of clays are two of the important reservoir parameters that affect entrapment of oil. Two other parameters, grain size sorting indices and standard deviation of grain size distribution at each depth, have also been plotted in figure 51 to determine their effect on distribution of water saturation.

### **Results of Correlations Studies**

In the following correlations between the various reservoir properties obtained from log and core data, it should be emphasized that the log data represent the average effect of 2 to 3 ft of rock, whereas the core data represent either point values or measurement over a much smaller distance.

The results of our correlation studies are summarized below:

1. Textural properties like grain size distribution and sorting strongly affect distribution of oil saturation in a clastic reservoir. As expected, grain size distribution was found to vary directly as permeability and inversely as water saturation. Porosity varies directly with grain size sorting.

2. The distribution of initial oil saturation in the very clean, high productive facies in well 26-4 was uniformly high (around 82%), indicating that the small amount of clay in the top part of the sand has not significantly affected distribution of initial oil saturation in this highly porous and permeable sandstone (This may not be true if detail values of cementation factor and saturation exponents were known.)

3. The effect of texture and clay content in the distribution of oil saturation are more pronounced in well P-2 drilled after 13 years of primary and waterflood production compared to that in well 26-4. This is believed to be due to non-uniform vertical sweeping efficiency of the waterflood process particularly in the presence of variable amounts of clays in sandstone reservoirs.

4. Distribution of oil saturation in the various facies of a barrier island sandstone varies because of variations in texture, lithology, sedimentary structure etc. Best petrophysical properties were observed in massive sandstones with large grain sizes and low angle dipping laminae and the poorest in clay rich bioturbated or burrowed sandstones.

### Application of Differential Oil-In-Place to Quantify the Effect of Geological Heterogeneities In Oil Production

#### **Determination of Oil-in-Place Distribution by Material Balance Equation**

The most commonly used methods to compute oil reserves using production data are decline curve analysis and material balance equation (MBE). The use of MBE for reserves or oil-in-place computations has been restricted to an entire reservoir rather than individual wells. Theoretically, a MBE is valid for a closed reservoir system, and its application to a single well may be misleading. However, when wells in a multiwell reservoir system are producing at the same time, it can be assumed that each well drains its 'own' volume for hydrocarbon production. Consequently, results of applying a MBE to a well can indicate its effective drainage volume and thus effective oil-in-place. Further, if the MBE calculated oil-in-place of a well is compared with that of volumetrics, the degree of discrepancy between these two values may serve as a quantitative reservoir heterogeneity index. A general material balance equation<sup>61</sup> (MBE) for calculating oil-in-place (OIP) of a reservoir or well at given reservoir pressure and temperature conditions is as follows:

$$N = \frac{N_p(B_o - R_s B_g) + (W_e - B_w W_p)}{B_o - B_{oi} + (R_{si} - R_s) B_g + m B_o (B_g - B_{gi}) / B_{gi}} \quad (1)$$

where

- N = original oil-in-place, STB
- N<sub>p</sub> = cumulative oil production, STB
- B<sub>o</sub> = oil formation volume factor, bbl/STB
- B<sub>oi</sub> = oil formation volume factor at the initial pressure, bbl/STB
- B<sub>g</sub> = gas formation volume factor, res bbl/STB
- B<sub>gi</sub> = gas formation volume factor at the initial pressure, bbl/STB
- R<sub>p</sub> = cumulative gas oil ratio, STB/STB, Also R<sub>p</sub> = G<sub>p</sub>/N<sub>p</sub>
- G<sub>p</sub> = cumulative gas production, STB, N<sub>p</sub>R<sub>p</sub>
- R<sub>s</sub> = solution gas oil ratio, STB/STB
- R<sub>si</sub> = solution gas oil ratio at the initial pressure, STB/STB
- W<sub>e</sub> = cumulative water influx, bbl
- B<sub>w</sub> = water formation volume factor, bbl/STB

- $W_p$  = cumulative water production, bbl  
 $m$  = ratio of initial reservoir free gas volume (gas cap) to initial reservoir oil volume, fraction

Using this equation, a computer program was prepared, debugged, and verified using the Bell Creek well production and PVT data.<sup>62</sup> As there was no known water drive, and the gas cap at initial reservoir conditions was very small,<sup>62</sup> both  $W_e$  and  $m$  terms shown in the above equation were assumed to be zero in using the MBE program. The program provides output results of well initial oil-in-place, recovery factor, and remaining oil-in-place at any given well pressure. The program was used to analyze all wells with primary production in the TIP area. Calculated initial oil-in-place values of each well based on 40-acre spacing were mapped using the Macgridzo™ mapping program (fig. 52). Fig. 52 shows that the central portion of the TIP contains the highest oil-in-place relative to adjacent areas. More than half of the wells contained more than 1 million bbl of oil each. This area of prolific oil reserves covers the southeastern part of section 22, southwestern part of section 23, northwestern part of section 26, and northeastern part of section 27. Previous studies of the TIP area have shown that this area has high storage capacity, high fluid flow capacity, and a low Dykstra-Parsons coefficient. All these three indices indicate this to be an area of high quality sandstones with highly recoverable oil reserves. Thus, the oil-in-place distribution of the TIP area using the data of MBE agreed well with the previous findings. Additionally, by subtracting known cumulative production data from these effective oil-in-place values, a map of remaining oil reserves of each well for the study area can be prepared.

#### Determination of Oil-In-Place Distribution by Volumetric Equation

A volumetric equation<sup>61</sup> for calculating oil-in-place (OIP) of a well with a specified spacing at given pressure and temperature conditions is:

$$N = \frac{7758 Ah \phi (1 - S_w)}{B_{oi}} \quad (2)$$

where

- $N$  = oil-in-place, STB  
 $A$  = well spacing, acres  
 $h$  = formation pay thickness, ft  
 $\phi$  = formation porosity, fraction  
 $S_w$  = water saturation, fraction  
 $B_{oi}$  = initial formation volume factor, bbl/STB

### **Differential Oil-in-Place Method**

The method examines the differential oil-in-place (OIP) of each well in a given reservoir. A map of the distribution of differential OIP will identify geological heterogeneities and their effects on oil production.

A well differential OIP, DOIP is defined by the equation:  $DOIP = \text{volumetric OIP at a given spacing} - \text{material balance equation OIP}$ .

A general material balance equation (MBE) and volumetric equation for calculating oil-in-place have been previously defined. The differential OIP is an indicator of the variation of individual well OIP, which could be due to a variety of reasons. Volumetric OIP can be considered as a static evaluation based on petrophysical (core and log) data. MBE OIP, on the other hand, represents the effective or recoverable OIP of a well from production data, and in this sense the MBE computation is dynamic.

A highly positive DOIP will indicate more oil reserves in the area than that calculated by production data, and the drainage efficiency in the area is probably low. A highly negative differential OIP will indicate that a well is draining more oil than is expected from the volumetrics, and the drainage efficiency in the area is probably high or the volumetric value of the OIP does not accurately account for all the parameters used in the calculation.

Geologically, positive differential OIP could be due to a variety of reasons such as high clay content, faults, or different types of flow barriers, whereas negative differential OIP may imply production affected by highly permeable clean sands, faults, fractures, etc. The essence of the differential OIP method is the use of MBE to compute OIP for an individual well and compare that with the volumetric OIP.

### **Testing of Differential Oil-in-Place Method**

The computer MBE program previously developed was used to analyze all available production data from wells in sections 22, 23, 26, 27, 28, 33, 34, and 35. To calculate volumetric OIP, available SP, induction, sonic, density, and gamma ray logs from 54 wells were interpreted to calculate porosity, clay content, pay thickness, and initial water resistivity and water saturation. These reservoir parameters, calculated at every foot interval, have been used to calculate the volumetric OIP for 40-acre areas surrounding each well by the application of Simandoux's method. The clay content for every foot of the pay thickness required for  $S_w$  calculations was obtained from interpretations of SP logs which were cross checked with core, density, and sonic log data. Where available, laboratory-measured porosity values, after compaction correction, were used for cross-checking log-derived values. Table 16 shows the analyzed well data of average initial water and oil saturation, average porosity and net pay thickness as well as the measured initial well flow rate. Table 17 shows the results of volumetric OIP (OIPVOL), MBE OIP

(OIPMBE), and differential OIP (DOIP). Several potentially useful indices also have been computed and are shown in the table. They are relative differential OIP (RDOIP = DOIP/OIPVOL), ratio of MBE OIP to volumetric OIP (OIPMBE/OIPVOL), and effective well drainage area (AREAMBE). Effective drainage area is calculated by using the volumetric equation and the computed MBE OIP. Shown at the bottom of the table are the mean ( $\bar{x}$ ), standard deviation  $\sigma$ ,  $\bar{x} - \sigma$ , and  $\bar{x} + \sigma$  of each related variable. The average volumetric OIP is 776,000 STB versus 729,000 STB for MBE OIP; the average differential OIP is 47,000 STB. Note that the mean effective well drainage area is 40.28 acres, which matches very well with the expected 40-acre well spacing. This close agreement indicates that the study sections as a whole unit are draining nearly 40 acres for each well.

The average effective drainage area for each section is as follows:

Section	22	23	26	27	28	33	34	35
No. of well data	12	9	16	11	2	1	2	1
Drainage area, acres	30.95	43.37	44.84	41.79	26.94	58.21	42.89	37.20

Among the four sections 22, 23, 26 and 27 that have enough analyzed well data to indicate a meaningful average effective drainage area, section 22 is the poorest drainage area (30.95 acres) while section 26 is the highest (44.84 acres). Both sections 23 and 27 are draining slightly more than the expected 40-acre spacing. These drainage areas results agree with the characteristics of the anomalous features and clay content, described in the next section.

Based on these results, a more dense well spacing than 40 acres may be needed to produce section 22, while a 40-acre spacing seems appropriate for sections 23, 26 and 27.

#### **Analysis of Differential Oil-in-Place (DOIP) Index in Unit 'A' of Bell Creek Field**

A plot of results of differential OIP calculations for 54 wells in the study area is shown in fig. 53. Areas of significantly negative and positive differential OIP anomalies are indicated. Significantly negative and positive differential OIP are those areas outside the lower bound "mean DOIP - standard deviation" and upper bound "mean DOIP + standard deviation" respectively. From table 17, the lower and upper bounds for DOIP are 193,000 and 288,000 STB, respectively.

The differential oil-in-place map was overlaid on 30 selected maps<sup>56,60</sup> showing variations in the study area in pertinent geological, and petrophysical properties or engineering data such as structural anomaly, clay content, porosity, permeability, Dykstra-Parsons coefficient, log-derived heterogeneity index (LHI), primary, secondary, and tertiary oil production. The purpose of this overlay was to determine if there is any relationship between the distribution of differential oil-in-place values and the superimposed variables.

Table 18 shows a qualitative analysis of the degree of correlation of distribution of each superimposed variable<sup>63</sup> with that of differential oil-in-place. The analysis of the overlays indicates correlations of various degrees between structural anomalies, clay content, log-derived heterogeneity index (LHI) and the distribution of differential oil-in-place values.

As an example, to determine if the linear structural features on the structural contour map constructed on the top of the Muddy barrier island sandstones in the study area<sup>57</sup> have in any way contributed to anomalies observed in the distribution of differential oil-in-place, the linear features from the structure contour map were transferred onto the differential oil-in-place map (fig. 53). From detailed construction of stratigraphic cross sections,<sup>46</sup> it is believed that linear feature no. 1 (LF1) indicated in fig. 53 is a deep valley incision which has contributed to NW-SE trending positive differential oil-in-place anomalies. Conductivity due to faults in this area is apparently augmented by the low clay content in sandstones from this area<sup>57</sup>. In a faulted area such as this, it may be expected that there will be many more smaller faults or fractures which are difficult to identify, but which nevertheless will contribute to variation in drainage volume.<sup>64</sup>

The highly positive differential oil-in-place in certain parts of the study area (for example, the western part of sections 27 and 22) coincide with areas having a high degree of clay content or areas having a greater thickness of low-permeability, valley-fill sediments. The poor drainage efficiency of the clay-filled western part of the study area is not improved by the presence of faults.

The overlay of the differential oil-in-place map (DOIP) on the log-derived heterogeneity index (LHI) map shows a weak correlation between DOIP and LHI. Fig. 54 shows a plot of LHI vs DOIP with a coefficient of correlation  $R = 0.559$  for a linear correlation analysis.

### **Conclusions**

Based on current findings, the newly developed differential OIP method can be used to (1) quantify the effect of geological heterogeneities on oil production; (2) characterize drainage efficiency of each well and its effective drainage volume; (3) determine optimal well spacing in each section of a given reservoir, (4) determine best injection and production well locations for waterflood, infill and EOR programs; and (5) determine best horizontal wells drillsites by orienting these wells in the highly negative differential oil-in-place areas. Two distinct advantages of this differential OIP method are indicated as follows: (1) it requires only readily available production and basic petrophysical data; that is, the method is inexpensive and efficient, and (2) it can be applied at or before the end of primary production; that is, valuable reservoir information can be obtained early during the producing life of a reservoir and used prior to planning and implementation of waterflood, infill, and EOR program.

However, determination of the best or worst producing areas for oil exploitation should be based on differential oil-in-place index and the absolute amount of oil reserves in the areas under consideration. Thus, areas with a highly positive differential oil-in-place index with significant oil reserves can be prospective ones at the end of primary production.

### Application of Fractals for Quantitative Reservoir Characterization

The R/S analysis method and its algorithm as shown by Feder's book<sup>65</sup> has been developed by NIPER, modified to one similar to that published by Hewitt,<sup>66</sup> and coded into Fortran as an application program for processing many types of data.

In general, reservoir features have a characteristic smallest length scale or lag, such as diameter of a grain of sand or the length of a gel/polymer molecule. This will be referred to as the lag.

We began the method by first normalizing the variables furnished by the well logs, displaying the input variables as a probability distribution, next finding the maximum and minimum range  $R(x, 1)$  for each value around  $x$  and also at any lag  $1 > 1$  and selected from  $0 < U < L$ , with a lag window between  $x$  and  $x + L$ .

Features include: ease of input/output file selection; default file extensions for both input and output files; a percent completion gauge for monitoring the iteration process; large array sizes for the input data; and graphic plots of input data, normalized input data, probability distribution, and the log-log curve in order to better visualize how the data are handled.

### The Method

Hurst<sup>67</sup> used fractal approach to study the water storage problem related to influx from the Nile river. Hurst called his newly invented statistical method "rescaled range analysis" or R/S analysis. The method appeared to be well suited to the analysis of yearly water influx data recorded over a long period of time. For any given period of years, up to 60 in this case, the annual average influx of water gave Hurst a good estimate of the overall yearly release of water from storage. The maximum and minimum values of the accumulated departures of each year's influx from the average yearly influx would show the range of the high and low water marks for the impounded water. The ratio of this range  $R$  to its standard deviation  $S$  is said to be a function of the period of time,  $\tau$  (tau). This function can be written as:

$$R/S = a \tau^H \quad (3)$$

The data to be subjected to Hurst's empirical law by following an R/S analysis is shown as the array  $\xi(t)$ . The average value of  $\xi$  over a dimensional period of  $1 < t < \tau$  is

$$\langle \xi \rangle_\tau = 1/\tau \int_0^\tau \xi(t) dt \quad (4)$$

The accumulated departure of  $\xi(t)$  from the average value  $\langle \xi \rangle$  is the next important algorithm needed to find range of deviation of  $\xi(t)$  as accumulated over the considerable period  $\tau$ . This is

$$X(t) \tau = \sum_{u=1}^{\tau} \{ \xi(u) - \langle \xi \rangle \tau \} \quad (5)$$

and is calculated for each value of  $t$  for  $u$  varying from 1 to  $\tau$ ,  $t$  from 1 to  $\tau$ .

The next algorithm finds the range  $R(\tau)$  or the difference between the maximum and the minimum values found in the ranges of  $X(t)\tau$ . In other words, a new array of  $X(t)$  is found for every value of  $\tau$ , selected in the  $\tau$ , loop. The resulting range  $R(\tau)$  is calculated as

$$R(\tau) = \max. X(t) - \min. X(t) \text{ for } t \text{ varying as } 1 \leq t \leq \tau \quad (6)$$

One more expression must be evaluated for each value of  $\tau$ , and this is the standard deviation of all  $\xi(t)$  in the dimensional span of  $\tau$ . The equation is

$$S = (1/\tau \sum (x(t) - \langle \xi \rangle \tau)^2)^{1/2} \quad (7)$$

Thus finding the range  $A$  and standard deviation  $S$  for each value of  $\tau$ , the ratio  $R/S$  is stored into an array along with another array for  $\tau$ . To determine the Hurst exponent  $H$ , the following relationship is observed.

$$R/S = (\tau/2)^H \quad (8)$$

### Results and Discussion

This first test of the program was made on a fractal function, known as the Weierstrass-Mandelbrot function.

$$C(t) = \sum_{n=0}^{\infty} (1 - \cos b^n t) / b^{(2-D)n} \quad (9)$$

$R/S$  analysis shows a straight line for the plot of  $\log(R/S)$  vs.  $\log t$  with a Hurst exponent ( $H$ ) of 0.9747. This is not a random function where  $H = 0.5$ , but it is a self-similar fractal function which must result in a straight line and have a fractal dimension.

When a rescaled range analysis was applied to the Weierstrass-Mandelbrot function using only lags which began at the origin, the  $\log R/S$  vs.  $\log t$  curve resulted in a straight line with  $H = 1.0$ . This is because the function is deterministically self-similar when beginning from the origin of the curve.

Bulk density well logs from wells P-2 and W-7 in Bell Creek field were subjected to a rescaled range analysis (or R/S analysis). Each represented about 300 observed points. The linear portion of each curve showed Hurst exponents which were in good agreement with other geological features reported by Hurst.<sup>65</sup> A regression plot of the R/S vs. lag curve of the bulk density log taken from well P-4 (fig. 55) revealed a Hurst value of 0.898. The curve in the figure remains very straight up to a lag value of 120 ( $\log 120 = 2.08$ ), and then begins to deviate from the straight line. This is explained by a high porosity zone (low bulk density) beginning at a lag of 120 or at 4,410 ft (fig. 56). An independent distribution can be shown in a histogram of the normalized data.

A Hurst exponent of 0.869 for density of W-7 (fig. 57) well porosity was calculated. In this case, the straight portion begins to deviate at a lag value of 100 ( $\log 100 = 2.09$ ) or the high porosity zone at 4,400 ft (fig. 58).

Based on a grain density of 2.65, the average porosity for the entire logged section of each well is 9.8 and 9.0%; however, the region between 4,407 and 4,422 ft in well W-7 is 15.8% and P-2 is 17.7%. The overall listed average reservoir porosity for Bell Creek is 26.0%.

Using neutron porosity well logs from three wells, in a West Texas carbonate, Hewett<sup>64</sup> published an overall R/S analysis of  $H = 0.87 \pm 0.07$ . His well spacing was 900 ft and thickness interval was 145 ft.

The next step is to build a mathematically generated field of porosity, based on fractally distributed characteristics self-similar to the original field. The method employs either a "stochastic interpolation" or a smooth interpolation technique otherwise known as "kriging." The stochastic interpolation preserves the original dispersion characteristics and heterogeneity of the reservoir.<sup>66</sup>

## CHAPTER V. - SUMMARY

NIPER's Reservoir Characterization Program (BE1) integrates geological and engineering information from reservoirs comprising a spectrum of examples representing end members from the shoreline barrier deposystem for improved prediction of fluid movement and trapping. Patrick Draw field is the second shoreline barrier reservoir to be investigated for generalization of the geological/engineering model. The first reservoir selected was Bell Creek field which exemplifies a microtidal shoreline barrier model, whereas Patrick Draw field represents a mesotidal type of shoreline barrier model. So far as we know, this project is the only one which systematically addresses the integration of geological and engineering parameters for all genetic varieties of a deposystem.

A summary of the work done during FY90 include:

1. A spectrum of the component parts of shoreline barriers was outlined. The end members of the deposystem were identified and their reported geological characteristics were listed. The depositional setting at Bell Creek (MT) field was classified according to this information. The classification provided a guideline for selection of a second shoreline barrier reservoir end member, Patrick Draw (WY) field.
2. Selection of Patrick Draw field was based on criteria including: type of deposystem and end member, prolific producer, data availability, outcrops, production history, and location. A list of 18 candidates were considered, of which the top five were subjected to a more detailed evaluation. Patrick Draw field was chosen from these candidates as the most suitable reservoir for generalization of the shoreline barrier reservoir characterization methodology.
3. Preliminary geological and engineering evaluation of the field was conducted. Significant effort was dedicated to locating, collecting, and organizing the data. Through examination of outcrop and reservoir cores, it was found that tidal inlet and channel deposits dominate the depositional facies at Patrick Draw field in contrast to the dominant shoreface and foreshore facies at Bell Creek field. In addition to the depositional aspects of the reservoir, preliminary investigations of tectonic, diagenetic, and geochemical features were made in order to identify critical geological heterogeneities present in Patrick Draw field.
4. Production/injection/pressure data, log signatures, core and fluid analysis data, petrographic information were integrated to identify heterogeneities and to quantify their effect on production injection performance.
5. An algorithm and a program for processing many types of data using the fractal method was developed and applied to the problem of recognition, quantification, and characterization of log signatures.

#### **ACKNOWLEDGMENTS**

The research team for Project BE1 gratefully acknowledges the counsel and guidance of Tom Burchfield of NIPER in performing this work. The team also acknowledges Mike Madden, Min Tham, and Bill Linville for their continued guidance throughout the continuation of this project. The support of Edith Allison, Project Manager, Bartlesville Project Office, U. S. Department of Energy is greatly appreciated. We appreciate the support of the U. S. Department of Energy for supporting this research through Cooperative Agreement DE-FC22-83FE60149. Special thanks are due to Frank Lim, Senior Staff

Engineer, Union Pacific Resources Co. Fort Worth, TX and Bob Skopec, ORYX Energy, Dallas, TX for providing field data and helpful comments. This manuscript was typed by Edna Hatcher.

## REFERENCES

1. Reinson, G. E. Barrier-Island and Associated Strand-Plain Systems, in Walker, R. G., *Facies Models*, Second Edition, Geoscience Canada. Reprint Series 1, 1984, p. 119-140. First edition published in 1979.
2. Evans, M. W., and A. C. Hine. Distribution and Infilling Sequences of Tidal Inlet Channels in the Open-Water Lagoons of Southwest Florida (Abs.) in, Davis, R. A. Jr., D. Nummedal, and R. W. Tillman, conveners, *Tidal Inlet and Related Sand Bodies: Modern and Ancient-Abstracts of Technical Program*. SEPM Research Conference, San Juan Basin, New Mexico, May 5-10, 1990.
3. Hayes, M. O. Barrier Island Morphology as a Function of Tidal and Wave Regime, in Leatherman, S. P., ed., *Barrier Islands from the Gulf of St. Lawrence to the Gulf of Mexico*. Academic Press, 1979, p. 1-27.
4. Donselaar, M. E. Flood Tidal Delta Sedimentation in the Late Cretaceous Menefee Formation (Mesaverde Group), San Juan Basin, Northwest New Mexico. *Geologie en Mijnbouw*, v. 63, 1984 p. 323-331.
5. Cuevas, M. M., E. Donselaar, and S. D. Nio. Eocene Clastic Tidal Deposits in the Tremp-Graus Basin (Prov. of Lerida and Huesce), in Mila, M. D., and J. Rosel, eds., 6th I.A.S. European Regional Meeting. *Excursion Guidebook*. Institut D'Estudis Illerdens (Lleida), 1985 p. 215-266.
6. Honarpour, M. Integrated Reservoir Assessment and Characterization Covering the Period October 1, 1985 - September 30, 1988. Final Report. Department of Energy Report No. NIPER-390, 1989.
7. Donselaar, M. E. Facies and Geometry of Fossil Flood-Tidal Deltas (Abs.), in, Davis, R. A. Jr., D. Nummedal, and R. W. Tillman, conveners, *Tidal Inlet and Related Sand Bodies: Modern and Ancient-Abstracts of Technical Program*. SEPM Research Conference, San Juan Basin, New Mexico, May 5-10, 1990.
8. Tillman, R. W. Personal Communication and Consulting Materials Provided to NIPER. July, 1990.
9. Szpakiewicz, M., R. Tillman, S. Jackson, and G. deVerges. Sedimentologic Interpretation of Barrier Island and Related Deposits in the Bell Creek Cores, Montana and Analogous Outcrops Near New Haven, Wyoming. NIPER Open File of Field Investigations, 1988. Available from the Authors.
10. Szpakiewicz, M., R. Schatzinger, M. Honarpour, M. Tham, and R. Tillman. Geological and Engineering Evaluation of Barrier Island and Valley-Fill Lithotypes in Muddy Formation, Bell Creek Field, Montana, in Coalson, E. B., ed., *Petrogenesis and Petrophysics of Selected Sandstone Reservoirs of the Rocky Mountain Region*. The Rocky Mountain Association of Geologists, Denver, Colorado, 1989, p. 159-182.
11. Schatzinger, R. A., M. Szpakiewicz, and B. Sharma. Applicable Correlations and Overall Characteristics of Barrier Island Deposystems. Department of Energy Report No. NIPER-427, August, 1989.
12. Campbell, C. V. Model for Beach Shoreline in Gallup Sandstone (Upper Cretaceous) of Northwestern New Mexico. New Mexico Bureau of mines and Mineral Resources, Circular 164, 1979.
13. Flores, R. M. Barrier and Back-Barrier Environments of Deposition of the Upper cretaceous Almond Formation, Rock Springs Uplift, Wyoming. *The Mountain Geologist*, v. 25, 1978, p. 57-65.

14. Wheeler, D. M., E. R. Gustason, and M. J. Furst. The Distribution of Reservoir Sandstone in the Lower Cretaceous Muddy Sandstone, Hilight Field, Powder River Basin, Wyoming. In: *Giant Oil and Gas Fields, A Core Workshop*. SEPM Core Workshop No. 12, 1988, p. 179.
15. Galloway, W. A. Reservoir Facies Architecture of Microtidal Barrier System. *AAPG Bull.*, v. 70, 1986, p. 787-808.
16. Dixon, J. Mobil Oil Co., Dallas, TX. January 1990 Personal communication.
17. Tillman, R. W. The Tocito and Gallup Sandstones, New Mexico, A Comparison, in R. W. Tillman, and R. G. Walker, eds., *Shelf Sands and Sandstone Reservoirs*. SEPM Short Course No. 13, 1985, p. 402-464.
18. Roehler, H. W. The Pintail Coal Bed and Barrier Bar G - A Model for Coal of Barrier Bar-Lagoon Origin, Upper Cretaceous Almond Formation, Rock Springs Coal Field, Wyoming. *USGS Prof. Paper* 1398, 1988.
19. Meyers, W. C. Environmental Analysis of Almond Formation (Upper Cretaceous) From the Rock Springs Uplift, Wyoming. Ph. D. Dissertation, University of Tulsa, 1977.
20. Asquith, D. O. Petroleum Potential of Deeper Lewis and Mesaverde Sandstones in the Red Desert, Washakie and Sand Wash Basins, Wyoming and Colorado. *Rocky Mountain Association of Geologists Symposium*, 1975, p.159-162.
21. Van Horn, M. D. Stratigraphy of the Almond Formation, East-Central Flank of the Rock Springs Uplift, Sweetwater County, Wyoming: A Mesotidal Shoreline Model for the Late Cretaceous. M.S. Thesis, Colorado School of Mines, 1979, 150 p.
22. Hale, L. A. Stratigraphy of the Upper Cretaceous Montana Group in the Rock Springs Uplift, Sweetwater County, Wyoming. *Wyo. Geol. Assoc. Guidebook*, 5th Ann. Field Conf., 1950, p. 49-58.
23. Weimer, R. J. Upper Cretaceous Stratigraphy, Rocky Mountain Area. *AAPG Bull.*, v. 44, 1960, p. 1-20.
24. Jacka, A. D. Sediment Economics of Upper Cretaceous Sandstones Rocky Mountain Region. *Wyo. Geol. Assoc.*, 22nd Ann. Field Conf. Guidebook, 1970a, p. 187-219.
25. Weimer, R. J. Time-Stratigraphic Analysis and Petroleum Accumulations, Patrick Draw Field, Sweetwater County, Wyoming. *AAPG Bull.*, v. 50, 1966, p. 2,150-2,175.
26. Asquith, D. O. Depositional Topography and Major Environments, Late Cretaceous, Wyoming. *AAPG Bull.*, v. 54, 1970, p. 1,184-1,224..
27. Hayes, M. O., and T. W. Kana. Terrigenous Clastic Depositional Environments. Coastal Research Division, Department of Geology, University of South Carolina, Technical Report 11-CRD, 1976, pt. 1, 131 p., pt. 2, 185 p.
28. Keighin, C. W., B. E. Law, and R. M. Pollastro. Petrology and Reservoir Characteristics of the Almond Formation, Greater Green River Basin, Wyoming. In Coalson, E. B., and others, eds., *Petrogenesis and Petrophysics of Selected Sandstone Reservoirs of the Rocky Mountain Region*. The Rocky Mountain Association of Geologists, 1989, p. 281-298.
29. Irwin, D. Arch and Monell Units, Patrick Draw-Table Rock Area, Sweetwater County, Wyoming-Upper Almond Sandstone Study, in, Unpublished Union Pacific Resources Co. Data Files, 1976.
30. Keyes, S. Union Pacific Resources Co. 1989, Personal communication.

31. Weimer, R. J., and R. W. Tillman. Sandstone Reservoirs. Pres. at the International Petroleum Exhibition and Technical Symposium of the SPE, Beijing, China, 1982, p. 1-5. SPE paper 10009.
32. Union Pacific Resources Co. Data Files Provided to NIPER. June, 1990.
33. Weimer, R. J. Rates of Deltaic Sedimentation and Intrabasin Deformation, Upper Cretaceous of Rocky Mountain Region. in Morgan, J. P., ed., Deltaic Sedimentation Modern and Ancient. Soc. Econ. Paleon. and Mineral., Spec. Pub. 15, 1970, p. 270-292.
34. Richers, D. M. Patrick Draw Oil Field. Preprint, To Be Published in: AAPG Treatise on Petroleum Geology, 1990.
35. Richers, D. M., J. R. Reed, K. C Horstman, G. D. Michels, R. N. Baker, L. Lundell, and W. Marrs. Landsat and Geochemical Study of Patrick Draw Oil Field, Sweetwater County, Wyoming. AAPG. Bull., v. 66, 1982, p. 903-922.
36. Law, B. E., M. R. Lickus, and M. J. Pawlewicz. Fluid Migration Pathways-Evidence from Thermal Maturity Mapping in Southwestern Wyoming. USGS Circular 0974, 1986, p. 35.
37. Szpakiewicz, M., and A. G. Collins. Hydrochemical Study of the Upper Cretaceous and Lower Tertiary Formations in the Uinta, Piceance and Greater Green River Basins; Implications for Oil and Gas Related Problems. Department of Energy Report No. NIPER-95, 1985, 70 p.
38. Jacka, A. D. Principles of Cementation and Porosity-Occlusion in Upper Cretaceous Sandstones, Rocky Mountain Region. Wyoming Geol. Assoc. 22nd Ann. Field Conf. Guidebook, 1970b, p. 265-285.
39. Kocurko, M. J. Action of Organic Matter and Crystallization of High Magnesium Calcite, South Louisiana, in Gautier, D. L., ed., Roles of Organic Matter in Sediment Diagenesis. Soc. Economic Paleo. and Mineralogists, Special Pub. 38, 1986, p. 13-21.
40. Pryor, W. A. Petrography of Mesaverde Sandstones in Wyoming. Wyoming Geol. Assoc. 16th Ann. Field Conf. Guidebook, 1961, p. 34-46.
41. Thomas, J. B. Diagenetic Sequences in Low-Permeability Argillaceous Sandstones. J. Geol. Soc. London. v. 135, 1978, p. 93-99.
42. Folk, R. L. Petrology of Sedimentary Rocks. Hemphills, Austin, Texas, 1968, p. 124.
43. McCubbin, D. G., and M. J. Brady. Depositional Environment of the Almond Reservoirs, Patrick Draw Field, Wyoming. The Mountain Geologist, v. 6, 1969, p. 3-26.
44. Priisholm, A., B. L. Nielson, and O. Haslund. Fines Migration, Blocking, and Clay Swelling of Potential Geothermal Sandstone Reservoirs, Denmark. SPE Formation Evaluation, v. 2, 1987, p. 168-178.
45. Pollastro, R. M. Mineralogical and Morphological Evidence for the Formation of Illite at the Expense of Illite/Smectite. Clays and Clay Minerals, v. 33, 1985, p. 265-274.
46. Sharma, B., M. M. Honarpour, S. R. Jackson, R. Schatzinger, and L. Tomutsa. Determining the Productivity of a Barrier Island Sandstone Deposit From Integrated Facies Analysis Based on Log and Core Data and Fluid Production. Pres. at SPE Tech. Conf. San Antonio, Oct. 1989, SPE paper 19584.
47. Sharma, B. and Susan Jackson. A Crossplot Technique for Determination of Various Sandstone Facies in Barrier Island Sandstone Deposits. Pres. at Poster Session NIPER/DOE Second International Reservoir Characterization Technical Conference, Dallas, June 1989.

48. Baptist, O.C., E.J. White, and C. S. Land. Laboratory Predictions of Water Sensitivity Compared with Field Observations of Well Damage-Patrick Draw, Wyoming. SPE Paper 839, 1964, 6 p.
49. Honarpour, M. M., T. E. Burchfield, Bill Linville: Reservoir Characterization Can Help Recovery Efficiency. American Oil & Gas Reporter, v. 32, no. 9. Sept. 1989, pp. 9-16.
50. Honarpour, M. M. and L. Tomutsa. Injection/Production Monitoring: An Effective Method for Reservoir Characterization. Pres. at 7th SPE/DOE Symp. on EOR, Tulsa, April 1990, SPE/DOE paper 20262.
51. Talash, A. W. An Overview of Waterflood Surveillance and Monitoring. SPE Distinguished Author Series, J. Pet. Tech., Dec. 1988, pp. 1539-1543.
52. Ramey, Jr., H. J. Pressure Transient Testing. SPE Distinguished Author Series, J. Pet. Tech. July 1982, pp. 1407.
53. Talash, A. W. and L. K. Strange. Summary of Performance and Evaluations in the West Burburnett Chemical Waterflood Project, J. Pet. Tech. Nov. 1982, pp. 2495-2502.
54. Moffitt, P. D. and D. E. Menzie. Well Injection Tests of Non-Newtonian Fluid. SPE paper 7177, 1978.
55. Honarpour, M. M., M. J. Szpakiewicz, R. A. Schatzinger, L. Tomutsa, H. B. Carroll, Jr. Integrated Geological/Engineering Model for Barrier Island Deposits in Bell Creek Field, Montana. Pres. at SPE/DOE Enhanced Oil Recovery Symposium, April 17-20, 1988, Tulsa, OK. SPE/DOE paper 17366.
56. Mishra, S. and H. J. Ramey. A Comparison of Pressure Transient and Tracer Concentration Time Data for Layered Reservoirs Under Injection. Pres. at SPE Ann. Tech. Conf. and Exhib., Las Vegas, Sept. 1985, SPE paper 14170.
57. Sharma, B., M. M. Honarpour, M. J. Szpakiewicz, and R. B. Schatzinger. Critical Heterogeneities in a Barrier Island Deposit and Their Influence on Primary, Waterflood and Chemical EOR Operations. Pres. at SPE Ann. Tech. Conf. and Exhib., Dallas, TX, Sept. 27-30, 1987. SPE paper 16749. SPE Formation Evaluation, March 1990, pp. 103-112.
58. Jackson, S. R., L. Tomutsa, M. J. Szpakiewicz, M. M. Chang, M. M. Honarpour, and R. A. Schatzinger. Application of an Integrated Methodology for Construction of a Quantitative Transmissivity Model-Bell Creek Field, a Barrier Island Reservoir. Pres. at the Second International NIPER/DOE Reservoir Characterization Symposium, Dallas, TX, June 25-28, 1989.
59. Buell, R. S., R. Kazemi, and F. H. Poettmann. Analyzing Injectivity of Polymer Solutions With Hall Plot. Presented at the 62nd SPE Ann. Tech. Conf. and Exhib., Dallas, TX, Sept. 27-30, 1987. SPE paper 16963.
60. Tood, M. R., J. K. Dietrich, A. Goldberg, and R. G. Larson. Numerical Simulation of Computing Chemical Flood Designs. Pres. at SPE Symp. on Improved Methods of Oil Recovery, Tulsa, OK, April 16-19, 1978. SPE paper 7077.
61. Craft, B. C. and M. F. Hawkins. Applied Petroleum Reservoir Engineering. Prentice-Hall Inc., Englewood Cliffs, NJ, 1959.
62. Gary-Williams Oil Producers Inc. 1969 Engineering and Geological Report, Bell Creek Field, Unit 'A'. Prepared by Frank E. Farnham, Gary-Williams Oil Producers, Inc., Denver, 1969.
63. Honarpour, M. et al. Integrated Reservoir Assessment and Characterization. Final Report Department of Energy Report No. NIPER-390, February 1989.

64. National Institute for Petroleum and Energy Research Quarterly Technical Report for January-March 31, 1990, v. 1, Energy Production Research. Department of Energy Report No. NIPER-470, 1990.
65. Feder, J. Fractals. Plenum Press, 1988.
66. Hewett, T. A. Fractal Distributions of Reservoir Heterogeneity and Their Influence on Fluid Transport. Pres. at Soc. Pet. Eng. Ann. Tech. Conf. and Exhibit, New Orleans, LA, 1986. SPE paper 15386.
67. Hurst, H. E. Long-term Storage Capacity of Reservoir. Trans American Soc. Civ. Eng., v. 116, 1951, pp. 770-808.
68. Sneider, R. M., F. Richardson, D. Paynter, R. Eddy, and I. A. Wyant. Predicting Reservoir Rock Geometry and Continuity in Pennsylvanian Reservoirs, Elk City Field, Oklahoma. J. Pet. Tech., 1977, pp. 851-866.
69. Tomkins, J. Q. Bisti Oil Field, San Juan County, New Mexico. AAPG Bull., v. 41, 1957, pp. 906-922.
70. McNeal, R. P. Hydrodynamic Entrapment of Oil and Gas in Bisti Field, San Juan County, New Mexico. AAPG Bull., v. 45, 1961, pp. 315-329.
71. Davies, J. L. A Morphogenic Approach to World Shorelines. Zeits. Geomorph., v. 8, 1964, p. 127-142.
72. Berg, R. R. Reservoir Sandstones. Prentice-Hall, Inc., Englewood Cliffs, NJ, 1986, p. 284.
73. Taylor, A. M. Depositional Environments of the Dakota Sandstone in Southeastern Colorado. Guidebook for SEPA Field Trip No. 3, 1980, p.69.

## Appendix A. -- References and Papers Examined for Selection of a Second Shoreline Barrier Reservoir System

This appendix provides the information collected during the literature search. The examined literature is tabulated according to major subject (eg. Almond Formation, Patrick Draw Field Studies, etc.) Critical statements have been highlighted with bold type.

### ALBERTA, CANADA

•Holmes, I.G., and Y.A. Rivard, 1976, A marine barrier island bar, Jenner Field, Southeastern Alberta: The Sedimentology of Selected Clastic Oil and Gas Reservoirs in Alberta: Canadian Soc. of Petroleum Geologists, p. 44-61.

No reasons given in this paper to support barrier island over strandplain with attached shoreface.

### ALMOND FORMATION

•Asquith, D.O., 1966, Geology of Late Cretaceous Mesaverde and Paleocene Fort Union oil production, Birch Creek, Sublette County, Wyoming: AAPG Bull., v. 50, p. 2176-2184.

South Birch Creek is located on the La Barge Arch in western Green River Basin, northwest of the Rock Springs Uplift. It is part of the Big Piney-La Barge producing complex. The close association of oil and most of the gas production with the Paleocene Fort Union lacustrine shales suggests that this shale is the source of hydrocarbons for the associated reservoirs. Close association of production in mesaverde reservoirs with an unconformity above it at the overlying shale, absence of distinct chemical differences in oils between Cretaceous and Paleocene reservoirs, and lack of significant production from areas lacking or with poorly developed Paleocene shale suggests that the source of hydrocarbons produced from Mesaverde reservoirs may also be the Paleocene lacustrine shales rather than the underlying Cretaceous marine shale and siltstone.

•Asquith, D.O., 1968, Origin of large kaolinite crystals in the lower Almond Formation in southwest Wyoming: Jour. Sed. Petrol., v. 38, p. 948-949.

Large kaolinite books up to 3 mm in diameter from near Rock Springs (WY.) is present as a 1-3" "underclay" in the lower nonmarine portion of the Almond. Grain size, crystallinity, and lack of abrasion of books indicate diagenetic rather than detrital origin.

•Asquith, D.O., 1975, Petroleum potential of deeper Lewis and Mesaverde sandstones in the Red Desert, Washakie and Sand Wash Basins, Wyoming and Colorado: RMAG Symposium, p. 159-162.

Almond (Upper Mesaverde) was deposited during a local regression in the overall transgression of the marine Lewis Shale over the Mesaverde. Production trend includes Patrick Draw, Table Rock and Desert Springs fields on the western flank of the Washakie Basin and Red Desert Basin.

•Baptist, O.C., E.J. White, and C.S. Land, 1964, Laboratory predictions of water sensitivity compared with field observations of well damage - Patrick Draw, Wyoming: SPE Paper 839 (preprint), 6 pp.

Actual formation damage due to invasion of fresh water is estimated from interpretation of DST's and rates of injection into two pilot waterflood wells where fresh water was injected into 1 well and brine into the other.

Indecisive results. Damage ratios from DST are high for gas sands but damage is rapidly removed by production. Damage ratios are less in oil sands than in gas, and are even less in water sands. Injection rates for fresh water were about the same as for brine. Rates of brine injection are close to those calculated from laboratory relative-permeability curves.

•Bryant, W.A., 1984, Paleoenvironmental interpretation based on foraminifera of coal-bearing Almond Formation, Little Snake River Coalfield, Wyoming (Abst.): AAPG, Bull., v. 68, p. 933.

Almond is about 450 ft thick and divided into two informal members, both of which contain coal. Coals in the upper 100 ft of the upper member are thin, however, coals in the lower member include several thick beds. Coal-bearing portions of both members are characterized by repetitive coarsening-upward bay-fill deposits of mudstone and ss, commonly overlain by coal. A major coarsening-upward sequence in the lower part of the upper member is capped by sandstone interpreted as marine shoreface.

Fine grained rocks in both members contain forams. Three foram assemblages: 1) low diversity agglutinated benthic assemblage interpreted as a hyposaline saltmarsh fauna from fine grained rocks of the lower member, 2) a high diversity mixed agglutinated and calcareous benthic assemblage interpreted as a hyposaline bay to lagoonal fauna in shales in the lower part of the upper member, 3) a moderate-diversity agglutinated benthic assemblage in fine-grained rocks in the upper part of the upper member interpreted as a hyposaline salt marsh to interdistributory bay fauna.

•Finley, R.J., 1983, Comparison of depositional systems and reservoir characteristics of selected blanket-geometry tight gas sandstones: (Abst.), AAPG Bull., v. 67, p. 460-61.

Upper Almond Formation of eastern Greater Green River Basin may contain more shallow marine and offshore bar than barrier strand plain facies. Occurs at depths of 6,000-15,000 ft, net pay of 14-18 ft.

•Flores, R.M., 1978, Barrier and back-barrier environments of deposition of the Upper Cretaceous Almond Formation, Rock Springs Uplift, Wyoming: *The Mountain Geologist*, v. 25, p. 57-65.

Depositional environments identified in Upper Almond of Rock Springs Uplift include shoreface, barrier island, tidal inlet, tidal delta, washover fan, tidal flat, lagoon, tidal creek, overbank, pond, and marsh. Tidal delta, tidal-inlet-channel, washover fan, and tidal-creek deposits significantly affected back-barrier accretion and lagoon filling. The complete filling of the lagoon led to coalescing of marsh on the back side of the barrier island with the marsh on the landward side of the lagoon. Thin, discontinuous coal beds which rapidly grade into carbonaceous shale formed in the marsh in close proximity to the barrier island. Thin to thick, laterally extensive coal beds that locally grade into carbonaceous shale formed in the marsh on emergent levee, overbank, and bayfill deposits at the landward side of the lagoon. Deposition of the above detrital deposits as well as tidal-creek channel sandstones caused splitting and merging of the coal beds.

•Jacka, A.D., 1965, Depositional dynamics of the Almond Formation, Rock Springs Uplift, Wyoming: Wyoming Geol. Assoc., 19th Field Conference Guidebook, p. 81-100.

Upper Almond cycles display the following sequence of deposits from the base upward: 1) marine and/or lagoonal shale, 2) barrier-island sandstone, 3) marsh or mudflat deposits, and 4) lagoonal-bay deposits. These sequences reflect the lateral shifting of three contemporaneously existing depositional entities: 1) marine environment in which "surfzone" and infra-surfzone" sands, and offshore muds accumulated; 2) the barrier-island environment consisting of foreshore beach, backshore beach, and fringing marsh or mudflat deposits; 3) the lagoonal-bay environment in which predominantly fine-grained sediment, carbonaceous shale, and oyster reefs accumulated.

Evidence indicates that seaward growth of barrier islands was accompanied by expansion of lagoons which resulted in a progressive flooding of the landward margins of the barrier. Thus positions previously occupied by a barrier island were successively blanketed with lagoonal deposits. As the distance between a seaward-advancing barrier island and the mainland increased, a threshold limit was approached beyond which the volume of sand supplied to the seaward face was insufficient to permit further seaward growth. The operation of negative processes (subsidence, compaction, erosion, and possibly an independent rise in sea level) soon brought about the submergence or drowning of an abandoned barrier island.

•Jacka, A.D., 1970, Sediment economics of Upper Cretaceous sandstones Rocky Mountain Region: Wyo. Geol. Assoc., 22nd Ann. Field Conf. Guidebook, p. 187-219.

Upper Cretaceous in Rocky Mts. commonly display the following sequence: a) marine and/or lagoonal shale; b) barrier island sandstone; c) marsh-mudflat deposits; d) lagoonal-bay deposits; e) alluvial-coastal plain sediments. Sequence displays seaward progradation of coastal plain in response to a large sediment supply. **Proposed Gulf Coast Barrier Island/Coastal plain as analogue for Upper Cretaceous (especially Almond Fm.) in the Rocky Mts.**

Paper based primarily on investigation of environments, paleogeography and depositional history of the Upper Cretaceous Almond Formation of the Rock Springs Uplift.

•Keighin, C. Wm, B.E. Law, and R.M. Pollastro, 1989, Petrology and reservoir characteristics of the Almond Formation, Greater Green River Basin, Wyoming: in Coalson, E.B., et al, (eds), Petrogenesis and Petrophysics of Selected Sandstone Reservoirs of the Rocky Mountain Region, RMAG, Denver, p. 281-298.

Production through 1986 was 100 MM bbl. oil and 07 TCF gas. SEM and thin section analysis indicate that pores in fn to v fn Almond Fm ss are small ( $< 20\mu$ ) and formed in part by dissolution of framework grains and authigenic cements. Intergranular micropores occur between crystals of authigenic clay. **Sandstone contains 15-30% clay, which is dominantly illitic. Local concentrations of kaolinite occur, but chlorite is rare. Smectite clay minerals were not detected.** Distribution of cements, as well as detrital feldspars, is variable.

Not only porosity, permeability, and depth, but also vitrinite reflectance seem to be related in both conventional and unconventional (tight) Almond reservoirs. It may be possible to define an approximate depth at which **overpressuring** may occur based on these data.

•Krystinik, L.F., 1990, Characteristics of cores from a wave-dominated barrier/tidal inlet deposit: Cretaceous Almond Formation, south-central Wyoming (Abst.): in Davis, R.A., D. Nummendal, and R. Tillman, eds., Tidal Inlet and Related Sand Bodies Modern and Ancient: SEPM Research Conference San Juan Basin, New Mexico, pages unnumbered.

East of Table Rock field in Sweetwater County, the UA-8 sandstone is a north-south trending barrier/lagoon complex which has been cored at several localities in barrier and back-barrier facies. In the Union Pacific Railroad Corporation Robinson Siding #1 well (11-19N-97W), a 59 ft continuous core was cut through a sandstone body interpreted to be a tidal inlet deposit. The tidal inlet is laterally equivalent to wave-dominated shoreface deposits along strike and to back-barrier lagoonal deposits to the west.

The tidal inlet deposit is a 45 ft thick, blocky- upper-fine to lower-medium-grained sandstone body. The inlet has a sharp basal scour on older lagoonal deposits, and the inlet fill is composed of a basal oyster-shell lag which grades upward into clean, massive to medium-scale trough cross-stratified sandstone. A number of oyster-shell lags occur within the cross-stratified inlet fill, and these slightly inclined horizons may mark lateral accretion surfaces, as observed in field exposures of Almond formation inlets. The cross-stratified sandstone becomes more massive to planar-laminated toward the top 3 ft of the sandstone body and may record foreshore deposition as spit accretion filled the inlet. The upper 6 ft of the core is composed of Ophiomorpha-burrowed sandstone which grades upward into a transgressive unit composed successively upward of burrowed argillaceous sandstone, gritty mudstone and black silty mudstone.

•Leckie, D.A., and L.F. Krystinik, 1989, Is there evidence for geostrophic currents preserved in the sedimentary record of inner to middle-shelf deposits?: Jour. Sed. Petrol., v. 59, p. 862-870.

Evidence from Almond indicates wave-ripple crests trend generally N-S, parallel to regional shoreline, while other shoreline indicators and HCS beds trend E-W, normal to shoreline orientation.

•Meyers, W.C., 1977, Environmental analysis of Almond Formation (Upper Cretaceous) from the Rock Springs Uplift, Wyoming: Ph. D. Dissertation, University of Tulsa

Micropaleontology and photos of the two "outcrop" 5 inch diameter cores taken 1/2 mile set back from outcrop face in the Rock Springs Uplift. T20N, R101W. Also 150 palynological species recorded.

•Miller, F.X., 1977, Biostratigraphic correlation of the Mesaverde Group in Southwestern Wyoming and Northwestern Colorado: Rocky Mountain Assoc.Geol., Symposium, p. 117-137.

•Newman, H.E., 1981, Greater Green River Basin stratigraphy as it relates to natural gas potential: SPE/DOE 9845, Presented at SPE/DOE Low Permeability Symposium, Denver.

Almond deposited in transitional coastal plain and nearshore during a transgression, however the barrier island sediments were deposited during stillstands or local regressions of the Lewis Sea. Almond barrier may have advanced seaward as much as 20 miles (Jacka, 1965).

•Richars, D.M., R.J. Reed, K.C. Horstman, G.D. Michels, R.N. Baker, L. Lundell, and R.W. Marrs, 1982, Landsat and soil-gas geochemical study of Patrick Draw oil field, Sweetwater County, Wyoming: AAPG Bulletin, v. 66, p. 903-922.

Anomalous hydrocarbon concentrations in soil-gas samples appear in those areas near lineaments mapped from Landsat images of the Patrick Draw field. These lineaments represent extensional faults and fractures produced during development of the Rock Springs Uplift to the west. Several of the lineaments extend to depth and are able to serve as conduits allowing preferential microseepage of hydrocarbons to the surface in the Patrick Draw area, indicating the nature of expected hydrocarbons at depth.

•Richers, D.M., V..T. Jones, M.D. Mathews, J. Maciolek, R.J. Pirkle, and W.C.. Sidle, 1986, The 1983 Landsat Soil-Gas geochemical survey of Patrick Draw area, Sweetwater County, Wyoming: AAPG Bull., v. 70, p. 869-887.

•Roehler, H.W., 1976, Lagoonal origin of coals in the Almond Formation in the Rock Springs Uplift, Wyoming: 1976 Symposium on the Geology of Rocky Mountain Coal, p. 85-89.

**Upper 300 ft-** coastal lagoon, mixed barrier bar, lagoon, shallow marine; saltwater deposition indicated by shark teeth, cephalopods.

**Middle 350 ft-** brackish water lagoonal environment. Brackish water deposition indicated by oysters and other mollusks.

**Lower 200 ft-** Freshwater coastal swamps. Freshwater environment indicated by dinosaur, crocodile, turtle and fish fossils.

**Depositional Model:** marine coastline with lagoons formed behind barrier island during westward transgressions of late Cretaceous sea. Evidence for lagoonal origin of coals is: intertonguing and juxtaposition of the coal beds and barrier islands, and by presence of fossil oyster beds containing coal-bearing sequences. Eighteen coal beds that range from 25 to 16 ft thick have been mapped in the Almond Formation.

•Roehler, H.W., 1988, The Pintail Coal Bed and Barrier Bar G - A Model for coal of barrier bar-lagoon origin, Upper Cretaceous Almond Formation, Rock Springs Coal Field, Wyoming: U.S. Geological Survey Professional Paper 1398, 60 p.

Early Maastrichtian Upper Almond barrier is 60 miles long and 4 miles wide. There are 18 miles of outcrops on the east flank of Rock Springs Uplift.

Study based on outcrops around Rock Springs Uplift: 104 measured stratigraphic sections plus 14 others that describe lithofacies and primary sedimentary structures. 4 widely spaced holes drilled and logged (no cores)

Barrier bar G: mesotidal (4.5-8 ft range); islands 5-7 mi long, roughly drumstick-shaped, washover fans present, but not common; numerous tidal inlets; flood-tidal deltas large (up to several miles wide); ebb-tidal deltas moderately large to small.

Divisions of Almond Fm: **Upper 100-400'**-very fine-grained to medium grained; deposited in shallow marine, barrier bar and lagoonal environments; saltwater fauna-marine mollusks, shark teeth, ammonites, numerous trace fossils. **Middle 125-250'**-brown carbonaceous shale and coal, some thin interbedded gray shale and gray, fine-grained crossbedded sandstone deposited in lagoonal environments; brackish water fauna of abundant oysters and brackish mollusks. **Lower 100-600'**-

swampy, coastal plain setting: fresh water fauna of dinosaurs, turtles, crocodile and fish bones.

Pintail coal bed deposited in a lagoon, landward of barrier bar G. As the barrier prograded, the back-barrier flat was progressively covered by swamp deposits that include the seaward wedgeout of the coal bed. The coal bed is massive and locally more than 6 feet thick. Splits and partings of carbonaceous shale are interpreted as tidal inlet and tidal creek deposits. His model demonstrates that the barrier and its lagoon evolved through saltwater to brackish-water to freshwater stages, with the times of maximum peat accumulation occurring in the freshwater stage.

•Van Horn, M.D., 1979, Stratigraphy of the Almond Formation, East-Central flank of the Rock Springs Uplift, Sweetwater County, Wyoming: A mesotidal-shoreline model for the Late Cretaceous: M.S. Thesis, Colorado School of Mines, 150 p.

•Wanner, J.J., D.A. Chesnut, and D.O. Cox, 1979, Gas production from tight Mesa Verde sands in Wyoming--A field case history: SPE 7934, p. 233-237.

Barrel Springs Field, Washakie Basin, WY. Production from Almond and Ericson sands in upper Mesaverde.

•Weimer, R.J., and R.W. Tillman, 1982, Sandstone Reservoirs: SPE 10009, Pres. at the International Petroleum Exhibition and Technical Symposium of the SPE, Beijing, China, p. 1-5.

Patrick Draw Field discovered in 1959. Approximately 56 million bbl oil and 11bcf gas have been produced (22 years). Reserves in place 200-250 mm bbl oil. Upper 60 ft of Almond Formation consists of two sands: UA-5 (upper sandstone), UA-6 (lower sandstone).

**UA-6 Sandstone:** Productive in West Desert Springs Field and northern part of Patrick Draw. Gray, very fine to fine grained calcareous sandstone, ranges from 0 > 25 ft; Average thickness 12 ft. Interpreted as tidal creek channels and tidal flats west of a shoreline sand trend based on erratic distribution of production, fine grain size, close association above and below with coal beds and lagoonal shale.

**UA-5 Sandstone:** Main producing zone in Patrick Draw. Overlain by marine Lewis Shale, by oyster coquina layers or by 5-10 feet of carbonaceous shale and impermeable sandstone. Sandstone is quartzose, gray, fine to medium grained, calcareous and contains abundant dark gray to black chert grains and minor amounts of feldspar, quartz-64%, chert 32%; feldspar (mostly plagioclase) 4%; trace amounts of biotite, muscovite, chlorite and zircon. Cements are dominantly silica, calcite, dolomite and clay minerals (kaolinite). Thickness is 0-30 ft, lateral extent of sandbody is 20 miles long, 6 miles wide. UA-5 pinches out updip at the western margin of Patrick Draw into impermeable coal-bearing shale and siltstone.

**Depositional Model:** UA-5 is shoreline sand deposit based on sedimentary structures and geometry. Unit has characteristics of prograding barrier island shoreline deposit: coarsening upward texture with burrowed sandstone near base, overlain by trough crossbeds in sets 1-2 ft thick with laminae of clay or carbonaceous material within the cross lamina. Ophiomorpha trace fossils indicate near normal marine salinity. Mesotodal range (4-8 ft) based on widespread occurrence and thickness of the channel sands.

•Weimer, R.J., K.W. Porter, and C.B. Land, 1985, Depositional modelling of detrital rocks with emphasis on cored sequences of petroleum reservoirs: S.E.P.M. Core Workshop No. 8, Golden, Colorado, p. 105-127.

•Winn, R.D., Jr., M.G. Bishop, and P.S Gardner, 1985, Lewis Shale, South-Central Wyoming: Shelf, delta front, and turbidite sedimentation: Wyo. Geol. Assoc. Guidebook, 36th Annual Field Conference, p. 113-130.

•Winn, R.D., Jr., M.G. Bishop, and P.S. Gardner, 1987, Shallow-water and sub-storm-base deposition of Lewis Shale in Cretaceous Western Interior Seaway, South-Central Wyoming: AAPG Bull, v. 71, p. 859-881.

Basinwide discussion of Lewis Shale (that overlies Almond Fm.), documents depositional environments of the Lewis Shale and shows tectonic and eustatic events that controlled its development. Western extent of Lewis sea in the area of the Rock Springs and Wind River uplifts. Cross sections are presented that go through Wamsutter Arch/Patrick Draw area.

#### ALMOND FORMATION, PATRICK DRAW FIELD STUDIES (by date)

•Burton, G, 1961, Patrick Draw area, Sweetwater county, Wyoming: Wyo. Geol. Assoc., 16th Ann. Field Conf., p. 276-279.

•Lawson, D.C., and C.W. Crowson, 1961, Geology of the Arch Unit and adjacent areas, Sweetwater County, Wyoming: WGA Guidebook, 16th Ann Field Conf, p 280-299.

•Cox, J.E., 1962, Patrick Draw area, Sweetwater County, Wyoming: Billings Geol. Soc., Paper no. 1, p 1-17.

•Weimer, R.J., 1966, Time-stratigraphic analysis and petroleum accumulation, Patrick Draw Field, Sweetwater County, Wyoming: AAPG Bull., v. 50, p. 2150-2175.

Field discovered in 1959. Although several sandstone reservoirs produce at Patrick Draw, the principal productive interval consists of two sandstone bars at the top of the Almond Formation. Spatial dimensions, lithologic character, and stratigraphic framework of the bars suggest that they are barrier-bar sandstone bodies deposited along the margin of the Lewis sea. The bars are linear and grade updip into impermeable shale and sandstone that was deposited in a swamp and lagoonal environment. **A second important productive interval is approximately 40 ft below the top of the Almond Fm. The areal distribution, lithologic character, and stratigraphic framework of the ss in this interval suggest that it was deposited as a tidal delta in a lagoon.** Each of the three major productive sand bodies have different oil-water contacts.

•McCubbin, D.G., and M.J. Brady, 1969, Depositional environment of the Almond reservoirs, Patrick Draw Field, Wyoming: The Mountain Geologist, v. 6, no. 1, p. 3-26.

Study supports Weimer (1966) that the main reservoir sandstone is a composite shoreline deposit, at least partly replaced updip by lagoonal shales.

**UA-5 at Patrick Draw consists of a "western bar" and a younger "eastern bar" that partly overlaps the western bar.** The western bar and, in places, the eastern bar rest with sharp contact on a widespread coal that forms the uppermost unit of the underlying cyclic sequence. Both sandstone bodies contain transported bivalves and some forams and show burrows including rare Ophiomorpha. Both sand bodies show a vertical sequence of stratification types interpreted as indicating deposition in nearshore-marine and beach environments on a seaward- prograding shoreline. Lateral changes in stratification types suggest that the seaward direction was to the east. Vertical and lateral variations in grain size of this record an initial transgression, followed by deposition in progressively more shallow environments during shoreline progradation.

**The lagoonal facies that overlies the western bar and appears to be at least partly equivalent to the eastern bar consist of silty to sandy shales and some thin sandstones.** Oysters are common and are a major constituent of "coquina" beds. The occurrence of large, whole, randomly oriented oyster valves in shaly matrix indicates that these oysters are in their **original place of growth**. Some of the shales contain a microfauna of arenaceous forams. Structures formed by burrowing animals are abundant in the silty or sandy shales.

Richers, D.M., V.T. Jones, M.D. Matthews, J. Maciolek, R.J. Pirkle, and W.C. Sidle, 1986, The 1983 Landsat soil-gas geochemical survey of Patrick Draw area, Sweetwater County, Wyoming: AAPG Bull., v. 70, p. 869-887.

Resampling the Geosat test site at Patrick Draw indicate that the 1980 assessment was correct: that **faults and fractures visible as linear features on satellite and aircraft imagery provide paths for active microseepage of hydrocarbons from depth to the near surface.** This association is particularly true near the earlier described 'blighted sage zones,' where a much wider area of anomalously high free soil-gas values and fluorescence was revealed.

Richers, D.M., (preprint, in press March 1990), Patrick Draw Oil Field: To Be Published in: AAPG Treatise on Petroleum Geology.

Discovered in 1959, the estimated reserves are 200-250 mm bbl oil. Patrick Draw is just one of many Cretaceous oil fields in Wyoming that produce from elongate sand bodies that were distributed along the margin of the Upper Cretaceous Sea. About 279 wells have been drilled (1979), although about 115 of these are currently used as injection wells. Divided into three producing units: (north to south) Patrick Draw North, Arch, Monell. Production is from Almond, although localized pay or shows in Lewis, Fox Hills, and Lance formations (Cretaceous), as well as from the Paleocene Ft. Union and Eocene Wasatch formations. Patrick Draw like most fields in the area is a stratigraphic trap. Almond is felt to represent near-shore barrier bar and beach front sands. As a result, reservoirs tend to be several miles long and less than 4 miles wide.

Patrick Draw represents the typical Cretaceous stratigraphic trap of the Western U.S. It is felt that about 30% of reserves are recoverable. Secondary recovery programs include water flood, and gas reinjection. Active gas reinjection is necessary to maintain oil drive; it is reported that the field has always been underpressured since the initial production in 1959.

Field is located on the eastern flank of the Laramide Rock Springs Uplift, and on the southern limb of the Wamsutter Arch. Present axis of the arch is about 10 miles north of the original axis formed at the end of the Cretaceous. Vitrinite reflectance date and thermal modelling indicate that Patrick Draw is currently in the oil window; Lewis Shale several miles east of Patrick Draw could have entered the oil window 18-20 my ago.

Oil production is viewed by Weimer as having migrated vertically from the Almond, along E-W trending faults. This production is also along the trend of surface geochemical anomalies associated with a sagebrush "blight" zone. **Stratigraphic nature of Patrick Draw is difficult if not impossible to resolve on the seismic lines available.**

Weimer et al. (1985) indicated that the Almond represents near-shore barrier bar and/or ancient shorelines, with some shallow tidal-flat facies. Generally the producing sandstone bodies are less than 2 miles wide and some are up to 20 miles in length. Lateral facies changes are abrupt, resulting in extreme porosity differences over a very small distance. Updip seal for stratigraphic traps is provided by facies change into less permeable coastal plain shales and siltstones. Overlying seal is provided by the Lewis Shale. There is some speculation that the Lewis could be the source of the oil at Patrick Draw and that the gas is sourced either from coals in coastal plain facies of the Almond, or from a biogenic source (Weimer, 1966, Weimer et al, 1985). UA-6 is productive only in the northern portion of the field, about 10 feet below the UA-5. UA-5 and UA-6 are generally separated by a dark gray shale and silty shale. Several other sands produce in this area and are discussed.

Weimer et al., 1985 concluded that the UA-5 sand is most probably a shoreline sand deposit: a mesotidal barrier island sequence. Sub environments also identified include back barrier tidal flats, marsh, lagoon, and tidal channel. Tidal channels are typically medium grained cross stratified sands containing organic plant debris. **The channels tend to be about 20 ft thick and contain reactivation channels with oyster shells and fragments in a dark organic-rich, silty sandstone.**

Tidal flats are represented as fine-grained, laminated and rippled mudstones and sandstones. Burrows are common. Evidence for small tidal creeks includes deformed and slumped features.

**Marsh environments are evidenced by dark, organic-rich very fine grained sand and mudstone. Some coal is also present.**

Oil samples had API gravity of 44.4 and a density of 0.7977 g/cc at 25 C; Street (1979) reported GOR between 600:1 to 1554:1 for Almond production. Whole oil chromatogram shows preponderance of lighter n-paraffin components-generally indicative of maturity because mature oils are generally enriched in the lighter components. Pristane to phytane ratios greater than 3.0 in high wax crude oils and condensates characterize input from terrigenous materials common to lacustrine, fluvial, and deltaic environments. This assessment fits Patrick Draw. A terrigenous source for Patrick Draw oils is strongly suggested.

Surface geochemical studies support: 1) fractures and faults are the preferred migration pathway of hydrocarbons leaking from the subsurface reservoir to the surface, 2) high surface hydrocarbon anomalies are repeatable over a period of years, 3) geobotanical anomalies exist over the gas cap in western up-dip portions of the field. A stressed sage community is located over the field.

•Tillman, R.W., 1990, Tidal channels in Almond barrier islands sandstones, Patrick Draw field, Wyoming (abst.): In Davis, R.A. Jr., D. Nummendal, and R. W. Tillman, Conveners, Tidal Inlet and Related Sand Bodies: Modern and Ancient; SEPM Research Conference, San Juan Basin New Mexico, May 5-10, pages unnumbered.

The reservoir produces from tidal channel sandstones designated as UA-5, which consist of a western barrier island and a younger overlapping eastern barrier island. In parts of the fields the barrier islands have been thoroughly dissected by what are interpreted as tidal inlet channels. The UA-4 and UA-5 reservoirs include tidal inlets, while the UA-6 sandstone may be predominantly tidal creeks. When western barrier, and in places the eastern barrier, rests with sharp contact on a widespread coal that forms the uppermost unit of the underlying cyclic sequence.

The tidal channel fill typically is coarsest grained and includes abundant transported oysters at the base. Oysters also are scattered throughout the lower half of the inlet fill. Current structures, including cross-lamination and asymmetrical ripples, dominate the inlet fill. Ophiomorpha and other burrows are scattered throughout the sandstone fill of the inlet.

## **ATKINSON FIELD**

•Bulling, T.P., and J.A. Bryer, 1986, Exploring for subtle traps with high-resolution paleogeographic maps: Reklaw 1 interval (Eocene), South Texas: AAPG Bull., v. 73, p. 24-39.

Results for Atkinson field: This field produces from a sand within the Reklaw 1 interval; the sand extends for 9 mi along strike and reaches a width of 2 mi and a max thickness of 60 ft. Four electrofacies are recognized: blocky, bell shaped, simple spike, and tapered spike. Electrofacies must be considered in context, including sand-body geometry and orientation. Most of the logs from the central part of the sand have blocky patterns. Environmental interpretations include barrier beach, barrier bar or barrier island, tidal inlet fill, washover fan, and seaward edge of barrier-all summarized in their Table 1. The shoreline-parallel sands at Atkinson field have lobes that extend updip into shales and represent washover fan deposits. This probably indicates a microtidal model. The Atkinson sand does not show upward coarsening pattern commonly associated with barrier islands. This barrier was built and subsequently drowned in place, it did not prograde.

Good documentation of upward shoaling of North Bunces Key from a subtidal shoal area without benefit of significant storm activity.

•Davidson-Arnott, R.G.D., and B. Greenwood, 1976, Facies relationships on a barred coast, Kouchibouguac Bay, New Brunswick, Canada: in, Davis, R.A., and R.L. Ethington, eds., Beach and Nearshore Sedimentation: SEPM Spec. Pub. No. 24, p. 149-168.

Excellent review of facies in longshore bars and shoreface environment.

- Davis, R.A., Jr., editor, Coastal Sedimentary Environments, Springer-Verlag, N.Y., 707 p.
- Davies, D.K., and F.G. Etheridge, 1975, Sandstone composition and depositional environment: AAPG Bull., v. 59, p.239-264.
- Davies, D.K., Etheridge, F.G., and R.R. Berg, 1971, Recognition of barrier environments: AAPG Bull. v. 55, p. 550-565
- Demarest, J.M., II, and J.C. Kraft, 1987, Stratigraphic record of Quaternary sea levels: implications for more ancient strata: Sea-Level Fluctuation and Coastal Evolution, SEPM Special Publication No. 41, p. 223-239.
- Dolan, R., and H. Lins, 1987, Beaches and barrier islands: Scientific American, July, p. 68-77.

This is a general article that emphasizes the continually changing nature of barrier islands and beaches. Most of the paper is oriented toward land usage and attempts at barrier/beach stabilization.

Donselaar, M.E., 1990, Facies and geometry of fossil flood-tidal deltas (Abst.): In Davis, R.A., Jr., D. Nummedal, and R.W. Tillman, Conveners, Tidal Inlet and Related Sand Bodies: Modern and Ancient: SEPM Research Conference San Juan Basin, New Mexico, May, 1990, pages unnumbered.

Preservation potential of flood-tidal deltas in a transgressive setting is high because of the protected lagoonal environment of deposition and the low stratigraphic position in the transgressive sequence. Two examples are presented.

The first example includes laterally and vertically-stacked flood-tidal sandstone bodies with lobate geometry in the Menefee formation. Individual sandstone lobes are 2-7 m thick and widths are 100-650 m. Upper surfaces are often wave rippled and have a goethite cap. Concave scours produced by tidal channels locally cut the upper surfaces of the sand lobes. Channel fill is either with coaly lagoonal shale or with cross-bedded sands. Internally the sandstones are characterized by lagoonward-inclined primary bedding planes and tabular to wedge-shaped, large-scale cross beds with foreset dips in the lagoonal direction. Tidal features include mud drapes on the foresets, occurrence of bundle sequences, and bimodal distribution of foreset dips with a dominant landward component.

The second example is a wedge-shaped flood-tidal sandstone in the Pano formation, Spain. The sandstone body had a maximum thickness of 12 m. Thickness of the sand body decreases lagoonward as the flood-tidal delta interfingers with lagoonal marl. Lagoonward-inclined primary bedding characterizes the internal arrangement of the sandstone. The upper part of the sandstone shows deep erosive scours. Scours are filled with cross-bedded sandstone. Tidal criteria comprise bundle sequences, mud drapes, and bimodal foreset dips with a dominant landward component.

•Evans, M.W., and A.C. Hine, 1990, Distribution and infilling sequences of tidal inlet channels in the open-water lagoons of southwest Florida (Abst.): In Davis, R.A., Jr., D. Nummedal, and R.W. Tillman, Conveners, Tidal Inlet and Related Sand Bodies: Modern and Ancient: SEPM Research Conference San Juan Basin, New Mexico, May, 1990, pages unnumbered.

switch pages 65-66 (out of order)

## BARRIERS- MODERN

•Belknap, D.F., and J.C. Kraft, 1981, Preservation potential of Transgressive coastal lithosomes on the U.S. Atlantic Shelf: *Marine Geology*, v. 42, p. 429-442.

Variable fractions of the transgressive sequence may be preserved, depending on pre-existing topography, depth of erosion, wave energy, sediment supply, erosion resistance, tidal range, and rate of relative sea-level change. However, their not too earth shaking conclusions are that materials at greater depth in the stratigraphic column are more likely to be preserved during transgression; there is better preservation on the outer shelf and more reworking on the inner shelf.

•Belknap, D.F., and J.C. Kraft, 1985, Influence of antecedent geology on stratigraphic preservation potential and evolution of Delaware's barrier systems: Chapter VI. Barrier Platforms; *Marine Geology*, v. 63, p. 235-262.

Delaware coast is dominantly transgressive. As Holocene coastal lithosomes migrate over the Pleistocene erosional surface, they fill pre-Holocene valleys first, and then thicken. Shoreface forms another erosional surface (ravinement unconformity) and these two surfaces determine the degree of preservation of the Holocene section.

•Bernard, H.A., Major, C.F., Jr., and B.S. Parrott, 1959, The Galveston barrier island and environs: A model for predicting reservoir occurrence and trend: *Transactions of the Gulf Coast Ass. of Geol. Societies*, v. IX, p. 221-224.

•Bernard, H.A., and R.J. LeBlanc, 1965, Resume of the Quarternary geology of the northwestern Gulf of Mexico province: in Wright, H.E., Jr., and D.G. Frey, eds., *The Quaternary of the United States*, Princeton University Press, pp. 137-185.

•Cant, D.J., 1984, Development of shoreline-shelf sand bodies in a Cretaceous epeiric sea deposit: *Jour. Sed. Petrol.* v. 54, p. 541-556.

•Clifton, H.E., 1990, A wave-dominated inlet on a mesotidal coast: Willapa Bay, Washington (Abst.): In Davis, R.A., Jr., D. Nummedal, and R.W. Tillman, Conveners, *Tidal Inlet and Related Sand Bodies: Modern and Ancient: SEPM Research Conference San Juan Basin, New Mexico, May, 1990*, pages unnumbered.

Willapa Bay is located on the coast of Washington, just north of the mouth of the Columbia River. Tidal range within the bay is 2-3 m. The Inlet is 8-9 km wide and consists of broad shallow subtidal and intertidal flats dissected by two narrow channels less than one km wide, which are 10-15 m and greater than 20 m deep, respectively. **A large ebb-tidal delta extends from the inlet into the Pacific Ocean. The flood-tidal delta is less pronounced and is truncated by the large tidal channel that forms the north-south axis of the bay.**

Where the tidal channel enters the bay, the ebb and flood tidal currents dominate different parts of the channel: **dunes on the shallower parts of the channel (its southern bank) are oriented in an ebb direction, whereas those in the deeper part of the channel (off its erosional northern bank) are oriented predominantly in a flood direction.** Wave-related processes dominate on the outer part of the ebb tidal delta.

Three-dimensional consideration of the sand body indicates that it is an asymmetrically northward-thickening accumulation that is dominated by tidal process in its deeper parts and on its bayward side and by wave processes in its shallower parts and on its oceanward side.

•Crowe, D.E., and R.A. Davis, Jr., 1984, Upward-Shoaling origin of an Eastern Gulf Coast barrier island (Abst.): *AAPG Bull.*, V. 68, p. 467.

Island first became emergent in 1960; has grown to length of 2 km (1.2 mi) with widespread vegetation and dunes which rise about 2 m (6 ft) above mean sea level.

The Charlotte Harbor system is low energy- 28 cm average wave height, and mixed tides with a 62 cm maximum average tidal range. Three sediment types comprise the estuarine fill: a mature, well sorted, fine quartz sand, a molluscan shell gravel, and a silt-dominated clayey mud. Cores indicate multiple fining-up sequences which are interpreted as tidal channel fill. These fills contain coarse shell layers a few cm to a meter thick at the base, and fine up to muddy sands. Thickness of fining upward sequences varies from 30 cm to more than 200 cm.

Similar sequences have been interpreted from nearby lagoons as storm overwash deposits, however, seismic data show channel structures rather than thin, widespread reflectors. Migration and infilling of tidal channels accounts for 50% of the Holocene lagoon and lower estuarine accumulation and has been the single most important depositional process in those areas.

•Galloway, W.E., 1986, Reservoir facies architecture of microtidal barrier systems: AAPG Bull, v. 70, p. 787-808.

First part of paper is good summary of barrier systems, their stratigraphy, and recognition. Second part of paper is about an example from West Ranch Field (Frio) in Texas.

•George, D.J., and B.M. Hand, 1977, Computer simulation of barrier-island migration: Computers and Geosciences, v. 3, p. 469-473.

•Hayes, M.O. and T.W. Kana (editors), 1976, Terrigenous clastic depositional environments, some modern examples: A Field Course Sponsored by the American Association of Petroleum Geologists: Technical Report No 11-CRD, Coastal Research Division, Dept. Geology, U. of South Carolina, pt. 1, 135 ; pt. 2, 185 p.

Very useful lecture notes, especially part of Chapter C on Beaches and Barrier Islands. Defines and compares mesotidal and microtidal barrier island geomorphical components:

1) microtidal: long elongated, washovers abundant, tidal inlets infrequent, large flood-tidal deltas, small to no ebb-tidal deltas.

2) mesotidal: stunted, drumstick shape, minor washovers, frequent tidal inlets, moderate size to no flood-tidal deltas, large ebb-tidal deltas with strong wave refraction effects.

A lot of other well organized information also available including 3 separate papers on mesotidal barriers and 4 papers on tidal inlets.

•Hayes, M.O., 1989, Modern clastic depositional environments, South Carolina: 28th International Geological Congress, Field Trip Guidebook T371, 85 p.

This is basically an updated version of Hayes and Kanna (1976). Includes very organized description of the coastal environments along the South Carolina/Georgia Bight, including barrier and related settings.

•Heron, D., 1990, A summary of tidal inlet and delta stratigraphy of a microtidal wave-dominated foreland, Cape Lookout, NC (Abst.): In Davis, R.A., Jr., D. Nummedal, and R.W. Tillman, Conveners, Tidal Inlet and Related Sand Bodies: Modern and Ancient: SEPM Research Conference San Juan Basin, New Mexico, May, 1990, pages unnumbered.

Cape Lookout is at the center of barrier system consisting of two limbs. The NE limb has a tidal range of only 0.47 m, and the SW limb has a tide range of 0.89 m. Wave energy on the NE limb is almost 3 times as high as that focused on the SW limb.

The sedimentary sequence in most tidal inlets fines up and consists of inlet floor, active inlet channel, spit platform and overwash facies. Sand dominates in all facies. The coarsest material forms the inlet floor lag and consists of coarse pebbly sands and heavy shell fragments. The active inlet channel is

cross-bedded coarse sand and shell. The spit platform is finer well-sorted sand with parallel lamination of sand and shell. The top overwash unit has the typical horizontal lamination of sand and shell and is rooted with Spartina and other plants. The overwash unit may be topped with dune sands. The thickness of this sequence is variable depending on the size and duration of an inlet. The section at the modern migrating Beaufort inlet is 18 m thick, and one relic inlet is 25 m thick.

Not all inlets have a simple fining-upward sequence. Detailed study of the active inlet channel facies typically shows a stacked fining upward sequence of normal graded fine- to coarse-grained sand and shell fragments. These small cycles vary in thickness, but 2 m is a common value.

Flood-tidal deltas have a similar facies sequence as tidal inlets, but they fine-up into a mud zone rather than overwash or wind-dune sands.

**About 35% of the Holocene section of the barriers in the Cape Lookout foreland is Inlet fill. When the associated flood-tidal delta deposits are added, the bulk of the barrier system is of tidal channel and delta origin. Since much of these sediments are deposited below wave base or in protected areas behind the barriers, they will have the best preservation potential of the barrier system.**

•Hoyt, J.H., 1967, Barrier island formation: Geol. Soc. America Bull., v. 78, p. 1125-1136.

Empirical data fail to substantiate classical theories of barrier island formation from offshore bars. Absence of open ocean beach and neritic sediments landward of barrier islands suggests that barriers have not developed from offshore bars. Formation of barrier islands from emergent bars is also rejected, because evidence from many areas of the world does not support a sea level higher than present during the Holocene. Also unacceptable is the hypothesis of continuous barrier development through the Holocene submergence because it does not explain the original formation. Barrier islands which form from barrier spits or, in some instances, from bars are accepted, but these methods are not regarded as the general mechanism.

**Hypothesis advanced in this paper maintains that barrier island is initiated by building of a ridge immediately landward of the shoreline from aeolian or water-deposited sediments. Slow submergence floods the area landward of the ridge and forms a barrier and lagoon. Slow submergence or negligible sedimentation is necessary to maintain the lagoon. Emergence in excess of lagoonal depth terminates the barrier system.**

(Not mentioned by the author, this theory could only work with a generally transgressive shoreline because it requires that a portion of the mainland must subside simultaneously with the formation of a neo-barrier.)

•Hunter, R.E., H.W. Clifton, and R.L. Phillips, 1979, Depositional processes, sedimentary structures, and predicted vertical sequences in barred nearshore systems, southern Oregon coast: Jour. Sed. Petrol., v. 49, p. 711-726.

Describes a shoreline barrier type consisting of elongate nearshore (submerged) bars that extend obliquely out from shore and that migrate alongshore.

•Imperato, D.P., Sexton, W.J., and M.O. Hayes, 1988, Stratigraphy and sediment characteristics of a mesotidal ebb-tidal delta, North Edisto Inlet, South Carolina: Jour. Sed. Petrol., v. 58, p. 950-958.

Bedforms and surface textures at North Edisto Inlet reflect typical ebb-tidal delta circulation patterns. The main ebb channel is dominated by large ebb-oriented bedforms, and channel sediments become finer in seaward direction. At the inlet throat, the coarsest available sediments forms a lag deposit. Marginal flood channels adjacent to the barrier islands are dominated by flood-oriented bedforms composed of med.-grained sand. Channel-margin linear bars flanked by bedforms with opposing orientations develop where flood channels approach the main ebb channel. The extensive swash platform is dominated by wave energy, which effectively sorts swash platform sediments.

Ebb-tidal delta stratigraphy is dominated by sequences deposited by shifting tidal channels and the migration of swash bars. **Proximally, ebb-tidal delta sequence dominated by thick tidal channel deposits which fine upward and have sharp, disconformable base.** Ebb-channel deposits up to 20 ft thick flank the channel and are composed of well-sorted, planar-bedded, fine-grained sandstone.

**Adjacent to barrier islands, marginal flood-channel deposits dominate the ebb-tidal sequence.** These channel sequences are composed of moderately to intensely burrowed, wavy to flaser-bedded sand and mud. Barrier island accretion in the vicinity of inlets often involves flood-channel switching; marginal flood channel deposits could comprise a significant portion of the barrier island lithosome in the vicinity of inlets.

Distally, wave-formed swash platform deposits dominate the ebb-tidal delta sequence. These are very well sorted, fine-grained sand and have planar bedded, landward-oriented crossbeds; coarse shell-hash layers; and extensively burrowed zones. Swash platform deposits interfinger with shoreface deposits laterally and at depth. **Distal ebb-tidal delta deposits are relatively thin and have an overall coarsening-upward grain-size trend.**

•John, C.J., 1977, Internal sedimentary structures, vertical stratigraphic sequences, and grain-size parameter variations in a transgressive coastal barrier complex: The Atlantic Coast of Delaware: Delaware Sea Grant College Program, College of Marine Studies, University of Delaware, Sea Grant Technical Report DEL-SG-10-77, 287 p.

This study provides detailed information on the internal sedimentary structures, vertical stratigraphic sequences, and grain-size variations in a transgressive coastal barrier complex. The barrier extends from Cape Henlopen in the north to Cottonpatch Hill in the south, along the Atlantic coast of Delaware. Major data is from 32 transverse cross sections and one longitudinal cross section.

Four major variations of the coastal transgressive barrier were found: 1) spit-beach-dune complex, 2) barrier against marsh, 3) beach against Pleistocene highland, and 4) barrier-tidal delta-lagoon, which included a baymouth barrier and a tidal inlet section.

Littoral transport carries sediment from south to north; the sands are mostly derived by coastal erosion of the Atlantic shoreline. **Washovers are the dominant mechanism for landward barrier migration.** Washovers and back-barrier marshes form part of the leading edge of the Holocene marine transgression.

The greater thickness of transgressive sequence deposits in ancestral stream valleys crossing the barrier complex, compared to that at other sections of the barrier complex, gives it a better potential for preservation under a cover of marine sediments. The current barrier is about 3,750 years old.

Vertical sedimentary sequences of coarse sediments over fine sediments occur in both transgressive and regressive coastal settings. **Shapes of geophysical logs may be funnel-shaped, columnar-shaped, and/or possibly bell-shaped in an overall transgressive coastal setting.**

•Kumar, N., and J.E. Sanders, 1974, Inlet sequence: a vertical succession of sedimentary structures and textures created by the lateral migration of tidal inlets: *Sedimentology*, v. 21, p. 491-532.

Based on Fire Island inlet, located 56 km east of New York City, which has migrated west-southwest at mean rate of 64m/yr during period 1825-1940. Deposition of sediment on the east side of the inlet has forced the tidal currents to erode the west side of the inlet, causing inlet migration. Lateral migration of the inlet along with changing hydraulic conditions that vary from channel floor to the subaerial part of the spit produce 5 major units:

- 1) **Spit with subenvironments**: steep and gentle, seaward to landward-dipping laminae.
  - 2) **Spit platform**: Steep seaward-dipping planar cross-strata, and small scale flood-oriented cross-laminae at top; ebb oriented cross-laminae at bottom.
  - 3) **Shallow channel**: parallel laminae
  - 4) **Deep channel**: Lenticular sets of ebb-oriented cross-laminae bounded by flood-oriented reactivation surfaces.
  - 5) **Channel floor**: Lag gravel composed of large shells, pebbles, and other coarse particles.
- Units 3-5 compose the inlet proper.** Because of the great variability in rates of lateral migration inlet sediments may be preserved as elongate lenses, or as widespread blankets.

•McBride, E.F., and M.O. Hayes, 1962, Dune cross-bedding on Mustang Island, Texas: *AAPG Bull.* v. 46, p. 546-551.

•McBride, R.A., and T.F. Moslow, 1990, Distribution of tidal inlets and shoreface sand ridges along wave-dominated barriers, Atlantic Inner shelf, USA (Abst.): In Davis, R.A., Jr., D. Nummedal, and R.W. Tillman, Conveners, *Tidal Inlet and Related Sand Bodies: Modern and Ancient*: SEPM Research Conference San Juan Basin, New Mexico, May, 1990, pages unnumbered.

Ebb-tidal deposits associated with migrating tidal inlets provide the initial sand body for development of shoreface-attached sand ridges. The oblique orientation and linear form of shoreface-attached sand ridges are a function of shoreline transgression, lateral inlet migration, and wave reworking of ebb-tidal delta deposits along an ebb-tidal delta retreat path. Shelf processes are important in the evolution of sand ridges after their initial deposition.

•McCubbin, D.G., 1982, Barrier-Island and strand-plain facies: in Scholle, P.A., and D. Spearing, eds., *Sandstone Depositional Environments*: AAPG, p. 247-279.

•Morton, R.A., and J.H. McGowen, 1980, Modern depositional environments of the Texas coast: *Bureau of Eco. Geol. Guidebook* 20, 167 p.

•Neese, K.J., 1984, Stratigraphy of a transgressive barrier island arc (abst.): *AAPG Bull.*, v. 68, p. 511.

Isles Derrieres, Holocene of Louisiana Gulf Coast. 10-13 ft thick.

•Penland, S., R. Boyd, and J.R. Suter, 1988, Transgressive depositional systems of the Mississippi delta plain: a Model for barrier shoreline and shelf sand development: *Jour. Sed. Petrol.* v. 58, p. 932-949.

Three transgressive stages of evolution: 1) erosional headland and flanking barriers, as transgression continues an intradeltaic lagoon forms and the stage 1 sandbody is separated from the shoreline. 2) a transgressive barrier island arc: landward-migrating barrier island arc is unable to keep pace with relative sea level rise and retreating mainland shoreline. This results in 3) inner shelf shoal: as the barrier island arc continues to be reworked into an inner shelf marine sandbody.

•Rampino, M.R., and J.E. Sanders, 1981, Evolution of the barrier islands of southern Long Island, New York: *Sedimentology*, v. 28, p. 37-47.

Holocene transgressive sequence.

•Reading, H.G., ed., 1980, *Sedimentary environments and facies*: Elsevier, New York, p. 152-169.

This is the section of Readings textbook that deals with tidal inlets, tidal deltas, lagoons, transgressive barriers, and ancient beach and barrier facies. Some general comments: The extent to which tidal inlets are developed and maintained in a barrier island is related to the tidal range, and microtidal and mesotidal barriers can be distinguished on this. **Three types of tidal inlet are recognized: overlap, symmetrical, and offset and each type is related to longshore drift characteristics.** Inlets generally range from several hundreds of meters to a few kilometers in width and may be **up to 20m deep**. The updrift bank tends to be constructional and the downdrift (relative to longshore drift) bank tends to be erosional. Dunes and sandwaves that cover the subtidal part of the inlet depositional bank are overlain by a series of wave-induced recurved spits attached to the channel margin.

Inlets can become extremely important because of their tendency to migrate laterally in the direction of longshore drift. The extent to which inlet deposits are developed depends on 1) frequency of inlets along the barrier, 2) rate and consistency of direction of inlet migration, 3) nature of barrier migration, whether transgressive, regressive, or stationary, and 4) rate of barrier migration relative to the rate of inlet migration. Rates of migration of inlets can be extremely high: on Sapelo Island inlet migration has produced a sandbody 1 km long parallel to shoreline and 10-13 km wide normal to the shoreline in 4,000 years. The western tip of Fire Island has migrated 8 km in 115 years at an average rate of 64 m/year.

•Reinson, G.E., 1984, Barrier-island and associated strand-plain systems: in, Walker, R.G., ed., *Facies Models*, Second Edition, Geoscience Canada Reprint Series 1, p. 119-140.

•Richardson, J.G., Sangree, J.B., and R.M. Sneider, 1988, Coastal barrier reservoirs: *Journal of Petroleum Technology*, v. 40, p. 1127-1128

•Swift, D.J.P., 1968, Coastal erosion and transgressive stratigraphy: *Jour. of Geology*, v. 76, p. 444-456.

Study of ravinements in the Bay of Fundy show that they are caused mainly by surf action along a narrow zone at the foot of the shoreface.

•Swift, D.J.P., 1975, Barrier-island genesis: Evidence from the Central Atlantic Shelf, Eastern U.S.A.: *Sedimentary Geology*, v. 14, p. 1-43.

Most barrier systems today appear to have retreated into their present positions from out on the continental shelf. The relative roles of coastwise spit progradation and mainland-beach detachment depend on coastal relief and slope, with steep, ragged coasts favoring spit progradation at the expense of mainland-beach detachment. Since most major barrier systems form on flat coastal plains, it would appear that mainland-beach detachment is the more important mode of barrier formation. During stillstands or periods of reduced rate of sea-level rise coasts can more nearly approach their climax configurations— with straight coasts and well developed shoreface.

## **BIGHORN BASIN, WYOMING-MONTANA**

•Uhlir, D.M., Akers, A., and C.F. Vondra, 1988, Tidal inlet sequence, Sundance Formation (Upper Jurassic), north central Wyoming: *Sedimentology*, v. 35, p. 739-752.

Sandstone and coquinas of uppermost 15-20 m of the Sundance Formation within Bighorn Basin represent deposits of Late Jr. prograding, barrier coastline. Previously proposed offshore sand body models do not explain the conformable relations between Sundance & Morrison formations. Study based on outcrops.

## **BISTI FIELD, NEW MEXICO**

•Curtis, B.F., Kirkbride, R.K., McCabe, W.S., Picard, M.D., and Pritchett, F.J., Jr., 1957, Nature of Rocky Mountain stratigraphic fields: AAPG Bull., v.41, p.813-822.

One of his examples is Bisti Field-in regressive Gallup Sandstone member of Mesaverde Fm. Notes micaceous shales that he interprets as lagoonal or tidal flat deposits. Clean sandstone grades updip into tight shaley lagoonal beds, basinward into marine silty and sandy shales.

•Devlin, F.J., and J.Q. Tomkins, 1957, The Bisti area, San Juan County, New Mexico: Four Corners Geological Society, Geology of SW San Juan Basin, Second Field Conference, p. 152-154.

A short history of Gallup/Tocito production and local stratigraphy.

•McNeal, R.P., 1961, Hydrodynamic entrapment of oil and gas in Bisto Field, San Juan County, New Mexico: AAPG Bull., v.45, p. 315-329.

Field is a series of narrow permeability lenses over 30 miles long. At west end of the field the oil column is more than 365 feet in height, and is sufficient to create cap. pressure of over 52 psi at the updip edge of the accumulation. Entry or threshold pressures for the better sands are about 22 psi. Favorable hydrodynamics is responsible for retaining additional oil that would otherwise have migrated updip.

•Sabins, F.F., Jr., 1963, Anatomy of stratigraphic trap, Bisti Field, New Mexico: AAPG Bull., v. 47, p. 193-228.

Depo history of Bisti field began with regressive deposition interrupted by a pulse of subsidence and possibly a minor unconformity after which the low SP interval was deposited. Wave action winnowed the mud from this sediment and concentrated the sand as a series of bars. A restricted marine environment (lagoon?) existed on the landward side of the bar complex and open marine environment on the seaward side. The abstract does not mention subaerial exposure at any time.

•Tomkins, J.Q., 1957, Bisti Oil Field, San Juan County, New Mexico: AAPG Bull., v. 41, p. 906-922.

Produces from Gallup Sandstone Formation, Mesaverde Group of Upper Cretaceous. Stratigraphic trap. Author identifies reservoir as an offshore sandbar.

•Van Couvering, M., 1958, Geology of southwestern San Juan Basin, by Four Corners Geological Society (Book Review): AAPG Bull., v. 42, p. 1100-1106.

Review mentions a paper about Bisti by Devlin and Tomkins.

## **DAKOTA SANDSTONE**

•Noon, P.L., 1980, Surface to subsurface stratigraphy of the Dakota Sandstone (Cretaceous) and adjacent units along the Eastern flank of the San Juan Basin, New Mexico and Colorado: M.S. Thesis, Bowling Green State Univ.

Deposition of Dakota Sandstone was in response to regional transgression of the Western Interior Sea during Cenomanian time. Within overall transgression there were minor regressions which may have been brought about by local progradation related to increased local sediment supply. The Cubero, Paguete, and Twowells sands were deposited by southward flowing paleocurrents oriented approximately parallel to the shoreline.

The authors environmental interpretations are less than earth shaking. Twowells, Paguate, and Cubero sandstone pods all show coarsening upward patterns on logs. NW trends of Twowells may represent offshore bars derived from a northwestern source, or linear sand shoals derived from shoreface sands.

•Taylor, A.M., 1980, Depositional environments of the Dakota Sandstone in southeastern Colorado: SEPM Field Trip Guidebook, 69 p.

Environmental summary: the Dakota Sandstone is interpreted as a prograding barrier island composed of a beach complex with seaward shoreface, inshore, and offshore deposits and landward marsh-swamp- estuarine deposits. This Barrier Island prograded seaward toward the northeast.

### **EAGLE SANDSTONE, NORTHERN ROCKY MTS.**

•Cobban, W.A., 1955, Cretaceous rocks of northwestern Montana: Billings Geological Society, 6th Annual Field Conference, p. 107-119.

Generally not useful. General stratigraphic nomenclature.

•Shelton, J.S., 1963, Measured sections of sandstones and shales: AAPG Bull., v.47, p. 2047-2050.

Example of graphic core/outcrop facies logging with an example from the Eagle Sandstone at Billings, Mt.

8Shelton, J.S., 1965, Trend and genesis of lowermost sandstone unit of Eagle Sandstone at Billings, Montana: AAPG Bull., v. 51, p. 2441-2461.

Barrier island originated as a bar in over 75 ft water more than 50 miles offshore. Built toward the mainland (transgressive); subaerial part of barrier removed by erosion.

### **ELK CITY FIELD, OKLAHOMA**

•Sneider, R.M., Richardson, F.H., Paynter, D.D., Eddy, R.E., and Wyant, I.A., 1977, Predicting reservoir rock geometry and Continuity in Pennsylvanian reservoirs, Elk City Field, Oklahoma: Jour. of Petroleum Technology, July, 1977, p. 851-866.

### **EMBAYED COASTS- MODELS**

•Roy, P.S., Thom, B.G., and L.D. Wright, 1980, Holocene sequences on an embayed high-energy coast: an evolutionary model: Sedimentary Geology, v. 26, p. 1-19.

Based on Southeastern Australia. Three primary Holocene embayments fills (**valley fills**): 1. open ocean, 2. barrier estuary, 3. drowned river valley.

### **ENVIRONMENTAL DISCRIMINATION-FACIES IDENTIFICATION TECHNIQUES**

•Anderson, J.B., C. Wolfteich, R. Wright, and M.L. Cole, 1982, Determination of depositional environments of sand bodies using vertical grain-size progressions: Gulf Coast Assoc. Geol.Soc. Transactions, v. 32, p. 565-577.

Attempts to distinguish modern fluvial, coastal barrier, and turbidite sands using grain size on two dimensional scatter diagrams yields poor results. Environmental subdivisions were too broad. It was possible to distinguish braided river, alluvial fan, meandering river, coastal barrier, and deep-sea fan sands using vertical progressions of grain size data. Test cases were from sandstones whose depositional setting had been previously established prior to their vertical grain size trend analysis.

## EROSIONAL SURFACES IN CLASTIC FACIES - SEE ALSO 'TRANSGRESSIONS'

•Larue, D.K., and P.A. Martinez, 1989, Use of bed-form climb models to analyze geometry and Preservation potential of clastic facies and erosional surfaces: AAPG Bull., v. 73, p. 40-53.

Authors propose a model that explains how erosion surfaces and vertical sequences of clastic strata are preserved where deposition occurs in channelized or locally erosional environments- including fluvial and submarine-channels, barred beaches, and transgressive (barrier) coastlines.

•Nummedal, D., and D.J.P. Swift, 1987, Transgressive stratigraphy at sequence-bounding unconformities: Some principles derived from Holocene and Cretaceous examples: In Nummedal, D., O.H. Pilkey, and J.D. Howard, eds., Sea-Level Fluctuations and Coastal Evolution, SEPM Special Publication No. 41, p. 241-259.

This paper aids in identifying key stratigraphic boundaries by emphasizing the sedimentology and different patterns of systems stacking above the sequence boundaries.

**Key stratigraphic surfaces** encountered in shallow marine sedimentary sequences are 1) **subaerial unconformities**, erosion by episodes of sea-level fall, and representing a significant hiatal break, and 2) **diastems**, surfaces represent relatively short interruptions in sedimentation. Most diastems in shallow marine and coastal settings are associated with transgressions. Diastems include the **ravinement diastem, which is formed by transgressive shoreface retreat**, channel-base diastems, and various marine erosion diastems.

## FOREIGN BARRIERS

•Bagnoli, E., 1990, The Mossoro Sandstone, Canto Do Amaro oil field, Late Cretaceous of the Potiguar Basin, Brazil: An example of a tidal inlet-channel reservoir (Abst.): In Davis, R.A., Jr., D. Nummedal, and R.W. Tillman, Conveners, Tidal Inlet and Related Sand Bodies: Modern and Ancient: SEPM Research Conference San Juan Basin, New Mexico, May, 1990, pages unnumbered.

Eight lithofacies are associated in inlet channel and flood-tidal delta associations within this field. The vertical sequence of lithofacies suggests that the deposition of the Mossoro Sandstone took place in a tide-dominated transgressive setting. The main reservoir sandstones comprise inlet channel deposits whose characteristics change across the field, suggesting decreased depositional energy from ENE to WSW.

Although diagenesis has significantly modified the amount and geometry of the pore spaces, it is the depositional environment that controls the porosity and permeability. The coarser lithofacies deposited by high energy processes are more porous and permeable than fine-grained lithofacies deposited by lower energy processes.

•Czapowski, G., 1984, "Upper Miocene barrier sediments in southern margin of the Holy Cross Mountains" (in Polish): Przegląd Geologiczny, 1984, No. 4, p. 185-194.

Regressive barrier island and associated facies identified: open marine, barrier zone, main barrier body, barrier flat and inlet, and lagoon/embayment.

## FOX HILLS SANDSTONE, ROCK SPRINGS UPLIFT, WYOMING

•Land, C.B. Jr., 1972, Stratigraphy of Fox Hills Sandstone and associated formations, Rock Springs Uplift and Wamsutter Arch area, Sweetwater County, Wyoming: A shoreline-estuary sandstone Model for the Late Cretaceous: Quarterly of the Colorado School of Mines, v. 67, No. 2, 69 p.

Upper Cretaceous Fox Hills Sandstone **outcrops** on the east flank of the Rock Springs Uplift is a regressive sequence of sandstone and siltstone which was deposited along a barrier island coastline in littoral, shallow neritic, and estuarine environments. It overlies and intertongues with marine Lewis Shale; and it is overlain by, and intertongues with the nonmarine Lance Formation.

Depositional Environments: Earlier report by Weimer interpreted the Fox Hills as a barrier island sequence similar to the modern barriers along the Gulf Coast. Weimer interpreted the shoreline to have been generally north-south oriented with lagoons and coastal swamps to the west and a deeper neritic environment to the east. Land is generally in agreement (p. 55) but points out some minor differences of interpretation:

1. Sands were deposited in migrating estuaries was important in Fox Hills. Scour at base of Weimers upper "G" sandstone is base of migrating estuary channel.
2. Lenses of *Ostrea* are reinterpreted as lag deposits in estuary channels.
3. Subsequent subsurface control indicates that shoreline trend is northeast-southwest.
4. Weimer (1961) compared Fox Hills environments to the Gulf Coast Barriers- where the barriers are separated by broad lagoons which are filling with clay and silt deposits. Land finds better analogy with the modern Georgia coast (brought to his attention by Weimer). Georgia coast has about 7 ft tides and the barrier chain is separated from the mainland by a saltmarsh-estuary channel complex. The high-energy environments of sand deposition in these estuaries is believed to be similar to the postulated Fox Hills environments.

#### **FRIO FORMATION, TEXAS GULF COASTAL BASIN**

•Galloway, W.E., D.K Hobday, and K. Magara, 1982, Frio Formation of the Texas Gulf Coast Basin- Depositional systems, structural framework, and hydrocarbon origin, migration, and exploration potential: Bur. Economic Geology, The University of Texas at Austin, Report of Investigations No. 122, 78 p.

The Frio Formation is one of the major Tertiary progradational wedges of the Texas Gulf Coast Basin and has yielded nearly 6 billion bbl of oil and 60 tcf gas. The Frio and its updip equivalent, the Catahoula Formation, consist of deposits of two large fluvial and associated deltaic systems centered in the Houston and Rio Grande Embayments. **These two major deltaic depocenters are separated by a vertically stacked, strike-parallel barrier and strandplain system.** Underlying, interbedded, and transgressive shelf, prodelta, and continental slope mudstone sequences provide principal source and sealing facies. Sparse organic geochemical data and regional thermal and compaction-history analyses show that large volumes of hydrocarbons have probably been generated within, and effectively expelled upward and landward from, normally to moderately undercompacted sequences of these mudstone facies.

**Two strandplain/barrier systems listed include 1) Buna, and 2) Greta/Carancahua. Within both of these systems vertical upbuilding of sands was the main depositional pattern.**

Greta/Canancahua barrier/strandplain system comprises a linear sandstone belt separating marine from brackish-water shales and extends from Nueces Co. in the west, where it is gradational with the Norias delta system, to the Houston delta system in the east.

**Massive, blocky, stacked barrier and strandplain sandstones dominate intervals of as much as 4,000 ft.** Shoreline conditions remained remarkably uniform during lower and middle Frio deposition. **To the south, a wave-dominated barrier coast, probably resembling the Padre/Mustang/Matagorda complex of modern Texas islands, underwent significant aggradation.** Northward, many small streams supplied sediment directly into the gulf, where sands were combined with strike-reworked sediment to form a complex assemblage of strandplain and delta-destructural facies. Large proportions of these barrier sands were preserved during ensuing transgressions because of continued subsidence. The lenticular and tongue-shaped sands along the landward margin of the Frio barrier trend are probably stacked washover-fan and flood-tidal-delta deposits.

•Galloway, W.A., 1986, Reservoir facies architecture of microtidal barrier system: AAPG Bull, v. 70, no. 7, p.787-808.

The first part of the paper is a good review of the geometry and occurrence of modern barriers. Paper discusses West Ranch Field, Texas.

### **GALLUP SANDSTONE, SAN JUAN BASIN AREA, NEW MEXICO**

•Beaumont, E.C., 1957, The Gallup Sandstone as exposed in the Western part of the San Juan Basin: Four Corners Geological Society, Geology of SW San Juan Basin, Second Field Conference, p. 114-120.

•Budd, H., 1957, Facies Development of the Gallup Formation: Four Corners Geological Society, Geology of SW San Juan Basin, Second Field Conference, p. 121-127.

Brief description of upper Cretaceous Gallup gradation from a porous massive sandstone on the southwest flank to a black calcareous shale on the northeast side of the San Juan Basin.

•Campbell, C.V., 1979, Model for beach shoreline in Gallup Sandstone (Upper Cretaceous) of northwestern New Mexico: New Mexico Bureau of Mines and Mineral Resources, Circular 164, 32 p.

This model includes a lower regressive beach sandstone overlain unconformably by an upper transgressive offshore-bar sandstone. Landward, the beach sandstones interfingers with coal-swamp deposits or is truncated and overlain by dune sandstones. Seaward, the beach sandstones grades through shoreface sandstones into a transition zone that gives way to offshore siltstone and mudstone. Offshore siltstone and mudstone overlie and, in part, grade laterally into offshore-bar sandstone which has no contiguous landward equivalents and transgresses all beach and related facies.

The author may have confused ancient barrier and offshore bar environments based on his citations of the literature. No mention of Tocito Sandstone is made.

•King, V.L., and S.A. Wengerd, 1957, The Hospah oil field, McKinley County, New Mexico: Four Corners Geological Society, Geology of SW San Juan Basin, Second Field Conference, p. 155-168.

Good summary of history of exploration, regional stratigraphy, structure, and production from the field. Production is from Hospah Upper Gallup interval, on a combination stratigraphic -structural trap. Hydrodynamic drive is strong in this field.

•Matheny, M.L., and D.M. Thomas, Jr., 1957, The Gallegos-Gallup field, San Juan County, New Mexico: Four Corners Geological Society, Geology of SW San Juan Basin, Second Field Conference, p. 147-151.

Gallegos-Gallup field is a stratigraphic oil field with updip gas cap. Production is primarily from fractures in siltstones and shaley sandstones of Gallup.

•Molenaar, C.M., 1973, Sedimentary facies and correlation of the Gallup Sandstone and associated formation, northwestern New Mexico: Four Corners Geological Society Memoir Book, p. 85-110.

The Upper Cretaceous Gallup Sandstone is regressive clastic wedge that prograded about halfway across the San Juan Basin from sources in southwestern Arizona. Numerous closely spaced outcrop sections were used to determine details of correlations of the complex of marine coastal barrier sandstones and associated nonmarine paludal mudstones, coal beds and fluvial channel sandstones that comprise the formation.

Useful discussion of barrier facies: lower shoreface, upper shoreface, and foreshore. Vertical succession in their fig.3 is classical coarsening upward barrier with root-mottled zone at top (barrier island).

•Speer, W.R., 1957, Verde-Gallup Pool, San Juan County, New Mexico: Four Corners Geological Society, Geology of SW San Juan Basin, Second Field Conference, p. 141-146.

Verde-Gallup pool produces oil from fractures within the final regressive phase of the Lower Gallup sandstone and shale interval. (This is probably Tocito?)

•Valasek, D.W., 1990, Compartmentalization of shoreface sequences in the Cretaceous Gallup Sandstone west of Shiprock New Mexico: Implications for the position of tidal deposits in the rock record (Abst.): In Davis, R.A., Jr., D. Nummedal, and R.W. Tillman, Conveners, Tidal Inlet and Related Sand Bodies: Modern and Ancient: SEPM Research Conference San Juan Basin, New Mexico, May, 1990, pages unnumbered.

Cretaceous Gallup Sandstone exposed west of Shiprock, New Mexico, is a seaward-stepping progradational unit capped by a transgressive sequence. The seaward progradational event is divided into eleven one to three km wide compartments bounded by time significant surfaces. Compartments are further divided into 0.1 to 0.5 km wide sub-compartments termed shingles. A wave to tidal dominated facies transition occurs within compartments.

The transgressive sequence (Tocito) is composed of thick clastic tidal deposits. Common sedimentary structures include double mud drapes, reactivation surfaces, dewatering structures, sigmoidal laminations and occupied an estuarine setting at the most seaward extension of the shoreline upon initial transgression. The tidal deposits thin and are transitionally replaced by bioturbated clastic shelf deposits landward.

## **GREATER GREEN RIVER BASIN**

•Annon., 1973, Oil Characteristics in the Greater Green River Basin: Wyo. Geol. Assoc. Guidebook, 25th Field Conf., p. 12-18.

•Hawkins, C.M., 1980, Barrier bar sands in the Second Frontier Formation, Green River Basin, Wyoming: Stratigraphy of Wyoming: 31st Ann. Wyo. Geol. Assoc. Field Conf. Guidebook, p. 155-161.

Based on logs and core cuttings from the gas productive area on the crest and flanks of the Moxa Arch at 7-12,000 ft. Interprets a classical upward coarsening, marine, shoreface, foreshore, dune, lagoonal package. This was a subsurface study of a gas productive barrier.

•Krueger, M.L., 1960, Occurrence of natural gas in the western part of Green River Basin: Wyo. Geol. Assoc. 15th Annual Field Conference Guidebook, Overthrust Belt of Southwestern Wyoming and Adjacent Areas, p. 195-209.

Green River Basin is one of the largest of the Rocky Mountain intermountain basins. Its maximum N-S dimension is approximately 180 miles, its maximum E-W dimension, near its southern end is 90 miles. The basin is bounded on the northeast by the Gros Ventre-Wind River Mountain Range, on the east by the Rock Springs Uplift, on the south by the east-west trending Uinta Mountains, and on the west by the east thrust front (Disturbed Belt) of the Hoback-Wyoming Range.

•Law, B.E., C.W. Spencer, and N.H. Bostick, 1980, Evaluation of organic matter, subsurface temperature and pressure with regard to gas generation in low- permeability Upper Cretaceous and lower Tertiary sandstones in Pacific Creek area, Sublette and Sweetwater counties, Wyoming: The Mountain Geologist, v. 17, p. 23-35.

The area for this report is 35 mi directly north of the Rock Springs Uplift. Onset of overpressuring occurs about 11,600 ft, at the base of the Upper Cretaceous Lance Formation. Generation of wet gas is apparently one of the main processes related to overpressuring. Reversal of SP curves near the top of overpressuring the authors believe is related to reduction of formation water salinity. **Small amounts of water produced during thermochemical decomposition of organic matter and the**

**dehydration of clays during clay transformation may provide enough low-salinity water to effectively dilute the original formation water.**

TOC averages 1.38% (range 0.25-7.84). Top of overpressuring and beginning of important wet-gas generation occurs at vitrinite reflectance values of 0.74-0.86.

•McDonald, R.E., 1973, Big Piney-La Barge Producing Complex, Sublette and Lincoln Counties, Wyoming: Wyoming Geol. Assoc., 25th Field Conf., p. 57-77.

Gas producer since 1956, major oil producer since 1960. Cumulative gas production over 1.2 tcf, total oil produced is about 65 mm bbl. Producing complex on and around the flanks of a Laramide anticlinal fold that was formed subjacent to a salient along the Disturbed Belt, west of Wind River Mts., in the northern part of the Green River Basin.

•Myers, R.C., 1977, Stratigraphy of the Frontier Formation (Upper Cretaceous), Kemmerer Area, Lincoln County, Wyoming: Wyo. Geol. Assoc. Guidebook, 25th Annual Field Conference, P. 271-292.

Turonian age---Older than Almond formation, the Frontier formation on the west side of the Green River Basin, WY., is a nearshore sequence of marine and nonmarine bentonites, shales, siltstones, sandstones, conglomerates, and coals. These strata represent two cycles of clastic shoreline progradation along the western fringe of the Cretaceous Seaway in the Western Interior of the US.

•Newman, H.E., 1981, Greater Green River Basin stratigraphy as it relates to natural gas potential: SPE/DOE 9845, Presented at SPE/DOE Low Perm. Symposium, Denver.

•Ritzma, H.R., 1955, Late Cretaceous and Early Cenozoic structural pattern, southern Rock Springs Uplift, Wyoming: Wyo. Geol. Assoc. 10th Annual Field Conference Guidebook, Green River Basin, p.135-137.

•Roehler, H.W., 1965, Summary of Pre-Laramide Late Cretaceous sedimentation in the Rock Springs Uplift area: Wyo. Geol. Assoc. 19th Field Conference Guidebook, Sedimentation of Late Cretaceous and Tertiary Outcrops, Rock Springs Uplift, p. 11-12.

•Stuart, W.J., Jr., 1965, Stratigraphy of the Green River Formation, West of the Rock Springs Uplift: Wyo. Geol. Assoc., 19th Field Conf. Guidebook, p. 159-166.

Based on exposures in the Green River Formation and equivalent tongues of the Wasatch Formation located the ENE margin of the 'Bridger Basin.'

•Thomas, G.E., 1973, Evanston Lineament Green River Basin, Wyoming: Wyo. Geol. Assoc. 25th Annual Field Conference Guidebook, Symposium and Core Seminar on the Geology and Mineral Resources of the Greater Green River Basin, p. 93-95.

•Wach, P.H., 1977, The Moxa Arch, an overthrust model?: Wyo. Geol. Assoc. Guidebook, 29th Annual Field Conf., p. 651-664.

Moxa Arch is a major N-S structural feature extending from Bridger Lake where it is over ridden by the North Uinta Thrust Fault, to at least the Big Piney-La Barge Platform, where it becomes lost in thrust faulting and attendant strike-slip faulting. Moxa Arch may serve as a model for buried or scalped arches in the Overthrust Belt.

•Winn, R.D., Jr., S.A. Stonecipher, and M.G. Bishop, 1984, Sorting and wave abrasion: Controls on composition and diagenesis in Lower Frontier sandstones, Southwestern Wyoming: AAPG Bull., v. 68, p. 268-284.

See discussion under "Petrography" heading.

## **HETEROGENEITY**

•Lewis, J.J.M., 1988, Outcrop-derived quantitative models of permeability heterogeneity for genetically different sand bodies: SPE paper 18153, Presented at the 63rd Annual Technical Conference and Exhibition, Houston, TX., p. 449-457.

## **LIVINGSTON FIELD, LOUISIANA**

•Johnston, D.D., and Johnson, R.J., 1987, Depositional and diagenetic controls on reservoir quality in First Wilcox Sandstone, Livingston Field, Louisiana: AAPG Bull., v. 71, p. 1152-1161.

Marine channel and barrier island. Barrier island deposit is 40-50 ft thick, at 9,917-10146 ft subsea. Reservoir quality is a direct result of diagenetic events that were strongly influenced by depositional facies. Early porosity was significantly reduced by authigenic clay, quartz, and carbonates. Dissolution of carbonates, feldspar, and labile rock fragments restored porosity to 65-75% of original values. Highest degree of secondary porosity was created in facies that had highest primary porosity. Late stage diagenetic clays have reduced permeability by blocking or reducing pore-throat openings.

## **LOCKHART CROSSING FIELD, SOUTHEASTERN LOUISIANA**

•Self, G.A., et al., 1986, Lockhart Crossing Field: New Wilcox trend in southeastern Louisiana: AAPG Bull., v. 70, p. 501-515.

Main reservoir is from a 40-80 ft Eocene marine sandstone. Dominant facies is a sequence of upward-coarsening very fine to fine-grained glauconitic sandstone deposited as a nearshore marine bar. Associated is a younger fining upward channel fill sequence. Primarily a structural field.

## **MESAVERDE GROUP--STRATIGRAPHY**

•Douglass, W.B., Jr., and T.R. Blazzard, 1961, Facies relationships of the Blair, Rock Springs and Ericson formations of the Rock Springs Uplift and Washakie Basin: Wyo. Geol. Assoc., 16th Annual Field Conf. Guidebook, p. 81-86.

Paper suggests revisions for nomenclature in the Rock Springs Uplift: rocks formerly correlated with the Rock Springs Formation are shown to be laterally equivalent with the Ericson Formation. From bottom to top the formations of the Mesaverde Group are Blair, Rock Springs, Ericson and Almond.

•Gosar, A.J., and J.C. Hopkins, 1969, Structure and stratigraphy of the southwest portion of the Rock Springs Uplift, Sweetwater County, Wyoming: in Lindsay, J.B., ed., Geologic Guidebook of the Uinta Mountains, Utah's Maverick Range, 16th Annual Field Conference, Intermountain Association of Geologists, p. 87-90

## **MUDDY SANDSTONE, INCLUDING BELL CREEK**

•Almon, W.R., and Davies, D.K., 1979, Regional diagenetic trends in the lower Cretaceous Muddy Sandstone, Powder River Basin: SEPM Special Pub No. 26, p. 379-400.

•Berg, R.R., and Davies, D.K., 1968, Origin of lower Cretaceous Muddy Sandstone at Bell Creek Field, Montana: AAPG Bull., v. 52, p. 1888-1898.

•Davies, D.K., and Etheridge, F.G., 1975, Sandstone composition and depositional environment: AAPG Bull., v. 59, p. 239-264.

Environmentally produced compositional changes are process dependent and are closely related to textural variations. Environmental imprint is recorded in relative abundance and size of individual detrital minerals. Example from Bell Creek.

•Gardner, M.H., and E.R. Gustason., 1987, Valley-fill sequences and onlap geometries, Lower Cretaceous Muddy Sandstone, Kitty Field, Powder River Basin, Wyoming (abst.): AAPG. Bull., v. 71, p. 558.

•Gustason, E.R., T.A. Ryer, and S.K. Odland, 1988, Stratigraphy and depositional environments of the Muddy Sandstone, Northwestern Black Hills, Wyoming: Wyoming Geol. Assoc., Early Science Bull., v. 20, p. 49-60.

These authors have a very different view of the Muddy sandstone as compared with the NIPER interpretation. They do not feel that the Muddy at Bell Creek field is a barrier island at all. They interpret the Muddy at Bell Creek field as a topographic feature formed during prolonged subaerial erosion of a once widespread regressive sand sheet.

•McGregor, A.A., and C.A. Biggs, 1968, Bell Creek field, Montana: A rich stratigraphic trap: AAPG Bull., v. 52, p. 1869-1887.

•Meyer, H.J., and H.W. McGee, 1985, Oil and gas fields accompanied by geothermal anomalies in Rocky Mountain region: AAPG Bull., v. 69, p. 933-945.

Principal cause for temperature gradient anomalies over oil and gas fields is lateral and upward movement of hot fluids (water). Cites Bell Creek as an example.

•Tillman, R.W., 1990, Sequence stratigraphy and sedimentology of non-tidal-inlet "channels" through a barrier island, Bell Creek field, Montana (Abst.): In Davis, R.A., Jr., D. Nummedal, and R.W. Tillman, Conveners, Tidal Inlet and Related Sand Bodies: Modern and Ancient: SEPM Research Conference San Juan Basin, New Mexico, May, 1990, pages unnumbered.

Only a single barrier was deposited in the area designated as production Units A and B. During a post barrier drop in sea level several narrow, possibly dendritic, valleys were cut into and locally entirely through the barrier island. These relationships are indicated by:

1. Ability to correlate barrier facies and thicknesses on either side of the valleys.
2. The fill of the valleys varies, bottom to top from continental to shallow marine.
3. Secondary clays formed as part of an inferred soil zone below an unconformity surface which separates the barrier island sandstones and the valley fill sandstones, siltstones, and shales.
4. Dendritic valleys which cut the barrier island may be connected to a larger valley system recognized over a large portion of the northern Powder River Basin in NE Wyoming.
5. Some valleys are entirely filled with marine shales.

Two periods of post-barrier erosion and sandstone and shale valley-fill are postulated to result from two falls in relative sea level. Earlier valley incisions are broad and relatively shallow and commonly involve erosion of only the top of the barrier. Younger valley fill deposits along the northwest side of Unit A are 30 ft thick where erosion has cut completely through the barrier island and the valleys are filled with marine shale.

One unconformity, interpreted to be a sequence boundary, occurs below the Muddy Sandstone barrier island and it separates back barrier and other facies of the barrier island from the underlying Albian marine Skull Creek Shale. A second sequence boundary occurs between the valley fill and the underlying barrier. No true barrier inlet fills are recognized in the portion of the field designated as Units A and B.

•Weimer, R.J., C.A. Rebne, and T.L. Davis, 1988, Geologic and seismic models, Muddy Sandstone, Lower Cretaceous, Bell Creek-Rocky Point area, Powder River Basin, Montana and Wyoming: Wyoming Geol. Assoc. 39th Field Conference Guidebook, Eastern Powder River Basin-Black Hills, p. 161-177.

The Muddy Sandstone in the northern Powder River Basin consists of two genetic units (members) that are separated by a widespread subaerial surface of erosion. The older sandstone member, comprising the reservoir rock at Bell Creek field, was deposited in shoreline and associated nearshore marine environments. The younger member is a valley fill deposit of fluvial, estuarine and tidal flat environments.

Deposition and distribution of these two genetic units was controlled primarily by relative sea level changes. The Bell Creek sandstone (the older unit) was deposited as a widespread regressive sandstone during a high stand of sea level. A following sea level lowstand caused valley cutting, erosion of all or portions of the Bell Creek sandstone, and paleosoil development causing early diagenesis. A rising sea level resulted in valley filling (the younger unit), coastal onlap and a transgressive surface of erosion that is overlain by black marine shale.

Recurrent movement on basement-controlled fault blocks appears to have controlled distribution of the Muddy members, drainage incision patterns, present structure and heat flow, and possibly petroleum migration.

Seismic modelling indicates that it is possible to seismically distinguish Muddy facies changes. A strong Muddy amplitude is associated with a thick valley fill facies, while a low amplitude corresponds to the Bell Creek sandstone.

•Weimer, R.J., J.J. Emme, C.L. Farmer, L.O. Anna, T.L. Davis, and R.I. Kidney, 1982, Tectonic influence on sedimentation, Early Cretaceous, east flank Powder River Basin, Wyoming and South Dakota: Quarterly of Colo. School of Mines, v. 77, no. 4.

#### **NEW MEXICO-GENERAL, CENTRAL**

•Hook, S.C., 1983, Stratigraphy, paleontology, depositional framework, and nomenclature of marine Upper Cretaceous rocks, Socorro County, New Mexico: 34th Annual New Mexico Geol. Soc. Field Conference Guidebook, p. 165-172.

Barriers are present in the following: (1) Atarque Sandstone member of Tres Hermanos formation is regressive coastal-barrier or shoreface complex. It was deposited along a low energy shoreline-wave energy was not great; tidal currents were important depositional agents. (2) The Fite Ranch Sandstone member of the Tres Hermanos formation is a well-developed coastal barrier sandstone with an upward coarsening sequence. (3) The Gallup Sandstone consists of a series of northeast prograding coastal-barrier or delta-front sandstones that grade seaward into the Mancos Shale, and intertongue landward with nonmarine coastal deposits. This study was based on outcrops, paleontology, and field mapping.

•Kirk, C.L., Montgomery, E.B., Knapp, R., Dow, R., Lukas, J.R., and K.A. Barrie, 1983, Bibliography of Theses and dissertations on New Mexico, 1968-1982: Mountain Geologist, v. 20, no. 2, p. 63-81.

Listed alphabetical by author.

•Ridgley, J.L., 1977, Stratigraphy and depositional environments of Jurassic-Cretaceous sedimentary rocks in the southwest part of the **Chama Basin**, New Mexico: New Mexico Geol. Soc. Guidebook, 28th Field Conf., San Juan Basin III, p. 153-158.

Environments of deposition in this area: Entrada Sandstone-eolian; Todilto Limestone-lacustrine; Morrison formation, a variety of continental fluvial and lacustrine environments. Burro Canyon(?) formation, a series of high-energy braided to meandering streams. Dakota Sandstone, basal part-dominantly fluvial, middle unit-fluvial and shallow marine, upper unit-a variety of near-shore littoral environments as the sea transgressed toward the south-southwest.

## OVERTHRUST BELT- STRATIGRAPHIC NAMES OF THE AREA

•Olson, G., 1977, Catalog of Jurassic, Cretaceous and Tertiary Rock Names for the Overthrust Belt and vicinity: Wyo. Geol. Assoc. Guidebook, 29th Annual Field Conf., p. 91-99.

•Pattison, L., 1977, Catalog of Triassic, Permian and Paleozoic Rock names for the overthrust Belt and vicinity: Wyo. Geol. Assoc. Guidebook, 29th Annual Field Conf., p. 81-90.

## PETROGRAPHY

•Cant, D.J., 1986, Diagenetic traps in sandstones: AAPG Bull., v. 70, p. 155-160.

Formation of diagenetic traps requires that parts of the sandstones react differently from one another. This can be caused by differences in 1) detrital mineralogy (depositional control), 2) early diagenetic mineralogy (largely controlled by depositional environment), 3) burial history, and 4) fluid content. Each of these factors can lead to differences in porosity and permeability of the sandstone sufficient to form reservoirs and seals.

•Jacka, A.D., 1970, Principles of cementation and porosity-occlusion in Upper Cretaceous sandstones, Rocky Mountain Region: Wyo. Geol. Assoc, 22nd Annu. Field Conference Guidebook, p. 265-285.

Upper Cretaceous sediments from the Rockies were chosen because they constitute good models for humid-subhumid climates, swampy coastal plain, barrier island-lagoon-bay, and deltaic facies with established structural and geological histories, and outcrops and subsurface data which may be compared.

Vadose cementation is restricted to hot arid and semi-arid regions where carbonate (caliche) is concentrated, and hot regions with wet-seasons. Rapid evaporation-triggered precipitation of carbonates, hydroxides, and oxides results in initial precipitation of finely crystalline **grain coating cement** films, which separate grains, causing an expanded or floating fabric, and which later replace terrigenous grains to form concretions.

Cementation below the water table in fresh or sea water occurs slowly resulting in coarsely crystalline cement that **tends to fill pore bodies**. Soon afterward, burial silica is precipitated as syntaxial overgrowths on quartz grains at shallow to moderate depths under conditions of low temperature, and slightly acid pH. At greater depths silica cementation is followed by calcite precipitation and replacement of quartz under higher temperature and pH. Silica mobilized at depth by replacement and solution of quartz, diffuses upward and carbonate diffuses downward where it precipitates on prior calcite "seeds".

Transportation of cementing material by opposing diffusion gradients, slowly through nearly static interstitial waters overcomes inadequacies inherent in supposition of transport by abnormally large volumes of water (as required by water from compacting clays).

•Keighin, C. Wm, B.E. Law, and R.M. Pollastro, 1989, Petrology and reservoir characteristics of the Almond Formation, Greater Green River Basin, Wyoming: in Coalson, E.B., et al, (eds), Petrogenesis and Petrophysics of Selected Sandstone Reservoirs of the Rocky Mountain Region, RMAG, Denver, p. 281-298.

Production through 1986 was 100 MM bbl. oil and 07 TCF gas. SEM and thin section analysis indicate that pores in fine to very fine Almond formation sandstones are small ( $< 20\mu$ ) and formed in part by dissolution of framework grains and authigenic cements. Intergranular micropores occur between crystals of authigenic clay. **The sandstone contains 15-30% clay, which is dominantly illitic. Local concentrations of kaollinite occur, but chlorite is rare. Smectite clay minerals were not detected.** Distribution of cements, as well as detrital feldspars, is variable.

Not only porosity, permeability, and depth, but also vitrinite reflectance seem to be related in both conventional and unconventional (tight) Almond reservoirs. It may be possible to define an approximate depth at which **overpressuring** may occur based on these data.

•Lanham, R.E., 1980, Petrography and diagenesis of low-permeability sandstones of the lower Almond Formation, Southwestern Wyoming: M.S. Thesis, Univ. of Colorado, 113 p.

Petrographic study of the lower Almond sandstones in the Tierney Gas Field, in the Wamsutter Arch area of southwestern Wyoming; the sandstones are fine grained sublitharenites containing chert fragments and little or no feldspar. Sandstones average 9% porosity and have very low permeabilities, averaging 0.10 md. Compaction and quartz cementation have reduced both  $k$  and  $\phi$ ; dissolution of unstable minerals has created varying amounts of secondary porosity.

Quartz cement averages 15% of rock volume and has inhibited compaction, but also occluded much porosity and has reduced permeability. In many instances cementation by quartz was hindered by detrital and authigenic clays. Where clay is common quartz cement is less abundant and intergranular microporosity is widespread.

Based on thin section analysis up to one-half of existing porosity of some sandstones is secondary, having been formed by dissolution of detrital and authigenic minerals. Much of the porosity was created by dissolution of siderite and possibly dolomite-ankerite. Some of the resulting pores were subsequently filled by authigenic quartz and kaolinite. (A complete solid solution between dolomite and ankerite appears to exist). Dissolution of chert grains also appears to have created a significant amount of secondary porosity. Chert dissolution first produces a microporous mass, but with continued leaching results in grain-size voids. Leaching of biotite and possibly feldspar created minor amounts of secondary porosity. Formation of secondary porosity was hindered by the presence of matrix, which inhibited access of leaching fluids to potentially soluble minerals. Good photomicrographs and SEM images.

•Pryor, W.A., 1961, Petrography of Mesaverde sandstones in Wyoming: Wyo. Geol. Assoc., 16th Annual Field Conf. Guidebook, p. 34-46.

This study was based on a systematic sampling of outcrops from uppermost, middle, and lower sandstone bodies in the Mesaverde section, from a number of formations including the Almond. Textural classification of Almond as a lithic graywacke (immature chert arenite) with 25% chert: Q58, F12, R30. Heavy minerals comprise less than 0.8% by weight of Mesaverde sandstone samples. Much of the report dwells on species and interpretation of heavy minerals (typical of many 1950-1960 petrography reports).

•Siever, R., 1983, Burial history and diagenetic reaction kinetics: AAPG Bull., v. 67, no. 4, p. 684-691.

This paper investigates the relations among burial histories deduced from stratigraphy, thermal regimes imposed by tectonic and sedimentation diagrams, plots of burial with respect to the sediment-water or sediment-air interface as a function of time since deposition. Paleogeotherms are estimated using assumptions about heat flow, thermal conductivities, compaction and cementation effects on porosity, and convecting formation waters. From these, one can deduce the temperature history of a sediment as a function of postdepositional time. This parameter (temperature as a function of time) is the relevant parameter for reaction kinetics. Deductions about when a sediment would have had sufficient time/temperature to accomplish a given reaction can then be compared with petrologic information on the time of origin of the given diagenetic phase.

•Thomas, J.B., 1978, Diagenetic sequences in low-permeability argillaceous sandstones: Journal of the Geological Society of London, v. 135, p. 93-99.

Based on Cretaceous sandstones from the Rockies, a regular sequence of mineral paragenesis is observed in low permeability sands. Diagenetic sequences in the coarser sandstones do not match the order of free energies of formation. This implies that early precipitation in very fine-grained sandstones probably occurs under nearly static conditions, whereas constant fluid throughput in coarser grained rocks

leads to a markedly different diagenetic sequence. Thus two potential sandstone reservoirs, one coarse and one very fine, commonly will have different authigenic mineral suites though their original pore waters were broadly identical.

The author uses examples from the Almond Formation; contrasts upper Almond (coarser, cleaner) with lower Almond (finer grained, tighter).

•Weaver, C.E., 1961, Clay mineralogy of the Later Cretaceous rocks of the Washakie Basin, Wyoming: Wyoming Geol. Assoc. 16th Annual Field Trip Guidebook, Symposium of Late Cretaceous Rocks, p. 148-154.

This is one of the earliest papers dealing with the subsurface mineralogy of the Mesaverde Group. Used XRD analyses of the clay size fraction of well cutting from Upper Cretaceous rocks in the Washakie Basin to determine that clay minerals in the Almond Formation are comprised of kaolinite, montmorillonite, chlorite, illite, and mixed-layer illite-montmorillonite. He reported that montmorillonite (smectite) does not occur at depths greater than 10,000 ft because of its presumable conversion to mixed-layer illite-montmorillonite. Weaver did not attempt to distinguish authigenic from detrital clays, but mentioned that some of the kaolinite might be of diagenetic origin.

•Wilson, M.D., and E.D. Pittman, 1977, Authigenic clays in sandstones: Recognition and influence on reservoir properties and paleoenvironmental analysis: J. Sed. Petrol., v. 47, p. 3-31.

Authigenic clays occur as pore linings, pore fillings, pseudomorphous replacements, and fracture fillings. Sandstones also contain detrital clays and clay clasts/grains. Authigenic origin can be established on the basis of clay composition, structure, morphology and distribution, and sandstone textural properties. No individual criterion is an infallible indicator of authigenic origin. The most reliable criteria include a) delicacy of clay morphology, b) clay as pore linings, absent only at grain contacts, c) composition radically different than associated detrital clay. Distinction between authigenic and detrital clays is difficult if recrystallized or if deformed by burial/tectonism.

Each of the major clay groups has distinctive morphologies: Smectite occurs as highly wrinkled or honeycomb-like pore linings, with individual flakes not resolvable. Illite forms pore lining overlapping flakes whose edges tend to curl away from the grain surface and from highly elongate lath like projections. Mixed layer smectite/illite morphologies resemble both smectite and illite. Chlorite occurs primarily as pore-lining pseudo-hexagonal flakes with a cardhouse, honeycomb, or rosette arrangement. Kaolinite and dickite have stacks of pseudo-hexagonal flakes.

•Winn, R.D., Jr., S.A. Stonecipher, and M.G. Bishop, 1984, Sorting and wave abrasion: Controls on composition and diagenesis in Lower Frontier sandstones, Southwestern Wyoming: AAPG Bull., v. 68, p. 268-284.

The lower Frontier Sandstone on Moxa Arch was deposited in wave-dominated, multi-river delta plain which prograded eastward into the Cretaceous Interior Seaway. Depositional hydrodynamics largely controlled diagenesis. **Fluvial sandstones contain a greater percentage of rock fragments and have less quartz than equivalent marine sandstones owing to the combined effects of sorting and wave abrasion.** The coarsest sands and gravels, which were trapped on the delta plain, were initially richer in rock fragments than finer-grained sands that were passed to the shoreline. These latter sands had a significant portion of unstable grains, including chert, destroyed by wave abrasion. Quartz-rich permeable marine sandstones were cemented early by silica (which preferentially formed as monocrystalline quartz), whereas primary porosity in quartz-poor fluvial sandstones was largely preserved through this stage. Fluvial sandstones were affected more by grain dissolution, calcite replacement, calcite precipitation in open pores, and by subsequent carbonate dissolution. Fluvial sandstones generally have the best porosity and permeability mostly due to creation of secondary porosity. Compaction in finer-grained sandstones destroyed permeability by squeezing clays into open spaces. Other major diagenetic processes are late-stage growth of kaolinite and continued precipitation of silica.

## **POWDER RIVER BASIN (EXCLUDING MUDDY SANDSTONE)**

•Sabins, F.F., and F.A. Petersen, 1961, Geology and petrography of Dead Horse Creek and Barber Creek fields: Wyoming Geol. Assoc. Guidebook, Symposium on Late Cretaceous Rocks Wyoming and Adjacent Areas, 16th Ann. Field Conf., p. 301-309.

Oil production is from the Ferguson and Parkman sands. Ferguson is a stratigraphic trap due to updip pinchout into shale. Called a linear bar; sandstone is regressive marine; contour maps are definitely elongate. No further depositional information available.

## **RECOGNITION OF ANCIENT BARRIER COASTLINES**

•Dickinson, K.D., Berryhill, H.L., Jr., and Holmes, C.W., 1972, Criteria for recognizing ancient barrier coastlines: In, Rigby, J.K., and W. K. Hamblin, eds., Recognition of Ancient Sedimentary Environments, SEPM Spec. Pub No. 16, p. 192-214.

This appears to be **one of the best relatively 'early' papers that describe modern barrier coastline attributes** (eg. facies, geometry, physiography, and fauna, internal structure of the sand bodies) as well as the ancient barriers. Numerous **examples of ancient barrier islands** cited and referenced including those from Bisti field (Gallup Sandstone), Eagle Sandstone (Montana), Bell Creek field (Muddy Sandstone), Bartlesville shoestring sands (Kansas), and ancient Gulf Coast barriers.

### **ROCKY MOUNTAIN BASINS-GENERAL**

•Baars, D.L., and 15 others, 1988, Chapter 8. Basins of the Rocky Mountain region: in Sloss, L.L., ed., Sedimentary Cover--North American Craton; U.S.: Boulder, Colorado, Geological Society of America, The Geology of North America, v. D-2, p.109-220.

Covers the following basins: Paradox, Eagle (northwestern Colorado), San Piceance Creek (Colorado/Utah), Greater Green River, basins of the Rio Grande Rift, Raton and Huerfano Park, South Park, Denver, Wind River, Bighorn, Powder River.

## **SAN JUAN BASIN, NEW MEXICO--GENERAL - SEE ALSO NEW MEXICO-GENERAL**

•Arnold, E.C., J.M. Hill, K.S., Hatton, L.B. Martinez, and D.A. Donaldson, 1978, Stratigraphy and oil and gas production of northwest New Mexico: in Fassett, J.E., N.D. Thomaidis, M.L. Matheny, and R.A. Ullrich, eds, Oil and Gas Fields of The Four Corners Area, Volume 1, Four Corners Geological Society, p. 46-61.

•Campbell, C.V., 1971, Depositional model-Upper Cretaceous Gallup beach shoreline, Ship Rock area, northwestern New Mexico: Jour. Sed. Petrology, v. 41, p. 395-409.

Gallup regressive beach deposits are overlain unconformably by upper Gallup transgressive offshore-bar sandstones. The offshore bars formed on a shallow shelf that may be up to 100 miles wide; one documented offshore bar that is contemporaneous to the studied shoreline sandstones is 12 miles offshore, but others are at several multiples of that distance. Deposition of offshore bars was localized at a seaward steepening or break in slope of the sea floor amounting to less than 1 degree increase in slope.

•Cumella, S.P., 1981, Sedimentary history and diagenesis of the Pictured Cliffs Sandstone, San Juan Basin, New Mexico and Colorado: M.S. Thesis, University of Texas, Austin, 219 p.

•Devine, P.E., 1980, Depositional patterns in the Point Lookout Sandstone, Northwestern San Juan Basin, New Mexico: M.S. Thesis, University of Texas, Austin, 238 p.

•Donselaar, M.E., 1989, The Cliff House Sandstone, San Juan Basin, New Mexico: Model for the stacking of "transgressive" barrier complexes: J. Sed. Petrol. v. 59, p. 13-27.

Deposition took place in regressive phases of an overall transgressive formation. Based on outcrop studies.

•Fassett, J.E., 1977, Geology of the Point Lookout, Cliff House and Pictured Cliffs Sandstones of the San Juan Basin, New Mexico and Colorado: New Mexico Geol. Soc. Guidebook, 28th Field Conf., San Juan Basin III, p. 193-197.

Point Lookout, Pictured Cliffs are regressive; Cliff House is more transgressive. Paper not helpful in defining depositional environments. Includes a table of subsurface wells used: purpose was to discuss the subsurface geometry of the three units in title.

•Fassett, J.E., and J.S. Hinds, 1977, Abstract: Geology and Fuel Resources of the Fruitland Formation and Kirtland Shale of the San Juan Basin, New Mexico and Colorado: New Mexico Geol. Soc. Guidebook, 28th Field Conf., San Juan Basin III, p. 207.

This is the abstract from USGS Prof. Paper 676, which is a companion volume to the N. Mex. Geol. volume. The 1971 USGS volume details the subsurface and surface stratigraphy of Pictured Cliff Sandstone, Fruitland formation, Kirtland Shale, and Ojo Alamo Sandstone throughout the San Juan Basin.

•Jacobs, J.L., 1977, Some Recent shallow Pictured Cliffs gas discoveries: New Mexico Geol. Soc. Guidebook, 28th Field Conf., San Juan Basin III, p.247-249.

Lists 4 small, shallow gas pools.

•Kirk, A.R., and Zech, R.S., 1977, The transgressive and regressive relationships between the Upper Cretaceous Mulatto Tongue of the Mancos Shale and the Dalton Sandstone Member of the Crevasse Canyon Formation, Gallup-Pinedale area, New Mexico: New Mexico Geol. Soc. Guidebook, 28th Field Conf., San Juan Basin III, p. 185-192.

Upper and lower units of the Dalton sandstone members are regressive coastal barrier sandstones. Lower shoreface, upper shoreface, and foreshore are overlain by paludal (swamp/marsh) deposits. Description is that of a strand plain backed by marshes or swamps. Outcrop study.

•Mannhard, G.W., 1976, Stratigraphy, sedimentology, and paleoenvironments of the La Ventana Tongue (Cliff House Sandstone) and adjacent formations of the Mesaverde Group (Upper Cretaceous), Southeastern San Juan Basin, New Mexico: Ph. D. Dissertation, The University of New Mexico, 182 p.

Study based on 7 measured sections along an outcrop belt that is nearly parallel to depositional dip. Delatic sedimentation in this area is represented in which the **Menefee formation** represents the fresh water aggradational delta plain deposits, the **La Ventana Tongue** the marine delta front transgressive and progradational deposits, and the **Lewis Shale** the offshore prodelta deposits.

Five facies recognized in the La Ventana Tongue: 1) fining upward destructional delta front sheet sandstone; 2) Thin bedded tabular sandstone deposited in the offshore area during storms; 3) Thick coarsening upward progradational delta front sheet sandstones from areas of relatively high sediment input; 4) tabular cross-stratified sandstone with shale interbeds, interpreted as channel mouth bar deposits, and 5) lenticular tidal inlet channel sandstones. **Virtually no mention of barriers in this interpretation.**

La Ventana delta prograded into shallow water gently sloping shelf under conditions of relatively high wave energy relative to sediment input. Stratigraphic framework is similar to the modern Rhone delta, the Pleistocene Surinam cusped delta, and abandoned shoal water Mississippi deltas.

•Molenaar, C.M., 1983, Principal reference section and correlation of Gallup Sandstone, Northwestern New Mexico: Contributions to Mid-Cretaceous Paleontology and Stratigraphy of New Mexico Pt. 2: N. Mexico Bur. Mines Mineral Resources Circular No. 185, p. 29-40.

Index Map shows the subsurface control throughout the basin. The principal reference section includes an interval interpreted as regressive coastal barrier overlying marine mudstones and overlain by paludal sediments. Study based on outcrops.

•Molenaar, C.M., 1977, Stratigraphy and depositional history of Upper Cretaceous rocks of the San Juan Basin area, New Mexico and Colorado, with a note on economic resources: New Mexico Geol. Soc. Guidebook, 28th Field Conf., San Juan Basin III, p. 159-166.

A good correlation chart that labels marine and coastal barrier sandstones. Author uses the term coastal barrier for barrier island and non-barrier island shoreline sandstones. Semilla Sandstone member of Mancos Shale is a discontinuous offshore sandstone bar in SE part of the basin. Semilla is offshore equivalent of and derived from the lower regressive coastal-barrier sandstone of the lower Gallup. Several elongate offshore bars occur above and seaward from the regressive Gallup (lower part). These sandstones bars are oil productive and have been referred to as transgressive Gallup, Tocito, or basal Niobrara sandstones. Dalton Sandstone is a regressive coastal-barrier ss that is included in the Crevasse Canyon formation, above the Gallup. The Dalton Sandstone member of the Crevasse Canyon is a typical regressive coastal-barrier sandstone. Hosta tongue of the Point Lookout Sandstone is a fining-upward deepening water sandstone. Mesaverde Group: basal Point Lookout Sandstone-regressive coastal-barrier sandstone. Middle unit- Menefee Formation is nonmarine-paludal to alluvial-plain landward of Point Lookout and Cliff House shorelines. Upper unit- the Cliff House Sandstone- shoreline-barrier, overall transgressive cycle but deposited during stillstands or regressions of shoreline. Pictured Cliff Sandstone- is regressive coastal barrier sandstone.

**Economic resources of the Upper Cretaceous units in San Juan Basin:** This basin contains the nations third largest gas field, Blanco gas field, with estimated recovery of 23 tcf gas plus significant amount of condensate. Dakota produces oil in several small structurally controlled fields on basin flanks-eg. Hogback, Table Mesa and Rattlesnake fields. Most oil in basin from stratigraphic traps in transgressive Gallup or basal Niobrara sands. Estimated ultimate recovery is 40 million bbl. Only production from regressive Gallup Sandstone is at Hospah field, which is structurally controlled, and produced 11 1/2 million bbls as of 1974.

•Noon, P.L., 1980, Surface to subsurface stratigraphy of the Dakota Sandstone (Cretaceous) and adjacent units along the Eastern flank of the San Juan Basin, New Mexico and Colorado: M.S. Thesis, Bowling Green State Univ.

Deposition of Dakota Sandstone was in response to regional transgression of the Western Interior Sea during Cenomanian time. Within overall transgression there were minor regressions which may have been brought about by local progradation related to increased local sediment supply. The Cubero, Paguata, and Twowells sands were deposited by southward flowing paleocurrents oriented approximately parallel to the shoreline.

The authors environmental calls are less than earth shaking. Twowells, Paguata, and Cubero sandstone pods all show coarsening upward patterns on logs. Northwest trends within the Twowells may represent offshore bars derived from a northwestern source, or linear sand shoals derived from shoreface sands.

•Parker, J.M., Riggs, E.A., and W.L. Fisher, 1977, Oil and gas potential of the San Juan Basin: New Mexico Geol. Soc. Guidebook, 28th Field Conf., San Juan Basin III, p. 227-234.

Mesozoic potential is limited, much of the section has been eroded or crops out. So little of this section is preserved in the subsurface that its resource potential is negligible. In the San Juan Basin most of the resource potential in Mesozoic section is proven, but undeveloped. The best potential for future development is within the Middle to Upper Paleozoic carbonate section.

•Peterson, F., and A.R. Kirk, 1977, Correlation of the Cretaceous rocks in the San Juan, Black Mesa, Kaiparowits and Henry Basins, southern Colorado Plateau: New Mexico Geol. Soc. Guidebook, 28th Field. Conf., San Juan Basin III, p. 167-178.

Correlations show general depositional environments for formations including coastal barrier and nearshore marine sandstones, especially in Toreva and Dakota sands.

•Peterson, J.A., Loleit, A.J., Spencer, C.W., AND Ullrich, R.A., 1968, Sedimentary history and economic geology of San Juan Basin, New Mexico and Colorado: AAPG Mem. No. 10, p. 186-231.

Good correlation chart, structural contour map, and **map of oil and gas fields of the San Juan Basin**, isopach maps by age and formation. Author notes that Gallup Sandstone is no longer considered the basal part of the Mesaverde Group, but stands alone.

•Reneau, W.E., Jr., 1957, Reservoir characteristics of Cretaceous sands of the San Juan Basin: Four Corners Geological Society, Geology of SW San Juan Basin, Second Field Conference, p. 40-43.

Good, short summary of Pictured Cliffs, Mesaverde Group, Gallup formation, Tocado, and Dakota fields.

•Woodward, L.A., and J.F. Callender, 1977, Tectonic framework of the San Juan Basin: New Mexico Geol. Soc. Guidebook, 28th Field Conf., San Juan Basin III, p. 209-212.

#### **TRANSGRESSIONS - HOLOCENE MARINE SEQUENCES - SEE ALSO 'EROSIONAL SURFACES'**

•Kraft, J.C., 1971, Sedimentary facies and geologic history of a Holocene marine transgression: Geol. Soc. America Bull., v. 82, p. 2131-2158.

Based on a study of the Delaware coast. The sediments are infilling a drowned topography with local relief of 70 ft. and possibly up to 125 ft. Thickness and areal extent of sedimentary bodies are to a large degree controlled by the morphology of the Pleistocene unconformity. Depositional units are thin, highly irregular in areal extent, extremely variable in thickness, and difficult to project.

•Kraft, J.C., and C.J. John, 1979, Lateral and vertical facies relations of transgressive barrier: AAPG Bull., v. 63, p. 2145-2163.

This paper appears to be a condensation for AAPG of the 1977 paper by Chacko J. John (Listed under Barriers-Modern).

Of particular interest are: 1) Coarse sediments overlying fine sediments, generally believed to be characteristic of regressive barriers, also are present in this transgressive example. 2) From the abstract "**Time lines clearly diverge and cross lithologic boundaries in both transgressive and regressive barrier sedimentary units. Hence, the transgressive or regressive nature of preserved barrier sequences cannot be positively identified on the basis of characteristic shapes of geophysical logs or sedimentary sequences.**" Everything except the last two words of this quotation seem reasonable.

## **WATER SENSITIVITY, ALMOND FORMATION**

•Baptist, O.C., E.J. White, & C. S. Land, 1964, Laboratory predictions of water sensitivity compared with field observations of well damage-Patrick Draw, Wyoming: SPE Paper No. 839, 6 p.

Actual damage is estimated from interpretation of drill stem tests and observation of rates of injection with brine, and with fresh water. Lab tests indicate that Almond sands should have a medium sensitivity to fresh water and less sensitivity to brine. Actual damage ratios from DST's indicate that damage increases from water sands to oil sands to much greater in gas sands. Injection rates are about the same for fresh water as for brine, which does not agree with laboratory predictions. Rates for brine injection are close to those calculated from lab relative-permeability curves.

## **WEST RANCH FIELD, TEXAS**

•Galloway, W.A., 1986, Reservoir facies architecture of microtidal barrier system: AAPG Bull, v. 70, no. 7, p.787-808.

The first part of the paper is a good review of the geometry and occurrence of modern barriers. Paper discusses West Ranch Field, Texas.

## **VIKING BARRIER SANDSTONE, ALBERTA, CANADA**

•Amajor, L.C., 1984, Lower Cretaceous Viking Barrier Island, Southwestern Alberta Canada (abst.): AAPG Bull., v. 69, p. 448.

The Viking trend is more than 120 km (75 mi) long and maximum thickness of over 30 m (100 ft). It prograded to the northeast as much as 24 km (15 mi).

The presence of an ebb-tidal delta and marine shelf shales beneath and above the middle shoreface facies, respectively lead the author to compare the Viking barrier more closely with Recent barriers of the South Carolina coast than with Galveston Island, TX., or the Muddy barrier, MT.

## Appendix B

This appendix contains an example from a spreadsheet that currently contains information from approximately 200 wells. Data concerning well location, core information, total depths and tops of formations, logs available, fluids, and production data are available on the complete listing, which is available of request.

### Key for Appendix B

% OIL- % oil recovered  
%CR- percentage of core recovered  
A- Abandoned  
AL- Almond formation  
CQI- Core quality index score  
DA- Dry and abandoned  
ER- Ericson formation  
FDL- Formation density log  
FH- Fox Hill formation  
G- Gas production  
GI- Gas injection  
GL- Ground level  
GR- Gama ray log  
GRAV- Oil gravity, ° API  
GV- Gas vent  
IND- Induction log  
IP- Initial production  
KB- Kelly bushing  
L- Lance formation (Fort Union)  
LOC- Location  
LW- Lewis formation  
MAX- Maximum depth of core  
MIN- Minimum depth of core  
ML- Micro log  
ND- Never drilled  
O- Oil production  
OG- Oil and gas production  
PA- Plugged and Abandoned  
PERF- Depths of perforated zones  
PH- Photographs of core taken  
RW- Range  
SEC- Section  
SH- Shots per foot for perforations  
SI- Shut in  
SON- Sonic log  
SP- Surface plug  
ST- Well status  
T- Type of core; S-slabbed F- full  
TA- Temporarily abandoned  
TD- Total depth  
TN- Township  
TOT- Total barrels recovered per 24 hours  
TP- Temporarily plugged (records indicate intention to re-enter well)  
WI- Water injection

PATRICK DRAW DATABASE

LOC	FW	IN	SEC	LIB	OPERATOR	NAME	T	M	MIN	MAX	PH	%CR	COI	IND	M	GR	LOG	ELEVATION	IP	%oil	PERFS	TD	L	11	LW	41	ER	ST			
SE SW	99	18	11	C810	EL PASO	5 PATRICK DRAW UNIT	S4978	5015	X	30	30	30	30	X	X	X	X	6720	6708	781	100	4980-5010	43.4	5036	0	35.14	3718	4980	W		
SE SW	99	18	16	A410	FOREST	76-61 GOV ARCH UNIT	S4898	4948	14	58	6	6	6	X	X	X	X	6810	6797	115	67	4987-4906	4	5032	2605	35.08	3742	1890	SP		
NW SE	98	19	7	A412	FOREST	36-74 ARCH UNIT	S5042	5060	14	58	4	4	4	X	X	X	X	6787	6775	180	99.7	5041-5054	4	5425	0	30.16	3848	5389	SI		
NW NE	98	19	7	B159	FOREST	32-77 ARCH UNIT	S4979	4988	X	39	69	69	69	X	X	X	X	6808	6796	40	99.8	5.5*@2460	4	5375	2688	35.14	3773	1969	5356	SP	
SE NW	98	19	9	B538	FOREST	1-9-6 UPRR ARCH UNIT	S5744	5779	X	12	127	127	127	X	X	X	X	6802	6791	0	0	5728-42	4	6900	0	4374	6056	6056	SP		
SE NW	98	19	10	B177	FOREST	80-10-1 ARCH UNIT	S5948	6013	X	25	60	60	60	X	X	X	X	6778	6770	33	66.7	5956-68	4	6200	0	35.14	4539	1638	5877	TA	
NW SW	98	19	18	B534	FOREST	17-18-1 ARCH	S4843	4873	X	40.5	75.5	75.5	75.5	X	X	X	X	6763	6750	324	100	4948-4968	4	5208	2524	33.38	3840	1943	A		
NW NW	98	19	18	A384	FOREST	9-18-2 ARCH UNIT	S4879	4904	48	70	70	70	70	X	X	X	X	6758	6745	232	100	4884-4899	4	5400	0	31.77	3757	1876	SP		
SE NW	98	19	18	B181	FOREST	26-18-3 ARCH UNIT	S5040	5055	X	25	55	55	55	X	X	X	X	6797	6784	504	100	5044-5064	4	5474	2637	3620	3927	5037	5409	SP	
SE NW	98	19	18	B185	FOREST	101-18-0 ARCH UNIT	S4998	5028	X	40	55	55	55	X	X	X	X	6784	6772	32	100	5003-5023	4	5090	0	35.68	3849	4993	SP		
NW SW	98	19	1	A411	FOREST	60-1-3 ARCH UNIT	S4553	4604	15	35	35	35	35	X	X	X	X	6945	6933	184	98	4592-4602	4	5300	0	32.13	3458	1545	SP		
NW NW	98	19	1	B533	FOREST	49-1-3 ARCH UNIT	S4580	4630	X	25	60	60	60	X	X	X	X	6990	6978	580	100		4	4959	0	32.40	3457	1507	4919	TA	
NW NE	98	19	1	A579	FOREST	70-1-8 ARCH UNIT	S4790	4815	48	111	111	111	111	X	X	X	X	6911	6898	68	30	4793-4810	4	4890	2564	34.15	3686	4787	SP		
SE NW	98	19	1	A398	FOREST	108-1-8 ARCH UNIT	S4532	4598	28	73	73	73	73	X	X	X	X	6901	6889	132	237	100	4527-43	64-72	4	4593	0	31.26	3387	4466	W
SE SE	98	19	2	A393	FOREST	63-2-2 GOV ARCH UNIT	S4475	4528	X	32	40	40	40	X	X	X	X	6826	6814	545	100	4484-4498	4	4553	0	31.31	3372	4471	TA		
SE SE	98	19	2	B182	FOREST	109-2-6 ARCH UNIT	S4485	4543	X	23	58	58	58	X	X	X	X	6952	6939	115	64.6	4523-4533	4	4286	0	29.45	3090	4185	TA		
SE SE	98	19	3	B183	FOREST	61-3-1 UPRR ARCH UNIT	S4205	4256	X	0	30	30	30	X	X	X	X	7025	7012	102	100	4230-4242	4	3859	0	29.83	3479	3759	TA		
SE SE	98	19	8	B056	FOREST	1-8 GOVERNMENT	S3485	3539	40	40	40	40	40	X	X	X	X	7114	7103	0	91		4	5300	0	33.45	3602	4758	5116	W	
SE SE	98	19	11	B175	FOREST	42-11-1 ARCH UNIT	S4510	4533	X	23	23	23	23	X	X	X	X	6878	6865	260	99.6	4495-4515	4	4895	0	31.48	3367	4489	4843	P-A	
NW NW	98	19	11	A392	FOREST	71-11-6 ARCH UNIT	S4261	4312	33	93	93	93	93	X	X	X	X	6865	6852	438	100	4294-4310	4	4970	3014	31.77	4257	4370	P-A		
NE NE	98	19	12	A408	FOREST	107-11-8 ARCH UNIT	S4465	4523	27	65	65	65	65	X	X	X	X	6904	6892	35	0.86	4497-4505	4	4525	0	31.90	3397	4451	W		
NE SE	98	19	12	A391	FOREST	103-12-12 ARCH UNIT	S4774	4808	26	66	66	66	66	X	X	X	X	6808	6786	38	32.6	4774-4801	4	4808	0	33.27	3610	4769	P-A		
SE SW	98	19	12	B184	FOREST	11-2-1 GOV ARCH UNIT	S4656	4700	21	56	56	56	56	X	X	X	X	6845	6833	146	97.6	4671-87	90-93	4	5000	0	32.33	3510	4651	TA	
SE NW	98	19	12	B184	FOREST	106-12-15 ARCH UNIT	S4830	4688	X	25	40	40	40	X	X	X	X	6889	6877	10	16.5	4633-4674	4	4790	0	32.45	3467	4616	TA		
SE SE	98	19	13	A163	FOREST	4-12-5 ARCH UNIT	S4858	4894	X	50	70	70	70	X	X	X	X	6814	6803	333	91		4	5400	0	33.45	3602	4758	5116	W	
SE SE	98	19	13	B184	FOREST	10-13-1 ARCH UNIT	S4712	4752	34	79	79	79	79	X	X	X	X	6750	6738	684	100	4871-4895	4	5400	0	32.14	3612	4718	5125	P-A	
NW NW	98	19	13	B535	FOREST	23-13-4 ARCH	S4592	4620	27	62	62	62	62	X	X	X	X	6848	6835	744	99.7	4596-4616	4	5050	0	31.80	3480	4583	P-A		
SE SW	98	19	13	B176	FOREST	39-13-7 ARCH	S4668	4786	13.6	75	75	75	75	X	X	X	X	6750	6740	0	2479	4882-4894	4	5100	0	32.40	3560	4664	5016	G	
NW NW	98	19	13	A413	FOREST	88-13-9 ARCH UNIT	S4712	4752	34	79	79	79	79	X	X	X	X	6761	6748	261	100	4706-4740	4	4793	0	32.13	3600	4701	P-A		
NW NW	98	19	14	B537	FOREST	74-14-6 ARCH UNIT	S4300	4308	X	22	55	55	55	X	X	X	X	6856	6847	112	99.7	50.5 *@2000	4	4850	0	27.6	3075	4189	4450	SP	
NW SE	98	19	14	A388	FOREST	22-14-1 ARCH UNIT	S4464	4482	28	62	62	62	62	X	X	X	X	6821	6808	1264	100		4	4950	0	31.13	3439	4553	4891	O	
SE SE	98	19	14	A438	FOREST	44-14-2 ARCH UNIT	S4552	4586	X	30	95	95	95	X	X	X	X	6895	6882	804	100		4	4848	0	31.10	3308	4446	4800	W	
NW NE	98	19	14	B536	FOREST	45-14-3 ARCH	S4449	4472	X	23	50	50	50	X	X	X	X	6915	6902	0	1123	0	4164-68	4	4300	0	27.67	3041	4125	SI	
SE NW	98	19	14	B180	FOREST	74-22-2 ARCH UNIT	S4155	4207	24	64	64	64	64	X	X	X	X	6828	6815	1578	100	4493-4518	4	4895	0	31.62	3394	4184	4837	SP	
NW NE	98	19	23	S395	FOREST	20-23-4 ARCH UNIT	S4497	4547	23	83	83	83	83	X	X	X	X	6804	6791	1752	100	4464-4495	4	4871	2238	30.70	3321	4452	4805	SP	
SE SW	98	19	24	A414	FOREST	18-23-2 ARCH UNIT	S4427	4461	20	80	80	80	80	X	X	X	X	6830	6818	212	100	4837-4865	4	5300	0	34.76	3720	4826	P-A		
SE NE	98	19	24	B260	FOREST	86-6-2 ARCH UNIT	F4906	4925						X	X	X	X	6855	6846	0	0		4	4925	0	35.0	3722	4904	P-A		
NW NW	98	19	7	S261	FOREST	16-7-1 ARCH	F4828	4859						X	X	X	X	6777	6764	1340	100	4837-58	4	5000	0	34.51	3699	4860	SP		
SE SE	98	19	7	S262	FOREST	17-7-2 ARCH	F4836	4860						X	X	X	X	6824	6812	360	95	4841-54	4	5300	0	34.9	3680	4836	5237	TA	
NE SE	98	19	7	S263	FOREST	48-7-6 ARCH UNIT	F5145	5172						X	X	X	X	6819	6806	252	100		4	5399	0	37.14	3987	5139	5486	SP	
NW SE	98	19	7	S264	FOREST	58-7-8 ARCH UNIT	F5103	5149						X	X	X	X	6806	6793	366	100	5126-5148	4	4860	0	34.47	3708	4860	SP		
NW SE	98	19	7	S265	FOREST	102-7-10 ARCH UNIT	F4863	4901						X	X	X	X	6765	6752	356	99.8	5.5*@2400	4	4860	0	36.13	3822	5118	SP		
NW SE	98	19	18	S268	FOREST	50-18-6 ARCH UNIT	F5097	5121						X	X	X	X	6733	6725	938	99.8	4567-4990	4	5400	0	35.63	3796	5000	SP		
NW NW	98	19	19	S268	FOREST	3-19-2 ARCH UNIT	F4949	5000						X	X	X	X	6739	6730	27	100	5008-5032	4	5048	0	35.63	3796	5000	SP		
NW NW	98	19	19	S269	FOREST	86-19-5 ARCH UNIT	F5001	5003						X	X	X	X	6744	6735	34	88	5870-5884	4	6050	0	41.47	4558	5789	SI		
NW																															

LOC.	FW	IN	SECLIB	OPERATOR	NAME	TMIN	MAX	IPH	%GR	CCI	IND	ML	GR	SOX	FD	KB	GL	LOI	GAS	%oil	PERFS	DEPTH	CL	GRAV	TD	L	FH	LW	AL	TOPS	FW	AL	RR	ST	
SESW	99	19	12	S277	FOREST	F4355	4404				X	X	X	X	X	6859	6946	755	100	4372-4384			4	44500	0	3079	3243	4335							
SENE	99	19	12	S278	FOREST	F4487	4538				X	X	X	X	X	6964	6952	1242	100	4521-37			4	49000	0	3141	3357	4469	4820			WI			
NWSE	99	19	12	S280	FOREST	F4209	4456				X	X	X	X	X	6967	6954	612	100	4446-4455			4	43180	0	3070	3290	4392				TA			
NWSE	99	19	11	S282	FOREST	F4204	4235				X	X	X	X	X	6980	6967	228	100	4232-4249			4	89850	0	3053	3232	4396	4728						
SENE	99	19	11	S283	FOREST	F4478	4526				X	X	X	X	X	6895	6884	130	77					4	48540	0	3127	3300	4461	4827	WI				
NWSE	99	19	11	S284	FOREST	F4413	4461				X	X	X	X	X	6923	6920	258	100	4444-4449			4	48250	0	3054	3330	4396				TA			
SENE	99	19	11	S285	FOREST	F4387	4421				X	X	X	X	X	6933	6920		100	4371-4377			4	4525	0	3071	3276	4334	4692	SP					
NWSE	99	19	11	S286	FOREST	F4498	4511				X	X	X	X	X	6849	6840	137	2213	99.9	4486-4506			4	4675	0	3012	3322	4474				P.A		
NWSE	99	19	12	S288	FOREST	F4558	4609				X	X	X	X	X	6874	6862	46	800	265.2	4584-4602			4	50000	0	3185	3454	4571				P.A		
NWSE	99	19	12	S289	FOREST	F4675	4727				X	X	X	X	X	6838	6826		99.7					4	0	0	3261	3525	4866				P.A		
NWSE	99	19	12	S290	FOREST	F4539	4578				X	X	X	X	X	6811	6800	756	99.7	4874-4893			4	0	0	3190	3409	4544					P.A		
NWSE	99	19	12	S291	FOREST	F4514	4563				X	X	X	X	X	6884	6851	308	99.6	4564.5-4565			4	0	0	3324	3559	4709					P		
NWSE	99	19	13	S292	FOREST	F4698	4747				X	X	X	X	X	6870	6857	118	99.6					4	48600	0	3168	3450	4504				P.A		
NWSE	99	19	13	S293	FOREST	F4798	4878				X	X	X	X	X	6749	6737	607	100	4836-62			4	49130	0	3421	3738	4829					SP		
NWSE	99	19	14	S294	FOREST	F4608	4821				X	X	X	X	X	6874	6854	228	99	4885-4862			4	5400	0	3384	3694	4795	5198	P.A					
NWSE	99	19	14	S295	FOREST	F4392	4420				X	X	X	X	X	6892	6850	1460	100	5.5*@2020			4	48000	0	3020	3292	4399	4739	SP					
NWSE	99	19	15	S296	FOREST	F4271	4322				X	X	X	X	X	6905	6883	18	45	100	4237-03*13-16			4	44000	0	2900	3154	4255					O-B	
NWSE	99	19	15	S297	FOREST	F4254	4304				X	X	X	X	X	6884	6871		28300	100	4213-4229.5			4	43220	0	2959	3138	4238					P.A	
NWSE	99	19	15	S298	FOREST	F4210	4262				X	X	X	X	X	6928	6814	0	100	5.5*@2200			4	47000	0	2865	3120	4208	4511	G					
NWSE	99	19	15	S299	FOREST	F4578	4608				X	X	X	X	X	6742	6730	1800	100	4573-4608			4	48000	0	3040	3318	4408	4757	SP					
NWSE	99	19	15	S300	FOREST	F4857	4908				X	X	X	X	X	6800	6787		100	4897-4802			4	5300	0	3500	3740						P.A		
NWSE	99	19	15	S301	FOREST	F4606	4824				X	X	X	X	X	6749	6737	148	100					4	48990	0	3163	3502	4611	4948					
NWSE	99	19	15	S302	FOREST	F4908	5195				X	X	X	X	X	6771	6759	1122	100	4928-4948			4	53500	0	3524	3768	4920	5277						
NWSE	99	19	15	S303	FOREST	F4961	5222				X	X	X	X	X	6796	6783	228	100	4868-82*71-84			4	5300	0	3610	3558	4959							
NWSE	99	19	15	S304	FOREST	F4647	4878				X	X	X	X	X	6798	6725	1020	100	4648-4668			4	4780	0	3225	3498	4637							
NWSE	100	18	12	CHANDLER	#1 VERBRUGGE GOVT						X	X	X	X	X	6868	6861		1500					4	2380	0	1400	2369	2704	P.A					
NWSE	100	18	12	CHANDLER	#2 VERBRUGGE GOVT						X	X	X	X	X	6862	6861		724					2	2559	350	1400	2300	SI						
NWSE	100	18	13	U.P. RAIL	#1-3 U.P. R.R.	154.5	1595				X	X	X	X	X	6937	6929	0	528			OH		4	1923	528	1497	1874	P.A						
NWSE	100	18	13	NEW MONT	#3 P.S.						X	X	X	X	X									4	358	0									
NWSE	100	18	13	BONNER	#1 FOREST FEDERAL						X	X	X	X	X	6639	6629							4	5250	0	367	685	290	P.A					
NWSE	100	18	13	CHANDLER	#1 BLACK BUTTES GOVT						X	X	X	X	X	6795	6755							4	2295	0	920	1954	2208	P.A					
NWSE	100	18	11	HOLSTON	#22-11 AMOCO-CHAMPL						X	X	X	X	X	6754	6740							4	2285	550	940	1160	2170	2490	P.A				
NWSE	100	18	11	PRENATA	12X- PRENATA CORP.						X	X	X	X	X	6767	6759							4	2400	356	844	1035	2262	SI					
NWSE	100	18	11	AMOCO	#1 CHAMP. 295 AM.-A						X	X	X	X	X	6830	6829							4	2800	0	2084	3202	3631	P.A					
NWSE	100	18	12	CHANDLER	B-1 VERBRUGGE						X	X	X	X	X	6825	6815		2306					4	3021	0	2084	3202	3631	P.A					
NWSE	100	18	12	CHANDLER	#1 WOLF-GOVT						X	X	X	X	X	6622	6616							4	2670	1235	2205	2570	2671	SI					
NWSE	100	18	12	PADON	#1 BLAIR-HAY LIVE. CO.						X	X	X	X	X	6687	6675							4	1597	0	900	1880	2190	P.A					
NWSE	100	18	22	LOON	#1 KELLY						X	X	X	X	X	6687	6675							4	5900	0	200	1206	1490	P.A					
NWSE	100	18	22	PHILLIPS	A-1 SWEETWATER						X	X	X	X	X	6643	6632							4	2600	0	982	1090	2220	D.A					
NWSE	100	18	24	MOUNTAIN	#1-24 SAND BUTTE						X	X	X	X	X	6757	6746							4	3451	992	1725	1915	3063	3383	P.A				
NWSE	100	18	25	ST. MICHA	#1-25 UPRR						X	X	X	X	X	6692	6673							4	3904	1635	2195	2410	3425	P.A					
NWSE	100	18	26	CHANDLER	#1 HOLBECK-GOVT						X	X	X	X	X	6680	6673							4	3400	0	1784	2903		P.A					
NWSE	100	18	36	CHANDLER	#2 CHORNEY STATE						X	X	X	X	X	6777	6772		700					4	4053	0	2252	3285	3640	P.A					
NWSE	100	18	36	ST. MICHA	#1-36 STATE						X	X	X	X	X	6288	6288							4	4031	0	2252	3285	3640	P.A					
NWSE	100	18	36	CHANDLER	#1 CHORNEY STATE						X	X	X	X	X	6280	6276							4	4157	2608	2610	3718	4020	P.A					
NWSE	100	18	36	ROLFAM	#44-36 STATE						X	X	X	X	X	6899	6889							4	6340	2875	4354	4516	5928	6282	A				
NWSE	98	19	17	CHAMPLIN	#1 CHAMPLIN ROCK						X	X	X	X	X	6728	6717	721	100	5092-5119			4	41.5	5244	0	5092								

LOC	LOC AT CN	OPERATOR/NAME	OCFE	LOG	ELEVATION	IP	PERFS	TD	TOYS	ST																		
LOC	FW TN/SEC/LIB	LIB	MIN	MAX	PH	%CR	COL	IND	ML	GR	SCN	FD	KB	CL	LOI	GAS	%OIL	DEPTH	SH	REV	TD	L	FI	LW	AL	ER		
NMSW	99 181	EL PASO #19 PATRICK DRAW						X	X				6711	6698	242		100	4894-4923	4	43.8	5269				4894	5269	WI	
SESW	99 181	EL PASO #10 UNIT PATRICK DRAW						X	X				6717	6707	1002		100	5027-5059	4	41.6	5182				5027	5180	WI	
NMSW	99 181	EL PASO #9 UNIT PATRICK DRAW						X	X				6753	6739	235		100	5228-5251	4	42.8	5326				5228	5326	WI	
SESW	99 181	EL PASO #11 UNIT PATRICK DRAW						X	X				6716	6704	365		100	4980-5052	4	41	5088				4990	5088	WI	
NMSW	99 181	EL PASO #10 UNIT PATRICK DRAW						X	X				6750	6733	637		100	5178-5198	2	41.8	5656				3730	3850	WI	
SESW	99 181	EL PASO #105 MONELL						X	X				6725	6713	84	183	100	5081-5081	2	43.9	5189				3608	3895	TA	
NMSW	99 181	EL PASO #106 MONELL UNIT						X	X				6767	6756	48	15	100	5311-5331	2	43.9	5227				3737	3845	O-R	
SESW	99 181	EL PASO #109 MONELL UNIT						X	X				6729	6717	192	122	100	5084-5114	2	43.9	5227				3737	3845	O-R	
NMSW	99 181	EL PASO #113 MONELL UNIT						X	X				6754	6743			100	5269-5308	2	43.9	5227				3737	3845	O-R	
SESW	99 181	EL PASO #114 MONELL UNIT						X	X				6733	6721	152	77	100	5162-5182	2	43.9	5228				3808	3868	O-R	
NMSW	99 181	EL PASO #115 MONELL UNIT						X	X				6702	6708	54	112	100	4841-4866	2	43.9	5067				3795	4935	O-R	
SESW	99 181	EL PASO #123 MONELL UNIT						X	X				6712	6700	80	134	100	4980-5021	2	43.9	5123				3638	3848	O-R	
NMSW	99 181	EL PASO #124 MONELL UNIT						X	X				6750	6738	22	21	100	5225-5249	2	43.9	5245				2405	3874	O-R	
SESW	99 181	EL PASO #25 PATRICK DRAW						X	X				6710	6697	141		100	4707-20*30-42	4	43.8	4815				4704	4815	WI	
NMSW	99 182	EL PASO #26 PATRICK DRAW						X	X				6752	6739	616		100	4561-4586	4	43.8	4924				4561	4924	WI	
SESW	99 182	EL PASO #24 PATRICK DRAW						X	X				6726	6713	303		100	4662-4694	4	42.8	4738				3520	4658	WI	
NMSW	99 182	EL PASO #21 PATRICK DRAW						X	X				6711	6697	295		100	4828-4856	4	43.8	5004				3720	4828	WI	
SESW	99 182	EL PASO #23 PATRICK DRAW						X	X				6713	6697	733		100	4750-4777	4	43.2	4888				3640	4750	WI	
NMSW	99 182	EL PASO #18 PATRICK DRAW						X	X				6711	6710	602		100	4749-4774	4	43.2	4852				3455	4602	WI	
SESW	99 182	EL PASO #28 PATRICK DRAW						X	X				6710	6697	560		100	4926-4961	4	43.2	5030				3773	4926	WI	
NMSW	99 182	EL PASO #27 PATRICK DRAW						X	X				6710	6698	192		100	4642-60*66-72	4	43.2	4952				3590	4641	WI	
SESW	99 182	EL PASO #23-2 FEDERAL						X	X				6709	6687			100	4725-4734	1	47.22	1923				3270	3590	WI	
NMSW	99 182	EL PASO #104 MONELL						X	X				6735	6723			100	4821-2196	3661	3561	4716				4716	WI		
SESW	99 182	EL PASO #110 MONELL						X	X				6709	6697	55	159	100	4936-4862	2	43.9	4975				3790	2145	WI	
NMSW	99 182	EL PASO #111 MONELL						X	X				6708	6697	72	122	100	4862-70*72-90	2	43.9	5005				2075	3466	O-R	
SESW	99 182	EL PASO #112 MONELL						X	X				6726	6715	31	300	100	4728-4742	2	44.3	4850				2160	3365	O-R	
NMSW	99 182	EL PASO #116 MONELL						X	X				6731	6719	212	471	100	4761-4781	2	43.9	4891				2200	3418	O-R	
SESW	99 182	EL PASO #117 MONELL						X	X				6720	6708	228	985	100	4584-4614	2	43.9	4765				3324	3449	O-R	
NMSW	99 182	EL PASO #122 MONELL						X	X				6729	6717	83	311	100	4635-4675	2	43.9	4765				3324	3449	O-R	
SESW	99 182	EL PASO #36 PATRICK DRAW						X	X				6711	6699	52	281	100	4797-4829	2	43.8	4932				2155	3452	O-R	
NMSW	99 183	EL PASO #32 PATRICK DRAW						X	X				6776	6763	447		100	4432-37*46-71	4	43.8	4523				3310	4432	WI	
SESW	99 183	EL PASO #35 PATRICK DRAW						X	X				6788	6775	380		100	43.2	4756	4	43.2	4756				3243	4389	WI
NMSW	99 183	EL PASO #31 PATRICK DRAW						X	X				6729	6716	418		100	43.8	4539	4	43.8	4539				3271	4428	WI
SESW	99 183	EL PASO #37 PATRICK DRAW						X	X				6715	6703	472		100	43.8	4449	4	43.8	4449				3240	4355	WI
NMSW	99 183	EL PASO #39 PATRICK DRAW						X	X				6710	6698	227		100	4327-4335	4	43.8	4406				3390	4552	WI	
SESW	99 183	EL PASO #33 PATRICK DRAW						X	X				6780	6768	613	400	100	4458-71*74-84	2	43.9	4588				1905	3114	O-R	
NMSW	99 183	EL PASO #103 MONELL						X	X				6707	6695	187	881	100	4365-4370*74-82	2	43.8	4499				1712	3064	O-R	
SESW	99 183	EL PASO #118 MONELL						X	X				6752	6740	85	1850	100	4428-33*36-58	2	43.9	4564				1895	3128	O-R	
NMSW	99 183	EL PASO #107 WATER INJECT.						X	X				6744	6731	193	1547	100	4388-94*04-14	2	43.8	4525				2299	3011	O-R	
SESW	99 183	EL PASO #34 PATRICK DRAW						X	X				6709	6698	29	427	90	4502-4526	2	43.8	4614				3107	3387	O-R	
NMSW	99 2032	EL PASO #44-35						X	X				6780	6768		241									3020	4120	O-R	
SESW	99 2035	LUFF, INC. #1-35	44643					X	X				7038	7026	70		100	4552-4562	4	4686	0				3366	4506	O-R	
NMSW	99 2035	UPRCOM #44-35R						X	X				7025	7013	180		100	4552-54*57-61	4	4628	0				0	3382	4511	O-R
SESW	99 2035	UPRCOM #42-35	44651					X	X				7069	7057	0		0								0	3440	4552	O-R
NMSW	99 2035	UPRCOM #1-35						X	X				7055	7044			0								0	3280	4382	O-R
SESW	99 2035	LUFF, INC. #2-35	44385					X	X				6972	6962			100	4824-34	4	43.6	4855				4116	4818	O-R	
NMSW	99 2036	LUFF, INC. #1-38						X	X				7041	7031	360		100	4743-4762	4	43.6	4855				3678	4818	O-R	
SESW	99 2036	COLORADO #2-36						X	X								100							3530	4693	5044		



LOC	FW	TN	SECLIB	OPERATOR	NAME	TIME	MAX	CORE	IND	LOG	ELEVATION	IP	PERFS	TOPS				ST						
														AL	LW	FW	LH							
LOC	FW	TN	SECLIB	OPERATOR	NAME	TIME	MAX	CORE	IND	LOG	ELEVATION	IP	DEPTH	DEPTH	%oil	sig	sig	TD	L	FW	LW	AL	ER	
SENE	99	19	35	TEXACO	#6-35 BEACON	4737	4789		X		6752	6742	669	100	4766-71-76-86	2	44.5	5150	1510	2630	3622	4764	5107	SI
SEWV	99	19	35	TEXACO	#24-35 BEACON	0	0		X		6762	6751	942	100	4615-21-27-35	4	44.5	4711	1430	2356	3479	4605	4674	TA
NWSE	99	19	35	TEXACO	#11-35 BEACON	0	0		X		6753	6742	1005	100	4731-25-31-36	2	44.6	4830	1495	2602	3590	4717	4796	WI
NWSE	99	19	35	TEXACO	#14-35 BEACON	0	0		X		6784	6753	560	100	4574-77-85-05	2	47	4679	1392	2618	3430	4570	4642	WI
SESW	99	19	35	TEXACO	#6-35 BEACON	0	0		X		6739	6729	573	100	4697-03-03-08	4	44.7	4793	1463	2558	3520	4688	4758	A
SESE	99	19	35	TEXACO	#5-35 BEACON	4782	4842		X		6730	6720	771	100	4790-08-06-17	4	44.4	4897	1560	2662	3663	4782	4857	WI
SWSE	99	19	35	EL PASO	#129 MONELL	4696	4706		X		6732	6720	663	483	100	4586-06-10-32	2	43.8	4882	2100	3426	3600	4695	P
SESE	99	19	35	EL PASO	#134 MONELL	4819	4950		X		6770	6758	336	161	100	4819-4850	2	43.9	4884	2165	3465	3680	4813	TA
NWSE	99	19	35	CHAMP	#22 MONELL	4939	4982		X		6721	6711				42	5002	3460	3518	3575	4935		A	
NWSE	99	19	35	CHAMP	#23 MONELL	4808	4938		X		6750	6740						4864	3400	3525	4808		WI	
NWSE	99	19	35	CHAMP	#29 MONELL				X		6717	6707						5248	3400	3514	4884	5180	A	
SENE	99	19	35	CHAMP	#30 MONELL				X		6719	6709	295	100	NOTCH AT 5077			5186	3568	3678	5058		WI	
NWSE	99	19	35	CHAMP	#32 MONELL				X		6711	6704						5426	3500	3612	4999	5562	A	
SESW	99	19	35	CHAMP	#33 MONELL				X		6754	6744						4945	3402	3516	4881		A	
SESE	99	19	35	EL PASO	#41 MONELL				X		6711	6701	1104	472	100	4950-64-66-80	2	42	5040	3470	3840	4982	WI	
SESE	99	19	35	EL PASO	#42 MONELL				X		6736	6725	182	100	5166-5187	2		5500	3762	3800	5187	5500	WI	
SWSE	99	19	35	EL PASO	#127 MONELL				X		6719	6706	65	133	100	5043-66	2	43.8	5015	3546	3755	4871	4886	TA
SWSW	99	19	35	EL PASO	#128 MONELL				X		6736	6723	40	220	100	4870-76-89-97	2	43.9	5071	3592	3805	4940	4936	TA
NESE	99	19	35	EL PASO	#135 MONELL				X		6722	6710	80	141	100	5101-26	2	43.9	5108	2442	3635	3825	4969	TA
SWNE	99	19	35	EL PASO	#139 MONELL				X		6717	6705	65	219	100	4977-97	2	43.8	5225	2340	3745	3960	5099	TA
SWNW	99	19	35	EL PASO	#140 MONELL				X		6741	6729	87	197	100	4848-71	2	43.9	4962	2170	3500	3705	4841	TA
SENE	99	19	35	EL PASO	#146 MONELL				X		6721	6709	51	179	100	4874-95	2	43.9	4990	2170	3528	3726	4861	TA
SENE	99	19	35	EL PASO	#147 MONELL				X		6719	6706	54	138	100	5034-57	2	43.8	5143	2280	3695	3680	5033	TA
SESW	99	20	29	LUFF	#1-28CHAMP				X		6902	6890	56	22	100	3246-58	43	5340	2982	3810	4026	5238	PA	
SESW	99	20	29	LUFF	#1-29CHAMP	5238	5265		X		6921	6909	124	100	5175-85	1	443	5260	2700	3704	3962	5167	P	
NWSE	99	20	29	LUFF	#2-28CHAMP	5162	5187		X									5700	4083	5330	5685	5703	PA	
SENE	99	20	29	PUBCO	14-29-G	5217	5240		X		6885	6873	0	0				5380	2720	3780	3990	5216	DH	
NWSE	99	20	30	PUBCO	16-30J				X		6982	6972						5462		3644	3822	5072	5412	TA
SENE	99	19	12	UPRR	#85 ARCH	4375	4425		X		7013							4530		4375	4406		TA	
SESW	99	19	11	CHAMP	#113 ARCH				X		6960	6975	39	81	84	4286-4306	2	45	4539		3396	4260		
NWSE	99	19	12	FOREST	#33 ARCH	0	0		X		6940	6928	0	716	0	4391-99-07-11	4		4554	2251	3003	4349	4390	PA
CSW	99	19	12	FOREST	W-12-1 ARCH	0	0		X		6845	6836	0	0				3567					PA	
SESW	99	19	12	FOREST	97-12-10 ARCH	0	0		X		6827	6818	126	100	4836-4854	4	4670	3212	3468	4616			A	
SWSW	99	19	12	FOREST	98-12-11 ARCH	0	0		X		6856	6847	185	100	4600-4615	4	4637	3192	3442	4581			A	
SESE	99	19	12	FOREST	93-12-9 ARCH	0	0		X		6803	6794	31	547	67.7	4742-4762	4	4792	3304	3596	4736		A	
SESE	99	19	12	FOREST	32-12-3 ARCH	0	0		X		6811	6800	312	100	4828-4848	2		3381	3683	4815	4921		A	
SWNE	99	19	12	FOREST	104-12-13	0	0		X		6851	6839	55	91	47.1	4728	4	4736	3327	3574	4709		A	
SWSE	99	19	13	UPRR	#116 ARCH	0	0		X		6740	6728	60	120	100	4770-4788	4	44.5	4922	2602	3354	3598	4768	
NWSE	99	19	13	FOREST	31-13-5 ARCH	0	0		X		6792	6781	226	100	4742-4766	2		5180	0	3320	3638	4733	5087	P
NWSE	99	19	13	CHAMP	#34 CHAMP				X		6802	6788	30	60	48.8	4630	2	43	4931		3229	3549	4663	
NWSE	99	19	13	CHAMP	#111 ARCH	0	0		X		6811	6802	12	9.69	33.3	4886-02-14-27	4	4734		3249	3554	5484		
SWNE	99	19	13	FOREST	94-13-11	0	0		X		6743	6743		100	3288-38-96-32	4	3660	2330	3286	3610			PA	
NWSE	99	19	13	FOREST	10-13-3	0	0		X		6763	6754	75	99	4800-4822	4	2790						PA	
NESE	99	19	13	FOREST	92-13-10				X		6741	6728			4836-62	4	49.13	2431	3421	3728	4829		DH	
SESW	99	19	13	CHAMP	#39 ARCH	0	0		X		6750	6740		2479	4882-4894	4	5055	0	3260	3560	4664	5016	GF	
NWSE	99	19	14	FOREST	78-14-6				X		6934	6921	137	100	4324-4342	4	6921	0	2900	3126	4286		SI	
NESE	99	19	14	FOREST	99-14-7				X		6859	6850	161	243	98	4508-4526	4	4556		3126	3372	4500		A

LOC	FW	IN	SEC	LIB	OPERATOR	NAME	T MIN	CORE		PHI	%CR	COI	IND	M	GR	LOG	ELEVATION	GL	IP	GAS	%oil	DEPTH	PERFS			SIG	TD	L	TOPS			ST
								MAX	MIN														GRAV	FW	LW				AL	BR		
NESE	99	19	15		CHAMP	#112 ARCH											6964	6978		1416		4030-48*65-73	4	4.490	4	42.15	2530	2800	2990	4030	GP	
MNSW	99	19	15		CHAMP	#118 ARCH																4030-48*65-73	4	4.490	4	42.15	2530	2800	2990	4030	GP	
SENE	99	19	15		UPFR	#123 ARCH																4268-4278	4	4.43	4.00	3004	3119	4256	4280		P	
MNSW	99	19	15		UPFR	#123 ARCH	4187	4247														4220-4238	4	4.43	4.33	2368	2922	4180	4204		P	
NESE	99	19	16		COASTAL	#1-16 PATRICK	3990	1461														3988-4003	4	4.292	0	1850	2129	3986	4282	GP		
SENE	99	19	23		CHAMP	#3-21 UPFR																4014-4022	4	4.124							CP	
SENE	99	19	23		FOREST	#19-23-3																4014-4022	4	4.124							GP	
SENE	99	19	23		FOREST	#30-23-6																4014-4022	4	4.124							GP	
SENE	99	19	24		UPFR	#4-24-1																4014-4022	4	4.124							GP	
SENE	99	19	24		UPFR	#120	4942	4966														4014-4022	4	4.124							GP	
SENE	99	19	24		CHAMP	#114																4014-4022	4	4.124							GP	
SENE	99	19	24		CHAMP	#110																4014-4022	4	4.124							GP	
MNSW	99	19	24		FOREST	#73-24-7																4014-4022	4	4.124							GP	
MNSW	99	19	24		FOREST	#73-24-7	4690	4717														4014-4022	4	4.124								GP
MNSW	99	19	24		FOREST	#73-24-7																4014-4022	4	4.124								GP
MNSW	99	19	24		FOREST	#73-24-7																4014-4022	4	4.124								GP
MNSW	99	19	24		FOREST	#73-24-7																4014-4022	4	4.124								GP
MNSW	99	19	24		FOREST	#73-24-7																4014-4022	4	4.124								GP
MNSW	99	19	24		FOREST	#73-24-7																4014-4022	4	4.124								GP
MNSW	99	19	24		FOREST	#73-24-7																4014-4022	4	4.124								GP
MNSW	99	19	24		FOREST	#73-24-7																4014-4022	4	4.124								GP
MNSW	99	19	24		FOREST	#73-24-7																4014-4022	4	4.124								GP
MNSW	99	19	24		FOREST	#73-24-7																4014-4022	4	4.124								GP
MNSW	99	19	24		FOREST	#73-24-7																4014-4022	4	4.124								GP
MNSW	99	19	24		FOREST	#73-24-7																4014-4022	4	4.124								GP
MNSW	99	19	24		FOREST	#73-24-7																4014-4022	4	4.124								GP
MNSW	99	19	24		FOREST	#73-24-7																4014-4022	4	4.124								GP
MNSW	99	19	24		FOREST	#73-24-7																4014-4022	4	4.124								GP
MNSW	99	19	24		FOREST	#73-24-7																4014-4022	4	4.124								GP
MNSW	99	19	24		FOREST	#73-24-7																4014-4022	4	4.124								GP
MNSW	99	19	24		FOREST	#73-24-7																4014-4022	4	4.124								GP
MNSW	99	19	24		FOREST	#73-24-7																4014-4022	4	4.124								GP
MNSW	99	19	24		FOREST	#73-24-7																4014-4022	4	4.124								GP
MNSW	99	19	24		FOREST	#73-24-7																4014-4022	4	4.124								GP
MNSW	99	19	24		FOREST	#73-24-7																4014-4022	4	4.124								GP
MNSW	99	19	24		FOREST	#73-24-7																4014-4022	4	4.124								GP
MNSW	99	19	24		FOREST	#73-24-7																4014-4022	4	4.124								GP
MNSW	99	19	24		FOREST	#73-24-7																4014-4022	4	4.124								GP
MNSW	99	19	24		FOREST	#73-24-7																4014-4022	4	4.124								GP
MNSW	99	19	24		FOREST	#73-24-7																4014-4022	4	4.124								GP
MNSW	99	19	24		FOREST	#73-24-7																4014-4022	4	4.124								GP
MNSW	99	19	24		FOREST	#73-24-7																4014-4022	4	4.124								GP
MNSW	99	19	24		FOREST	#73-24-7																4014-4022	4	4.124								GP
MNSW	99	19	24		FOREST	#73-24-7																4014-4022	4	4.124								GP
MNSW	99	19	24		FOREST	#73-24-7																4014-4022	4	4.124								GP
MNSW	99	19	24		FOREST	#73-24-7																4014-4022	4	4.124								GP
MNSW	99	19	24		FOREST	#73-24-7																4014-4022	4	4.124								GP
MNSW	99	19	24		FOREST	#73-24-7																4014-4022	4	4.124								GP
MNSW	99	19	24		FOREST	#73-24-7																4014-4022	4	4.124								GP
MNSW	99	19	24		FOREST	#73-24-7																4014-4022	4	4.124								GP
MNSW	99	19	24		FOREST	#73-24-7																4014-4022	4	4.124								GP
MNSW	99	19	24		FOREST	#73-24-7																4014-4022	4	4.124								GP
MNSW	99	19	24		FOREST	#73-24-7																4014-4022	4	4.124								GP
MNSW	99	19	24		FOREST	#73-24-7																4014-4022	4	4.124								GP
MNSW	99	19	24		FOREST	#73-24-7																4014-4022	4	4.124								GP
MNSW	99	19																														

PATRICK DRAW DATABASE

LOC	FW	IN	SEC	LIB	OPERATOR	NAME	LOC AT CN	TIME	MAX	COE	PH	%DR	COI	IND	M	GR	LOG	SCN	FDI	KB	TELEVA	TION	IP	%coll	DEPTH	PERFS	sl	priv	TD	L	FW	LW	AL	ER	ST				
NEVE	99	18	15		EL PASO	#30 UNIT B2		4572	4622					X	X									100	4570-76*79-87	4	43.8	4935		0				3395	4570				
NESW	99	18	15		UPRR	#1		0	0					X	X									100	4958-4966	4	5065	2830	3395	3665	3665	4812				P			
SESW	99	18	15		UPRR	#178		4760	4793					X	X									100	4750-56	4	44	4925	2008	3324	3582	4750				P			
NANE	99	18	16		CHANDLER	#1		4372	4423					X	X									100	DRYHOLE	4	4812					3233	4354	4670		DH			
SENE	99	18	16		GULF	#1		0	0					X	X									100	DRYHOLE	4	4900	3066	3137	3293	4486	4610				DH			
SWNE	98	19	23		COLORADO	TABLE ROCK SWD#1		0	0					X	X									100	DRYHOLE	4	7512							6442	6874		PA		
SENE	98	19	23		LUFF	#1-23		0	0					X	X									100	DRYHOLE	4	6543	0	4850	4977	6520					PA			
SESE	98	19	23		CHAMP	CPC#1		0	0					X	X									100	DRYHOLE	4	6069									P			
SWNW	98	19	19		CHAMP	#1 UPRR 12D-19		0	0					X	X									99.8	?		5400												
SWNW	98	19	19		FOREST	#3-19-2 ARCH#3		0	0					X	X									99.8	?		5400												
SWNW	98	19	19		CHAMP	#1 UPRR 12B-19		0	0					X	X									99.8	?		5400												
NWSE	98	19	19		FOREST	#19-3 UPRR (ARCH #4)		0	0					X	X									99.8	?		5400												
SESW	98	19	19		FOREST	#2 UPRR 19-1		0	0					X	X									99.8	?		5400												
SESW	98	19	19		FOREST	#38-19-4		0	0					X	X									99.8	?		5400												
NWAW	98	19	19		FOREST	#5-19-3		0	0					X	X									99.8	?		5400												
NEVE	98	19	18		TEXAS	#1-18		0	0					X	X									99.8	?		5400												
NESW	98	19	18		FOREST	#95-18-8		0	0					X	X									99.8	?		5400												
SWSW	98	19	18		FOREST	#91-18-8		0	0					X	X									99.8	?		5400												
SWNW	98	19	18		FOREST	#80-18-7		0	0					X	X									99.8	?		5400												
SESW	98	19	18		FOREST	#37-18-5		0	0					X	X									99.8	?		5400												
NWNE	98	19	18		FOREST	#28-18-4		0	0					X	X									99.8	?		5400												
NWAW	98	19	17		LUFF	#1-17		0	0					X	X									99.8	?		5400												
SWNE	98	19	16		FOREST	#75-16-1		0	0					X	X									99.8	?		5400												
SESE	98	19	13		CHAMP	CPC#1 UPRR44-13		0	0					X	X									99.8	?		5400												
ONE	98	19	11		FOREST	#82-11-1		0	0					X	X									99.8	?		5400												
NENE	98	19	8		TEXAS	#2-8		0	0					X	X									99.8	?		5400												
NENW	98	19	8		TEXAS	#1-8		0	0					X	X									99.8	?		5400												
SWSE	98	19	7		FOREST	#89-7-9		0	0					X	X									99.8	?		5400												
SEAW	98	19	7		FOREST	#40-7-5		0	0					X	X									99.8	?		5400												
SESW	98	19	7		FOREST	#35-7-3		0	0					X	X									99.8	?		5400												
NWNE	98	19	6		LUFF	#1-6		4860	5002					X	X									99.8	?		5400												
SENE	98	19	6		COLORADO	#42-6-19-88		0	0					X	X									99.8	?		5400												
SEAW	98	19	6		LUFF	#2-6		4904	4935					X	X									99.8	?		5400												
SEAW	98	19	5		LUFF	#3-5		5200	5223					X	X									99.8	?		5400												
NWAW	98	19	5		LUFF	#2-5		5159	5197					X	X									99.8	?		5400												
NWSW	98	19	5		LUFF	#1-5		0	0					X	X									99.8	?		5400												
SESW	98	19	5		LUFF	#1		0	0					X	X									99.8	?		5400												
NESE	98	19	4		FOREST	#84-4-1		0	0					X	X									99.8	?		5400												
SWNE	98	19	3		FOREST	#77-3-1		0	0					X	X									99.8	?		5400												
NWAW	98	19	2		LUFF	#1-2		0	0					X	X									99.8	?		5400												
NWAW	98	19	2		CHAMP	CPC#1		6477	6557					X	X									99.8	?		5400												
NWSW	98	19	2		HELENS	USA #1-24		0	0					X	X									99.8	?		5400												
SWSW	98	19	2		COLORADO	#1-24		0	0					X	X									99.8	?		5400												
NWNE	98	19	2		COASTAL	#2-24V		6412	6575					X	X									99.8	?		5400												
SWNW	98	19	2		COASTAL	#3-24V		0	0					X	X									99.8	?		5400												
SESE	98	19	2		COASTAL	#3-24		0	0					X	X									99.8	?		5400												
SESE	98	19	2		TEXACO	#28		0	0					X	X									99.8	?		5400												
SESE	98	19	2		TEXACO	#36 SOUTH OF #24		0	0					X	X									99.8	?		5400												
SESE	98	19	2		TEXACO	#45		0	0					X	X									99.8	?		5400												
SESE	98	19	2		TEXACO	#75		0	0					X	X									99.8	?		5400												



TABLE 1. - Oil fields producing from shoreline barrier deposit. Initial candidates for comparative study and generalization of geological-engineering model

Atkinson	Texas
Bisti	New Mexico
Brent (North Viking Graben)	North Sea
Desert Springs	Wyoming
Echo Springs	Wyoming
Elk City	Oklahoma
Hilight	Wyoming
Jackson-Yegua	S. Texas
Livingston	Louisiana
Lockhard	Louisiana
Milbur	Texas
North Marklam-North Bay City	Texas
Patrick Draw	Wyoming
Pollard	Alabama
Sun Ranch	Wyoming
South Carlton	Alabama
Table Rock	Wyoming
West Ranch	Texas

TABLE 2. - Top five shoreline barrier reservoir candidates for comparison with Bell Creek field

Field/State	Basin	Formation	Depth, ft	Operator	Cores available	References
1. Patrick Draw, WY	Green River	Almond	4,000-5,000	UPRC	USGS, Denver	<sup>18</sup> Roehler, 1988 <sup>28</sup> Keighin et al., 1989
2. Hillight, WY (Springer Ranch Member)	Powder River	Muddy	2,200-9,800	Inexco Oil Co.	RPI International Inc.	<sup>14</sup> Wheeler, et.al. 1988
3. West Ranch, TX						
Greta Reservoir	Gulf Coast	Frio	5,100	Mobil	Mobil, Dallas	<sup>15</sup> Galloway, 1986
Glasscock Reservoir	Gulf Coast	Frio	5,500	Mobil	Mobil, Dallas	<sup>15</sup> Galloway, 1986
41-A Reservoir	Gulf Coast	Frio	5,700	Mobil	Mobil, Dallas	<sup>15</sup> Galloway, 1986
4. Elk City, OK	Anadarko	Penn SS	9,400	Shell	Unknown	<sup>68</sup> Sneider et al., 1977
5. Bisti, NM	San Juan	Gallup	4,920	Shell Chevron Texaco & an Independent	Unknown	<sup>69</sup> Tomkins, 1957 <sup>70</sup> McNeal, 1961

TABLE 3. Comparison of depositional setting, some rock, and some fluid properties for Bell Creek field Unit "A", and the top five candidates for a comparative study

Field/reservoir	Reported environments	Avg net pay, ft	Avg porosity, %	Avg permeability, md	Water saturation, %	Estimated OOIP, MM bbl	Oil gravity Avg, °API
1. Patrick Draw	Barrier Island and Inlet Fill	14	19	50	--	200-250	42
2. West Ranch							
Greta	Aggrading Barrier Island	35	31	1,000+	33	223	24
Glasscock	Transgressive Barrier Island	20	29	540	45	127	31
41-A	Progradation Barrier Island	31	30	900	28	149	32
3. Elk City	Associated Delta and Barrier Bar	40	20	375	--	100	--
4. Bisti	Barrier Bar System	10	15	28	25	150	39
5. Hilight (Springer Ranch Member)	Progradational Barrier Island/spit and tidal inlet deposits	3 to 33 ft	--	--	--	--	40+
6. Bell Creek	Barrier Island and Valley Fill	23	28.5	2,250	26	127	32

TABLE 4. -Shoreline barrier outcrops considered for generalization of reservoir models

---

Almond Sandstone	Wyoming
Cliff House Sandstone	New Mexico
Eagle Sandstone	Montana
Ferron Sandstone	Utah
Fox Hills	Wyoming
Gallup Sandstone	New Mexico
Highway Roadcut	Kentucky
Holy Cross Mts. Miocene sandstone	Poland
Lower Jurassic	South England
Muddy Sandstone	Wyoming
Pictured Cliff Sandstone	New Mexico
Point Lookout Sandstone	New Mexico
Tocito Sandstone	New Mexico
Viking Sandstone	Alberta, CA

---

TABLE 5. - Modern shoreline barriers considered for generalization of reservoir models

---

Atlantic Coast, USA

The Outer Banks  
Wassaw Island

North Carolina  
Georgia

Baltic Sea Coast

Hel Pennisu  
VistulaBarrier Bar  
Kuronsky Barrier Bar

Poland  
Poland  
USSR

Gulf of Mexico

Galveston Island  
Padre/Mustang Islands  
North Bunces Key

Texas  
Texas  
Florida

North Sea Coast

East Frisian Islands  
Terschelling Island

Germany  
Netherlands

---

TABLE 6. - Reservoir data and history for Patrick Draw field

	Patrick Draw	Bell Creek 'A'
Discovered	1959	1967
OOIP - Arch unit, MM STB	97.6	
OOIP-Monell unit, MM STB	112.5	
Total OOIP, MM STB	220-250	127
Primary	Solution Gas	Solution Gas
Arch, %	17.7	-
Monell, %	20.0	-
Bell Creek, %	-	17.3
Secondary	Five-spot waterflood	Linedrive WF
Arch, %	12	-
Monell	15	-
Bell Creek, %	-	36.7
Total recovery, MM STB	78.5 (35% OOIP)	68.6 (54%)
ROS after waterflood, % PV	39	35
Sor. % PV	19.5	30
Oil viscosity, cP	0.52	2.76
Porosity, %	19.8 (12-22)	28.5
Permeability, md	35.9 (5-200)	915 (50-7000)
Interstitial water saturation, %	30-50	20-35
Gas-oil contact, ft	+2525	+2475
Water-oil contact, ft	+1450	+1635
Oil gravity, °API	42	32.5
Initial oil formation volume factor vol/vol	0.52	0.76
Temperature, °F	121	110
Initial pressure, psi	1790 @ +2000'	1204 @ -800'
Saturation pressure, psi	1790 @ +2000'	1204 @ -800'
Initial solution GOR, SCF/bbl	450	200
Net pay, ft	20	22.9
Field size, acres	16,540	7,219
Length - width, miles	9-3	5-2
Depth, ft	5100	4500
DIP, degrees	4	1
HC Porosity	0.13	0.2
Dominant clay	Kaolinite/Illite-Smectite	Kaolinite

TABLE 7. - Chemical composition of a Patrick Draw oil sample. After Richers<sup>34</sup>

Oil Weight	Normal C9+	Saturates	Aromatics	Resin	Asphaltene
0.1087 g	0.0608 g 55.93 %	0.0450 g 41.40 %*	0.0114 g 10.49%*	0.0008 0.74%*	0.0035 3.22%*
Hydrocarbons	Saturates	Aromatics	Resin	Asphaltene	
92.82%**	74.07%**	18.75%**	1.39%**	5.79%**	
Normal Paraffin	Branched Paraffin		Cyclic Paraffin		
70.30%**	11.88%**		17.82%**		

\* Percentage relative to total oil sample

\*\* Percentage relative to nC9+ recovery

TABLE 8. - Range and mean of whole-rock X-ray diffraction analyses (in wt %) of 46 sandstone and 30 shale samples from the upper Almond formation. From Keighin, Law, and Pollastro, 1989<sup>28</sup>

	Shallow core samples (4,500 - 7,500 ft)		Deep core samples (9,600 - 13,700 ft)	
	Sandstone	Shale	Sandstone	Shale
Quartz:				
range	25 - 81	22 - 52	38 - 91	22 - 43
mean	57	37	67	33
Clay:				
range	13 - 25	44 - 67	3 - 26	47 - 72
mean	18	51	18	59
Carbonates:				
range	0 - 55	0 - 19	0 - 42	0 - 31
mean	20	10	12	5
calcite	8	2	3	<1
dolomite	4	5	3	3
ankerite	8	<1	6	<1
siderite	-	<1	<1	1
Feldspar:				
range	0 - 15	2 - 5	0 - 12	1 - 6
mean	5	3	3	3
Pyrite:				
mean	-	2	-	2

TABLE 9. - Mean clay-mineral compositions of sandstone and shale (in wt %) from the upper Almond formation as determined by X-ray diffraction. From Keighin, Law, and Pollastro, 1989<sup>28</sup>

	Shallow core samples (4,500 - 7,500 ft)		Deep core samples (9,600 - 13,700 ft)	
	Sandstone	Shale	Sandstone	Shale
Illite	23	36	44	41
Illite/smectite	30	48	51	47
Kaolinite	47	14	5	9
Chlorite	0	2	0	3

TABLE 10.- Whole rock X-ray diffraction analysis, in weight percent, for samples from Patrick Draw upper Almond formation core samples

Well	Depth, ft	Quartz	Plagioclase	K Feldspar	Calcite	Dolomite	Ferrous Dolomite	Siderite	Pyrite	Kaolinite	Illite/Mica	Illite/Smectite
7-18-1 <sup>1</sup>	4,945	61	4	4	3	-	21	-	3	3	1	tr
45-14-3 <sup>2</sup>	4,450	5	-	tr	93	-	tr	-	-	2	tr	tr
49-1-3 <sup>3</sup>	4,515	69	-	2	1	10	15	-	1	1	1	tr
74-14-6 <sup>4</sup>	4,305	78	2	3	5	5	tr	2	1	2	2	tr

1 Tightly cemented, cross laminated sandstone.

2 Oyster rubble in silty fine sandstone.

3 Faintly cross laminated fine sandstone

4 Ripple laminated sandstone and interbedded mudstone.

TABLE 11. - Characteristics of sands encountered in corehole #2 deposited under different environmental conditions

Depth of sand, ft	Depositional environment from geological studies	Clay content in sandstone <sup>1</sup> mean, % S.D. <sup>4</sup>	Porosity of sandstone <sup>2</sup> mean, % S.D.	Grain size distribution <sup>3</sup> Mean, $\mu\text{m}$ range, $\mu\text{m}$
56-90	Distributary channel	3.85 3.87	23.30 1.81	225 150-300
149-163	Shallow marine, interpreted as uppershoreface	15.23 3.50	22.19 1.50	135 100-200
184-236	Barrier beach	9.08 6.93	26.41 3.12	250 125-350
246-267	Marine, uppershoreface	175.00 2.98	21.19 1.63	170 125-200
282-297	Tidal channel	7.54 6.29	11.44 4.30	254 125-300
346-364	Marine, interpreted as uppershoreface or delta mouth bar	14.50 3.08	18.50 1.98	179 135-275
507-514	Fluvial channel	7.04 6.15	17.52 1.73	-- --

<sup>1</sup> Calculated from gamma ray logs, so the effect of potassium deficient kaolinite clays will be practically absent.

<sup>2</sup> Porosity calculated from density logs.

<sup>3</sup> From visual examination of cores.

<sup>4</sup> Standard deviations.

TABLE 12. - Characteristics of sand in corehole #1

Depth of sand, ft	Depositional environment	Clay content,		Porosity		Grain size Distribution	
		Mean, %	S.D.	Mean,	S.D.	Mean, $\mu\text{m}$	Range $\mu\text{m}$
261-289	Shallow marine sandstone and shale consisting of upper and lower shoreface facies/tidal delta	47.96	10.02	11.7	2.9	115	90-150
293-316	Tidal Delta	37.7	12.36	20.22	1.7	182	125-250
319-337	Distributary channel incised into barrier facies	17.5	3.4	23.1	2.1	203	104-250

TABLE 13. - Permeability reduction of core samples from Patrick Draw field as a result of fresh water injection, after Baptist, White, and Land<sup>37</sup>

Porosity, %	Air permeability, md	Fresh water permeability, md	Ratio of water to air permeability
17.9	<sup>1</sup> 30 <sup>2</sup> 26	<sup>1</sup> 15 <sup>2</sup> 13	0.5 0.5

<sup>1</sup>Arithmetic average for all core samples.

<sup>2</sup>Geometric average for all core samples.

TABLE 14. - Injectivity reduction as a result of chemical injection, TIP, Unit "A", Bell Creek field.

Chemical Injection well	Hall's initial slope, psi-days/bbl	Hall's final slope, psi-days/bbl	Ratio of final to initial slope
C-1	0.46	1.21	2.63
C-2	0.74	-	-
C-2x	-	1.44	1.95
C-3	0.55	2.85	5.18
C-4	1.04	2.85	2.74
C-5	0.52	1.33	2.55
C-6	1.02	1.55	1.52
C-7	0.69	3.07	4.45
C-8	0.88	2.68	3.05
C-9	0.38	1.6	4.37

TABLE 15. - Comparison of water relative permeabilities from well test analysts with those from core analysis

Well	kh core/log md-ft	k <sub>wh</sub> pressure transient md-ft	k <sub>wh</sub> Hall plot md-ft	S Skin factor	k <sub>rw</sub> pressure transient %	k <sub>rw</sub> Hall plot %	k <sub>rw@SOR</sub> <sup>1</sup> core %
C-3	22,000	2,840	2,060	5.4	12.9	9.3	6.4 (1.8-11.5)
C-4	38,000	5,975	1,750	13.1	15.7	4.6	
C-6	42,000	8,420	3,900	37.4	20.0	9.3	
C-8	52,300	9,334	1,600	8.4	17.8	3.1	

<sup>1</sup>Unsteady-state relative permeability and basic flood measurements conducted on core samples from well 22-9 (W-5).

TABLE 16. - Analysis of petrophysical data in Bell Creek field, Unit 'A'

Number	Well name	SW %	So %	$\phi$ %	h ft	q <sub>o</sub> B/D
1	22-01	25.7687	74.2313	23.9789	18.0000	728.00
2	22-03	42.7682	57.2318	20.2625	24.0000	796.00
3	22-05	42.5876	57.4124	21.7408	26.0000	571.00
4	22-08	23.2972	76.7028	21.6950	27.0000	580.00
5	22-09	30.4319	69.5681	24.8067	26.0000	700.00
6	22-10	23.7791	76.2209	21.6439	24.0000	738.00
7	22-11	31.4718	68.5282	21.6874	25.0000	640.00
8	22-12	34.8137	65.1863	19.6716	27.0000	828.00
9	22-13	35.6226	64.3774	23.4711	26.0000	782.00
10	22-14	33.5713	66.4287	22.0770	30.0000	786.00
11	22-15	33.9769	66.0231	23.6846	27.0000	746.00
12	22-16	32.4029	67.5971	20.9663	26.0000	777.00
13	23-01	50.9440	49.0560	22.9070	5.0000	140.00
14	23-03	30.8263	69.1737	23.9114	16.0000	816.00
15	23-04	27.3633	72.6367	22.1497	19.0000	867.00
16	23-05	25.2592	74.7408	22.9388	20.0000	621.00
17	23-07	39.9980	60.0020	20.0122	14.0000	799.00
18	23-10	39.4914	60.5986	20.2169	9.0000	802.00
19	23-12	16.4894	83.5106	27.5971	16.0000	720.00
20	23-14	17.0232	82.9768	26.4499	16.0000	483.00
21	23-16	54.4281	45.5719	23.8139	12.0000	320.00
22	26-01	42.9552	57.0448	213.6852	11.0000	217.00
23	26-02	30.4461	69.5539	25.9269	13.0000	720.00
24	26-03	34.5261	65.4739	29.5175	19.0000	612.00
25	26-04	30.4663	69.5337	23.2494	25.0000	840.00
26	26-05	30.2271	69.7729	24.4288	22.0000	754.00
27	26-06	37.9048	62.0952	27.7117	10.0000	712.00
28	26-07	30.9214	69.0786	23.8915	12.0000	761.00
29	26-08	38.0356	61.9644	22.3100	14.0000	272.00
30	26-09	32.5790	67.4210	25.2507	9.0000	272.00
31	26-10	37.2676	62.7324	24.2404	12.0000	419.00
32	26-11	33.3932	66.6068	27.2232	16.0000	865.00
33	26-12	30.3130	69.6870	28.7134	13.0000	680.00
34	26-13	21.1248	78.8752	21.6681	8.0000	380.00
35	26-14	32.0692	67.9308	27.7057	11.0000	397.00
36	26-15	24.0667	75.9333	28.1657	12.0000	380.00
37	26-16	27.7150	72.2850	27.6565	8.0000	422.00
38	27-02	45.2651	54.7349	20.7823	30.0000	820.00
39	27-03	38.2900	61.7100	21.1303	28.0000	690.00
40	27-04	35.4146	64.5854	23.7572	25.0000	610.00
41	27-05	37.7249	62.2751	22.9025	27.0000	754.00
42	27-07	39.1856	60.8144	19.4559	33.0000	940.00
43	27-09	27.0114	72.9886	22.4881	14.0000	680.00
44	27-11	51.9390	48.0610	20.2164	23.0000	425.00

TABLE 16. - Analysis of petrophysical data in Bell Creek field, Unit 'A' (Continued)

Number	Well name	SW %	So %	$\phi$ %	h ft	q <sub>o</sub> B/D
45	27-12	39.5710	60.4290	22.6830	24.0000	530.00
46	27-14	39.7982	60.2018	19.5527	19.0000	574.00
47	26-15	37.8862	62.1138	22.2913	16.0000	490.00
48	27-16	27.0972	72.9028	23.0632	12.0000	413.00
49	28-08	48.5022	51.4978	23.3901	21.0000	495.00
50	28-16	46.8010	53.1990	19.9908	21.0000	303.00
51	33-02	55.1298	44.8702	22.2917	15.0000	254.00
52	34-02	33.5628	66.4372	22.8329	15.0000	572.00
53	34-03	36.5315	63.4685	21.2841	17.0000	482.00
54	35-03	36.6920	63.3080	23.9160	11.0000	3492.00
	XMEAN	34.8653	65.1347	23.3140	18.5000	599.20
	SIGMA	8.5351	8.5351	2.5204	6.8846	197.64
	XM-S	26.3302	56.5996	20.7935	11.6154	401.56
	XM+S	43.4004	73.6698	25.8344	25.3846	696.84

TABLE 17. - Analysis of differential oil-in-place in Bell Creek field, Unit 'A'

Number	Well name	OIPVOL STB	OIPMBE STB	DOIP STB	RDOP frac	OIPM/OIPV frac	REAMBE acres
1	22-01	897263	791593	105670	0.1178	0.8822	35.29
2	22-03	779774	754177	25597	0.0328	0.9672	38.69
3	22-05	909492	753675	155817	0.1713	0.8287	33.15
4	22-08	1258814	841785	417029	0.3313	0.6687	26.75
5	22-09	1257355	1012221	245134	0.1950	0.8050	32.20
6	22-10	1110299	862532	247767	0.2232	0.7768	31.07
7	22-11	1042912	734009	308903	0.2962	0.7038	28.15
8	22-12	971700	842099	129601	0.1334	0.8666	34.66
9	22-13	1102986	546942	556044	0.5041	0.4959	19.83
10	22-14	1236345	683915	552430	0.4468	0.5532	22.13
11	22-15	1181100	752147	428953	0.3632	0.6368	25.47
12	22-16	1032778	1134693	-101915	-0.0987	1.0987	43.95
13	23-01	157618	201628	-44010	-0.2792	1.2792	51.17
14	23-03	741355	682370	58965	0.0795	0.9205	36.82
15	23-04	855605	859990	-4385	-0.0051	1.0051	40.21
16	23-05	960348	886498	73850	0.0769	0.9241	36.92
17	23-07	471377	510902	-39525	-0.0838	1.0838	43.35
18	23-10	309159	565837	-256678	-0.8302	1.8302	73.21
19	23-12	1034430	884846	149584	0.1446	0.8554	34.22
20	23-14	985627	705679	279848	0.2840	0.7160	28.64
21	23-16	366124	418814	-52690	-0.2439	1.1439	45.76
22	26-01	418328	327334	90994	0.2175	0.7825	31.30
23	26-02	658598	661524	-2926	-0.0044	1.0044	40.18
24	26-03	1028701	880147	148554	0.1444	0.8556	34.22
25	26-04	1133458	1534428	-400970	-0.3538	1.3538	54.15
26	26-05	1050413	1325201	-274788	-0.2616	1.2616	50.46
27	26-06	484167	511072	-26905	-0.0556	1.0556	42.22
28	26-07	557391	622952	-65561	-0.1176	1.1176	44.70
29	26-08	545348	646703	-101355	-0.1859	1.1859	47.43
30	27-09	433475	489481	-56016	-0.1292	1.1292	45.17
31	26-10	514229	633073	-118844	-0.2311	1.2311	49.24
32	26-11	816303	604615	211688	0.2593	0.7407	29.63
33	26-12	729983	1017526	-287543	-0.3939	1.3939	55.76
34	26-13	385017	740516	-355499	-0.9233	1.9233	76.93
35	26-14	581249	659140	-77891	-0.1340	1.1340	45.36
36	26-15	725935	427524	298411	0.4111	0.5889	23.56
37	26-16	451306	532093	-89787	-0.1790	1.1790	47.16
38	27-02	956365	912920	43445	0.0454	0.9546	38.18
39	27-03	1022469	642351	380118	0.3718	0.6282	25.13
40	27-04	1079009	762925	316084	0.2929	0.7071	28.28
41	27-05	1078333	722506	355827	0.3300	0.6700	26.80
42	27-07	1093064	839779	253285	0.2317	0.7683	30.73
43	27-09	643759	1112908	-469149	-0.7288	1.7288	69.15
44	27-11	625828	603056	22772	0.0364	0.9636	38.54

TABLE 17. - Analysis of differential oil-in-place in Bell Creek field, Unit 'A' (Continued)

Number	Well name	OIPVOL STB	OIPMBE STB	DOIP STB	RDOP frac	OIPM/OIPV frac	REAMBE acres
45	27-12	923105	839090	84015	0.0910	0.9090	36.36
46	27-14	627629	747150	-119521	-0.1904	1.1904	47.62
47	27-15	621076	1139464	-518388	-0.8347	1.8347	73.39
48	27-16	567543	660656	-93113	-0.1641	1.1641	46.56
49	28-08	709861	423390	286471	0.4036	0.5964	23.86
50	28-16	625946	469712	156234	0.2496	0.7504	30.02
51	33-02	421042	612742	-191700	-0.4553	1.4553	58.21
52	34-02	640697	845324	-204627	-0.3194	1.3194	52.78
53	34-03	644809	531826	112983	0.1752	0.8248	32.99
54	35-03	471089	438070	33019	0.0701	0.9299	37.20
XMEAN		776444	728585	47859	-0.0069	1.0069	40.28
SIGMA		278008	240360	240397	0.3273	0.3273	13.09
SM-S		498436	488244	-192538	-0.3342	0.6796	27.18
SM+S		1054452	968945	288257	0.3204	1.3342	53.37

TABLE 18. - Analysis of overlay results of differential oil-in-place on various geological and engineering variables, Bell Creek field, Unit 'A'

Variable*	Correlation
Diagenetic clay	Not obvious; TIP area only
Average matrix	Fair; TIP area only
Total clay content	Fair; TIP area only
Maximum matrix	None; TIP area only
Net pay (core)	Fair
$\phi$ (core)	Not obvious
$k_{air}$ (arithmetic)	Bad to fair
h	Not obvious
Dykstra-Parsons coeff.	Fair to good
LHI	Good
Net pay (log)	Not obvious
$\phi$ (log)	Not obvious
clay (log)	Fair
$R_i$	Not obvious
$R_i$ ratio	Not obvious; TIP area only
ROS (1980, core)	Not obvious; TIP area only
ROS (1980, simulation)	Not obvious; TIP area only
$q_{oi}$	Fair
Primary reserve	Fair
Maximum prim. prod. rate	Fair
Prim. cum. prod.	Fair to good
Prim. cum. prod.	Fair to good
Tertiary cum. prod.	Fair
20% water cut	Front direction normal to DOIP contours
70% water cut	Front direction normal to DOIP contours
70% water cut	Front direction normal to DOIP contours
Streamlines-preflush	More dense streamlines in - DOIP areas
Streamlines-chem. inj.	More dense streamlines in - DOIP areas

\*Source map may be found in Report No. NIPER-390, February 1989.

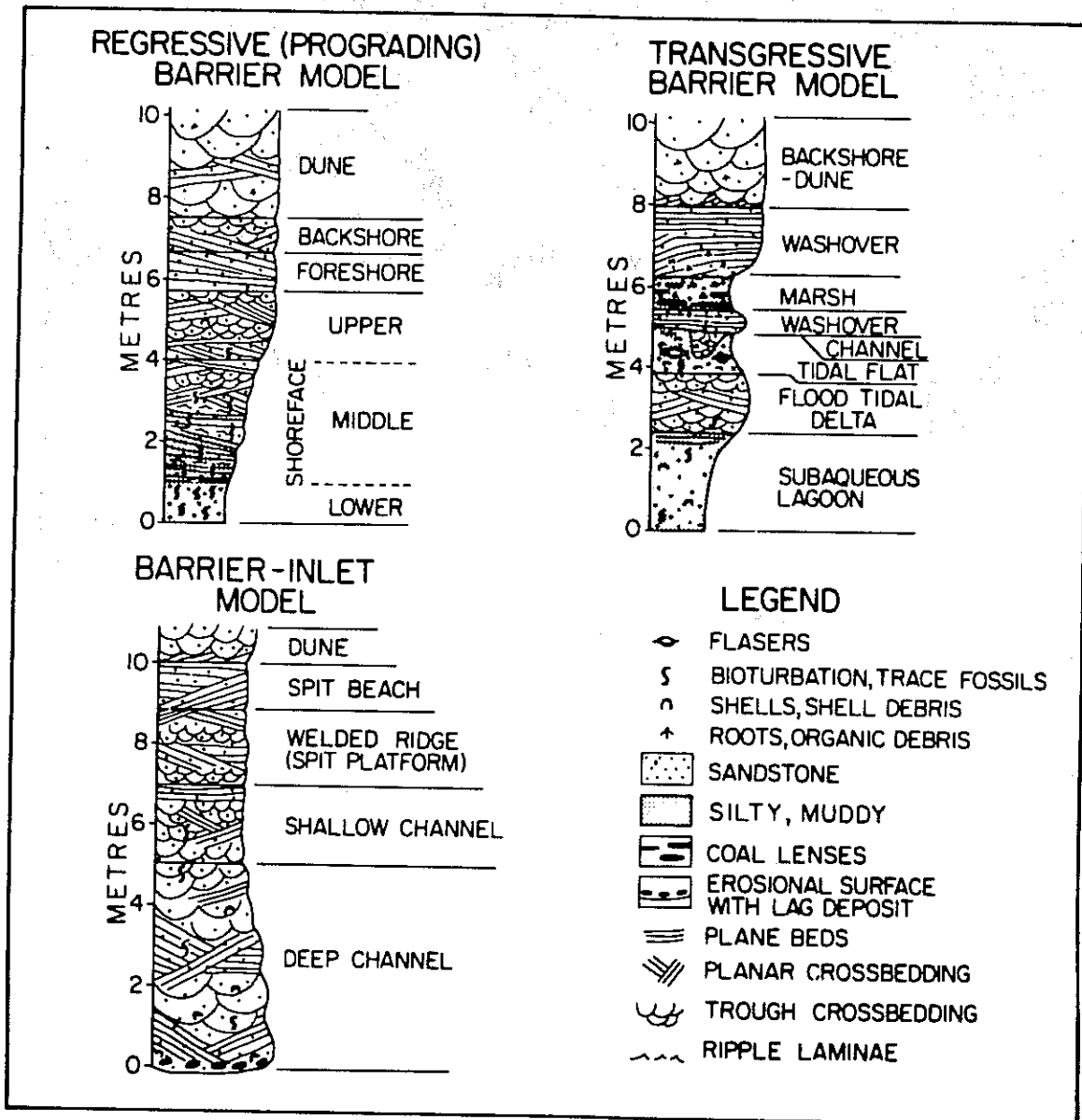


FIGURE 1. - Three "end-member" facies models of barrier island stratigraphic sequences. Although each section has been standardized to 10 m, thicknesses could range up to a few tens of meters. From Reinson, 1979<sup>1</sup>



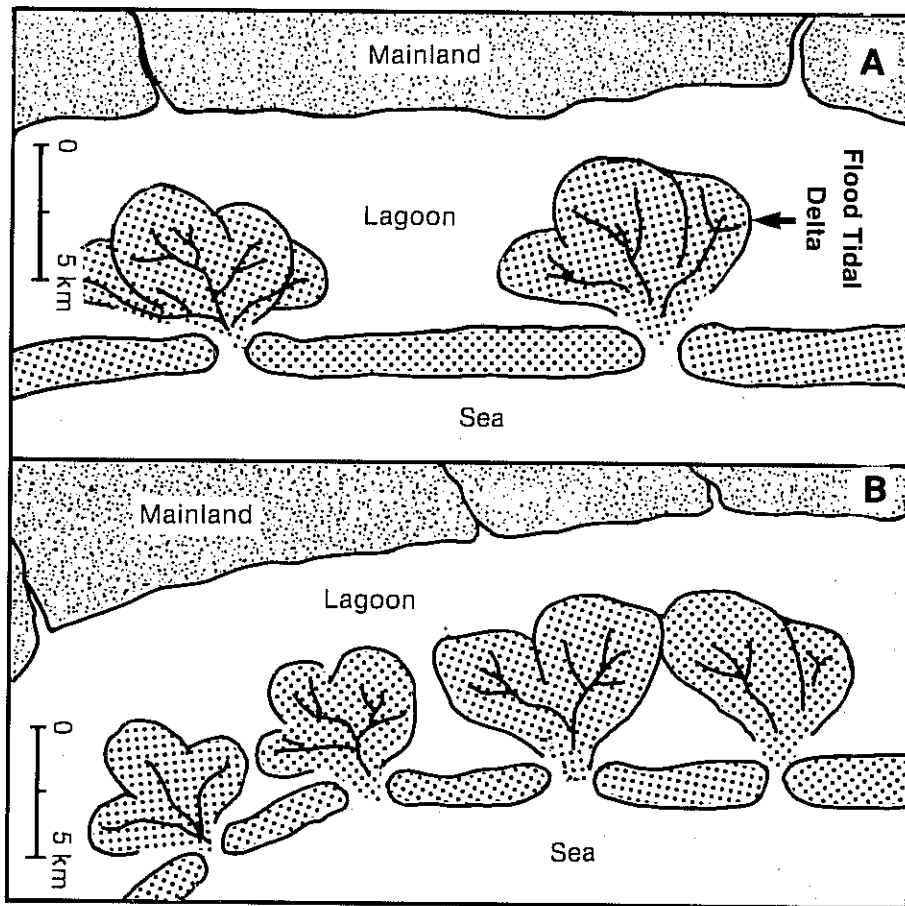


FIGURE 3. - The influence of inlet spacing on the interconnectedness ratio of tidal delta deposits. A - microtidal coast (Bell Creek core); B - mesotidal coast (Patrick Draw core). After Donselaar<sup>4</sup>.

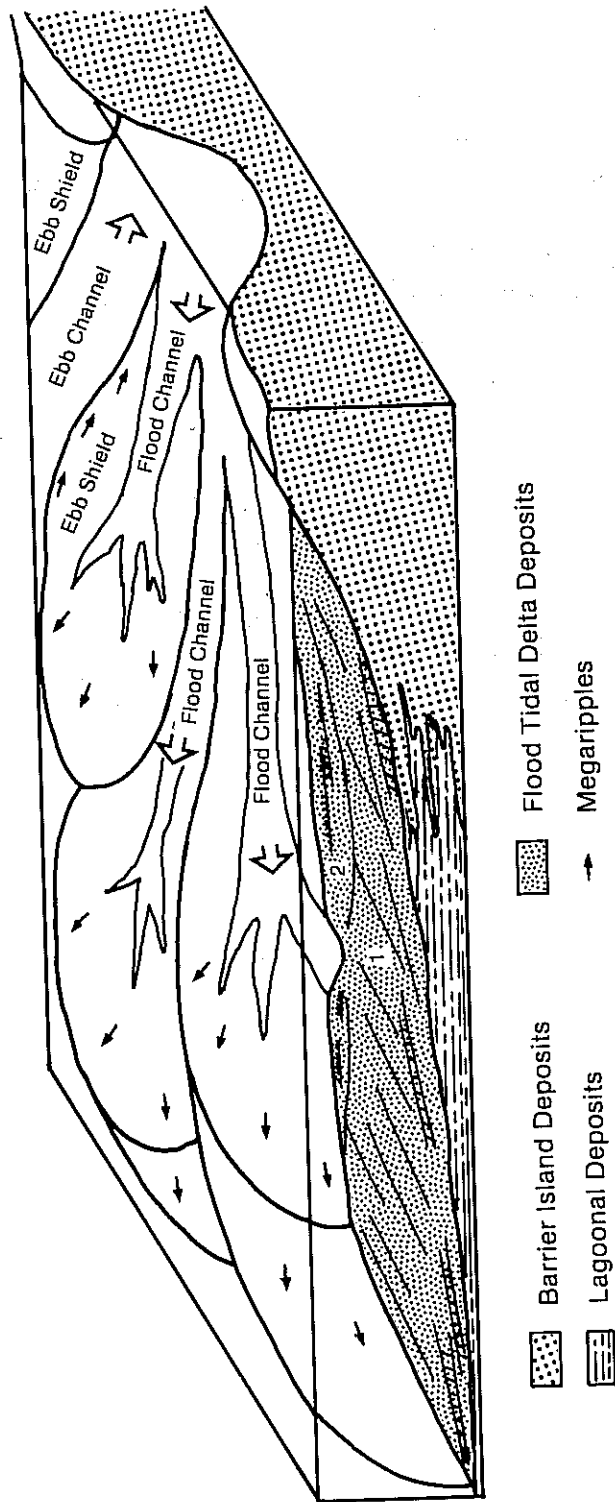


FIGURE 4. - Reconstruction of a landward expanding flood-tidal delta. Lower part (1) is made up of landward dipping megaripples and avalanche foresets, generated by sediment transport down the delta slope. Upper part (2) consists megaripples and channel fills, formed on the ebb-shields and flood-shields, and by migration of the channels on the delta top. After Donselaar<sup>4</sup>.

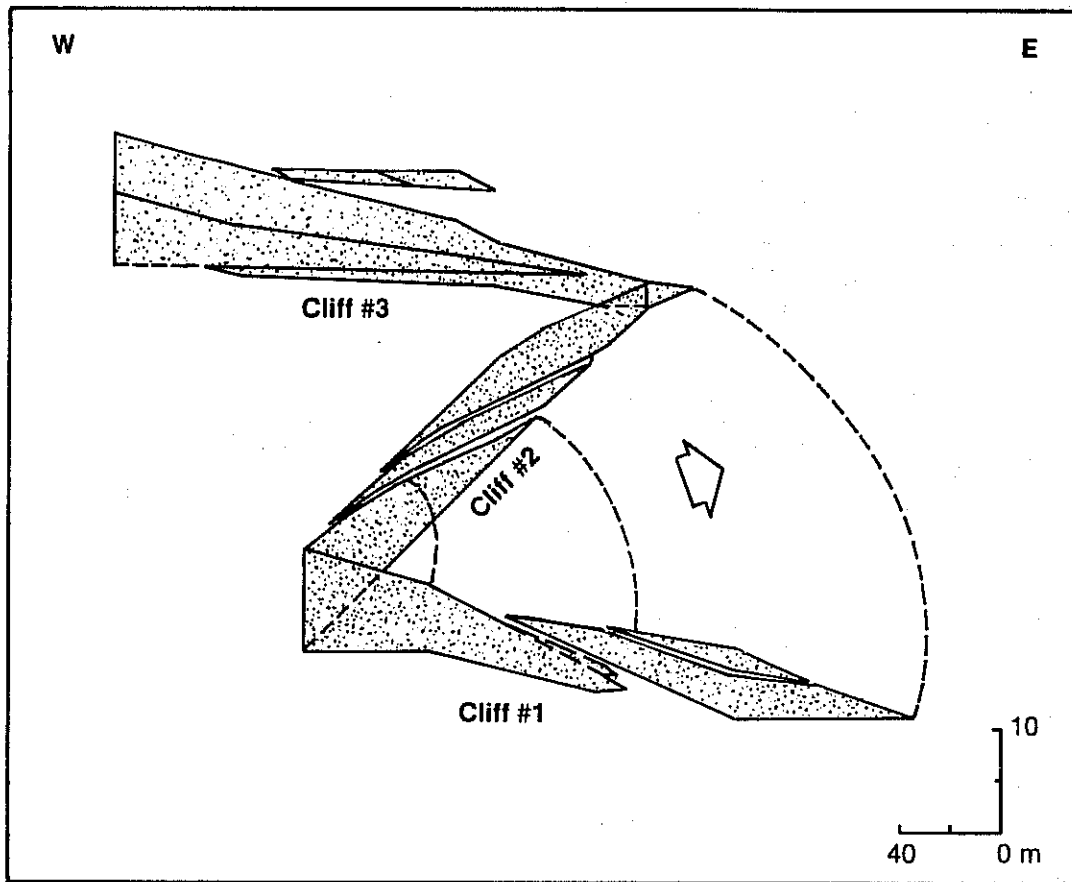


FIGURE 5. - Three-dimensional reconstruction of the wedge-shaped geometry of flood tidal delta sandstone. The illustrated wedges-out in a distance of about 700 ft. Arrow indicates direction of flood tide. After Cuevas<sup>5</sup>.

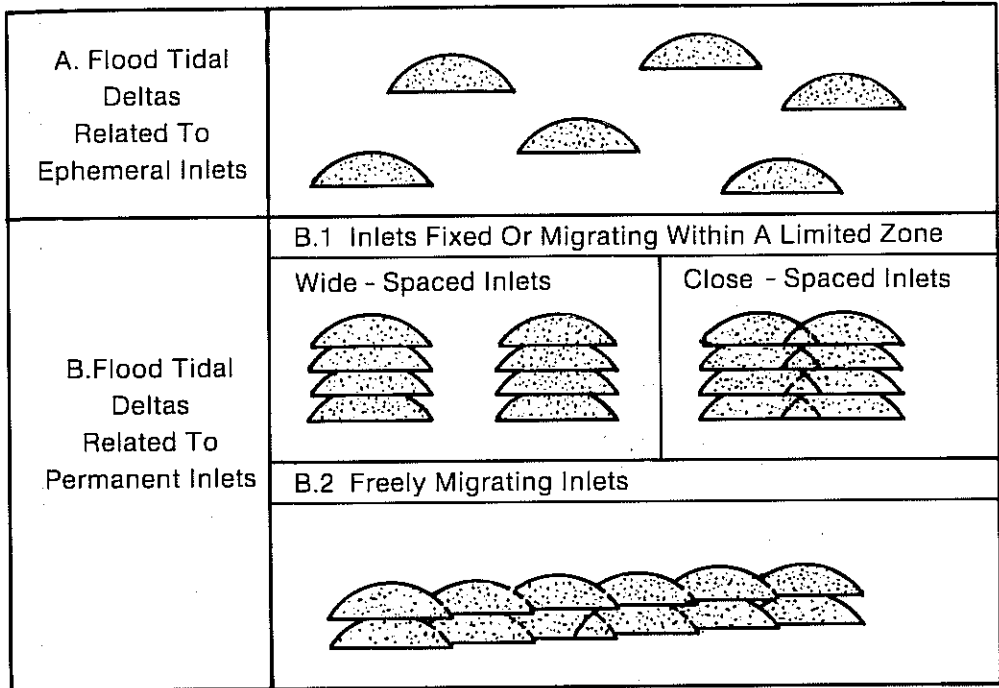


FIGURE 6. - Models for the vertical stacking of flood tidal deltas in an environment of relative rise of sea level. After Donselaar<sup>4</sup>.

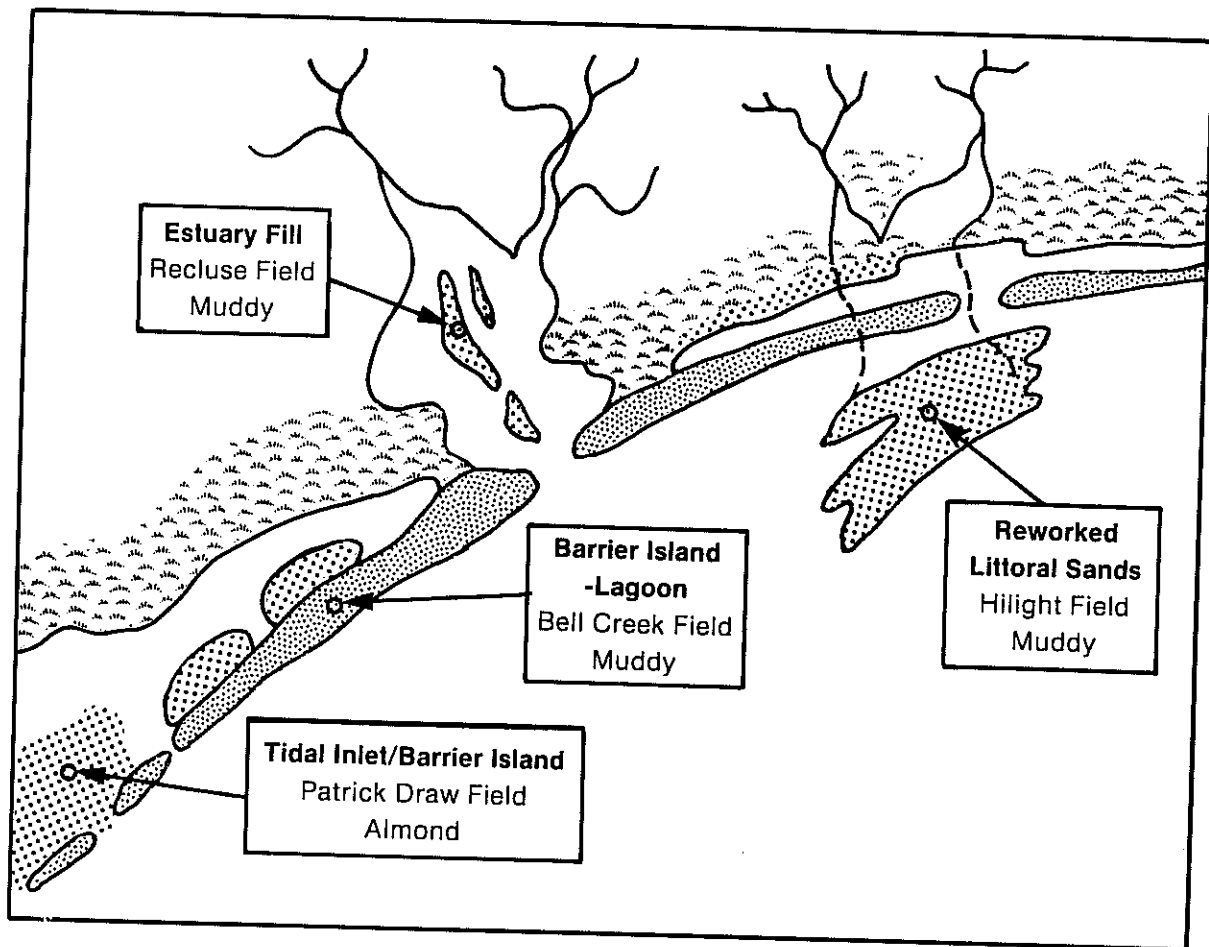


FIGURE 7. - Diagrammatic map showing relative locations of ancient oil productive shoreline barrier sandstones in Wyoming and Montana. Modified from Berg.<sup>72</sup>.

CORE HOLE #1

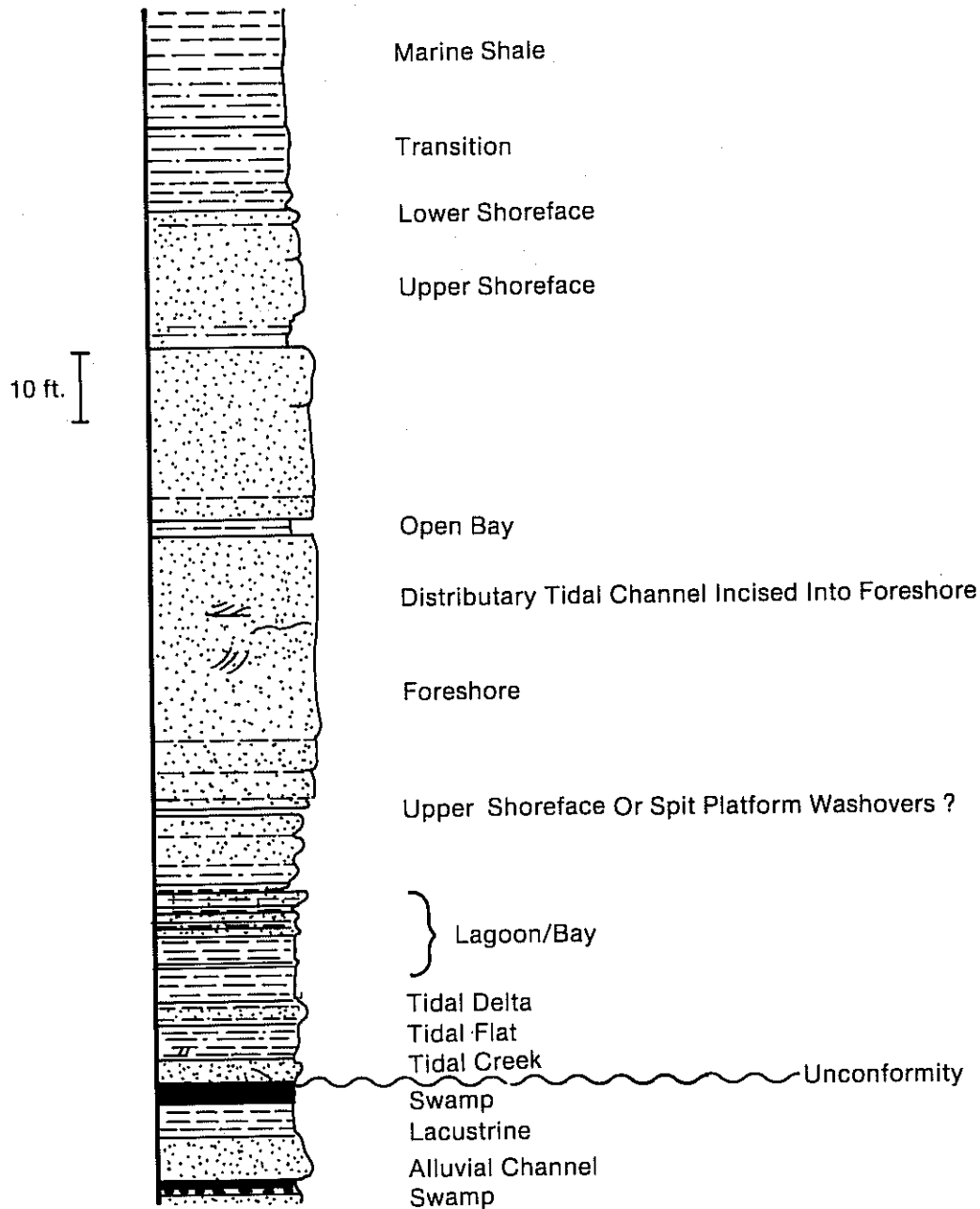


FIGURE 8. - Vertical sequence of facies from outcrop core hole #1, Almond formation.

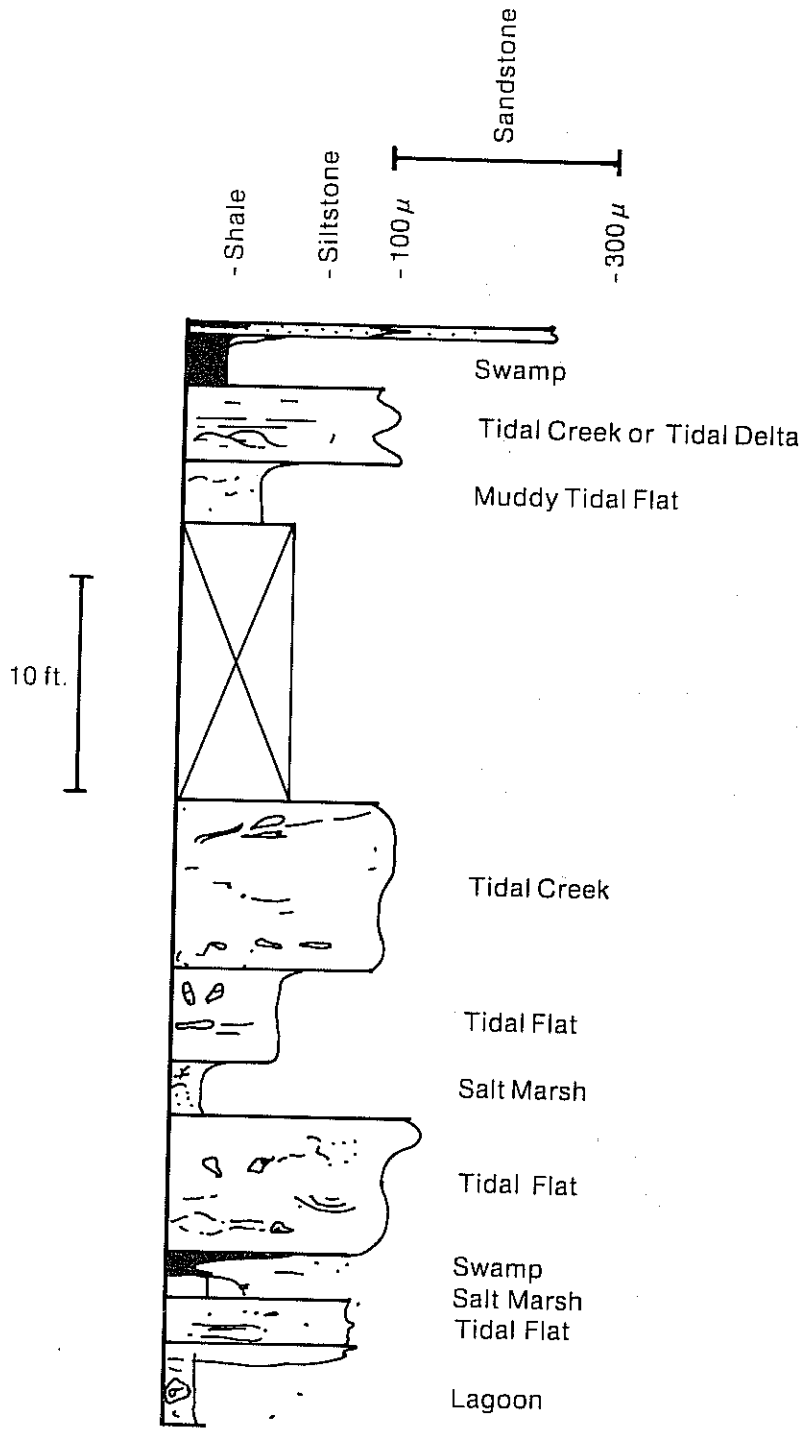


FIGURE 9. - Vertical sequence of facies in cored interval from well Arch 78-14-6, Patrick Draw field, WY, with grain size distribution.

TIDAL CHANNEL  
BAR

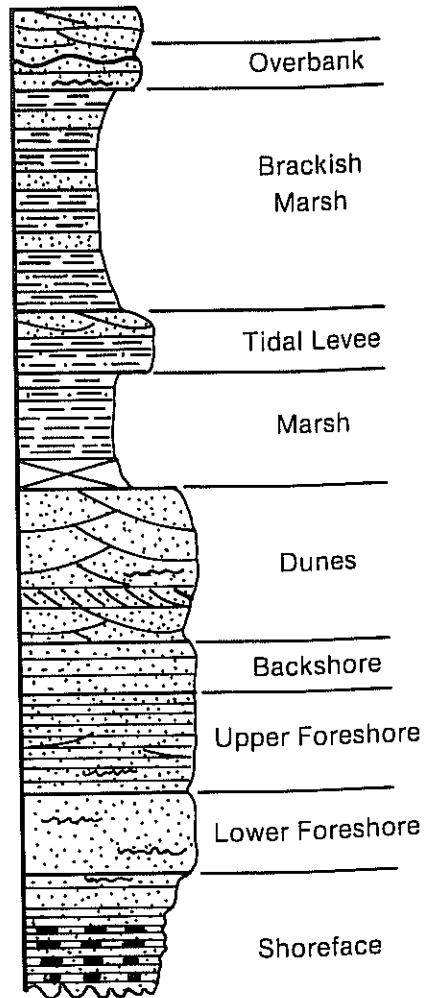


FIGURE 10. - Typical regressive sequence of the shoreline barrier sediments in Southeastern Colorado; the lower and upper Cretaceous Dakota Sandstone with an average thickness of 80 feet. The sequence represents barrier island facies (lower half) and backbarrier facies of tidal origin (upper half) of the profile. After Taylor<sup>73</sup>.

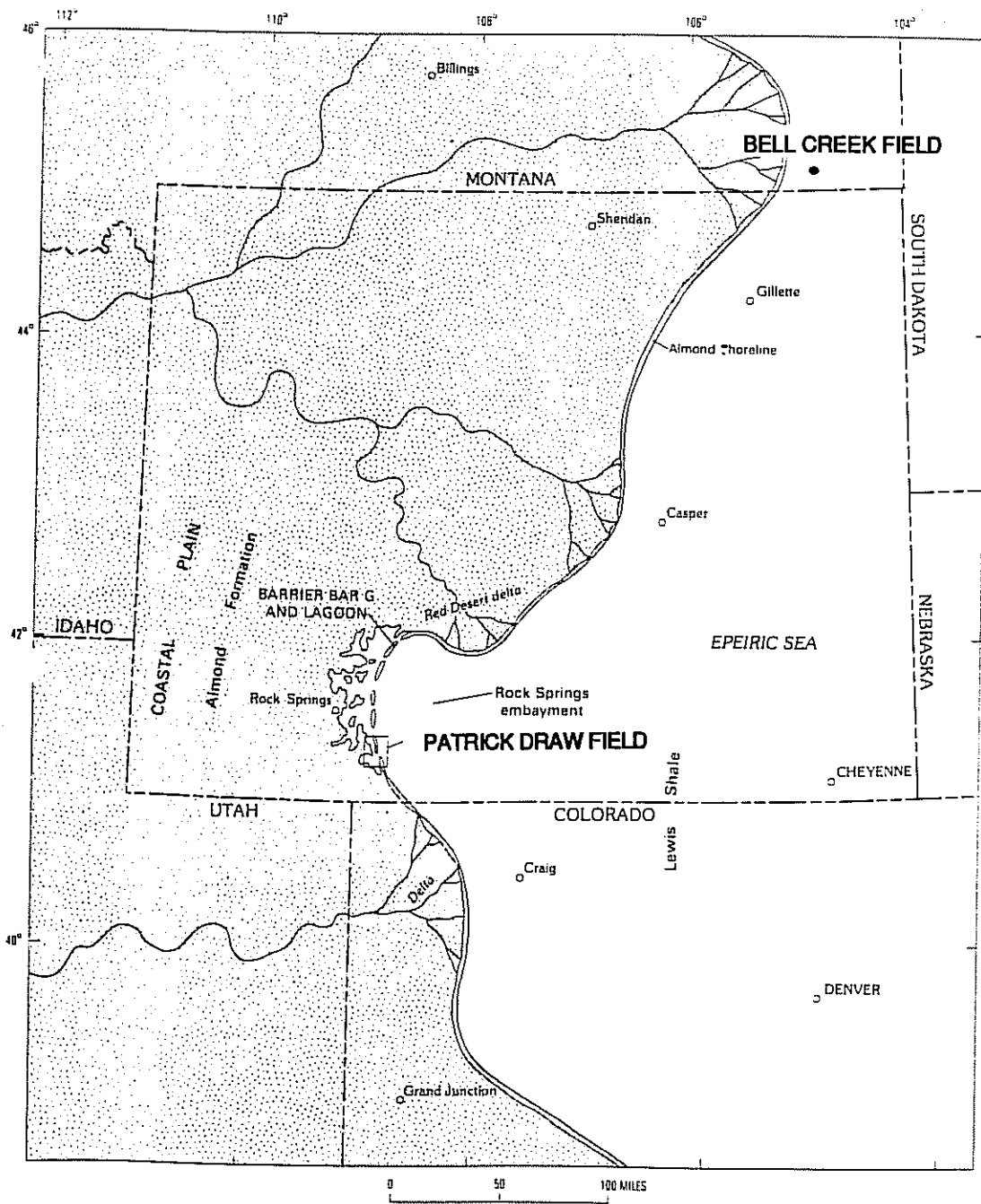


FIGURE 11. - Paleogeographic setting of the Almond formation shoreline/barrier island system on the western shoreline of the Late Cretaceous epeiric sea. After Roehler<sup>18</sup>.

**EXPLANATION**

1. Flood ramp
2. Flood channel
3. Tidal-oyster flat
4. Ebb shield
5. Ebb spit
6. Spillover lobe
7. Back barrier flat swamp
8. Vegetated dune ridge
9. Recurved spit
10. Beach
11. Main ebb channel
12. Marginal flood channel
13. Swash bar
14. Terminal lobe
15. Channel margin linear bar

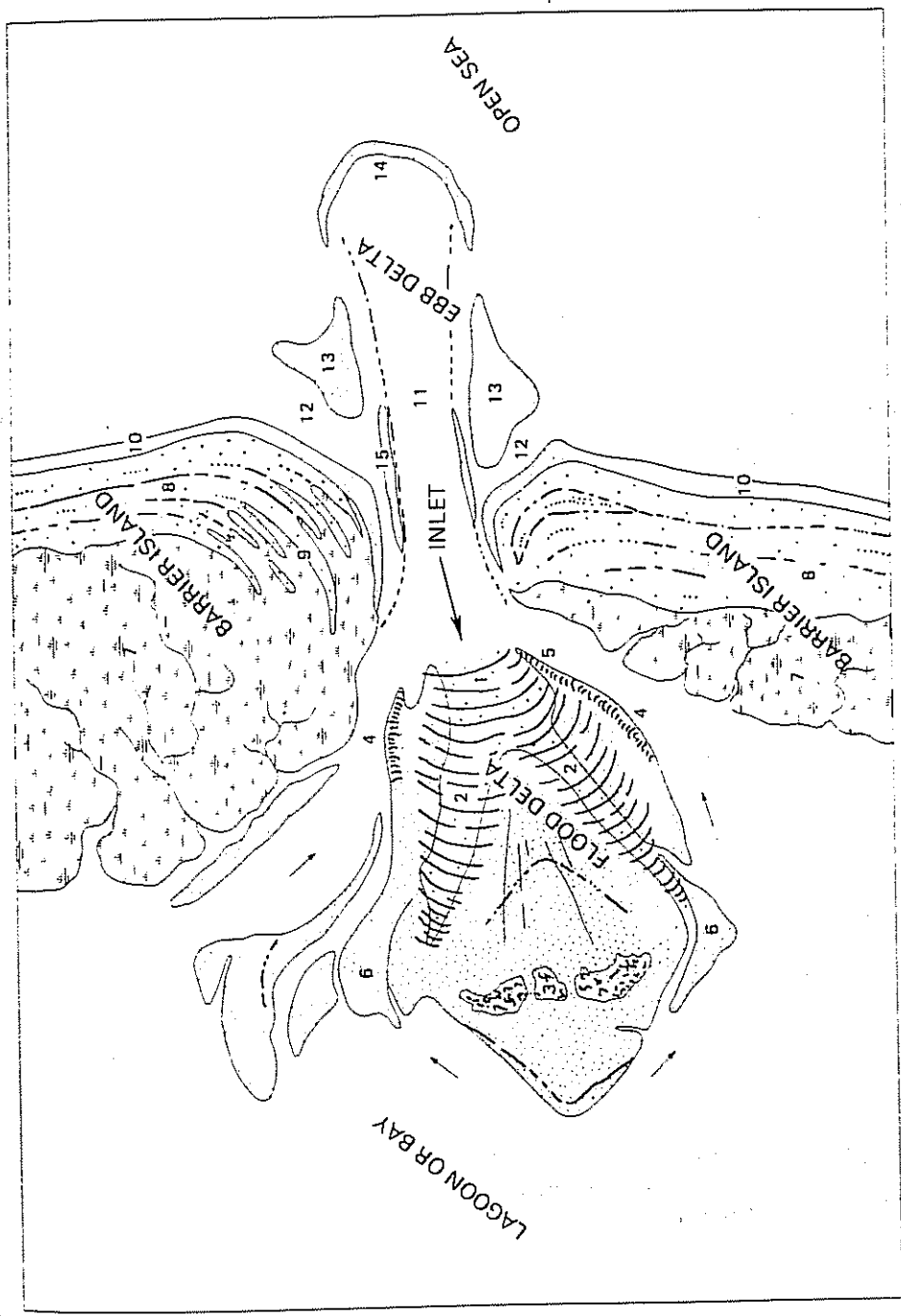


FIGURE 12. - Nomenclature and anatomy of facies deposited in a mesotidal barrier island system. After Hayes and Kana, 197627.

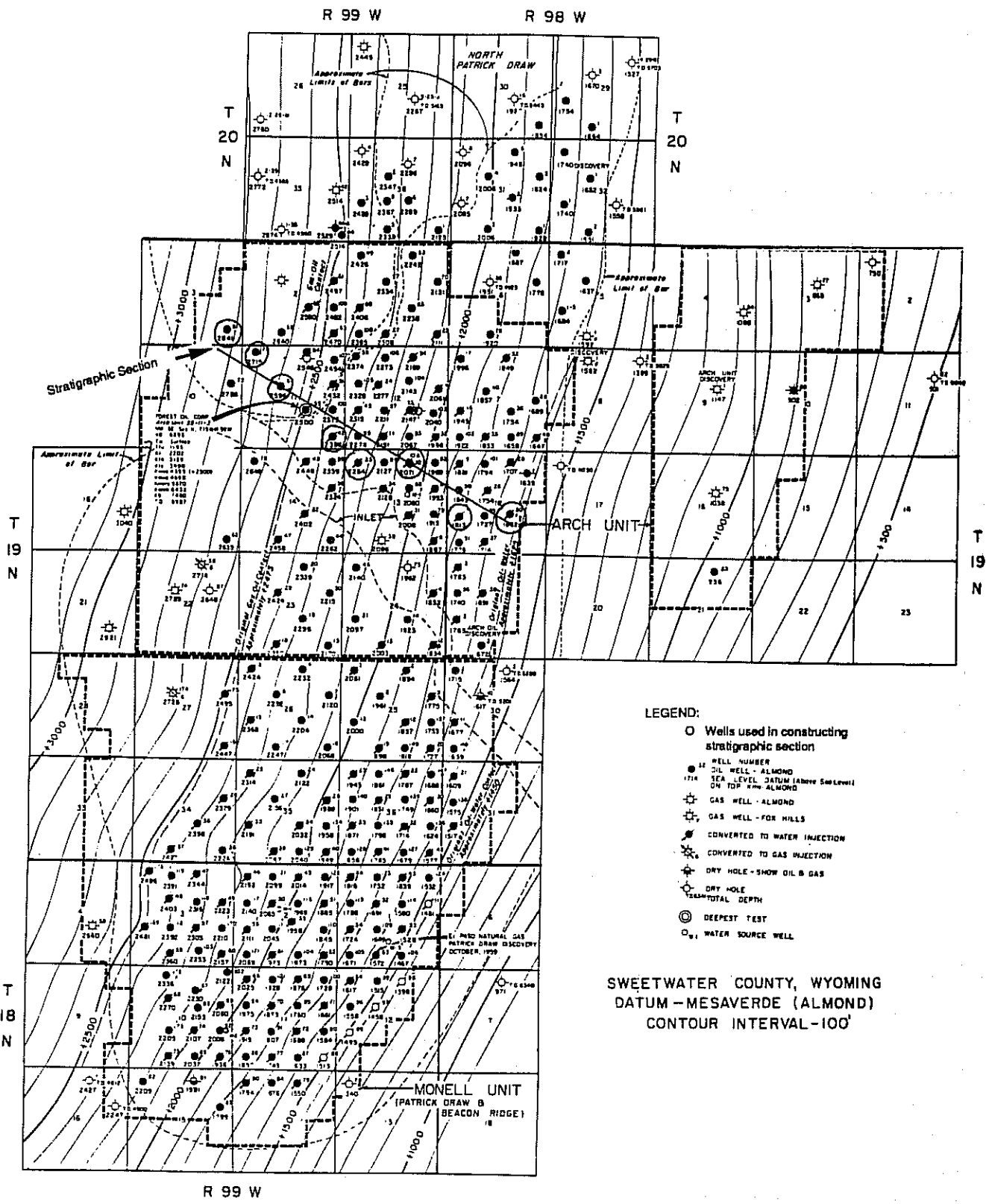


FIGURE 13. - Map showing location of wells within Arch and Monell units of Patrick Draw field and location of log-based dip-oriented stratigraphic section illustrated in fig. 31.

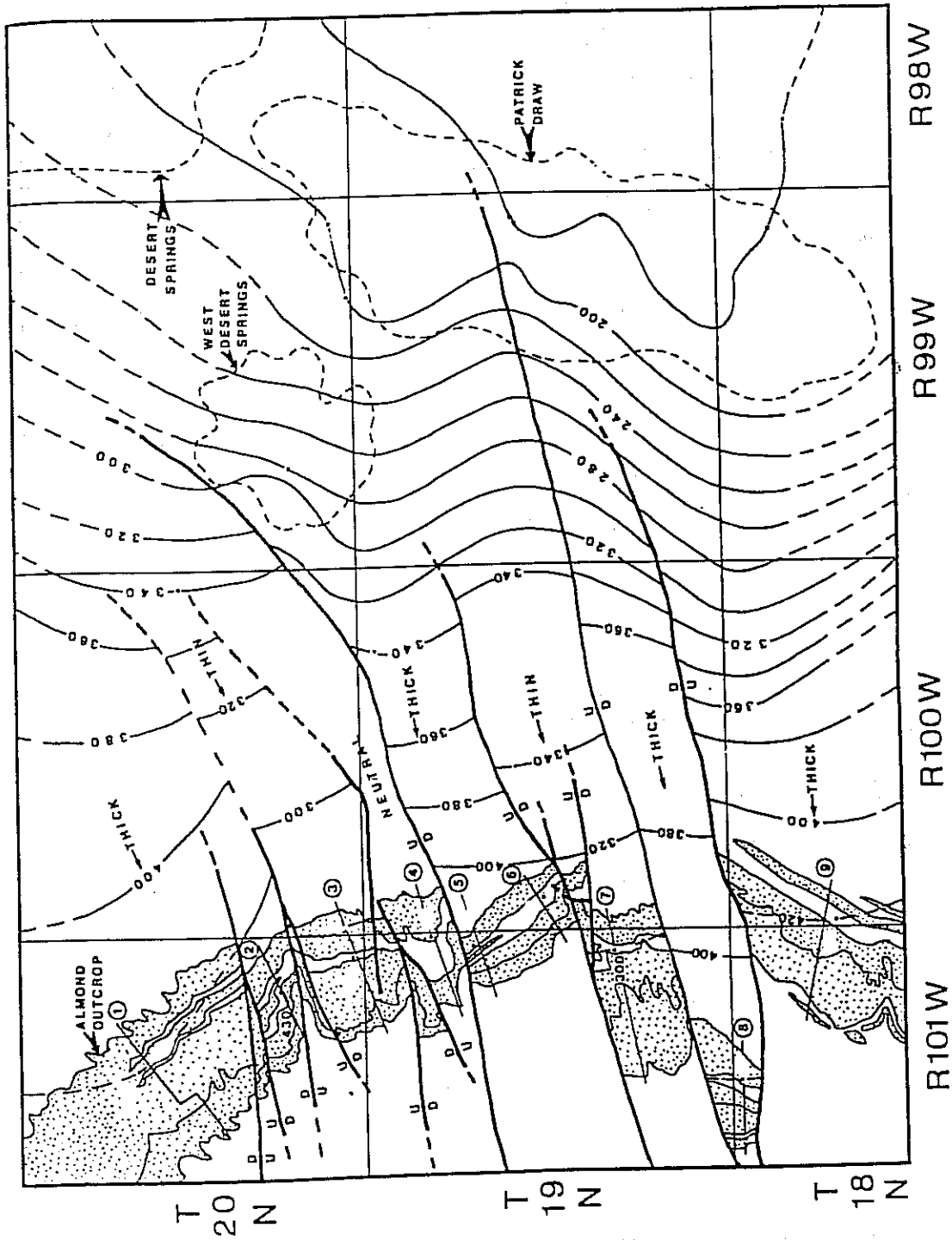


FIGURE 14. - Isopach map of interval from the "A" marker bentonite to the top of the lower Almond (same as interval 2 of Weimer, 1966) approximately equivalent to the upper Almond sequence in the outcrop. A series of thickness variations associated with the east-northeast faults that cut the area strongly indicates that rates of subsidence varied between fault blocks (syndepositional fault movement). Contour interval is 20 ft. From Van Horn, 1979<sup>21</sup>.

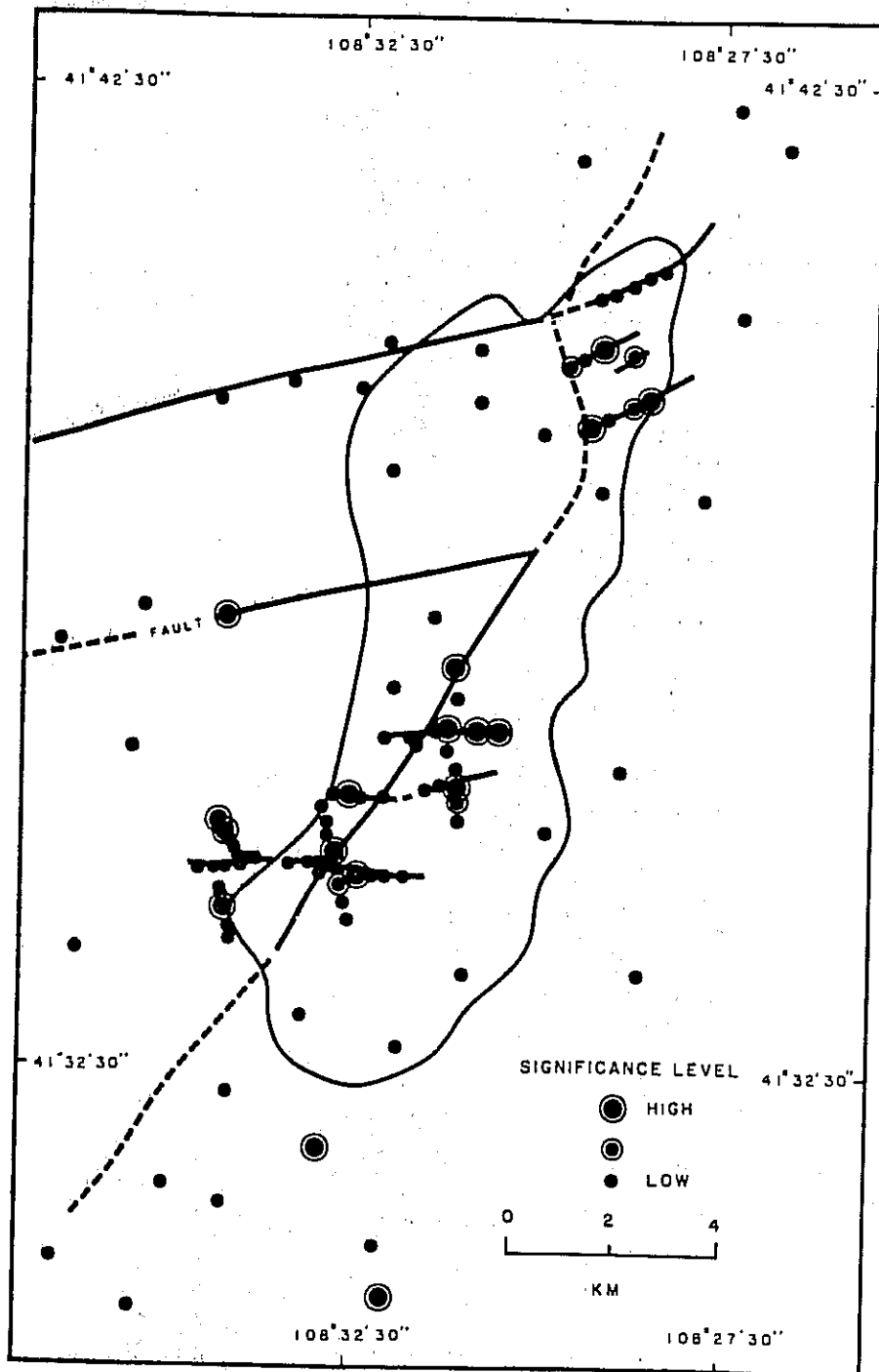


FIGURE 15. - Combined geochemical anomalies and faults at Patrick Draw oil field from the 1980 Geosal study. After Richers, 1982<sup>34</sup>.

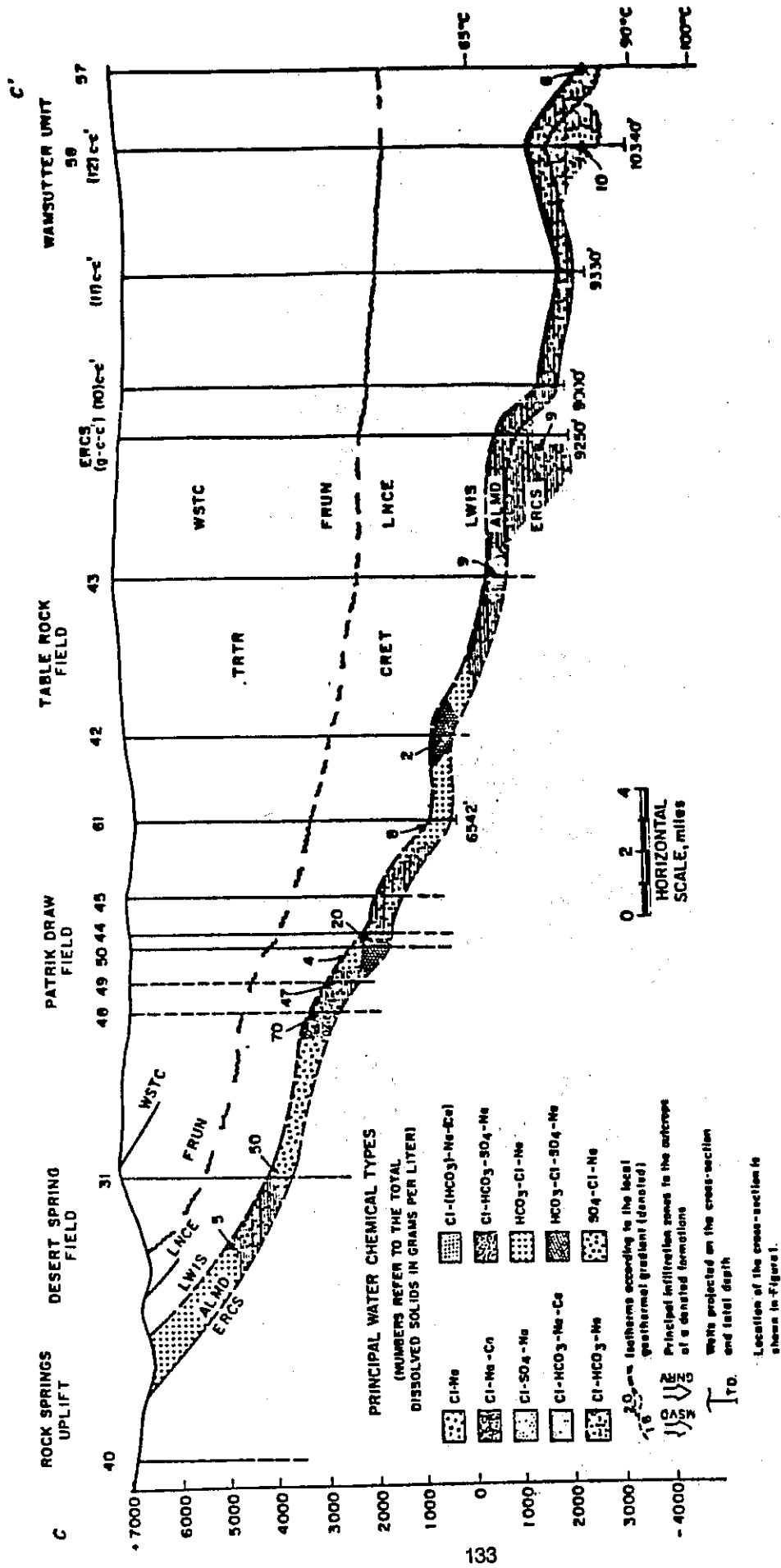


FIGURE 16. - Hydrochemical cross-section east of the Rock Springs Uplift, Greater Green River Basin. Almond formation interpreted. Geology based on the log correlation by Tyler, 1979 (cross section C-C'). After Szpakiewicz and Collins, 1985:37.

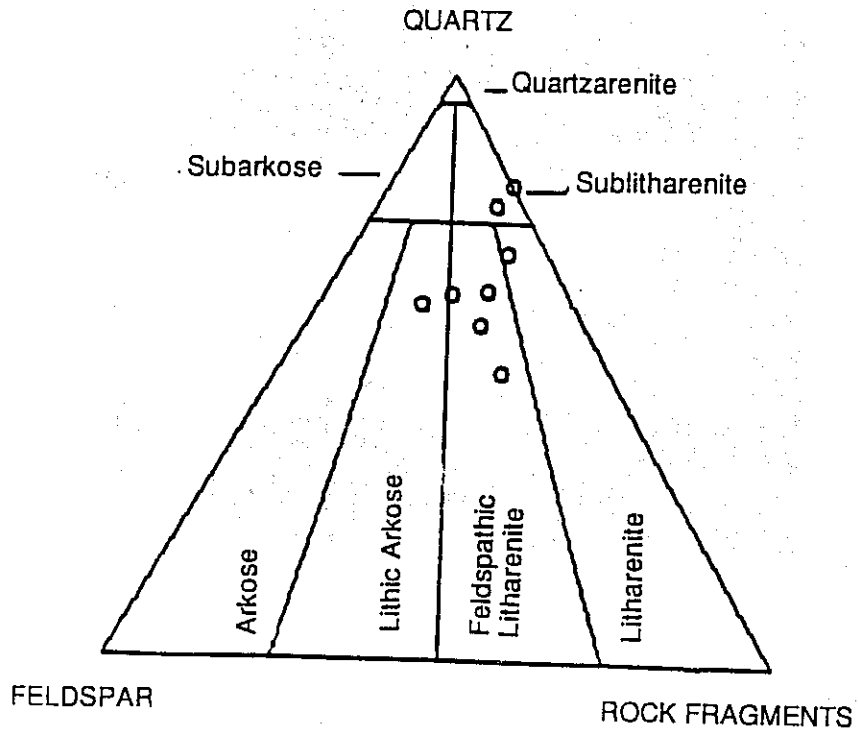


FIGURE 17. - Quartz-feldspar-rock fragment composition and rock type classification<sup>42</sup> for thin section samples from the upper Almond formation at Patrick Draw field.

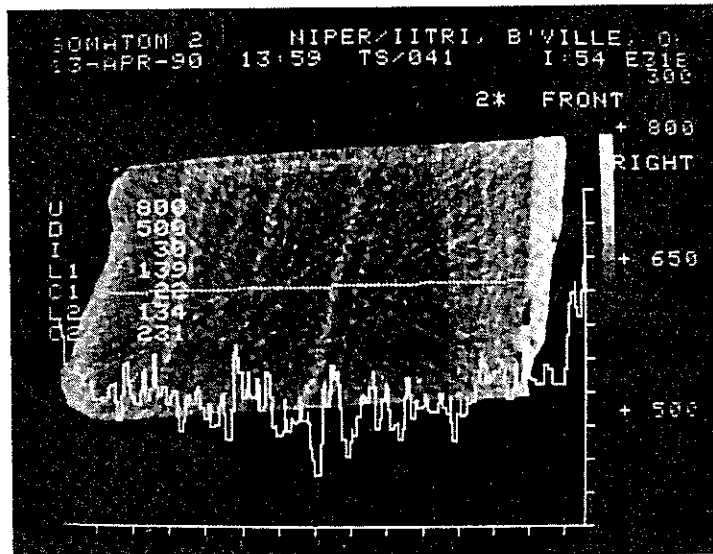


FIGURE 18. - CT scan and density profile for porous, cross bedded sandstone from Patrick Draw field well 49-1 3 at 4,552 ft. CT density varies from about 600 to 700 H.U.

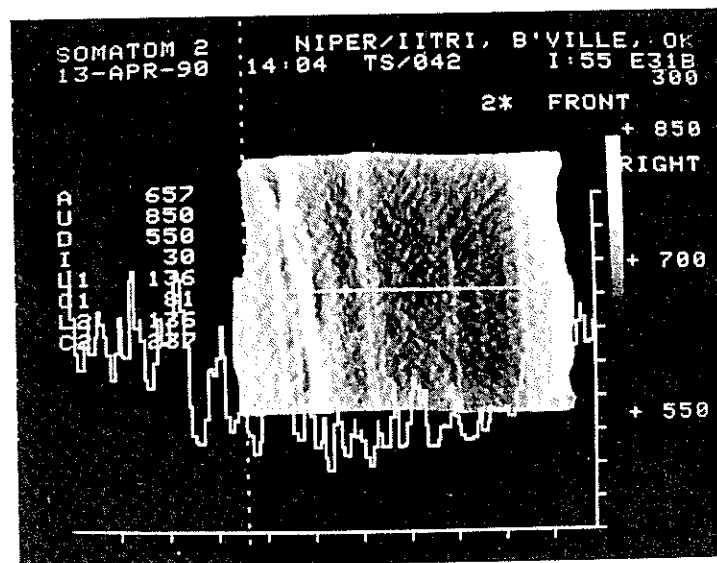


FIGURE 19. - CT scan and density profile for thinly laminated sandstone from Patrick Draw field well 49-1 3 at 4,531 ft. CT density varies from about 650 to 750 H.U.

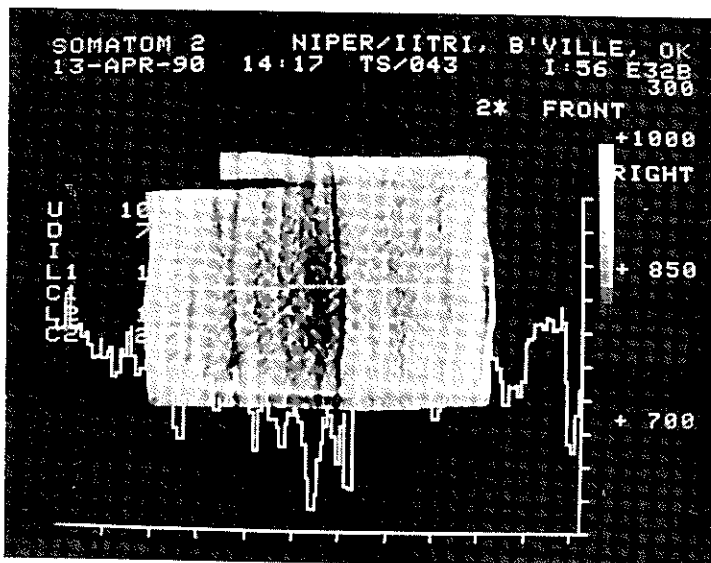


FIGURE 20. - CT scan and density profile for interlaminated silty, very fine sandstone and silty shale from Patrick Draw field well 7-18-1 at 4,957 ft. CT density varies from about 750 to 850.

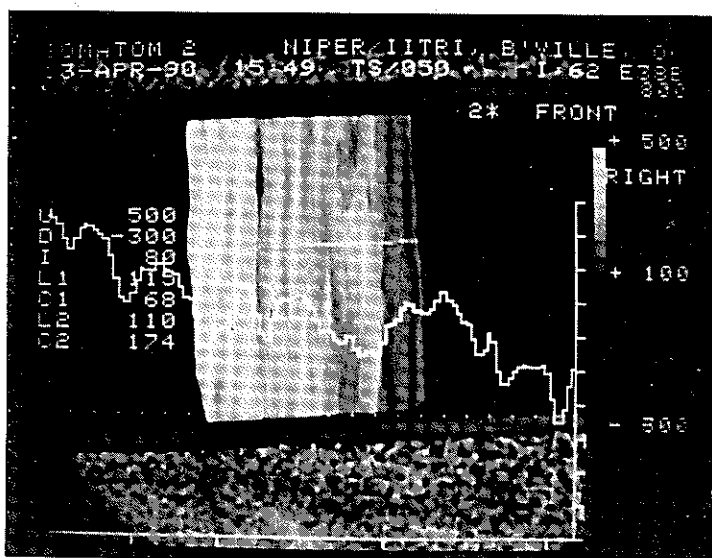


FIGURE 21. - CT scan and density profile for black, coaly siltstone and shale from Patrick Draw field well 78-14-6 at 4,344 ft. CT density varies from 0 to 450 H.U.

Diagenesis

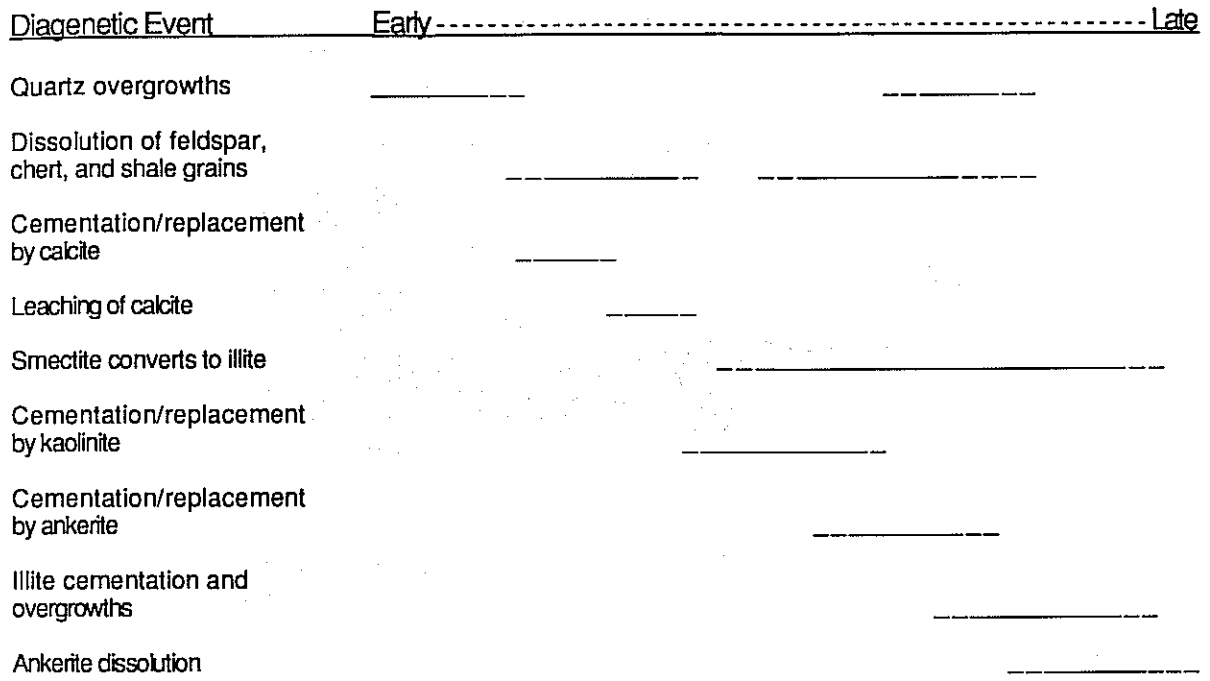


FIGURE 22. - Diagenetic sequence for upper Almond Formation, typical of Patrick Draw field. Modified from Keighin, Law, and Pollastro, 1989<sup>28</sup>.

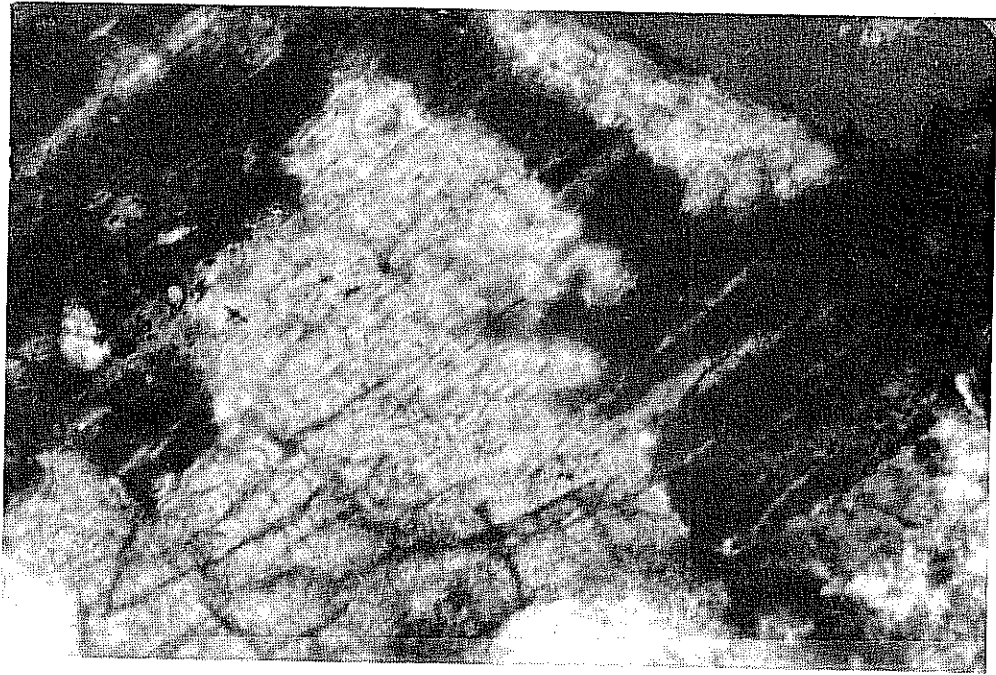


FIGURE 23. - Dolomite is dominantly cement, however, it locally replaces framework grains. Light-colored area in center of photomicrograph is dolomite which has replaced a twinned feldspar (darker area). Solution of such replacement dolomite provides secondary porosity. Well 7-18-1, 4,955 ft. Length of photomicrograph is 9 microns.

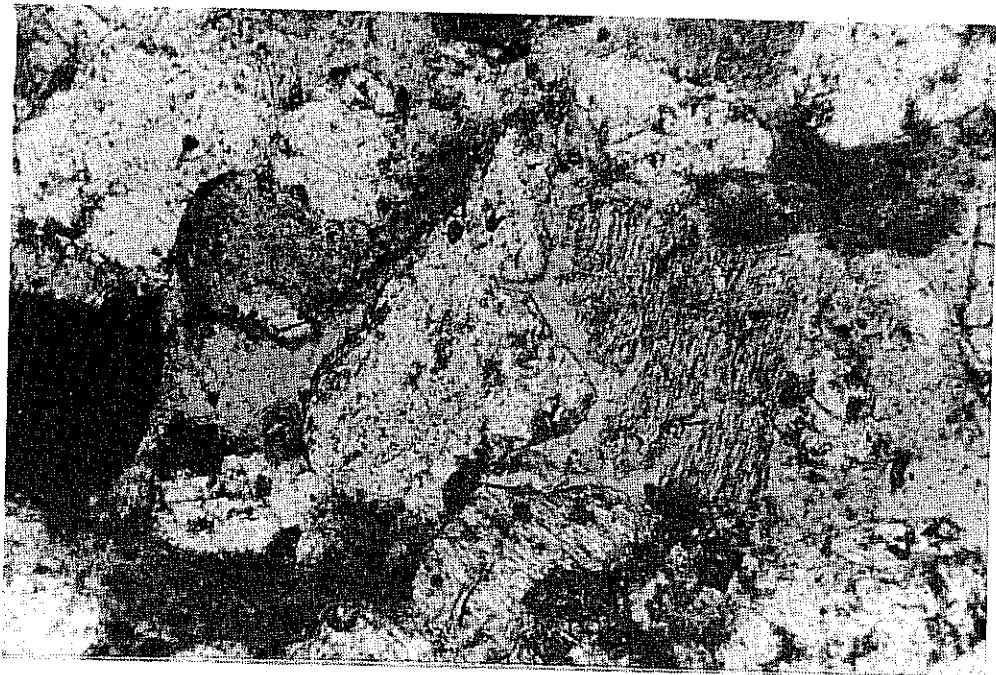


FIGURE 24. - Feldspar (right of center) has been severely leached leaving kaolinized remnants and secondary intercrystalline microporosity. Note overgrowths on margin of quartz grain (center). Well 7-18-1, 4,951 ft. Length of photomicrograph is 78 microns.

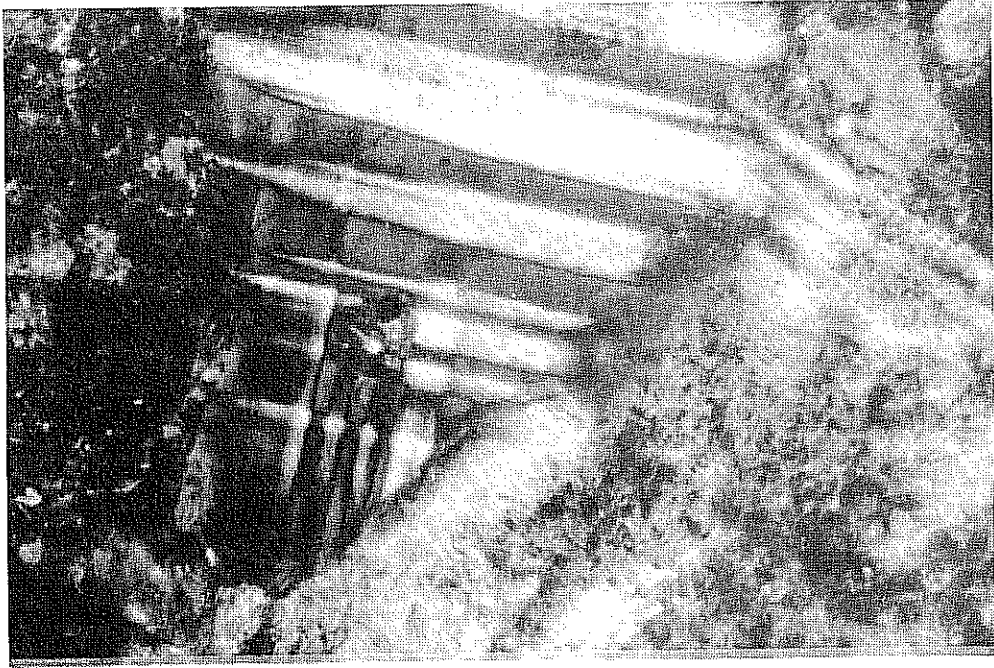


FIGURE 25. - Microcline with characteristic crossed spindle twinning (left) is not corroded while another grain of feldspar immediately adjacent (right) has had its center leached and kaolinized resulting in a significant increase of secondary intercrystalline microporosity. Well 7-18-1, 4,955 ft. Length of photomicrograph is 9 microns.

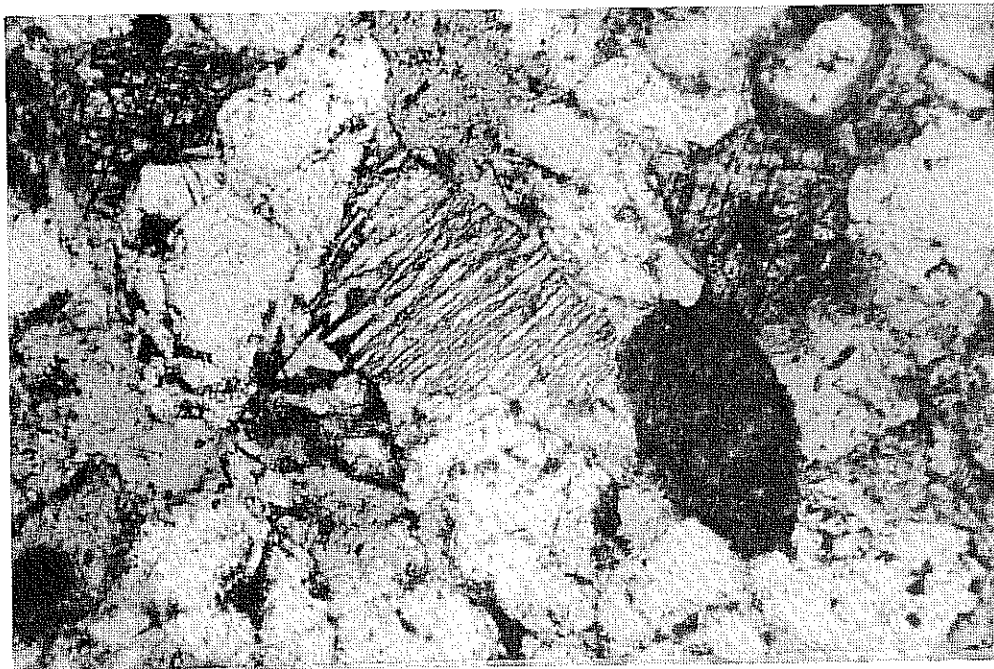


FIGURE 26. - Strongly leached feldspar with abundant secondary intraparticle porosity (center) could not have been transported to the site of deposition in its current state of preservation. It must have been affected by diagenetic processes after deposition. Note that dark colored sedimentary rock fragment (to right) has apparently not been affected by leaching. Well 7-18-1, 4,955 ft. Length of photomicrograph is 78 microns.

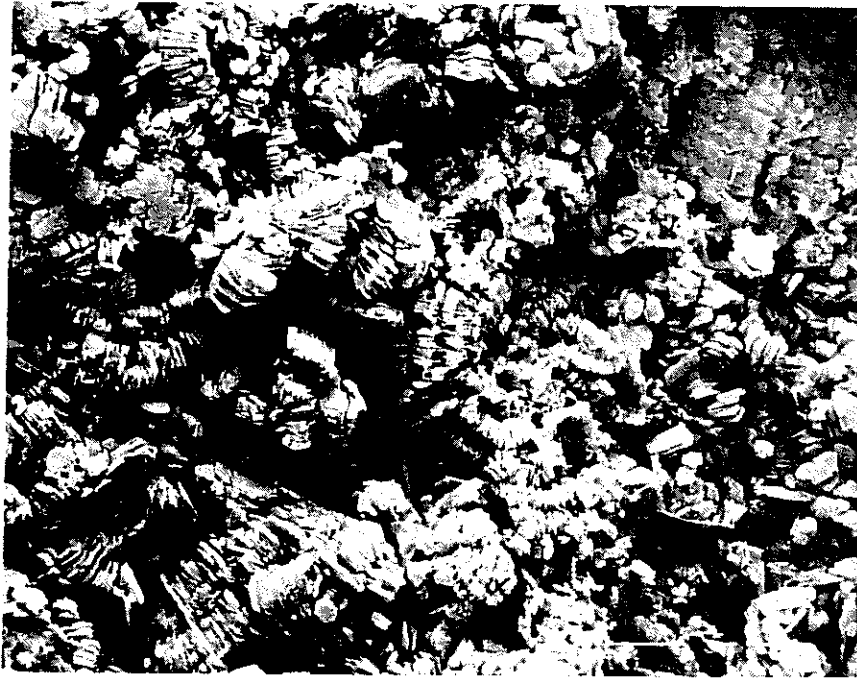


FIGURE 27. - Scanning electron image shows well-developed books and scattered flakes of kaolinite cement within interparticle porosity. Such cement generally reduces permeability, however, the resulting micropore system may be only slightly less porous than in many cleaner sandstones. Well 45-14-3, 4,524 ft. Length of image is 11.5 microns.

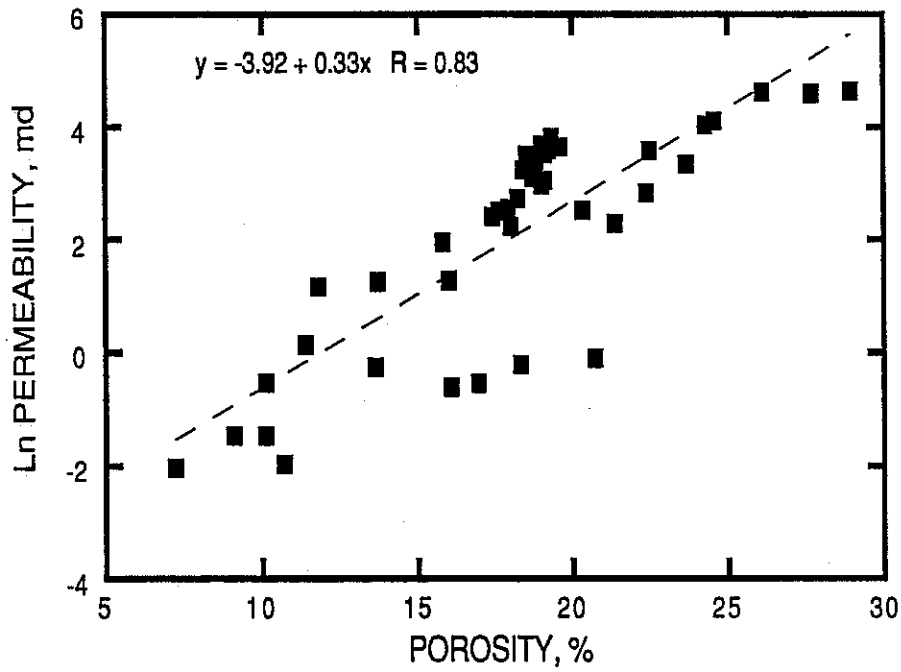


FIGURE 28. - The relationship between natural log of permeability (Ln) and porosity for core analysis from the upper Almond formation at Patrick Draw field.

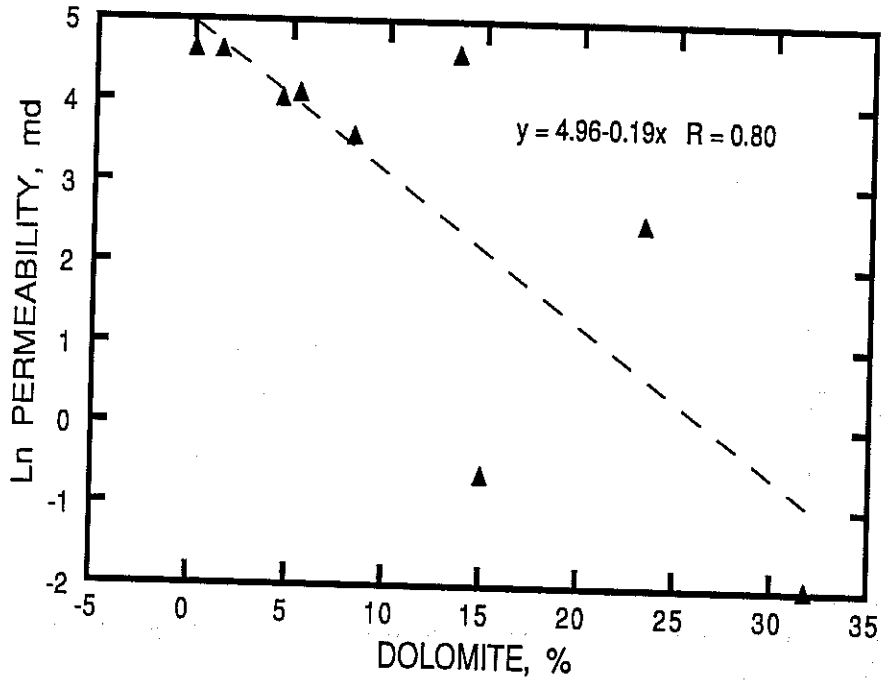


FIGURE 29. - The relationship between natural log (Ln) of permeability and amount of dolomite cement in reservoir sandstones from the upper Almond formation at Patrick Draw field.

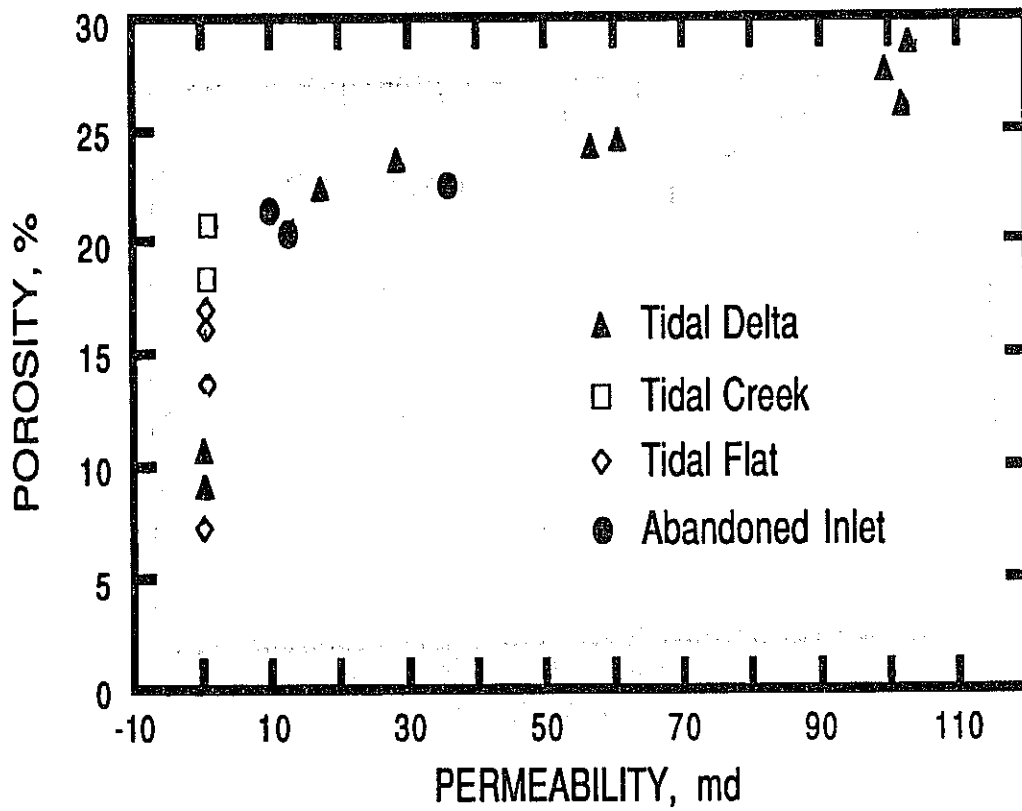


FIGURE 30. - Porosity and permeability plotted for samples from various depositional facies recognized in the upper Almond formation at Patrick Draw field. Notice the two straight-line segments, and the general segregation of facies along these trends.

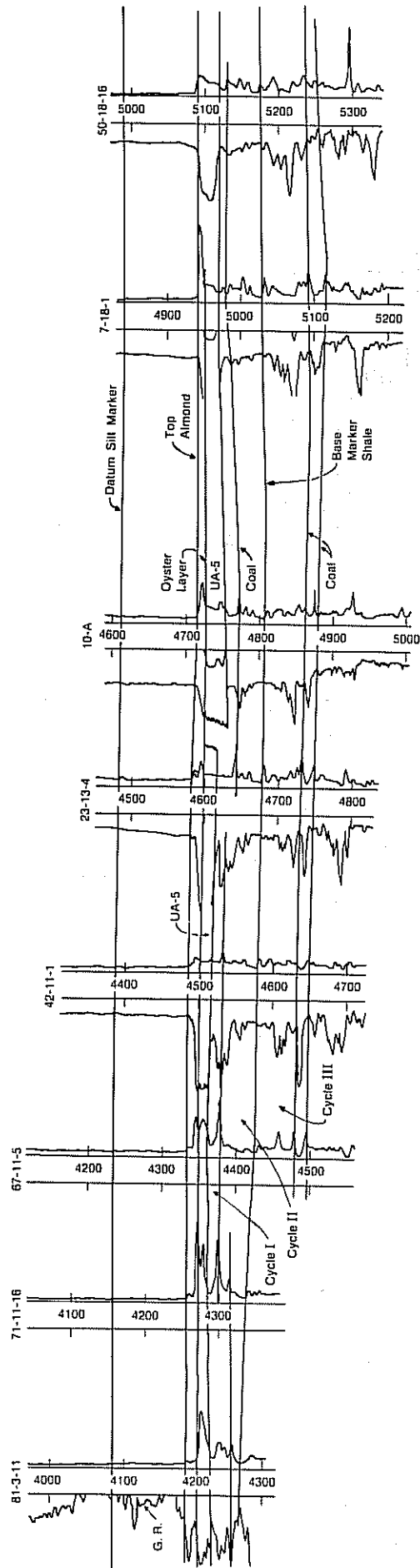


FIGURE 31. - Stratigraphic cross section of upper Almond formation, showing major stratigraphic units. Track 1 (left side) in well 81-3-11 is Gamma Ray, and in all other wells it is SP. Track 2 (right side) in all wells is Induction Log. See fig. 13 for location.

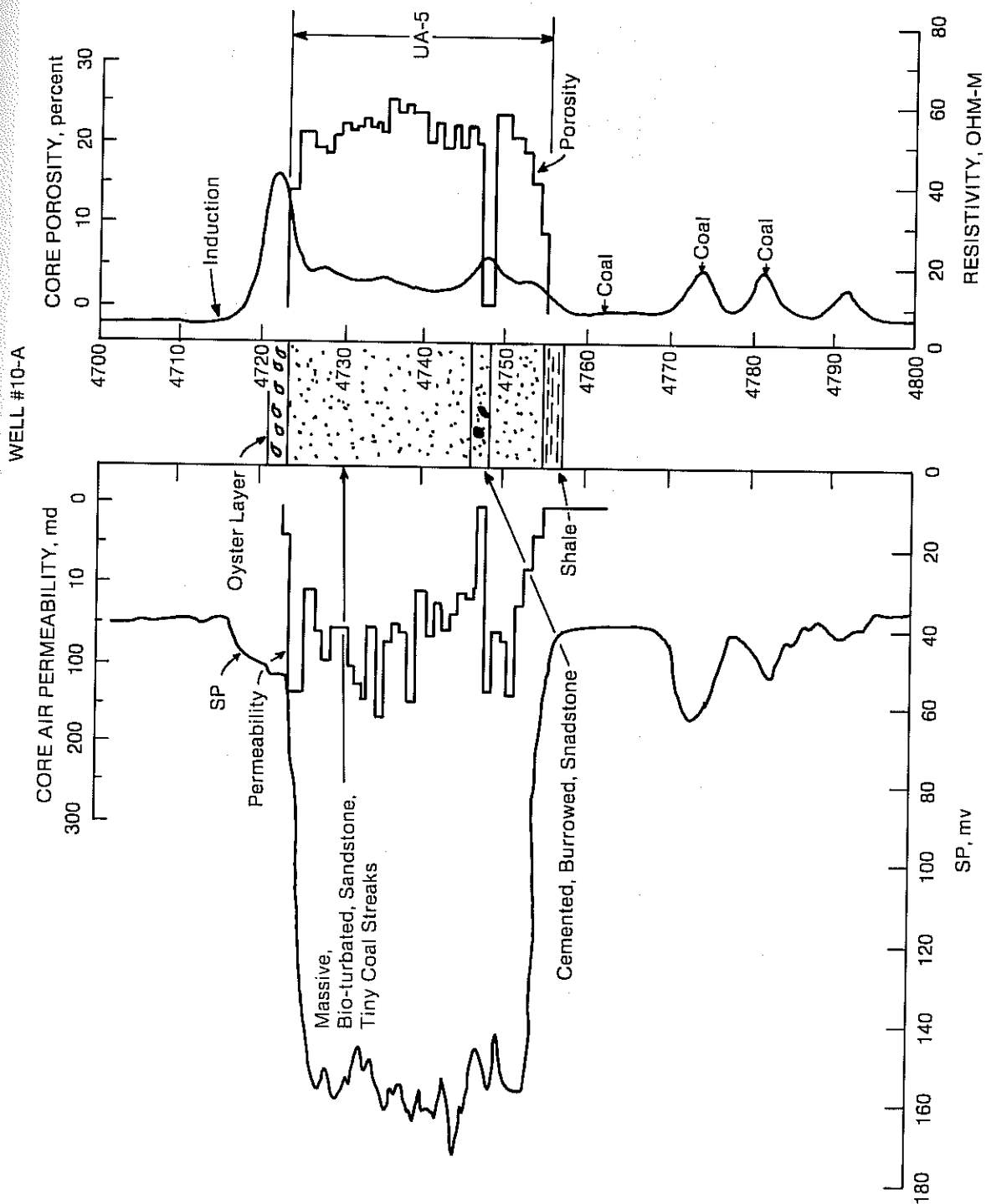


FIGURE 32. - Log responses and petrophysical properties of producing UA-5 sandstone and other geological features of the Upper Almond formation, Patrick Draw field, well no. 10-A. After Union Pacific Resources Office Records.

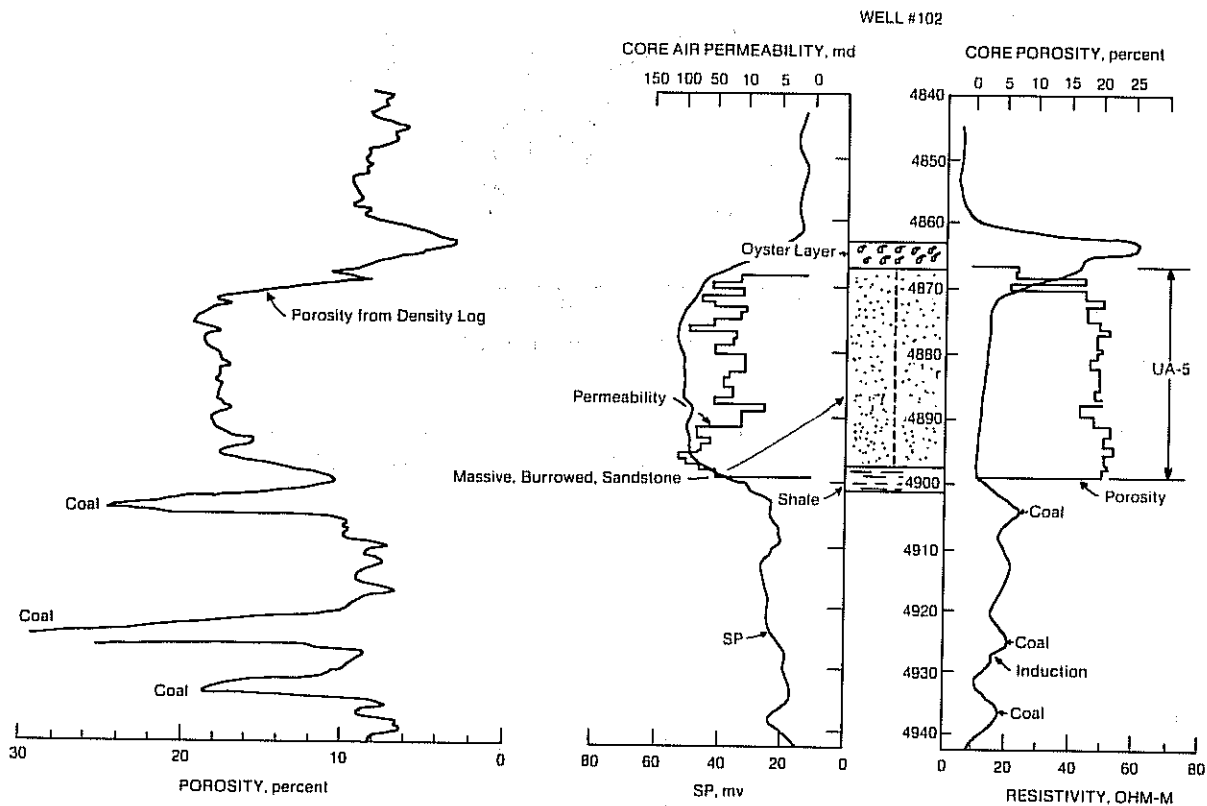


FIGURE 33. - Log responses and petrophysical properties of producing UA-5 sandstone and other geological features in upper Almond formation, Patrick Draw field, well no. 102. After Union Pacific Resources Office Records.

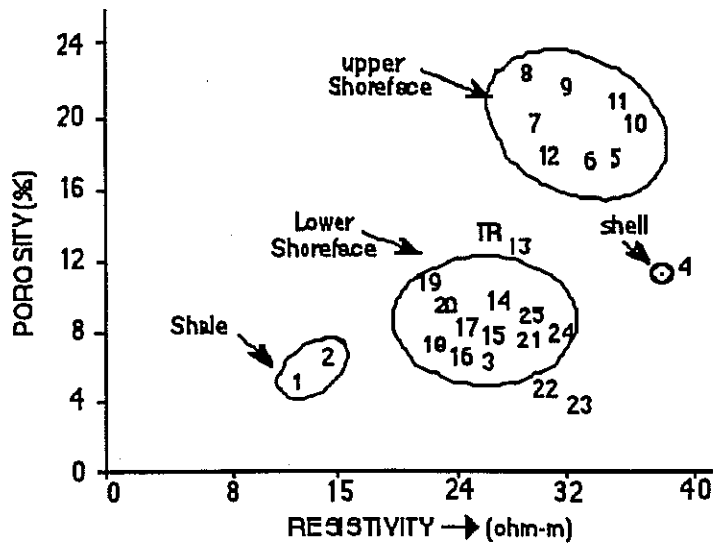


FIGURE 34. - Depth sequential crossplot of resistivity and porosity to distinguish various facies in the 140 ft sand in corehole No. 1 in the Almond formation.

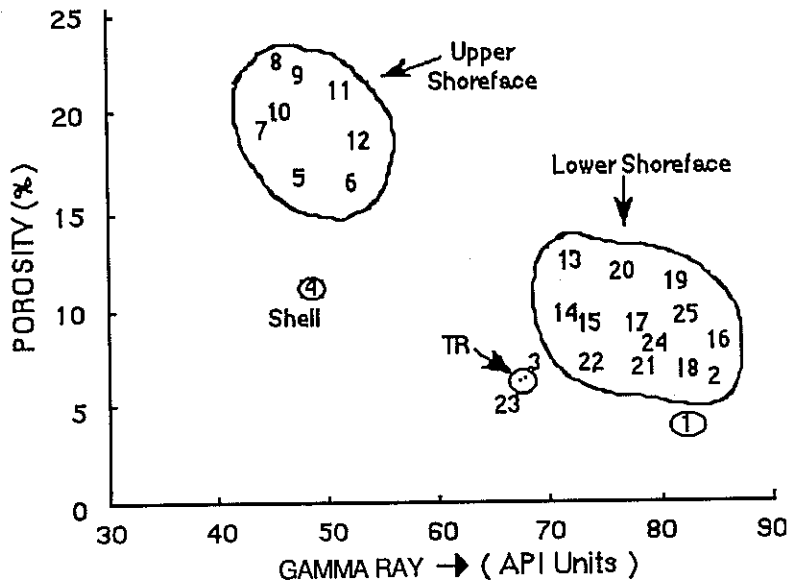


FIGURE 35. - Depth sequential crossplot of gamma ray and porosity to distinguish various facies in the 140 ft sand in corehole No. 1 in the Almond formation.

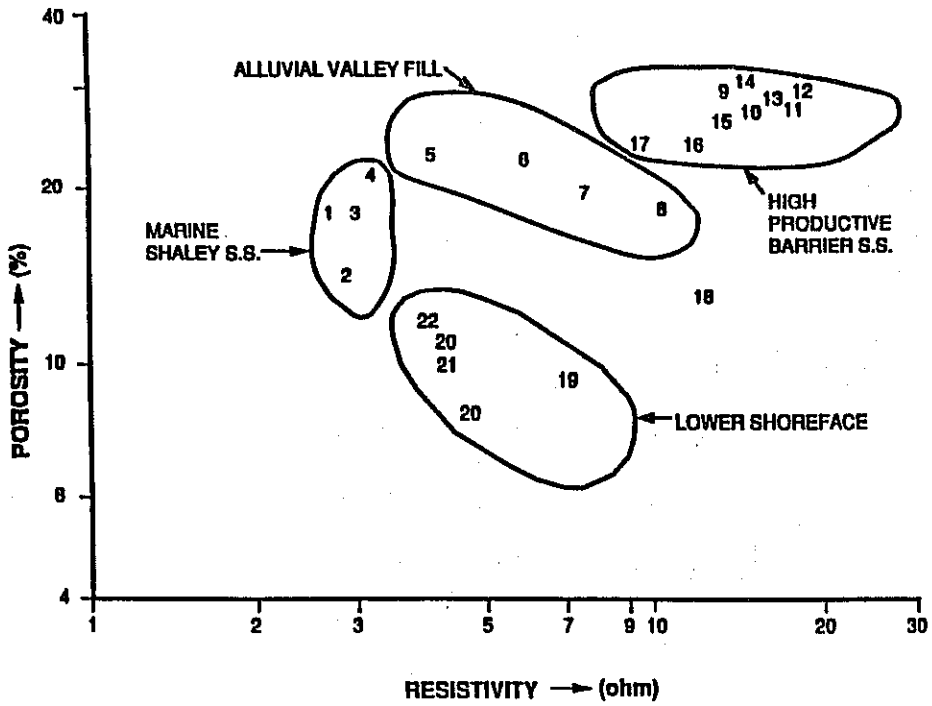


FIGURE 36. - Depth sequential crossplot of resistivity and porosity todistinguish various sandstone facies in well W-4 from Bell Creek (MT) field.

# NIPER / IITRI

## OIL-WATER RELATIVE PERMEABILITY

COMPANY Champlin Petroleum Company  
 WELL No. 1 CPC 12B-19 (19-98)  
 FIELD Patrick Draw  
 DEPTH, ft. \_\_\_\_\_  
 PERMEABILITY,  $K_o(S_{wi})$ , mD 39  
 CONNATE WATER, % P.V. 45

FORMATION Almond  
 COUNTY Sweetwater  
 STATE/COUNTRY WV  
 POROSITY, % B.V. \_\_\_\_\_  
 OIL VISCOSITY, cP \_\_\_\_\_  
 BRINE VISCOSITY, cP \_\_\_\_\_

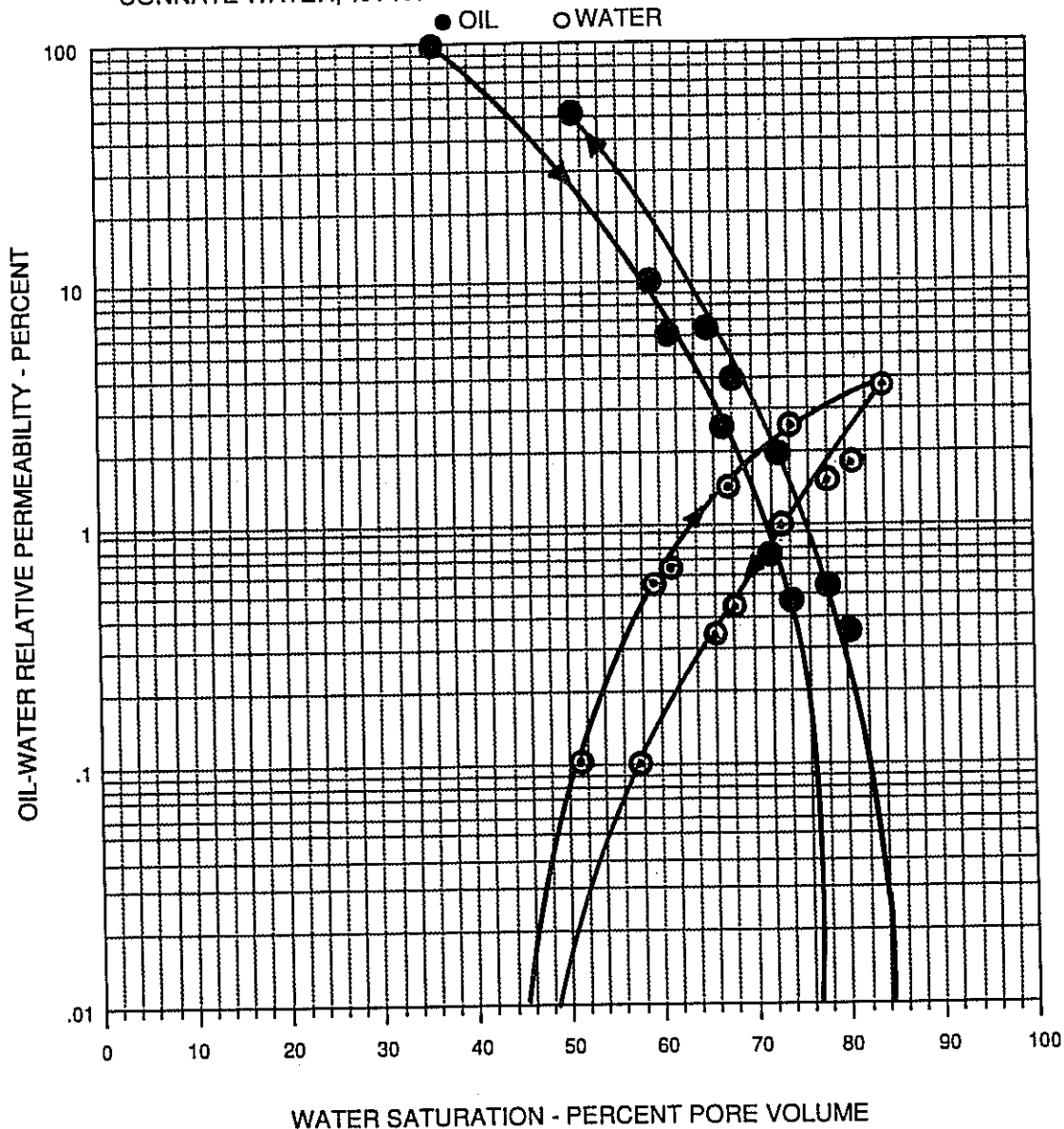


FIGURE 37. - Imbibition and drainage oil-water relative permeability analysis conducted on a core sample from the Almond formation at Patrick Draw field. Well identified as Champlin Petroleum Company No. 1, depth unknown.

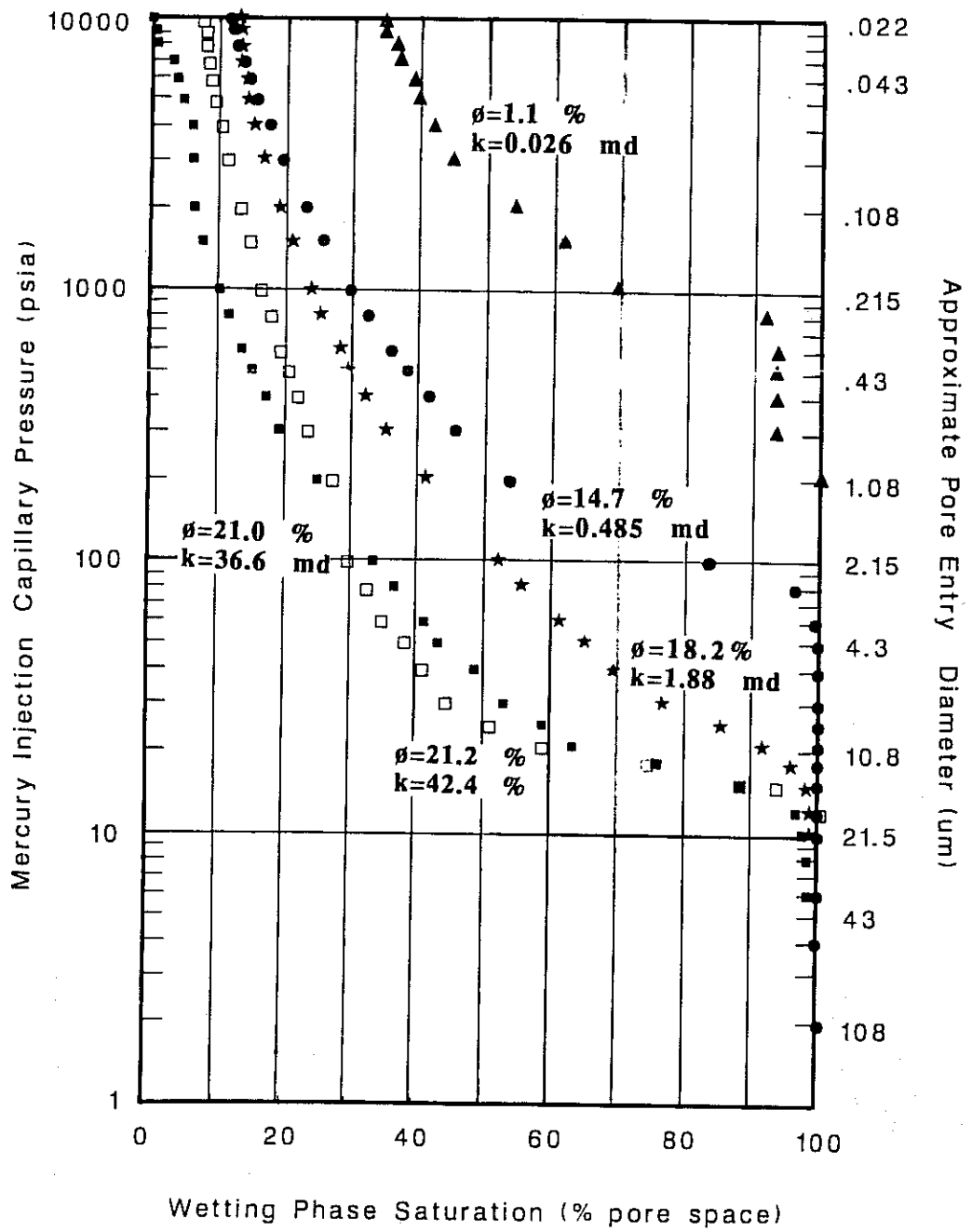


FIGURE 38. - Mercury capillary pressure test results on five core samples from well no. 15, Arch unit, Patrick Draw field. After Keighin, Law, and Pollastro, 1989<sup>28</sup>.

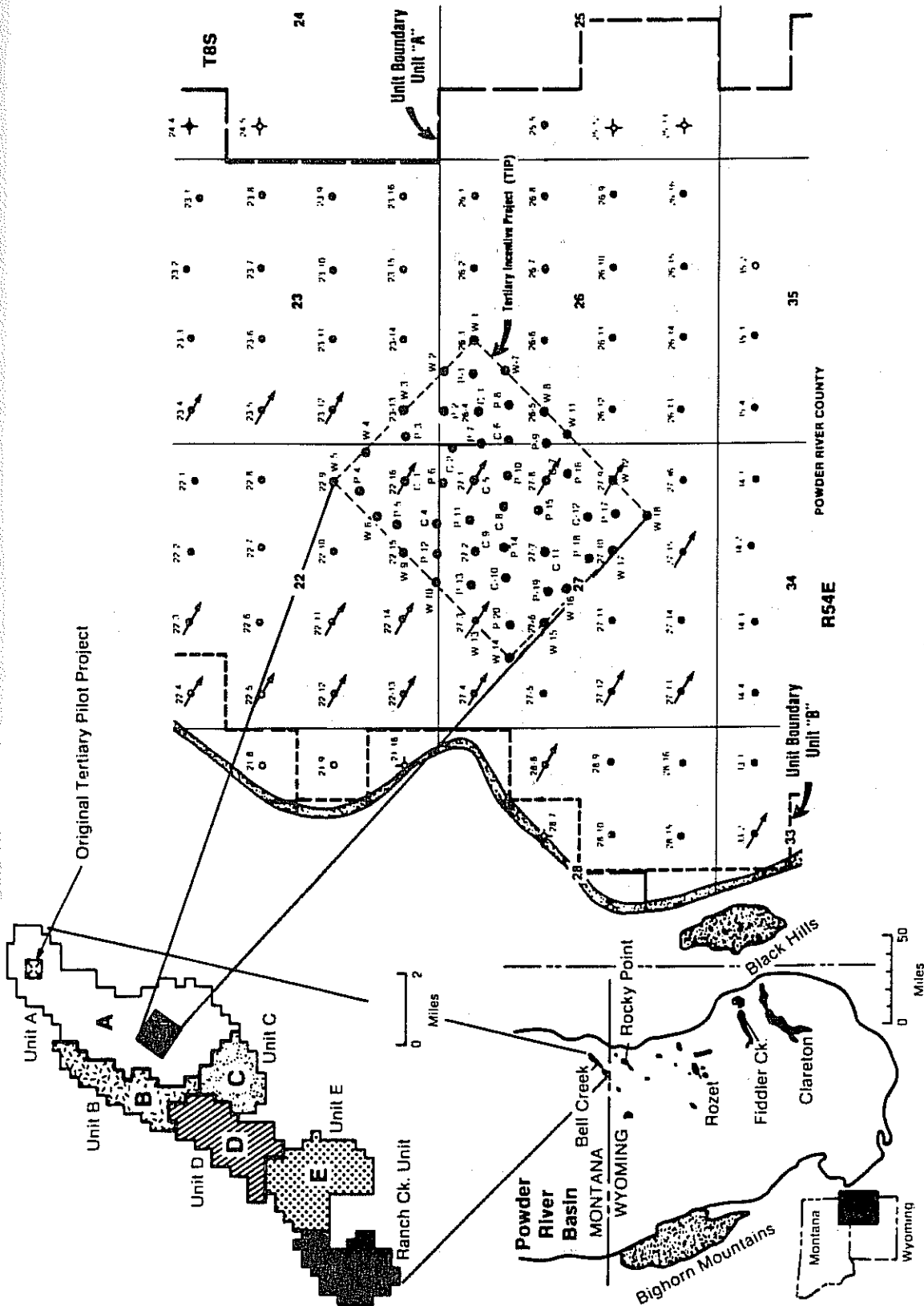
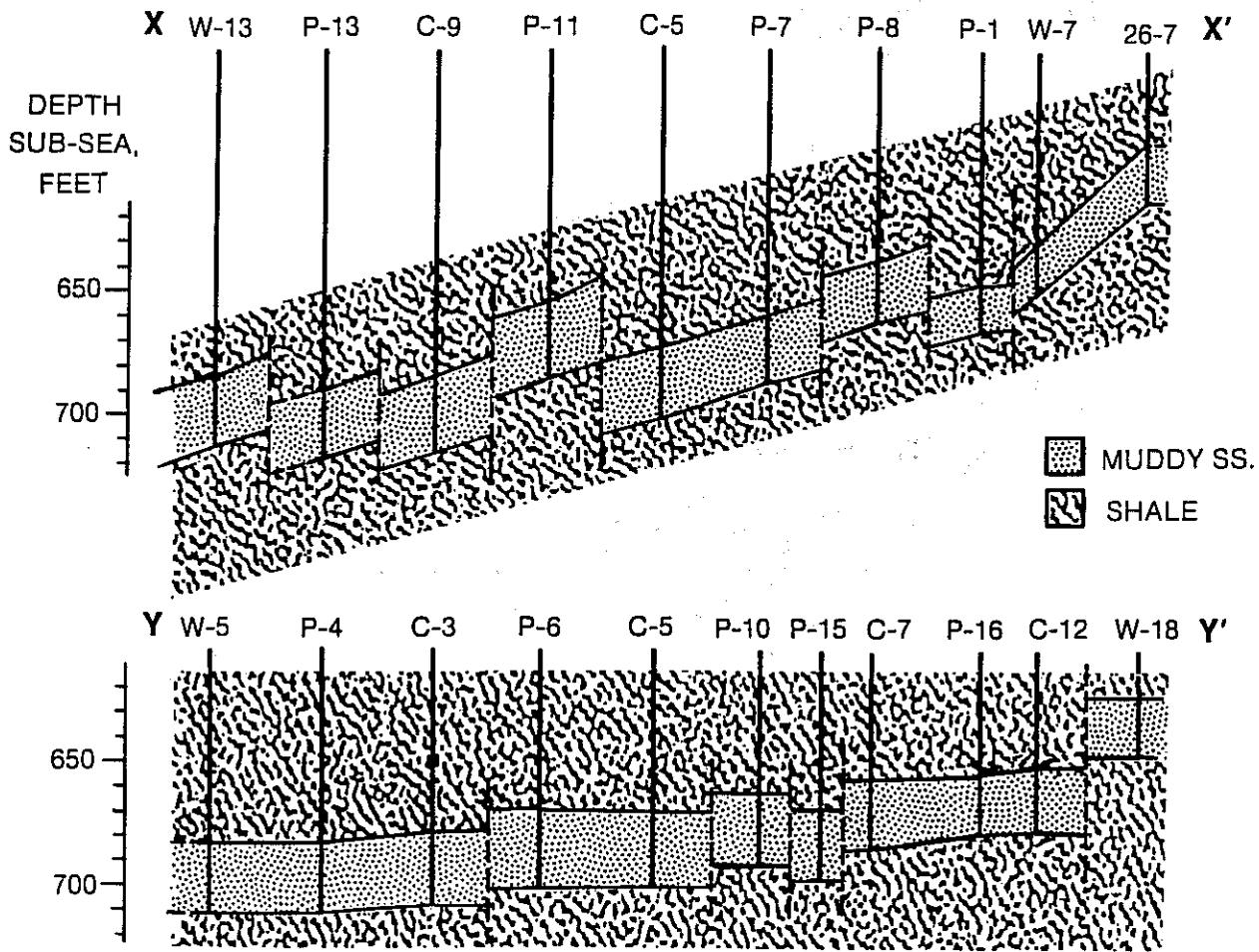


FIGURE 39. - Location map of Bell Creek (MT) field, Unit 'A', tertiary incentive project (TIP) area. Location of production (P) wells, tertiary injection (C) well, and water injection wells (w) are shown as well as location of cross section X-X' and Y-Y'42.



AFTER SZPAKIEWICZ, 89

FIGURE 40. - Structural cross-sections across TiP area parallel to the dip (X - X') and strike (Y - Y') of Muddy formation. Note vertical displacement and position of wells within fault blocks.

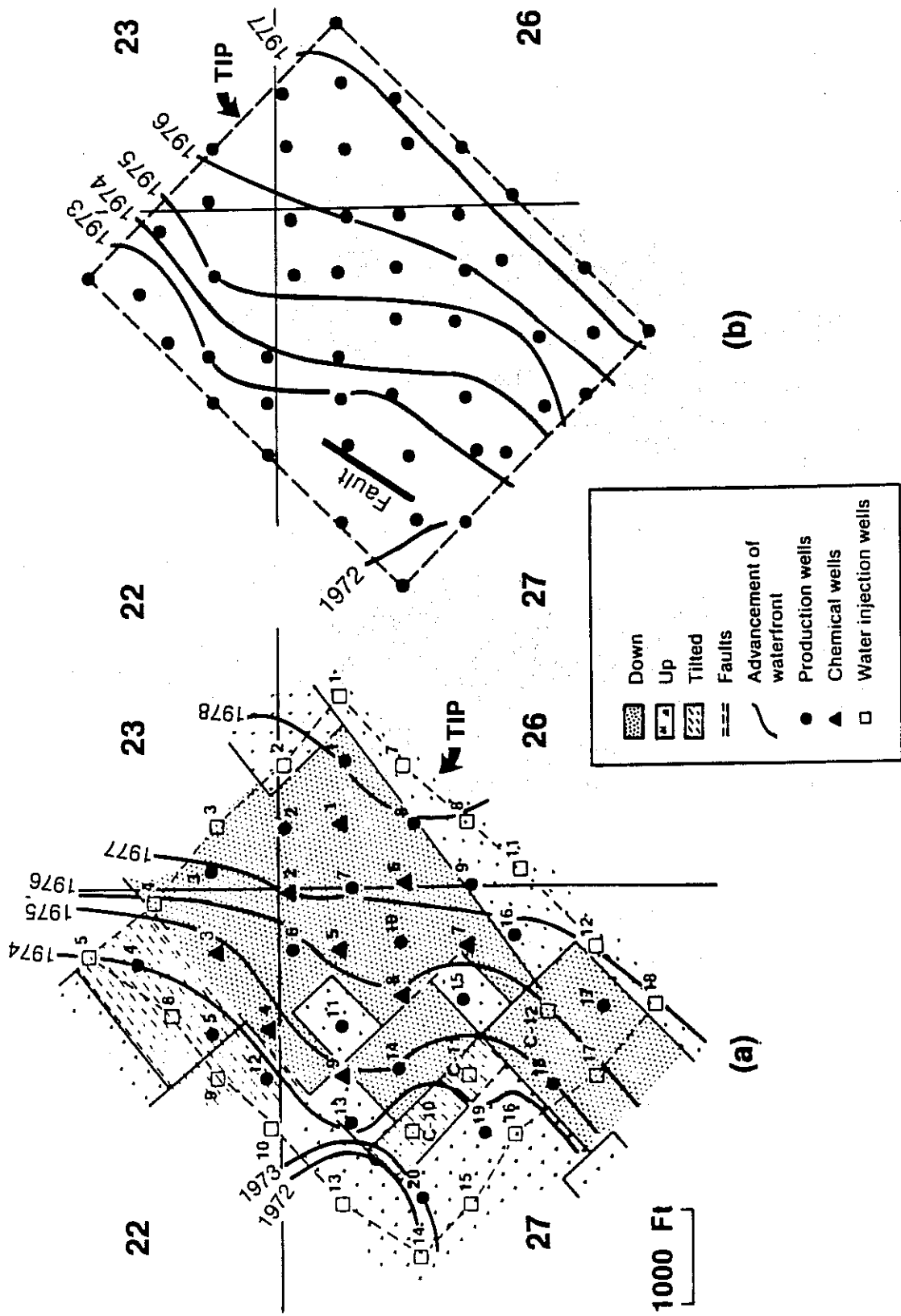


FIGURE 41.- Comparison of the location of 70% water-cut advancement superimposed on fault map (a) and that from the full-scale areal simulation (b) of TIP area.

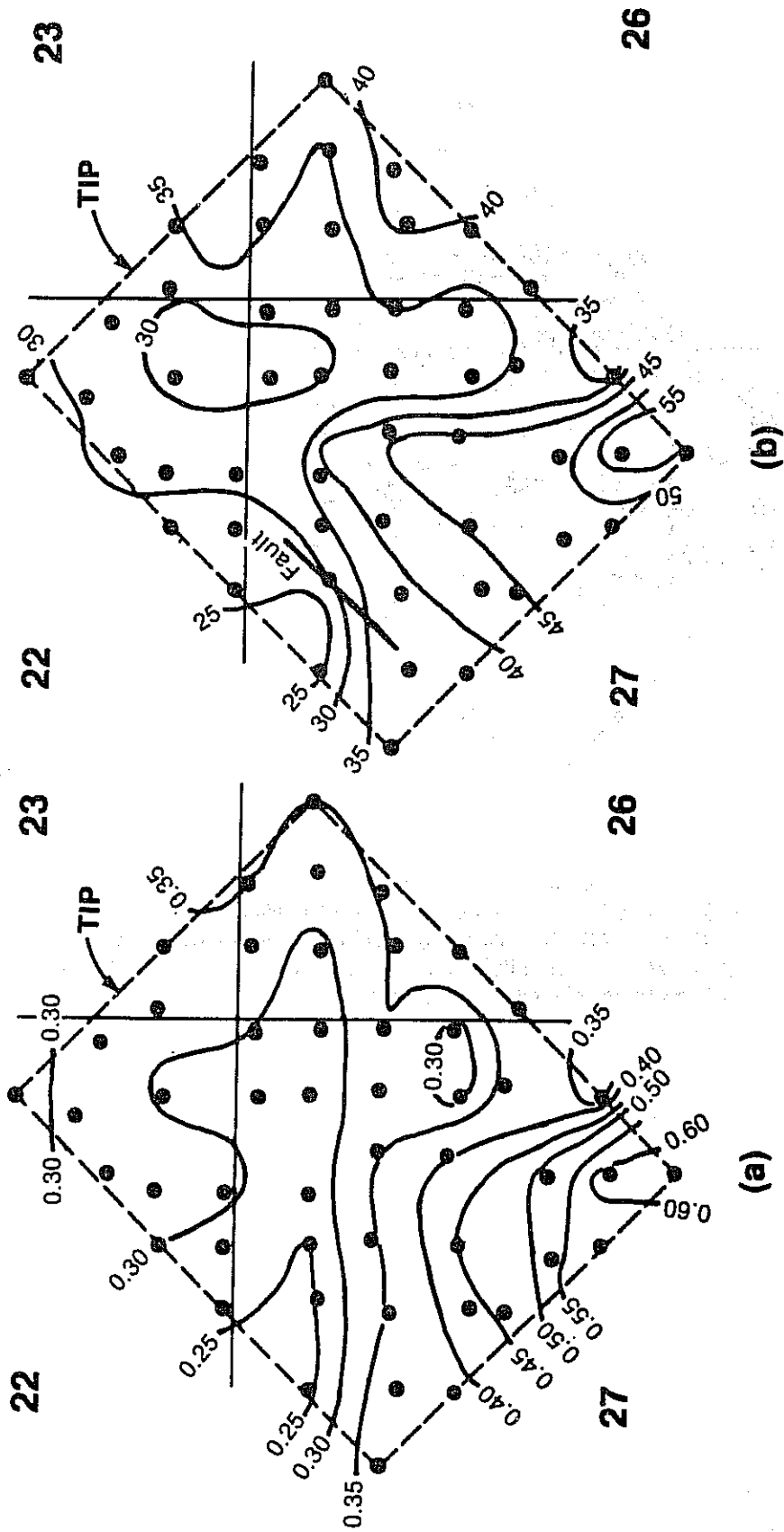


FIGURE 42.- Comparison of residual oil saturation distribution after 10 years of linedrive waterflooding, obtained by full-scale simulation without the inclusion of a major fault, in % (a) and with the inclusion of a major fault (b).

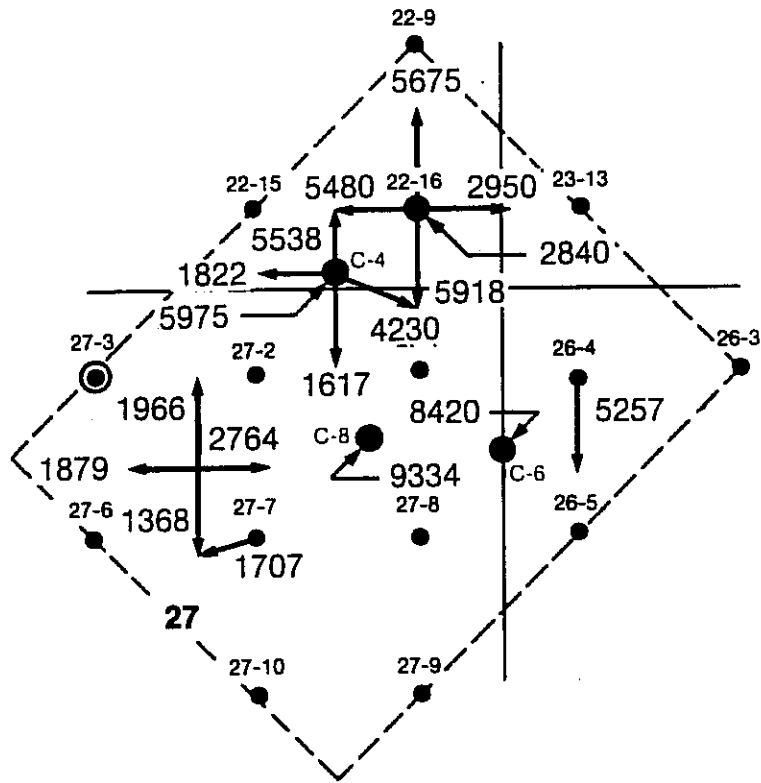


FIGURE 43. - Pressure-pulse and falloff test results prior to initiation of chemical flooding. The large numbers beside an arrow indicate water flow capacity ( $k_{wh}$ ) in the indicated direction. Numbers indicated on the side of straight arrows represent pulse test results, while numbers next to the bent arrows represent falloff test results.

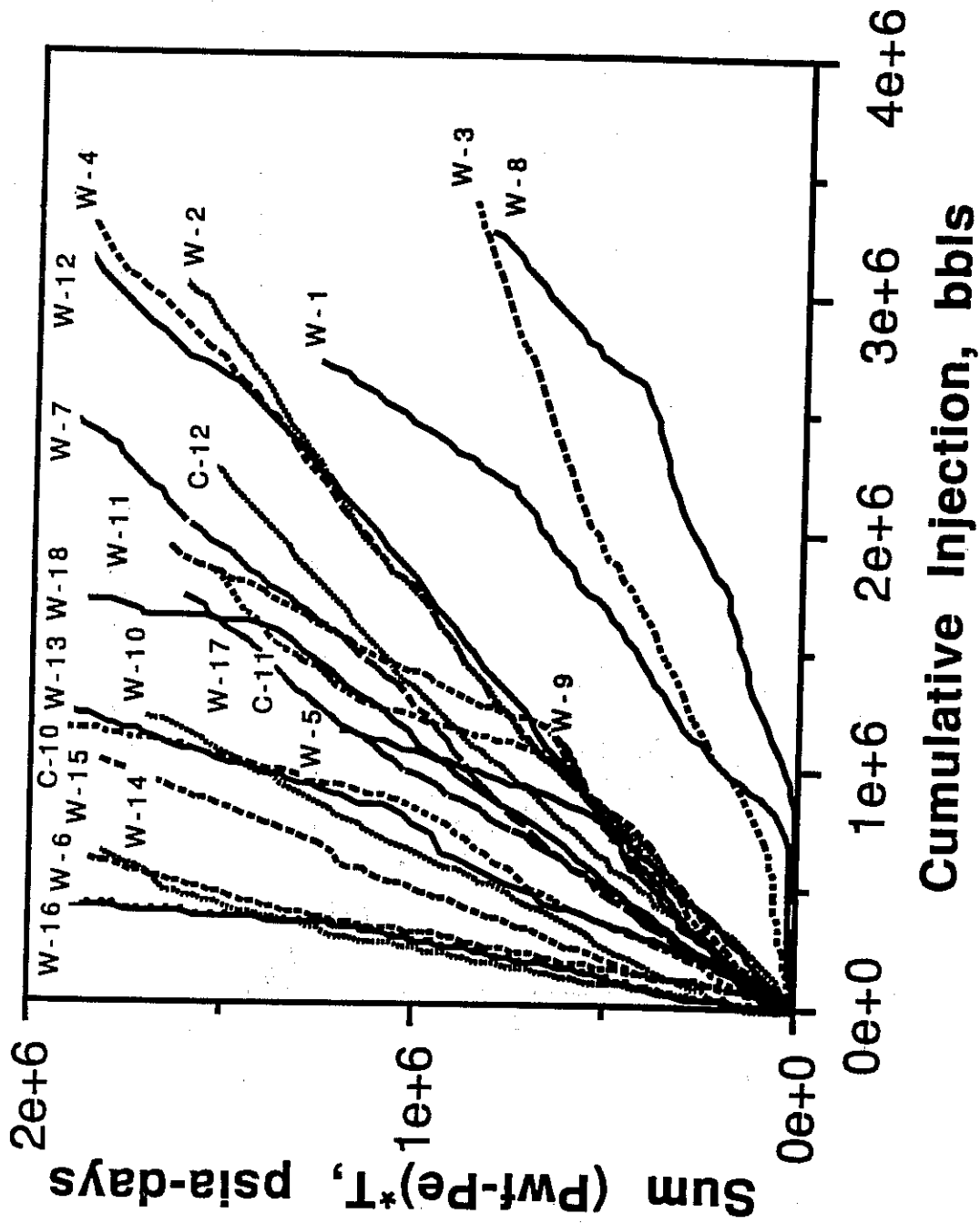
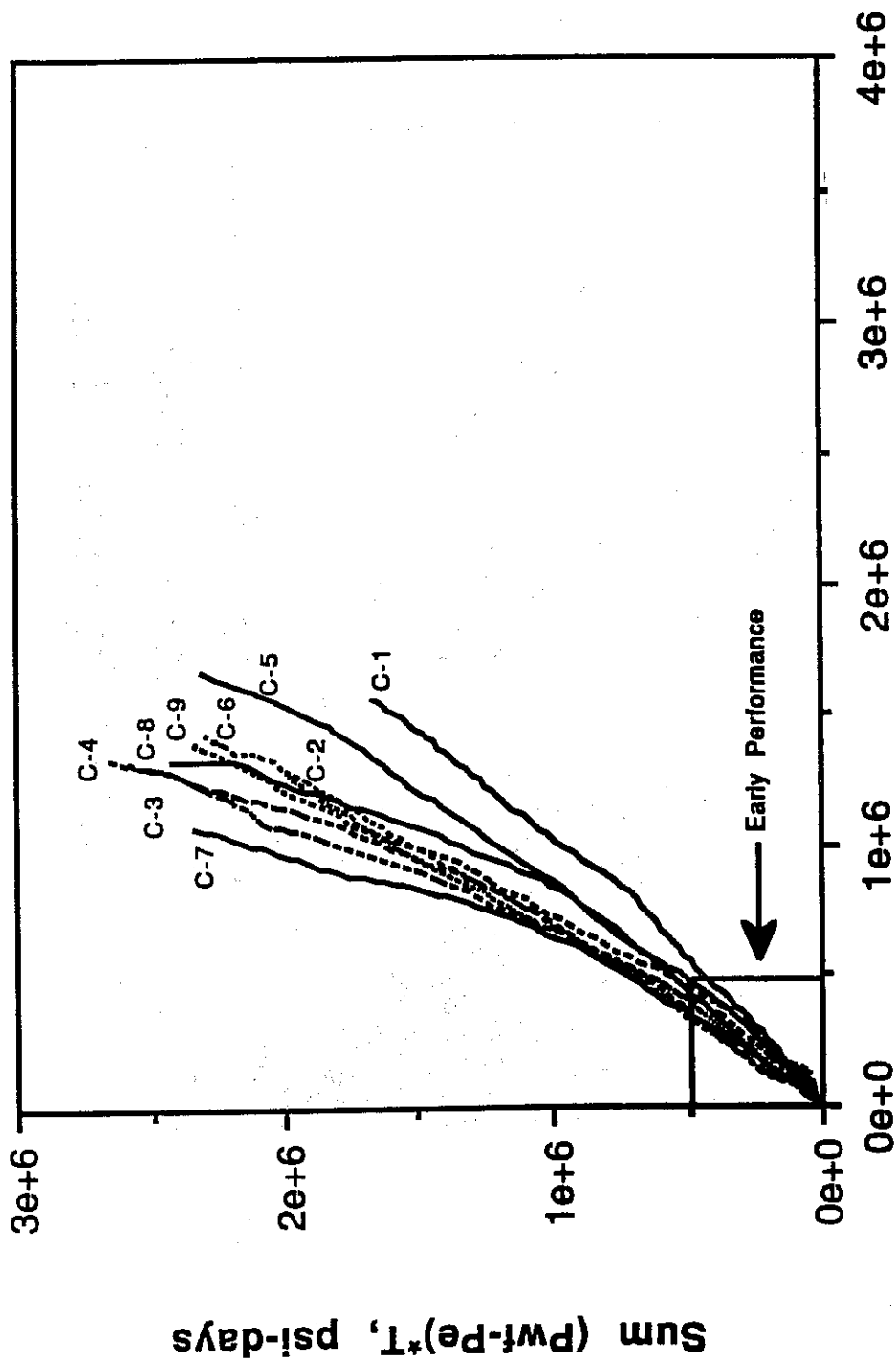


FIGURE 44. - Half plot of injection performance of all pattern water injection wells in TIP area.



### Cumulative Injection, bbls

FIGURE 45. - Hall plot of injection performance of all chemical injection wells in TIP area. The early performance of all chemical injection wells is shown in fig. 48.

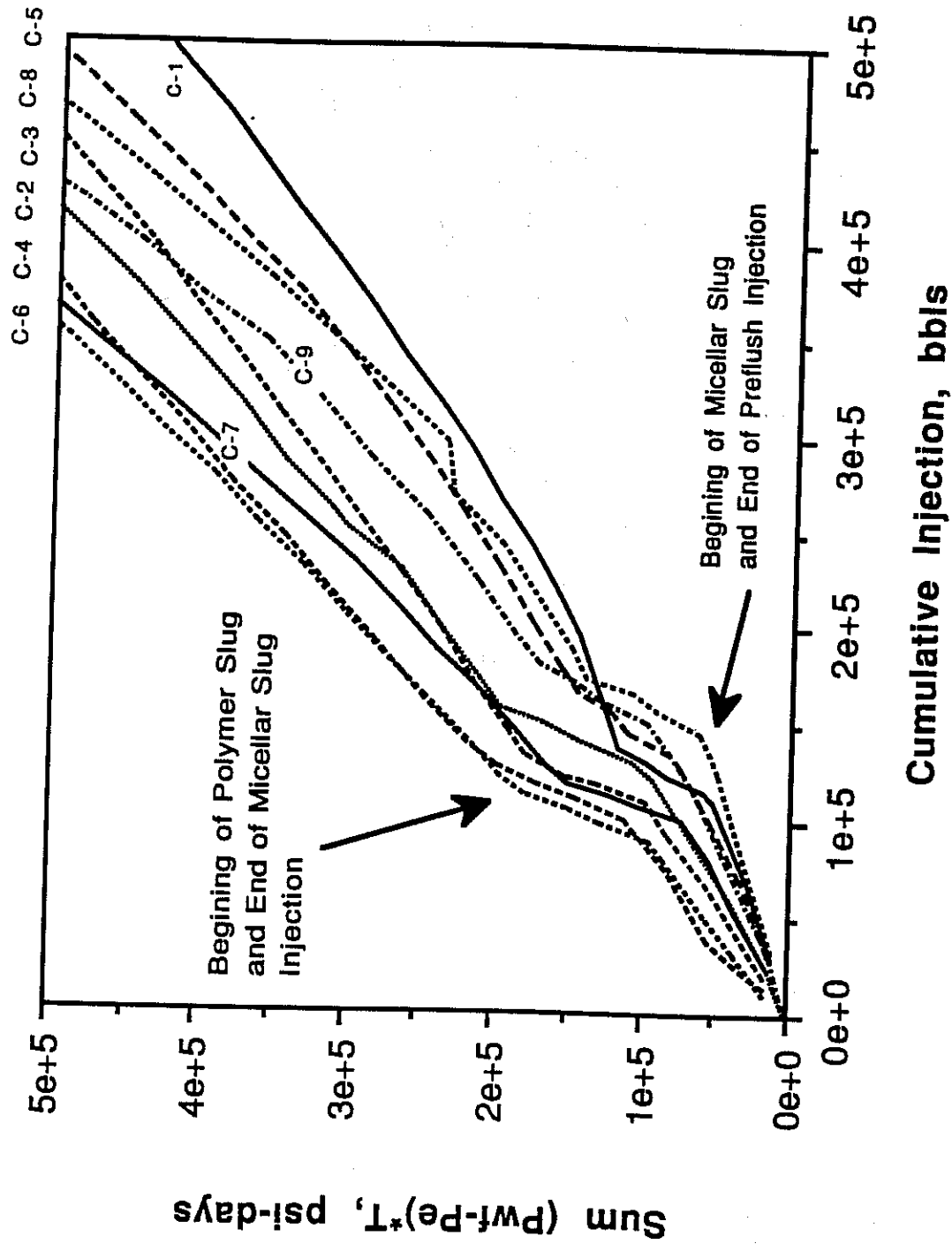


FIGURE 46. - Hall plot of early performance of all chemical injection wells in TIP area.

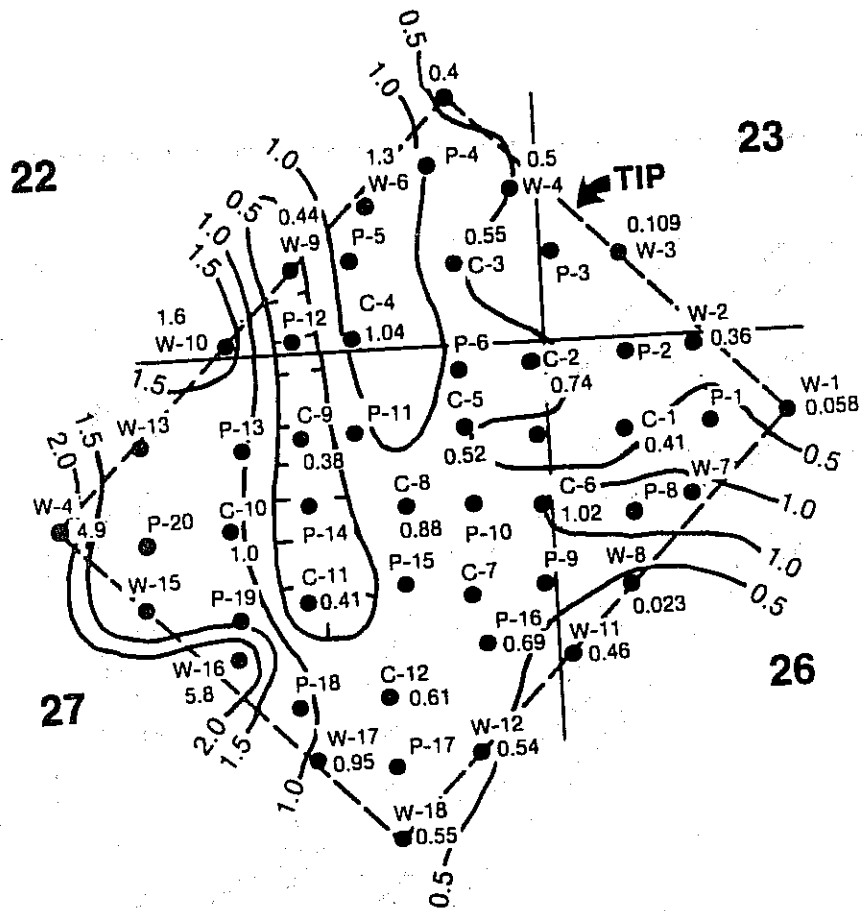


FIGURE 47. - Distribution of Hall plot slopes based on performance of water injection and early performance of chemical injection wells, TIP area.

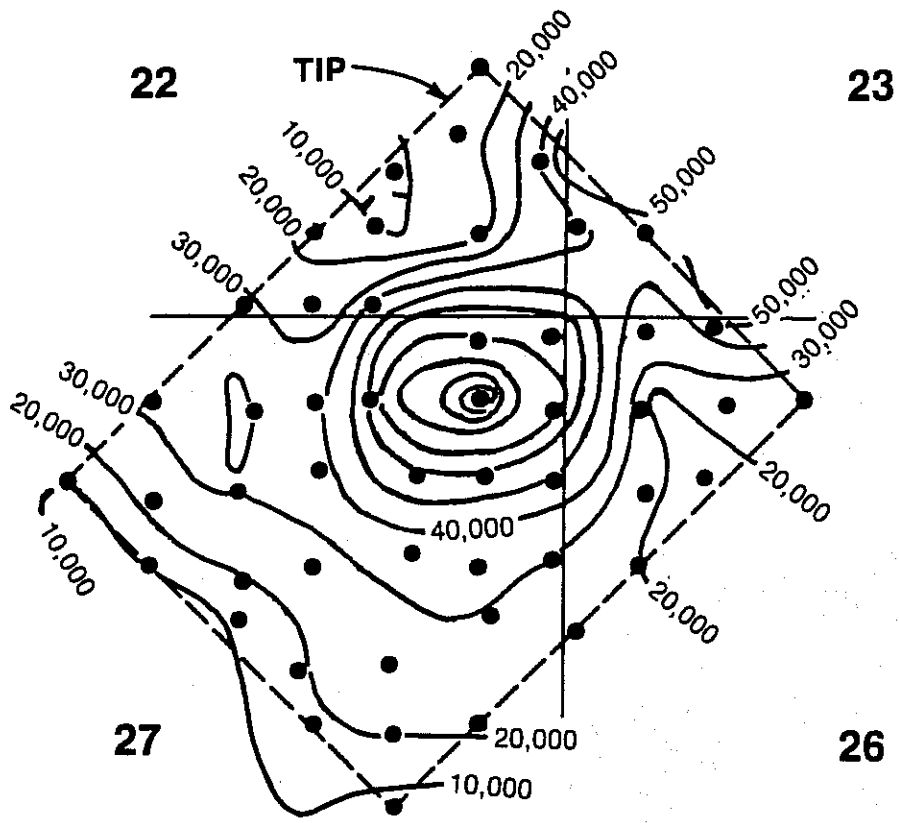


FIGURE 48 - Average transmissivity map. Product of horizontal air permeabilities measured on core samples and net pay in md-ft of Muddy formation, Unit 'A' of Bell Creek field, in TIP area.

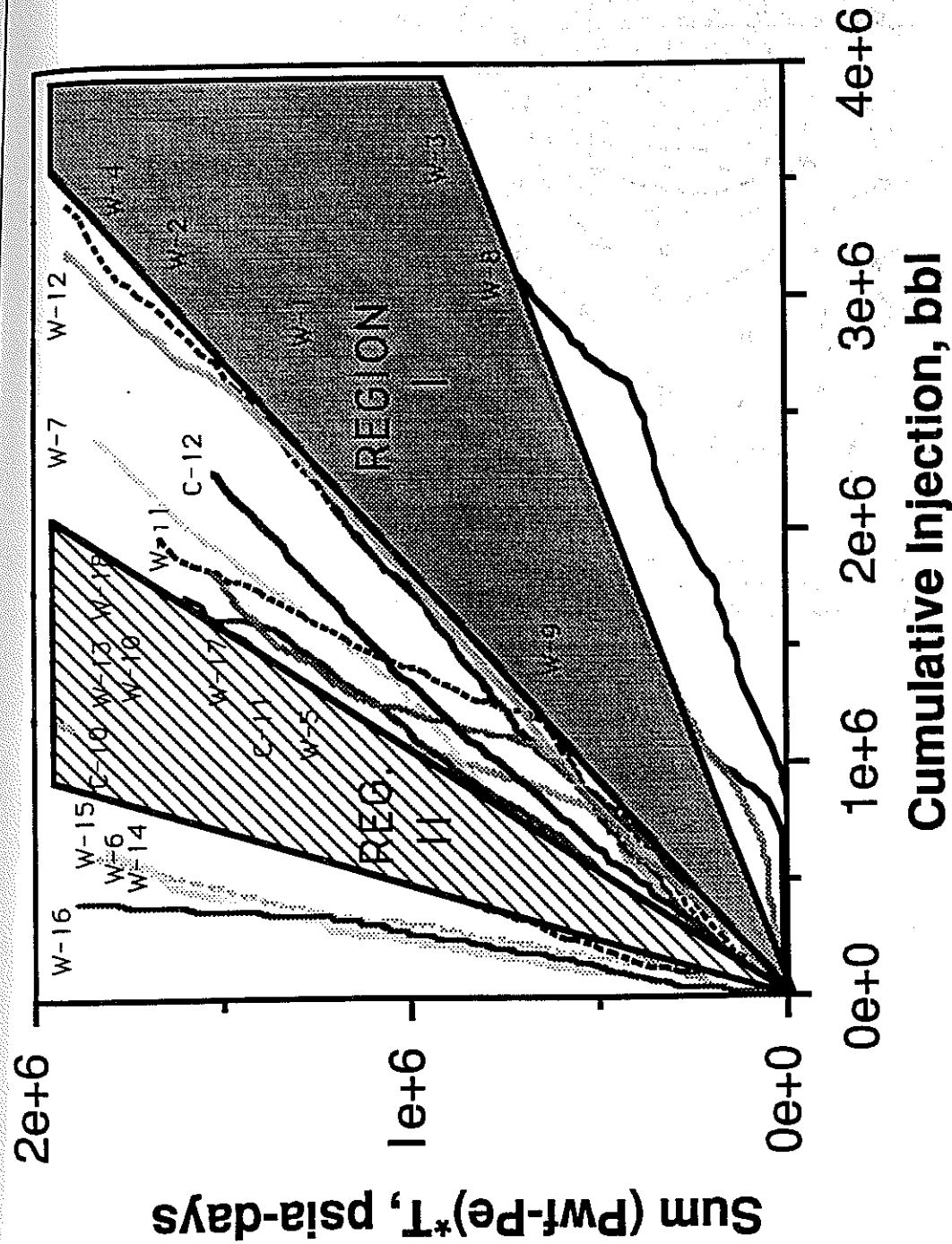


FIGURE 49. - Superposition of projected Hall plot chemical injection wells (Region I) based on their early performance and their actual performance (Region II) of Hall plot of water injection wells.

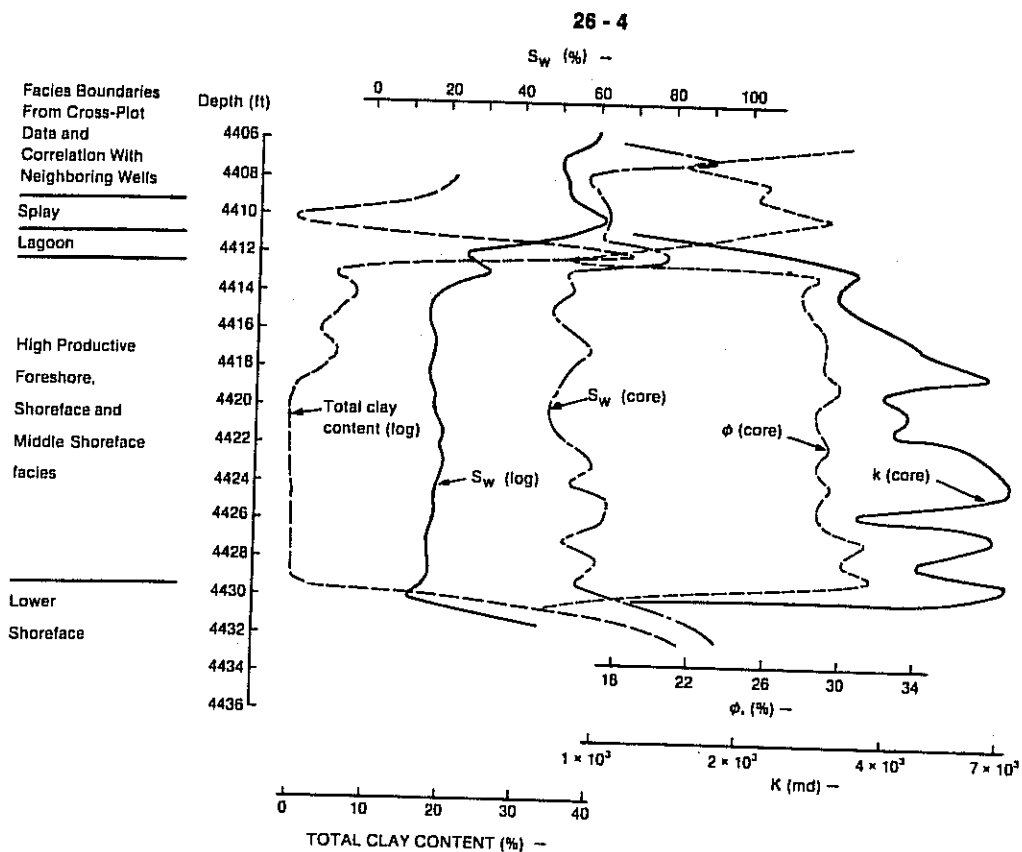
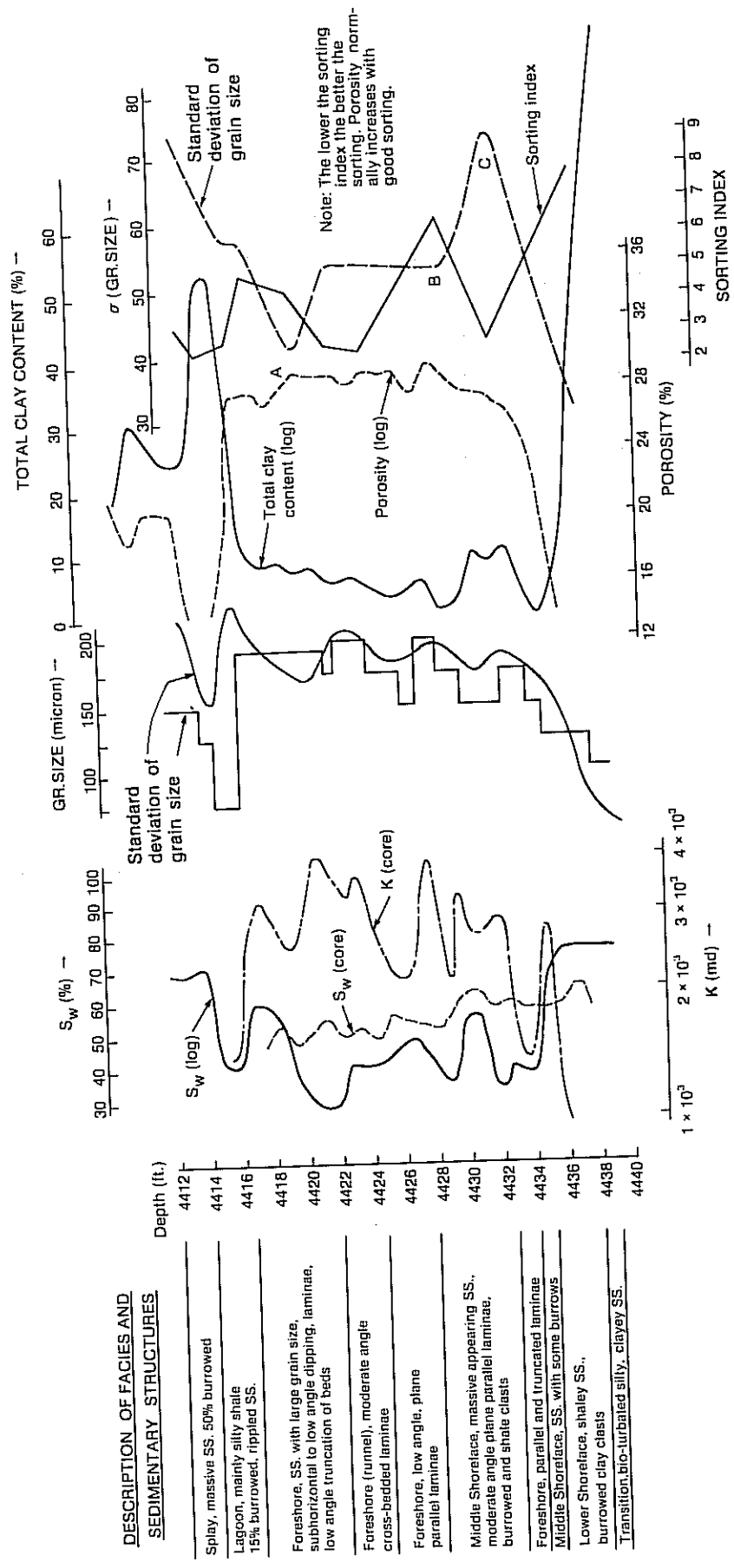


FIGURE 50. - Distribution of initial oil saturation and other reservoir properties in well 26-4.



DESCRIPTION OF FACIES AND SEDIMENTARY STRUCTURES

Depth (ft.)	Description of Facies and Sedimentary Structures
4412	Splay, massive SS. 50% burrowed
4414	Lagoon, mainly silty shale
4416	15% burrowed, rippled SS.
4418	
4420	Foreshore, SS. with large grain size, subhorizontal to low angle clipping, laminae, low angle truncation of beds
4422	
4424	Foreshore (runnel), moderate angle cross-bedded laminae
4426	Foreshore, low angle, plane parallel laminae
4428	
4430	Middle Shoreface, massive appearing SS., moderate angle plane parallel laminae, burrowed and shale clasts
4432	
4434	Foreshore, parallel and truncated laminae
4436	Middle Shoreface, SS. with some burrows
4438	Lower Shoreface, shaley SS., burrowed clay clasts
4440	Transition, bio-turbated silty, clayey SS.

FIGURE 51. - Distribution of water saturation and other reservoir properties in well P-2 drilled after 13 years of combined primary and waterflood production.

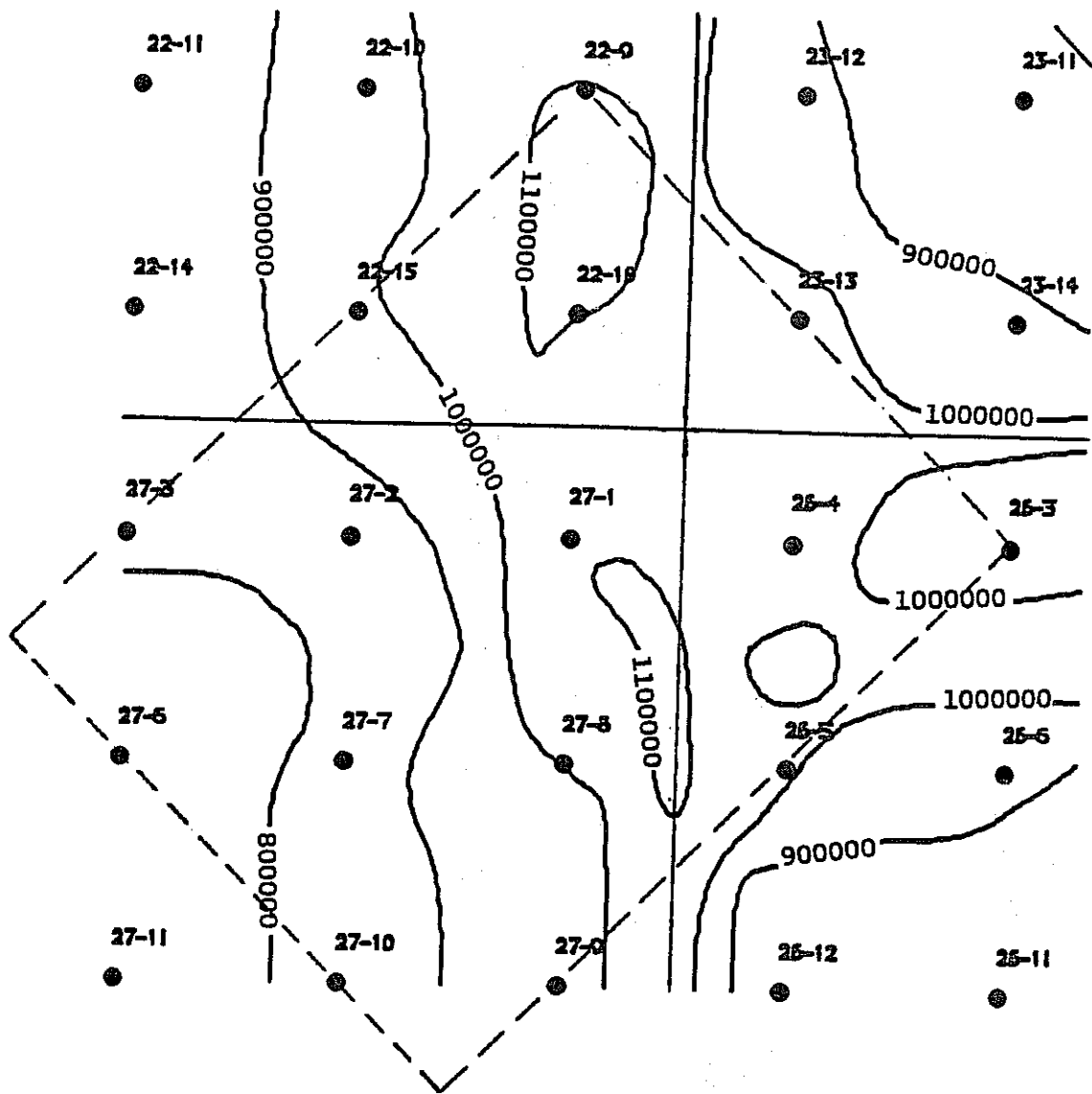


FIGURE 52. - Oil-in-place distribution in TIP area of Bell Creek (MT) field using material balance equation. Contour interval = 100,000 STB oil.

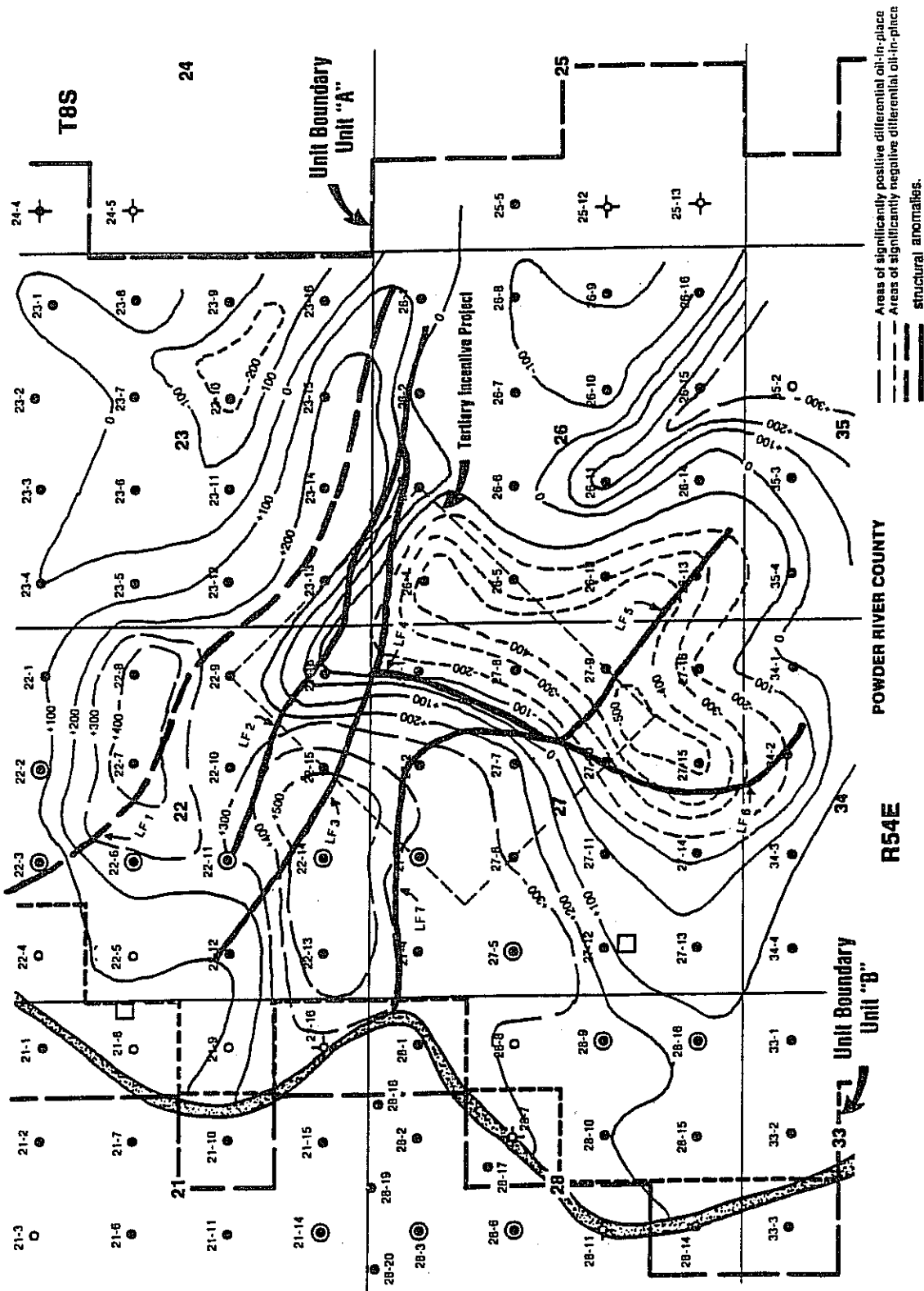


FIGURE 53. - Differential oil-in-place for the four sections surrounding the Tertiary Incentive Project area. Contours are in thousand of barrels oil difference between MBE and volumetric methods of oil-in-place calculation, LFI are interpreted structural anomalies.

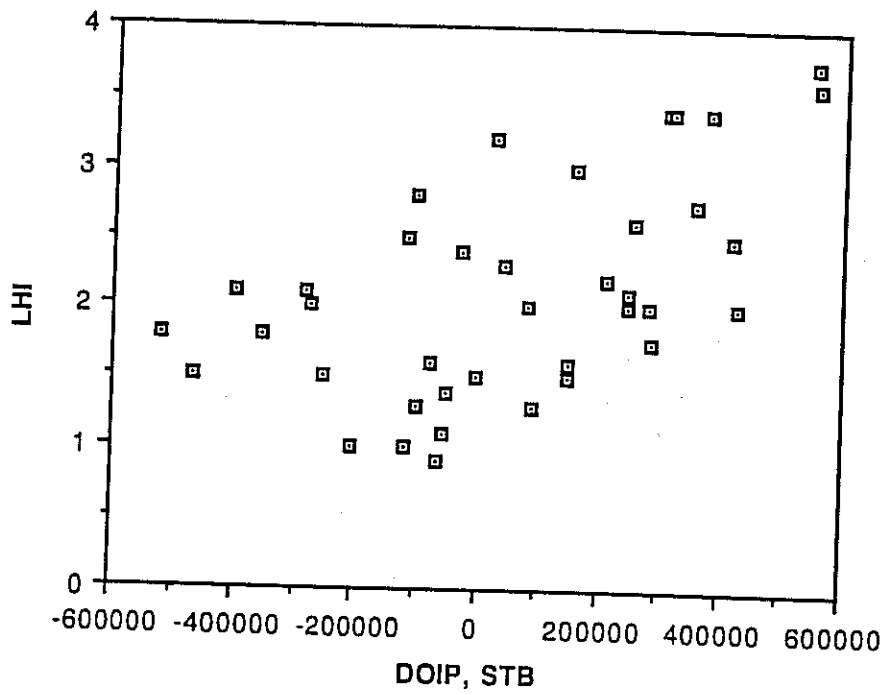


FIGURE 54. - Log derived heterogeneity index (LHI) vs. differential oil-in-place (DOIP), Bell Creek field, unit 'A'.

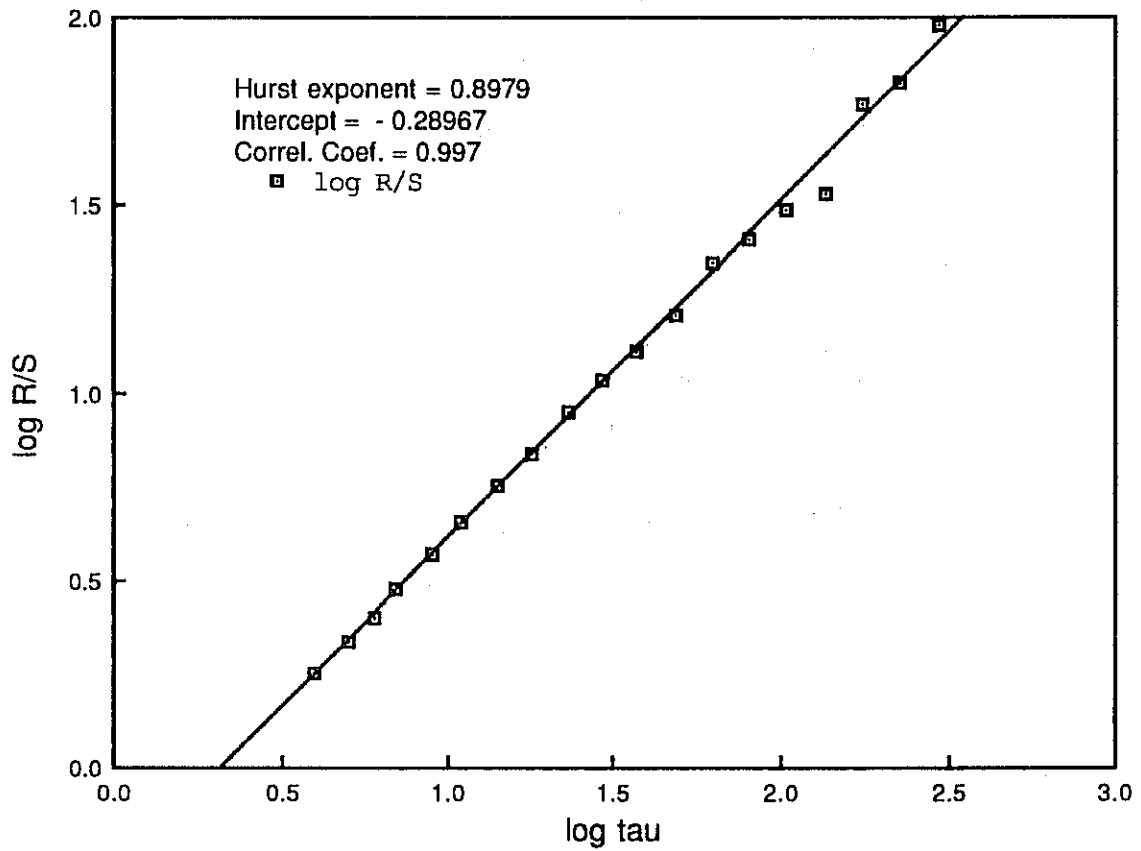


FIGURE 55. - R/S analysis regression curve of bulk density log as measured in well P2 of the Bell Creek field.

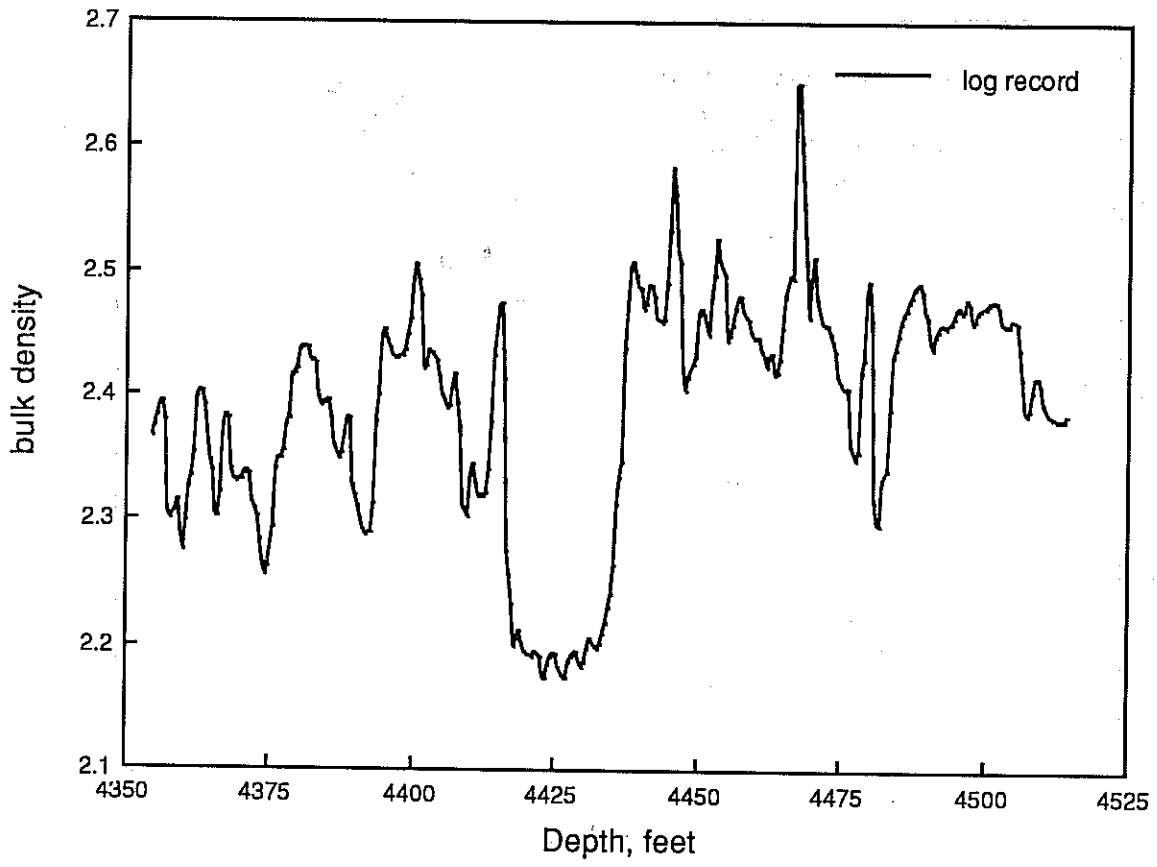


FIGURE 56. - Bulk density log for well P2, Bell Creek field.

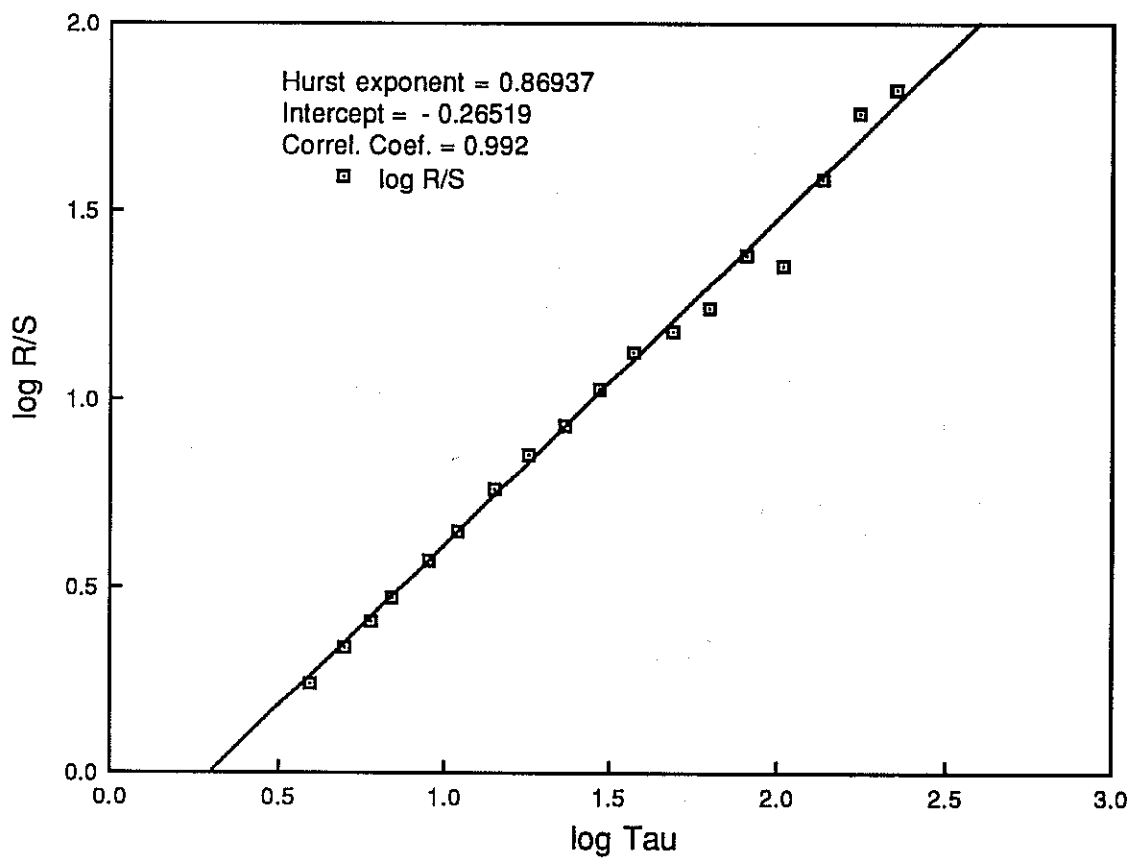
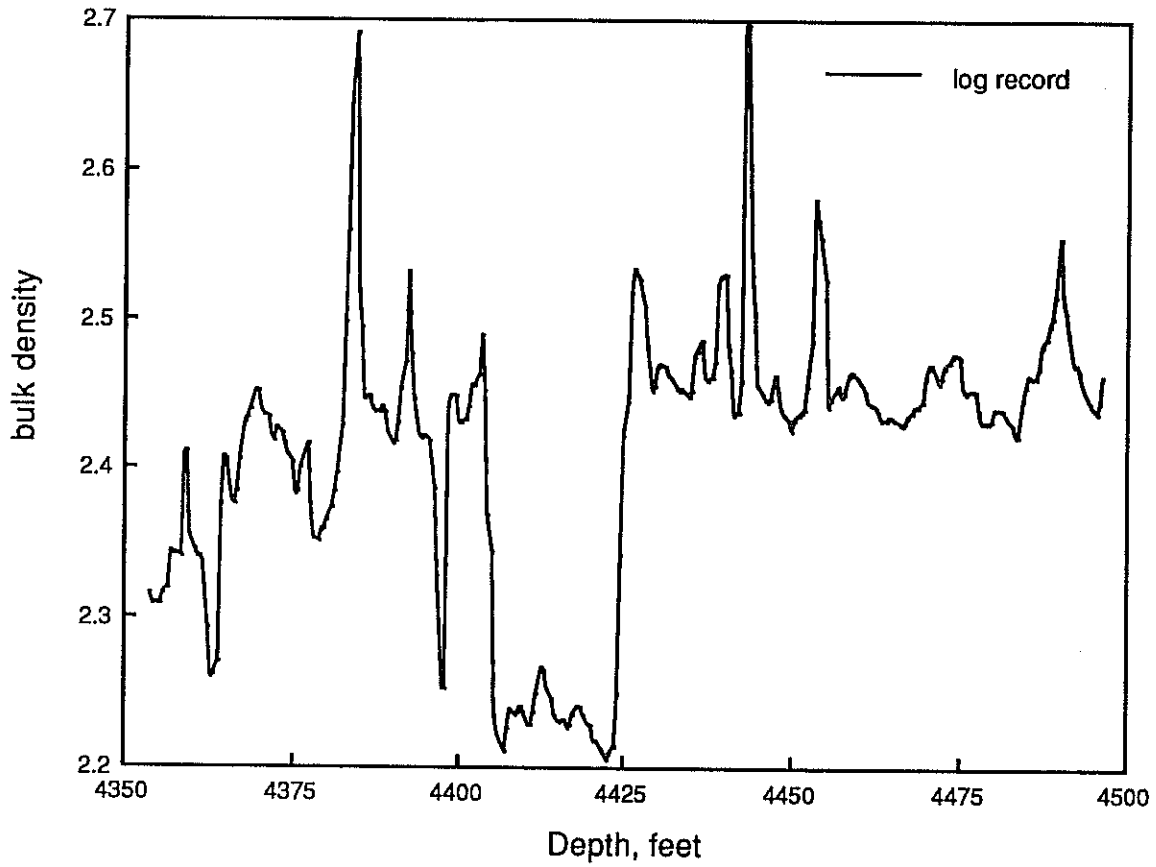


FIGURE 57. - R/S analysis regression curve of bulk density log as measured in well W7 of the Bell Creek field.



FIGURER 58. - Bulk density log for well W7 Bell Creek field.